Università di Brescia

Department of Civil and Environmental Engineering, International Cooperation and Mathematics

DOTTORATO DI RICERCA IN

Ingegneria Civile, Ambientale, della Cooperazione Internazionale e di Matematica

SETTORE SCIENTIFICO DISCIPLINARE

ICAR09

CYCLE

XXXVII

Sprayed Fibre Reinforced Concrete for Permanent Tunnel Lining

Ph.D. Candidate:

Mesfin Zenebe Gezahegn

Supervisor: Prof. Giovanni A. Plizzari

Co-supervisor: Prof. Giuseppe Tiberti

Dr. Ivan Trabucchi

March 2026

Declaration

I hereby declare that this thesis is my own original work, except where specific reference is made to the work of others. It has not been submitted, in whole or in part, for the award of any other degree or qualification at this or any other university.

Furthermore, this thesis contains no material that has been previously published or written by another person, except where due acknowledgement is given in the text and references.

Signed: Mesfin Zenebe Gezahegn

Date: 9th March 2026

Sommario

Nelle infrastrutture sotterranee, la costruzione di gallerie convenzionali prevede generalmente un rivestimento primario temporaneo in calcestruzzo proiettato, seguito dall'installazione di una membrana impermeabile e da un rivestimento secondario in calcestruzzo armato gettato in opera. Sebbene il processo di applicazione del calcestruzzo proiettato come rivestimento permanente (PSCL, Permanent Sprayed Concrete Lining) sia ormai ampiamente noto, nella pratica comune il calcestruzzo proiettato assolve convenzionalmente solo la funzione di rivestimento temporaneo. Il calcestruzzo fibrorinforzato spruzzato si è affermato come un materiale promettente per i rivestimenti permanenti delle gallerie, offrendo un'alternativa più efficiente e sostenibile nell'ambito dei metodi convenzionali di scavo delle gallerie, che attualmente comportano inefficienze in termini di costi, tempi e utilizzo dei materiali. I recenti sviluppi nella tecnologia del calcestruzzo fibrorinforzato proiettato comportano, inoltre, vantaggi significativi, tra cui la riduzione dei costi di investimento e di esercizio ed un'impronta carbonica inferiore rispetto ai sistemi di rivestimento tradizionali.

Le opzioni attualmente disponibili per la progettazione di rivestimenti in calcestruzzo fibrorinforzato spruzzato - rivestimenti a doppio strato (Double Shell Lining-DSL), rivestimenti compositi (Composite Shell Lining-CSL), rivestimenti a strato singolo (Single Shell Lining-SSL) - incorporano sempre più spesso il calcestruzzo fibrorinforzato spruzzato come materiale permanente, sia per il rivestimento secondario che per entrambi i rivestimenti, primario e secondario, a seconda delle opzioni di progettazione applicate. Tuttavia, mancano ancora procedure consolidate per la classificazione del calcestruzzo fibrorinforzato spruzzato per applicazioni di rivestimento permanente di gallerie; le linee guida di progettazione sono limitate e la fiducia nelle metodologie e

negli approcci standard esistenti è insufficiente.

Lo studio vuole valutare l'idoneità del calcestruzzo fibrorinforzato proiettato per i rivestimenti permanenti di galleria come soluzione efficace, valutandone le prestazioni meccaniche, il comportamento post-fessurativo e la conformità alle norme e alle linee guida di progettazione esistenti. Il lavoro di ricerca ha sfruttato appieno l'attuale metodologia per la caratterizzazione meccanica post-fessurativa del calcestruzzo fibrorinforzato proiettato da utilizzare nel PSCL (Permanent Sprayed Concrete Lining), obbligatoria per il processo di progettazione di queste strutture permanenti. Considerando anche campioni convenzionalmente gettati in casseri, si possono ottenere utili possibili correlazioni tra le prestazioni post-fessurative degli elementi di riferimento in calcestruzzo proiettato e quelli gettati. Lo studio, inoltre, esplora se esistono relazioni consolidate tra le proprietà delle fibre e il comportamento post-fessurativo osservato nel caso del calcestruzzo fibrorinforzato proiettato e indaga l'influenza del processo di proiezione del calcestruzzo sulla resistenza a compressione del calcestruzzo rispetto a quella del FRC (Fibre Reinforced Concrete) gettato. La ricerca mira anche a fornire dati affidabili sulla resistenza residua post-fessurativa ottenuta da prove su pannelli intagliati ed a sviluppare leggi costitutive uniassiali post-fessurative accurate da utilizzare nella modellazione numerica e nel processo di progettazione dei rivestimenti permanenti in calcestruzzo spruzzato (PSCL).

Per raggiungere questi obiettivi è stata condotta una vasta campagna sperimentale. La campagna comprende prove su campioni di riferimento in calcestruzzo proiettato rinforzato con fibre d'acciaio e anche campioni provenienti dallo stesso getto di calcestruzzo confezionati in casseri. Sono state inoltre utilizzate anche fibre macro-sintetiche per la preparazione di campioni gettati in casseri. Sono stati studiati il comportamento post-fessurativo e la tenacità, compresi la resistenza alla compressione, il modulo elastico ed il ritiro. È stata applicata la metodologia di prova in termini di resistenze residue (EN 14488-3:2023, Method B), recentemente inclusa nella norma europea EN 14487-1:2023 sul calcestruzzo proiettato per la caratterizzazione meccanica post-fessurativa del calcestruzzo proiettato finbrorinforzato. Similmente, è stata condotta la prova di capacità di assorbimento di energia, prova su pannello EN 14488-5, raccomandata

anche dalla norma EN 14487-1:2023 e comunemente applicata nei rivestimenti delle gallerie. È stata, inoltre, eseguita la prova di flessione a tre punti, EN 14651, consigliata dall'Eurocodice 2 e dal Model Code 2010 per valutare le prestazioni dell'FRC per l'uso generalmente in tipiche strutture gettate convenzionalmente. La maggior parte delle ricerche e dei casi di studio sul PSCL utilizzano infatti ancora questa norma (EN 14651), anche se si riferisce principalmente a campioni gettati in casseri. È stata inoltre effettuata un'indagine numerica utilizzando un approccio di analisi inversa applicato a travette con intaglio gettate in casseri ed è stata proposta l'applicazione di questo metodo anche alla prova su pannelli spruzzati con intaglio. Infatti, l'obiettivo principale è quello di fornire leggi costitutive post-fessurative uniassiali accurate rappresentative del comportamento effettivo del calcestruzzo spruzzato FRC da utilizzare nella simulazione numerica del corrispondente rivestimento permanente in calcestruzzo proiettato.

Lo studio ha stabilito chiare relazioni tra le prestazioni del calcestruzzo fibrorinforzato spruzzato e quello gettato, sottolineando l'importanza di utilizzare campioni proiettati rappresentativi per una caratterizzazione meccanica accurata, fornendo un quadro coerente per una caratterizzazione e una progettazione affidabili dei rivestimenti permanenti in calcestruzzo spruzzato (PSCL).

Keywords: Rivestimento permanente in calcestruzzo proiettato (PSCL); Calcestruzzo proiettato rinforzato con fibre; 3PBT su pannello quadrato proiettato con intagli; 3PBT su travette con intagli; Resistenza residua post-fessurativa; Caratterizzazione meccanica; Legge di trazione uniassiale.

Abstract

Within underground infrastructures, conventional tunnelling generally involves a temporary primary lining of sprayed concrete, followed by the installation of a waterproof membrane and a cast in-situ reinforced concrete secondary lining. Although the process of application of sprayed concrete as a Permanent Sprayed Concrete Lining (PSCL) is now widely recognised, the conventional practices, where sprayed concrete serves only as a temporary lining, remain the most common. Sprayed Fibre Reinforced Concrete has emerged as a promising material for permanent tunnel linings, offering a more efficient and sustainable alternative within conventional tunnelling methods, which often result in inefficiencies in cost, time, and material use. Recent developments in fibre-sprayed concrete technology have also demonstrated significant advantages, including reduced capital and operational costs and a lower carbon footprint compared to traditional lining systems.

The currently available sprayed fibre reinforced concrete lining design options - Double Shell Linings (DSL), Composite Shell Linings (CSL), Single Shell Linings (SSL), increasingly incorporate sprayed fibre reinforced concrete as a permanent material, either for the secondary lining or for both primary and secondary linings, depending on the design approach adopted. However, there remains a lack of well-established procedures for classifying sprayed FRC for permanent tunnel lining applications, along with limited design guidelines and insufficient confidence in existing methodologies and standard approaches.

The study aims to investigate the suitability of sprayed fibre-reinforced concrete as an effective solution for permanent tunnel linings by assessing its mechanical performance, post-cracking behaviour, and compliance with existing standards and design

guidelines. The research fully exploits the current methodology for the mechanical post-cracking characterisation of sprayed fibre-reinforced concrete for use in PSCL, which is a mandatory step for the design process of these permanent structures. By also considering conventional cast-in-mould samples, the study identifies useful possible correlations between post-cracking performance of reference sprayed concrete elements and cast ones. In addition, the study explores whether established relationships between fibre properties and post-cracking behaviour observed in case of sprayed FRC and investigates the influence of the spraying process on the compressive strength of sprayed fibre reinforced concrete compared with cast FRC. The research also aims to provide reliable post-cracking residual strength data from notched panel tests and to develop accurate uniaxial post-cracking constitutive laws to be used in the numerical modelling and design process of Permanent Sprayed Concrete Linings (PSCL).

A comprehensive experimental campaign was conducted to achieve these objectives. The campaign included tests on reference sprayed Steel Fibre Reinforced specimens and also cast-in-mould samples from the same concrete batch. In addition, macro-synthetic fibres were used for preparing cast-in-mould specimens. The post-cracking behaviour and toughness including compressive strength, elastic modulus, and shrinkage were studied. The residual strength test methodology (EN 14488-3:2023, Method B), recently included in European sprayed concrete standard EN 14487-1:2023 for the mechanical post-cracking characterisation of FRC sprayed concrete was applied. Similarly, the energy absorption capacity test, EN 14488-5 panel test, which is also recommended by EN 14487-1:2023 and commonly applied in tunnel linings, was conducted. Additionally, the three-point bending beam test, EN 14651, advised by Eurocode 2 and Model Code 2010 for evaluating the performance of FRC for use generally in typical conventionally cast structures, was carried out. In fact, most research and case studies of PSCL still utilise this standard (EN 14651) even though it mainly refers to cast-in-mould samples. A numerical investigation was also performed using inverse analysis approach applied to notched cast-beam and the application of this method to notched sprayed panel tests was proposed. In fact, the main goal was to provide accurate uniaxial post-cracking constitutive laws representative of the actual behaviour of

FRC sprayed concrete for use in numerical simulation of the corresponding Permanent Sprayed concrete lining.

The study established clear relationships between the performance of sprayed and cast fibre-reinforced concrete, highlighting the importance of using representative sprayed test specimens for accurate mechanical characterisation and providing a consistent framework for the reliable characterisation and design of PSCL.

Keywords: Permanent Sprayed Concrete Lining (PSCL); Fibre-reinforced sprayed concrete; 3PBT on notched sprayed square panel; 3PBT on notched beam; Residual post cracking strength; Mechanical characterisation; Uniaxial tensile law.

Acknowledgements

First and foremost, I would like to express my sincere gratitude to Almighty God for His guidance, strength, and grace in making this work possible in His perfect time.

I would like to express my deepest appreciation to my supervisor, Professor Giovanni Plizzari and to my co-supervisors Professor Giuseppe Tiberti and Dr Ivan Trabucchi, for their invaluable guidance, continuous support, and encouragement throughout my PhD journey. I am also grateful to all the laboratory technicians of the Structural Laboratories at the University of Brescia for their technical support. In addition, I would like to extend my thanks to the administrative and academic staff of the University of Brescia for their support throughout the entire process and for providing me with this opportunity.

I am deeply grateful to my parents and friends for their unconditional love, support, and prayers. I would also like to express my sincere thanks to Brurktawit Ewune for her patience and understanding.

Contents

List of Figures

List of Tables

Chapter 1

Introduction

Within underground infrastructures, conventional tunnelling generally involves a temporary primary lining of sprayed concrete, followed by the installation of a waterproof membrane and a cast-in-situ reinforced concrete secondary lining. Although the process of application of sprayed concrete as a Permanent Sprayed Concrete Lining (PSCL) is now widely recognised, the conventional practices, where sprayed concrete serves only as a temporary lining, remain the most common. Sprayed Fibre Reinforced Concrete has emerged as a promising material for permanent tunnel linings, offering a more efficient and sustainable alternative to conventional tunnelling methods, which often result in inefficiencies in cost, time, and material use. Recent developments in fibre-sprayed concrete technology have also demonstrated significant advantages, including reduced capital and operational costs and a lower carbon footprint compared to traditional lining systems.

The currently available sprayed concrete lining design options can be broadly categorized into three types. The first one is Double Shell Linings (DSL), which involve a sacrificial primary lining that carries the temporary loads and a secondary lining that withstands the permanent loads. The second type is Composite Shell Linings (CSL), where the primary lining carries the temporary loads and a proportion of the permanent loads through composite action with the secondary lining. The third type is Single Shell Linings (SSL), which use a single lining for the temporary and permanent loads, although it may be built up in several passes.

Within these design options, FRC sprayed concrete is increasingly utilised as a permanent material, either for the secondary lining or for both primary and secondary linings, depending on the design options applied. Consequently, understanding in detail the mechanical properties, as well as the mechanical characterisation in terms of post-cracking performance and classification of fibre reinforced sprayed concrete, is essential for its use in the design process and for supporting its implementation in permanent tunnel lining practice. However, there remains a lack of well-established procedures for classifying sprayed FRC for permanent tunnel lining applications, along with limited design guidelines and insufficient confidence in already existing test methodologies and standard approaches.

The *fib* Model Code 2010 and Eurocode 2 Annex L are nowadays used as reference documents for Fibre Reinforced Concrete and recommend EN 14651 three-point bending (3PBT) on notched samples for material characterization and classification. Likewise, ITA Report No.16 and *fib* Bulletin 83 provide guidance for FRC segmental tunnel linings and also refer to the EN 14651 test. This beam geometry and testing method are mainly suitable for cast-in-situ tunnel linings or precast FRC tunnel segment structural applications, but not for fibre-reinforced sprayed concrete.

The former European sprayed concrete standard EN 14487-1:2006, specifically conceived for sprayed concrete, describes various methods to evaluate the post-cracking toughness of fibre-reinforced sprayed concrete, including residual strengths according to EN 14488-3 (four-point bending test) on beams and energy absorption capacity determined from EN 14488-5 panel test. The energy values obtained from EN 14488-5 are typically considered when designing a temporary sprayed FRC lining and are not generally used for material characterisation and classification in permanent tunnel lining design. The residual strength four-point bending tests on unnotched samples of EN 14488-3 are not completely incongruent with the MC 2010 and conducting these tests on the saw cut beams taken from sprayed panels does not seem practical or feasible.

To align with the MC 2010, and using a sample representative of the spraying process, EFNARC produced guidance recommending the use of the three-point bending

tests on notched sprayed panels with the same geometry as EN 14488-5 (Energy absorption capacity test) and proposed a correlation between parameters of the EFNARC notched panel test and the EN 14651 notched beam test to prove the comparability of their corresponding residual strengths. More recently, the European sprayed concrete standard EN 14487-1:2023 has been updated to include the notched panel test, and the corresponding standard EN 14488-3 incorporates the 3PBT on notched panel as Method B, alongside the four-point bending beam test as Method A. It is worth noting that even though EN 14487-1:2023 is specifically intended for sprayed concrete, it frequently mentions the EN 14651 test method a test developed for cast or poured concrete, without clearly explaining how to produce beam samples representative of the spraying process adopted for tunnel linings.

Within this framework, this Ph.D. study aims to investigate the suitability of sprayed fibre-reinforced concrete as an effective solution for permanent tunnel linings by assessing its mechanical performance, post-cracking behaviour, and compliance with existing standards devoted to sprayed concrete. The research fully exploits the current methodology for the mechanical post-cracking characterisation of sprayed fibre-reinforced concrete for use in PSCL, which is a mandatory step in the design process of these permanent structures. By also considering conventional cast-in-mould samples, the study identifies possible useful correlations between post-cracking performance of reference sprayed concrete elements and cast ones. In addition, the study explores whether established relationships between fibre properties and post-cracking behaviour observed in conventional cast FRC are applicable to sprayed FRC, and investigates the influence of the spraying process on the compressive strength of sprayed fibre reinforced concrete compared with cast FRC. The research also aims to provide reliable post-cracking residual-strength data from notched panel tests and to develop accurate uniaxial post-cracking constitutive laws to be used in the numerical modelling and design process of Permanent Sprayed Concrete Linings (PSCL). Additionally, current guidelines and standards, such as the *fib* Model Code 2020 and Eurocode 2 Annex L, provide frameworks for the characterisation and classification of fibre-reinforced concrete (FRC). However, these documents do not specify explicitly whether the same

classification procedures are applicable to fibre-reinforced sprayed concrete. Therefore, this research aims to assess the applicability of these classifications to sprayed FRC.

In developing the research methodology, the study began with a comprehensive review of literature on fibre-reinforced sprayed concrete. Relevant standards and design guidelines were reviewed, along with case studies of tunnel linings that employed sprayed fibre-reinforced concrete as a permanent structural material. In addition, previous research on mix design approaches for fibre-reinforced sprayed concrete was reviewed to identify key parameters influencing performance. These case studies and literature findings were analysed to understand the design concepts adopted, the types and quantities of materials used, and the practical considerations in mix proportioning. The insights gained from this review formed the foundation for selecting the materials, fibre types, and mix proportions used in the experimental investigation.

The investigation involves a detailed experimental study that includes tests on reference sprayed steel-fibre-reinforced specimens and also cast-in-mould samples from the same concrete batch. Additionally, macro-synthetic fibres were used to prepare cast specimens. The post-cracking behaviour and toughness including compressive strength, elastic modulus, and shrinkage were studied. The residual strength test methodology (EN 14488-3 Method B), recently included in European sprayed concrete standard EN 14487-1:2023 for the mechanical post-cracking characterisation of FRC sprayed concrete was applied. Similarly, the energy absorption capacity test, EN 14488-5 panel test, which is also recommended by EN 14487-1:2023 and commonly applied in tunnel linings, was conducted. Additionally, the three-point bending beam test, EN 14651 advised by Eurocode 2 and Model Code 2010 for evaluating the performance of FRC for use in typical structures, was carried out. In fact, most research and case studies of PSCL still utilise this standard even though it mainly refers to cast-in-mould samples. Moreover, within EN 14487:2023 that also refers to the EN 14651 test methodology, to produce samples representative of the spraying process adopted in PSCL, sprayed panels ($15 \times 80 \times 200\,\text{cm}$) were made and beams (that comply with the dimensions specified by EN 14651) were saw-cut from them. These sprayed beams, sawn from the panels, were tested in accordance with the test set-up of EN 14651, providing more

reliable residual properties than those obtained from cast-in-mould beams.

In addition to experimental methods, numerical techniques are employed to study the post-cracking properties of sprayed FRC. A numerical investigation was performed using an inverse-analysis approach generally applied to notched beams, and the application of this method to notched sprayed panel tests was proposed. In fact, the main goal was to provide accurate uniaxial post-cracking constitutive laws representative of the actual behaviour of sprayed FRC concrete for use in numerical simulations of the corresponding Permanent Sprayed concrete lining.

The study established clear relationships between the performance of sprayed and cast fibre-reinforced concrete, highlighting the importance of using representative sprayed test specimens for accurate mechanical characterisation and providing a consistent framework for the reliable characterisation and design of PSCL.

The structure of the thesis is as outlined in Figure 3.1 and organized as follows:

The first chapter introduces the research, covering the background, problem statement, research objectives and questions, scope and delimitations, and an overview of the methodology and structure of the thesis.

The second chapter reviews the state of the art, providing a detail description of fibre reinforced concrete and in-depth discussion of sprayed concrete, including innovations in materials and technology. The chapter also includes a literature survey on the mix design of sprayed concrete and case studies exploring the use of sprayed fibre-reinforced concrete for permanent tunnel lining applications. Additionally, it identifies knowledge gaps and unresolved questions, particularly regarding the mechanical properties of sprayed FRC in using for permanent tunnel lining applications.

The third chapter highlights the research significance, its contributions to the advancement of knowledge in the field, and practical implications in the construction industry.

Chapter 4 presents the experimental investigations undertaken in this research. It outlines the experimental programme, provides detailed descriptions of the materials and mixture proportions, and explains the procedures adopted for specimen preparation, spraying and casting. The chapter also describes the experimental setups for all tests conducted and presents the corresponding results and discussions.

The experimental programme comprises a comprehensive study using standard test methods to evaluate the mechanical properties of fibre-reinforced concrete (FRC). The residual strength test, EN 14488-3 Method B (three-point bending panel test), was carried out in accordance with the European Sprayed Concrete Standard EN 14487-1:2023 on sprayed notched panels, in addition notched cast panels were also tested. Similarly, the energy absorption capacity test, EN 14488-5 panel test, also recommended by EN 14487-1 and commonly used in tunnel lining applications, was performed on sprayed concrete panels as well as on cast panels. Furthermore, the three-point bending beam test, EN 14651, referenced in Eurocode 2 Annex L and the *fib* Model Code 2020 for assessing the performance and mechanical characterisation of cast FRC, was conducted. In addition, notched sprayed beams sawn from sprayed panels were tested. The latter will be referred to herein as sprayed beams. Complementary tests, including compressive strength, elastic modulus measurements and shrinkage measurements, were also undertaken.

The experimental investigations were performed on sprayed concrete, including cast FRC specimens from the same batch prepared with different fibre types, properties, and contents. The overall experimental programme is summarised in Section 4.1. This chapter presents the results obtained from each test method and analyses the performance of the material under different casting and testing conditions. The post-cracking properties of sprayed FRC are evaluated for each test, and the characterisation and classification of the material are determined and discussed in detail. In this regard, it is worth noting that the post-cracking performance was evaluated and compared by means of energy absorption on panels (EN 14488-5), while the mechanical characterisation was based on residual post cracking strengths (f_{Ri}). The latter were obtained from 3PBT on notched panels (EN 14487-1:2023) and on notched beams (EN 14651).

In this chapter, these residual strengths (f_{Ri}) were directly compared, even though these parameters derive from different test set-ups. The correlation and comparability of these parameters are investigated in Chapter 6.

Chapter 5 focuses on the numerical investigations carried out in this research. It presents the background of the numerical modelling approach, the description of the finite element modelling (FEM) framework, and the procedures adopted for inverse analysis and model validation. The chapter integrates the results obtained from the uniaxial post-cracking laws with the flexural tensile strength results derived from the experimental programme. Inverse analyses were performed for different fibre types and casting methods to establish uniaxial tensile laws corresponding to each combination.

For each specific FRC composition, it is essential to establish the σ–w relationship that most accurately reflects the tensile behaviour of the composite. Ideally, a direct tension test should be performed to establish the σ–w relationship. However, this test is complicated. An alternative approach, currently under extensive investigation, involves using the load–displacement response from 3PB tests to drive the σ–w curve of the material through inverse analysis. Most researchers have focused on the behaviour of notched beams under three-point bending loads, while inverse analysis using 3PB notched panel tests, which is the reference test methodology for characterising FRC sprayed concrete, has been scarcely addressed in the literature. To address this gap, the research performed inverse analyses on both notched beam and notched panel tests to determine the σ–w relationships for various fibre types and casting methods, and to investigate the post-cracking behaviour of sprayed fibre-reinforced concrete.

Chapter 6 presents the investigation into the correlation of the main displacement parameters of 3PBTs and in particular their comparability in terms of a similar crack-width range investigated. According to the European sprayed concrete standards EN 14488-3 Method B:2023 and EN 14487-1, the crack mouth opening displacement (CMOD) measured in beam tests (EN 14651) and that obtained from panel tests (EN 14488-3) are generally considered equivalent when determining the residual strength of sprayed fibre-reinforced concrete (FRC). However, due to the geometrical differences

between the beam and panel specimens, the loading configurations, and differences in notch depth between the two test methodologies, the CMOD measurements cannot be regarded as fully equivalent. In this study, the relationship has been analysed, verified, and established using analytical, experimental, and numerical methods.

Finally, Chapter 7 presents the overall conclusions of the research, synthesising the key experimental and analytical findings.

Chapter 2

State of the Art

This chapter provides an overview of sprayed fibre reinforced concrete used in permanent tunnel linings, along with a broader overview of Fibre-Reinforced Concrete (FRC), as the foundation for discussing the main topic, fibre-reinforced sprayed concrete for permanent tunnel linings. It examines the applications, mechanical properties, and mix design of both sprayed and cast FRC, supported by relevant research, case studies, and practical experiences in tunnel lining applications. The chapter also identifies existing knowledge gaps and unresolved questions, particularly regarding the mechanical performance of sprayed FRC when used as a permanent structural material in tunnel lining.

In addition, regional standards and design guidelines related to the mechanical characterization and design of FRC are reviewed, with emphasis on their limitations for sprayed applications. The discussion highlights the constraints of standards originally developed for conventional FRC and evaluates their applicability to sprayed FRC, particularly in the context of permanent tunnel lining design.

2.1 Fibre Reinforced Concrete

Fibre reinforced concrete (FRC) is a composite material consisting of a cementitious hydraulic cement, and aggregate of various sizes, incorporating discrete, discountinuous fibres, characterised by an enhanced postcracking tensile residual strength, also defined as toughnes, due to the fibre reinforcement mechanisms provided by fibres bridging the

crack surface [1, 23–25]. The inclusion of these fibres enhances the material's post-cracking tensile residual strength by allowing the fibres to bridge crack faces through a pull-out mechanism [1].

Fibre-reinforced concrete has demonstrated its reliability in a wide range of construction applications, including in various complex architectural forms, precast elements, industrial pavement, highways and airport runways, in sprayed concrete tunnel linings, in precast bridge sections and decks as transverse reinforcement, in ground-supported concrete floors and others. Fibre reinforced concrete sections can be significantly reduced in thickness compared to traditional rebar reinforced concrete, leading to material savings, lower labour costs, and a decrease in greenhouse gas emissions associated with cement production.

Plain, unreinforced cement-based materials have low tensile strength and limited tensile strain capacity, making them brittle. Traditional reinforcement bars (rebars) are typically used in structures at specific points to resist tensile and shear forces. In contrast, fibres are discontinuous and are usually dispersed randomly throughout the concrete matrix. The mechancical properties of a cementitious matrix are modified when fibres are added. However, elastic properties and compressive strength are not significantly affected by fibres, unless a high percentage of fibres is used [1] see Figure 2.1. High-modulus fibres for structural application, low -modulus fibres and small size (length of few millimetres and diameter of few microns) for reduction of shrinkage cracking and enhancement of fire resistance. Higher fibre volumes and fibres with a high elastic modulus would be more efficient in controlling crack openings, resulting high post cracking performance as shown in the Figure 2.2.

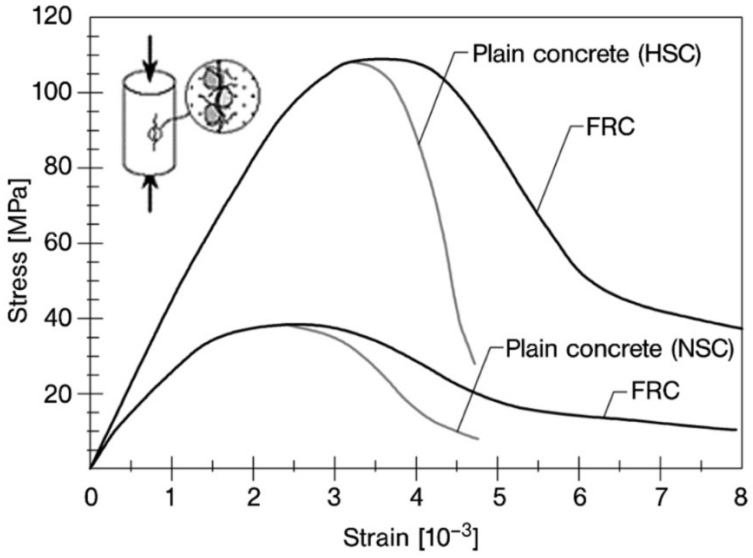

Figure 2.1: Main differences between plain and fibre reinforced concrete having both normal and high strength under uniaxial compression.

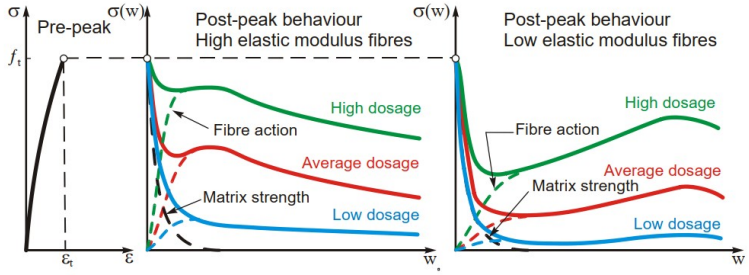

Figure 2.2: Difference between the performance of high-elastic-modulus and low-elastic-modulus fibres (Summer School presentation on FRC, August 2024, by Professor Lucie Vandewalle).

2.1.1 Types of Fibres

The main categories of fibres include steel fibres, synthetic fibres like polypropylene, glass, carbon, polyolefin, and polyvinyl, as well as fibres derived from waste materials. However, in structural FRC, steel, macro synthetic fibres, glass fibres and natural fibres are the main types of fibre, which are used as a replacement for conventional steel fabric reinforcement.

A sub-classification is often used based on the size and functionality of the fibres;

hence, fibres can be classified as microfibers or macrofibers with the fibre diameter of 0.3 mm as the separating limit. Macro fibres bridge macro crackes and micro fibres bridge micro cracks. Steel fibers and polymeric synthetic fibres are the most-used types of fibers in fibre reinforced concrete compared to other types.

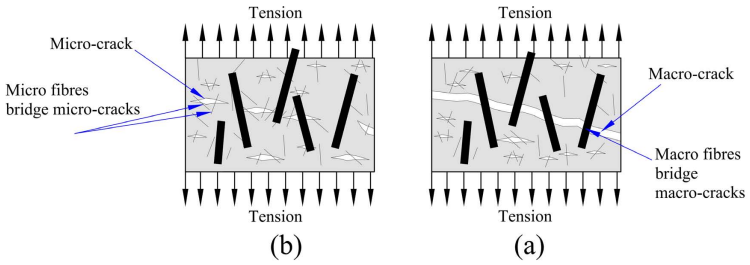

Figure 2.3: Macro fibres bridging macro cracks (a) and Micro fibres bridging micro cracks (b) under imposed tensile load on FRC elements.

2.1.1.1 Steel Fibre

Currently, Steel Fibre Reinforced Concrete (SFRC) is the most commonly used fibre-reinforced concrete. Steel fibres significantly alter the behaviour of concrete, turning it from a brittle material into a ductile one that can endure substantial deformations without losing its load-bearing capacity. This ductility allows for load redistribution and enhances the structure's bearing capacity, while the mechanical properties of the original concrete material remain unchanged.

Steel fibers come in many geometries, including rectangular, flat, cylindrical, and variations or combinations of these. In addition, fiber anchorage mechanisms in concrete include continuous deformations such as twists, dimples or crimps, end anchorage such as hooks, or simply bond for undeformed fibers. Bond to the concrete matrix is enhanced by mechanical anchorage, surface area, alloying, surface roughness, or a combination of these. Fiber geometry and anchorage significantly affects resistance to pullout forces and overall performance of FRC. Another characteristic is the aspect ratio or the ratio of the length to diameter. Typically, for the same mixture proportions, as the fiber aspect ratio increases, so does the reinforcing performance. Steel

macrofibers have typical diameters in the range of 0.3 to 1.3 mm and a length in the range of 30 to 65 mm.

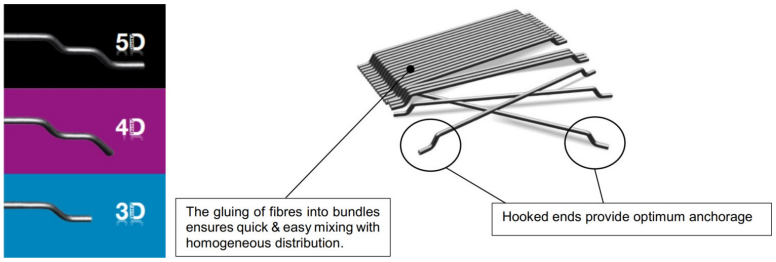

Figure 2.4: Technical concept of steel fibre (Images sourced from the manufacturer's data sheet).

2.1.1.2 Synthetic Fibre

Synthetic fibres in fibre-reinforced concrete includes macro and micro fibres. The main goal of adding fibres, such as macro-synthetic fibres, is to replace conventional steel reinforcement and improve the ductility and post-cracking strength of concrete. Synthetic fibers are made with polyolefin materials, which typically include polypropylene and polyethylene. Synthetic macrofibers have typical diameters in the range of 0.3 to 1.0 mm and a length in the range of 25 to 65 mm. Non-structural synthetic micro-fibers are generally 6 to 19 mm in length and a diameter of a few tens of μm.

Numerous studies have emphasized that the inclusion of macro-synthetic fibres enhances the residual strength and toughness of the concrete, [26–28] and also substantial post-peak load carrying capacity and continued resistance with increasing crack separation [29, 30].In contrast to steel fibers, macro-synthetic fibers have relatively low tensile strengths and low elastic modulus. However, due to the low elastic modulus of fibre, residual strengths tend to be more positively influenced at larger deflections or wider crack openings this phenomenon was observed in some studies.

The main advantages of using fibers are observed in the post-cracking phase where there is an increase in the residual tensile flexural stresses with the increase in the fiber content. The polypropylene macro-synthetic FRC exhibits a nonmonotonous post cracking behaviour marked by a first drop of the load-CMOD curve of EN 14651 after

cracking to more than 67% for a CMOD = 0.5 mm, followed by a strength recovery up to stress stability. The low elastic modulus of polypropylene fibers compared to steel fibers explains this drope [31]. Macro-synthetic fibers are starting to gain popularity due to their corrosion resistance relative to steel [31].

Figure 2.5: Various types of macro-synthetic fibres (Images sourced from manufacturer's data sheet).

2.1.1.3 Glass Fibre

Glass fibres are made in a process in which multiple filaments are drawn simultaneously from a container of molten glass, usually, 204 filaments are drawn simultaneously and they solidify while cooling outside the heated tank [23, 32]. The typical glass fiber varies from 6 to 18mm with an average density of 2.60 g/cm3. The tensile strength of glass fibres ranges from 1000 MPa to 3400 MPa with elastic modulus from 29 to 84 GPa. Furthermore, glass fibre has a significantly higher modulus of elasticity than synthetic fibres, although not as high as steel or carbon fibres [33].

2.1.1.4 Basalt Fibre

Basalt fibre is a kind of inorganic fiber made by the extrusion of melted basalt rock through melting process. The basalt rocks can be so finely divided into small particles that it is possible to produce into a form of fibres. Basalt fibres can be used in concrete as chopped fibres to make basalt fibre-reinforced to replace steel rebar. Basalt fibres are being has comparable mechanical strength with other fibres, higher durability than glass fibres, lesser cost than carbon fibres, sustainability due to abundant raw material, and environment-friendly production process [34].The modulus of elasticity (E) varies between 75 and 115 GPa and tensile strength between 2175 and 4840 MPa [34].

2.1.2 Mechanical Properties of FRC

The mechanical properties of fibre-reinforced concrete (FRC) are influenced by the characteristics of the fibres (such as material type, volume fraction, shape, and orientation), the concrete's properties (including aggregate size, strength, and elastic modulus), and the interaction between the fibres and the concrete matrix. The mechanical properties of FRC, like those of ordinary concrete, differ between the fresh state and the hardened state, and need to be considered separately.

2.1.2.1 Fresh State Properties

Factors which affect the mechanical performance of the FCR significantly related the fresh properties of FRC. The properties of fresh concrete are typically described by its workability, flowability, consistency, mobility, compatibility, pumpability, and finish ability. Among those terms such as workability, flowability, consistency, and mobility have been used to characterize the rheological behaviour. Rheology is an effective tool for assessing workability, flowability, consistency, as well as predicting stability, pumpability and shoot ability. The state of fibre distribution, which is closely related to the rheological properties of fresh concrete matrix, is actually influenced by both the fibre dispersion during mixing process and the stability of the plain concrete during casting. Additionally, fibre orientation and dispersion significantly affect workability, which in turn has a strong impact on the mechanical performance of fibre- reinforced concrete (FRC).

The fresh state is a crucial prerequisite for the use of fibre-reinforced cementitious composites, and numerous researchers have validated the potential correlations between concrete flowability and its mechanical properties [35–39]. Optimizing the fresh and rheological properties of fiber-reinforced concrete (FRC) is essential for improving its mechanical strength and durability in the hardened state. Generally, increasing fiber length, content, aspect ratio, or fiber factor reduces workability, while fibers tend to raise the yield stress and viscosity of cement-based materials [35]. Stiffer or hooked-end

fibres have a greater impact on concrete flowability and passing ability compared to flexible or straight fibres. In addition, the orientation of fibers is mainly governed by the deformation of the fluid, good fiber orientation promotes workability and vice versa, moreover, favorable rheological performance facilitates fiber dispersion [35].

2.1.2.2 Hardened State Properties

Among the properties of the hardened state, compressive strength is the most important. It is typically the primary property specified and used to classify concrete due to the relative ease of its testing compared to other properties. Additionally, many other characteristics of concrete, such as modulus of elasticity, tensile strength, and permeability, are tought to be influenced by compressive strength and can often be inferred from its data. However, compressive strength cannot be served as a substitute for all properties, particularly for the increased residual strength or toughness seen in fibre-reinforced concrete (FRC). Therefore, specific toughness measures and alternative testing methods are necessary to properly evaluate fibre reinforced concrete.

Table 2.1 presents the ranges of various mechanical properties for cement-based materials, including cement and concrete. The Table 2.1 includes values for the following properties: compressive strength (f_c), tensile strength (f_t), modulus of elasticity (E), fracture energy (G_F), and characteristic length (l_{ch}). The characteristic length provides an indication of the material's brittleness and is defined in Equation 2.1:

$$l_{ch} = \frac{E_C \times G_F}{f_t^2} \tag{2.1}$$

In normal-strength concrete, the aggregate is considerably stronger and stiffer than the cement paste; however, in high-strength concrete, their strength and stiffness are more comparable. When fibres are incorporated into the matrix, the concrete exhibits increased ductility (see Figure 2.7, with the primary benefit being their ability to resist the growth of longitudinal cracks. The inclusion of fibres is especially beneficial for enhancing the mechanical properties of high-strength concrete under compressive loads,

Table 2.1: Assessed ranges of mechanical properties in cement-based materials [2].

Material	f_c **[MPa]**	f_t **[MPa]**	**E [GPa]**	G_F **[Nm/m²]**	l_{ch} **[mm]**
Cement	10–25	2–10	10–30	10	5–15
Mortar	-	1–10	10–30	10–50	100–200
NSC	20–80	1.5–5	25–40	50–150	200–400
HSC	>80	4–5	40–50	100–150	150–250
FRC	20–80	1.5–5	25	>500	>1000

as it significantly reduces its inherent brittleness. Overall, it can be concluded that conventional steel fibres used at moderate dosages (less than 1%) do not impact the pre-peak properties, but they do increase the strain at crack localization and the failure strain. In contrast, using high fibre volumes (greater than 1%) can lead to an increase in compressive strength [2]. Generally, Fibres do not modify the compressive strength of the matrix, but reduce the brittleness in compression, especially in high or ultra-high strength concrete and in the cases where fibres are predominantly oriented orthogonally to the compressive force [1].

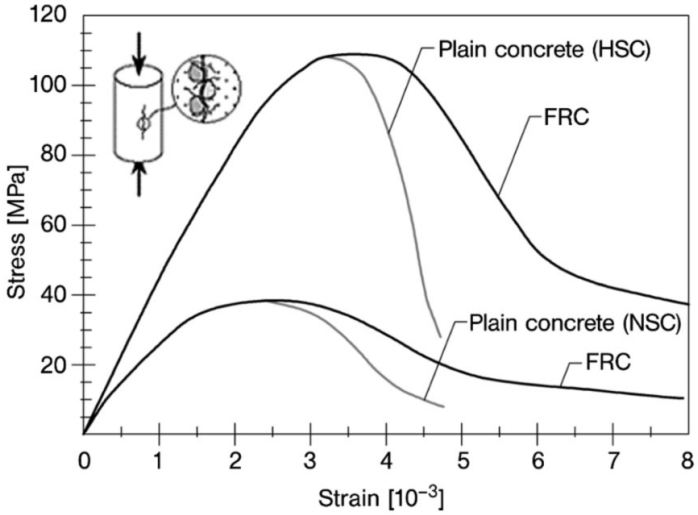

Figure 2.6: Schematic description of the behaviour of plain concrete (normal and high strength concrete) and FRC in compression [1].

When we come to the tensile properties of FRC. The most reliable way to classify the tensile behaviour of fibre-reinforced concrete is based on the material's uni-axial

response [40–42]. The tensile behaviour of fibre-reinforced concrete can be classified into two types: strain-softening or strain-hardening. Strain-softening materials, which are quasi-brittle, develop a single localized crack after reaching peak stress, and the stress decreases once the matrix cracks. In contrast, strain-hardening materials, also known as high-performance fibre-reinforced concrete, exhibit post-cracking strength greater than the cracking strength, displaying a strain-hardening (elastic-plastic) response refer to Figure 2.7.

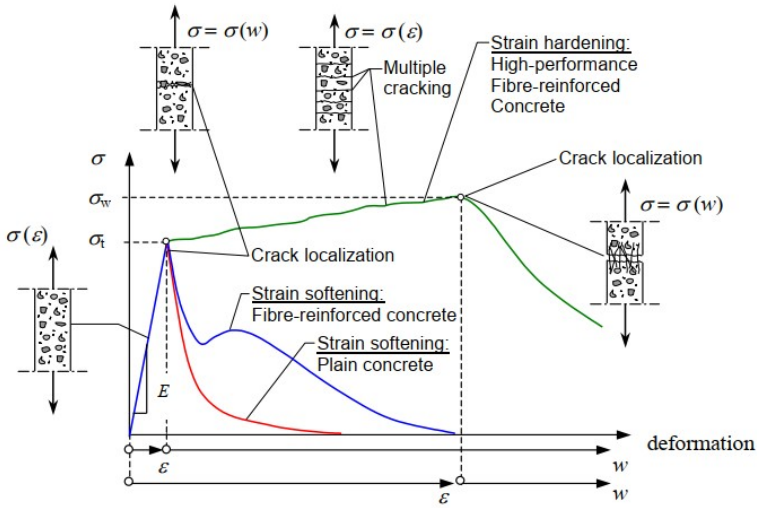

Figure 2.7: Classification of tensile behaviour of concrete and fibre-reinforced concrete [2].

In plain concrete, the primary mechanism for transferring shear stresses across a crack is typically attributed to aggregate interlock and friction along the crack surfaces. In fibre-reinforced concrete, with low to moderate fibre content, the cracking strength remains unaffected; however, once the matrix cracks, the fibres are engaged and begin to pull out, leading to a significant toughening effect. In summary of the mechanical properties of FRC, for concrete with a low to mideam volume fraction commonly called $V_f < 1.0\%$, fibres have minimal impact on both tensile and compressive strength [2]. Their main contribution is in enhancing post-cracking behaviour and toughness, the ability to transfer stresses after matrix cracking and increasing tensile strain capacity at failure.

2.1.3 Testing Methodologies for Post-cracking Performance of Fibre-reinforced Concrete

The experimental determination of the tensile constitutive behaviour of fibre-reinforced cementitious composites is a critical step in material characterization, classification, and the development of design methods for structural elements made from fibre-reinforced concrete. To achieve this, international standards and guidelines suggest conducting either direct tension tests, bending tests, or both, often combined with an inverse analysis process.

To assess the post-cracking tensile properties of FRC can be used with the following types of tensile tests: indirect (non standard) tensile test, direct uniaxial tensile test and flexural (bending) tests. Indirect (non-standard) tensile tests and direct uniaxial tensile tests are briefly introduced in Section 2.1.3. However, the bending test discussed in detail in 2.1.3.3, as evaluation of the performance of sprayed FRC and cast FRC with that test methodology is a key focus of this thesis.

2.1.3.1 Indirect Non-standard Tensile Test

The type of indirect non-standard tensile tests includes, the Wedge Split Test (WST) and Double Punch Test (DPT). The WST is a suitable method for establishing splitting tensile strength, which is related to tensile strength and fracture energy and provides the stress – crack width curve and is independent of specimen size (Figure 2.8). The DPT is performed on cylinders 150mm high by 150mm in diameter. By applying compressive load through the punches, uniform tensile stresses are generated over diametric planes, and tensile cracks occur along these diametric planes. The Double Punch Test (DPT) and Wedge Splitting Test (WST) on specimens weighing approximately 2 kg have been utilized to assess the post-cracking behaviour of FRC [43]. Both the DPT and WST tests enable the characterization of FRC cores extracted from the structure [43].

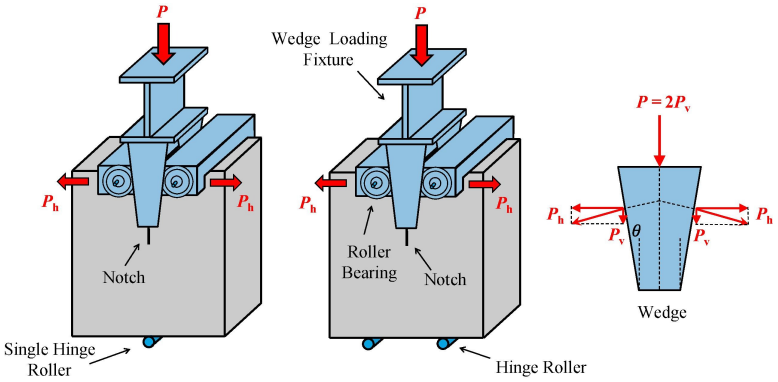

Figure 2.8: Typical wedge splitting test schematic [3].

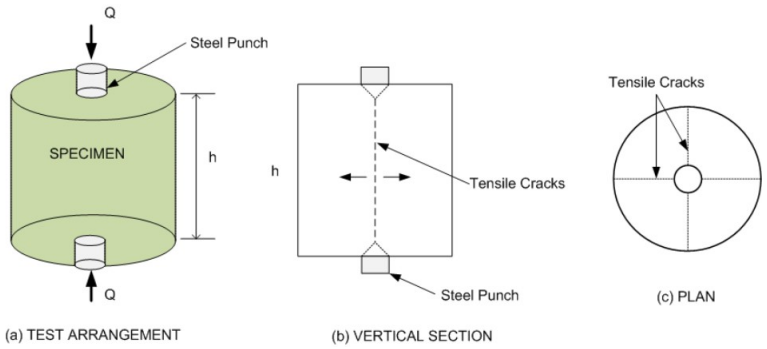

Figure 2.9: Typical schematic view of double punching test [4].

There is also indirect tensile testing called Double Edge Wedge Splitting (DEWS) test which has been developed at the Politecnico di Milano for thin-walled fibre cementitious composite structures. The test can directly provide the tensile stress versus crack opening behavior of the material, without requiring back analysis, by conducting an "indirect" test, where a compressive load is applied to the specimen [5].Though performing an indirect test, by applying a compressive load to the specimen, it directly yields the tensile stress versus crack opening as shown in the Figure 2.10a and 2.10b. The test is simple, with compact specimen geometry and a preordained fracture plane, allowing easy alignment with fibre orientation. This makes it perfect for analysing how fibre orientation influences material behaviour in customized casting processes.

Numerous studies in the literature have examined the characterization of fibre re-

inforced concrete using indirect non-standard tensile tests. However, it is important to note that these tests are non standardize and have not yet been validated by any international standards organization. As a result, they should not be used alone as a substitute for standardized beam/panel bending tests or full-scale segment testing.

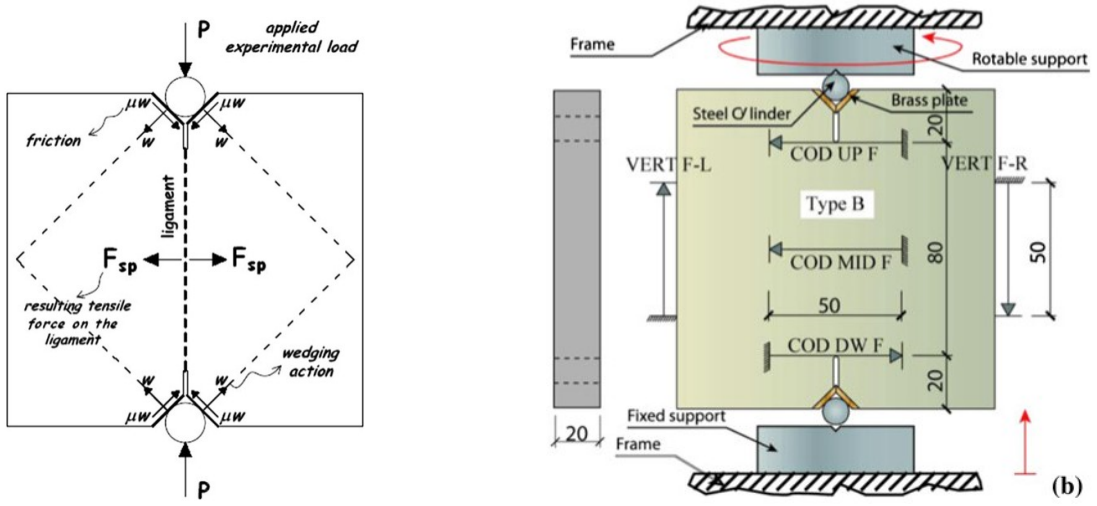

(a) (b)

Figure 2.10: Force diagram (a) and details of specimen geometries (b) in double edge splitting test [5].

2.1.3.2 Direct Uniaxial Tensile Test

The second type of test involves applying a direct uniaxial tensile load to the specimen as shown in the Figure 2.11. Direct tensile tests can be used to characterize various properties of SFRC, including tensile stress-strain behaviour, post-peak response, tensile modulus of elasticity, and tensile strength [6]. These tests allow the tensile stress-strain and tensile stress-crack width curves to be derived directly from the testing, without the need for analytical manipulation. However, this test is well-known for its difficulty and complex set-up, difficult to guarantee rigid-fixed end conditions and a uniform application of stress.

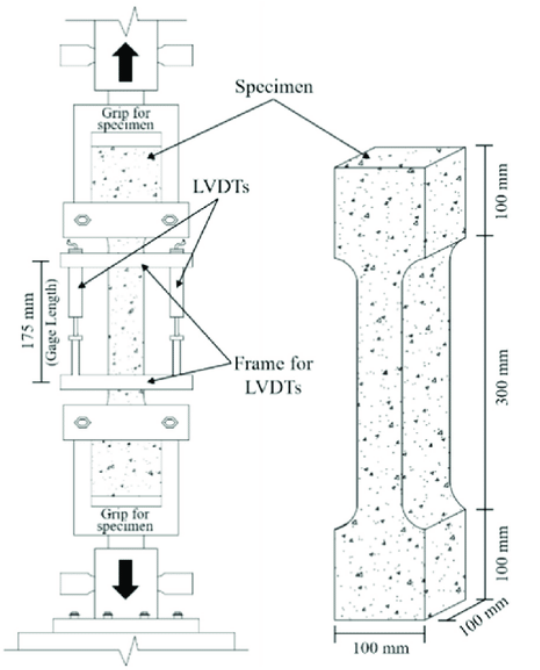

Figure 2.11: Typical schematic view of direct tensile test [6].

2.1.3.3 Bending Test (Notched Beam Test)

The most commonly used test methods for FRC material characterization involve bending tests of beams. The main advantages of the three-point bending beam test are it is well-established, relatively easy to perform, supported by an extensive database for comparative studies, and consistent with existing design guidelines. The notched three-point bending beam test is a standard test method for FRC, as seen in standard such as EN 14651, RILEM TC-162 TDF, and JCI-S-002-2003. However, the focus of this thesis is on EN 14651 [7].This is a flexural tensile test on a beam specimen with nominal dimensions of 150 mm in width and depth, and a length (L) of 550 mm $\leq L \leq$ 700 mm as shown in the Figure 2.12.

The test specimens shall be prisms conforming to EN 12390-1 [44] and the procedure for filling the mould is according to the standard EN 14651 [7], Section 7.2. The test specimens shall be cast and cured in compliance with EN 12350-1 [45] and EN 12390-2 [46]. A notch with a maximum width of 5 mm and a height of 25 mm is sawn.

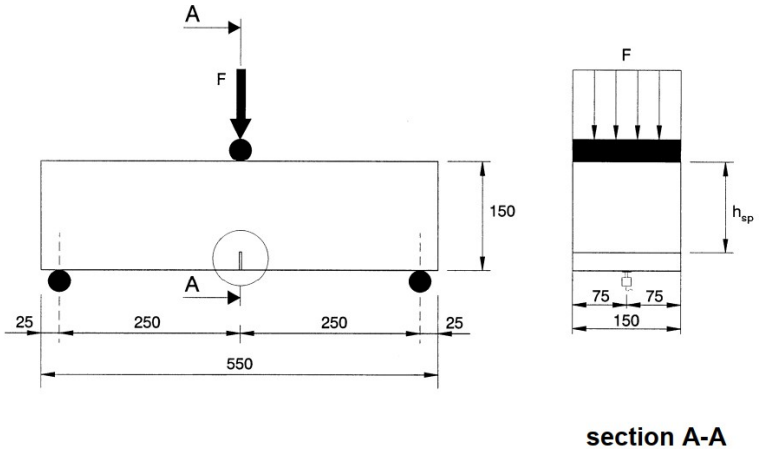

Figure 2.12: Test setup according to EN14651 three-point bending test [7].

The notch allows the creation of a weak section where cracks can spread quickly. In correspondence with the notch, the depth of the section is equal to 125 mm as shown in Figure 2.12.

The test is deflection control or CMOD control, in case of a testing machine controlling the rate of increase of CMOD, the machine shall be operated so that CMOD increases at a constant rate of 0.05 mm/min. when CMOD = 0.1 mm, the machine shall be operated so that CMOD increases at a constant rate of 0.2 mm/min. In case of a testing machine controlling the rate of increase of deflection, the CMOD related parameters are transformed into deflection related parameters, can be correlated as per Equation 2.2.

$$\text{CMOD} = \frac{\delta - 0.04}{0.85} \tag{2.2}$$

Where: δ is deflection, in millimetres; CMOD in millimetres.

The results of the test include the limit of proportionality (LOP) and the residual tensile strength. These expressions are derived from the bending moment at mid-span of the test specimen, corresponding to the center-point load F in the Figure 2.12 and represented by Equation 2.3. Assuming a linear stress distribution, as illustrated in Figure 2.14b, the LOP is given by Equation 2.4, and the residual flexural tensile

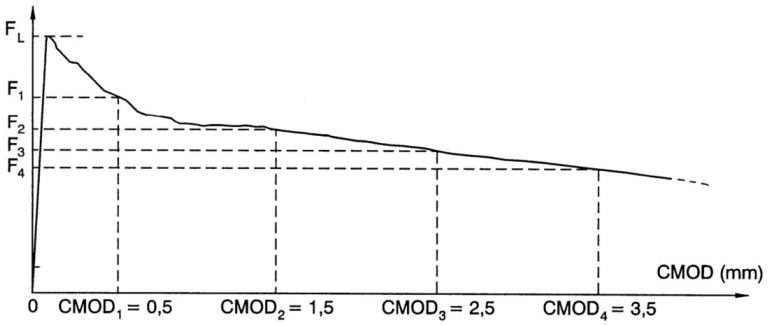

Figure 2.13: Load-CMOD diagram and F_j (j = 1, 2, 3, 4) [7].

strength f_R, j (j = 1,2,3,4) is provided by the expression in the Equation 2.5.

$$M = \frac{F}{2} \times \frac{l}{2} \tag{2.3}$$

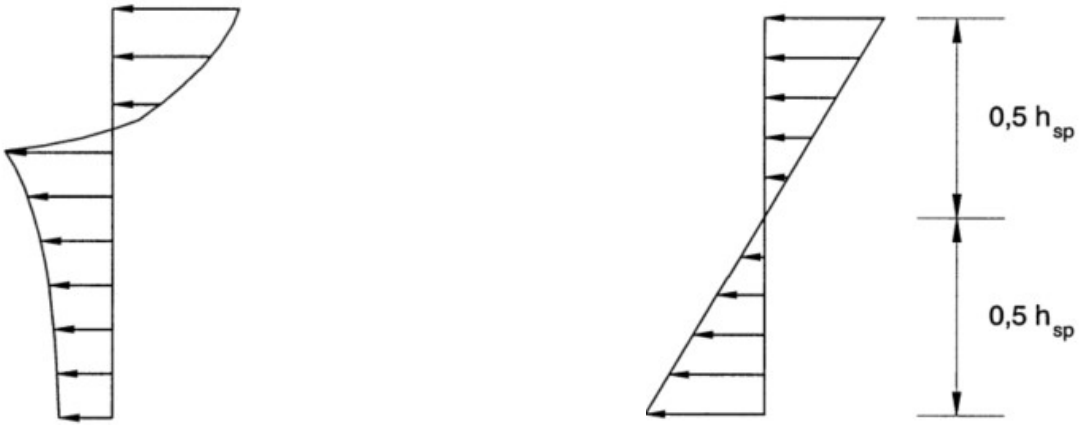

(a) (b)

Figure 2.14: Stress distribution (a) Real stress distribution and (b) Assumed stress distribution.

$$f_{\frac{f}{ctL}} = \frac{6 \times M_L}{b \times h_{sp}^2} = \frac{3 \times F_L \times l}{2 \times b \times h_{sp}^2} \tag{2.4}$$

$$f_{R,j} = \frac{6 \times M_J}{b \times h_{sp}^2} = \frac{3 \times F_j \times l}{2 \times b \times h_{sp}^2} \tag{2.5}$$

where

$f^f_{ct,L}$ is the LOP in MPa;

$f_{R,j}$ is the residual flexural tensile strength corresponding with CMOD = CMOD$_j$ or $\delta = \delta_j$ $(j = 1, 2, 3, 4)$ in MPa.

F_L is the load corresponding to the LOP, in N;

F_j is the load corresponding with CMOD = CMOD$_j$ or $\delta = \delta_j$ $(j = 1, 2, 3, 4)$ in N.

M_L is the bending moment corresponding to the load at LOP;

M_J is the bending moment corresponding to the load at F_j $(j = 1, 2, 3, 4)$;;

b is the width of the specimen;

h_sp is the un notched height;

After finding the LOP and the residual tensile strength material, characterization and classification can be assessed according to Model Code 20 [8] and EN 1992-1-1:2023 Annex L [9] or as detailed in Subsection 2.1.5 of this PhD thesis. In general, testing the structural performance of FRC is essential to characterize its post-crack behaviour and to derive tensile strength parameters for use in design analysis.

2.1.4 Behaviour in Tension

When unreinforced concrete fails under uniaxial tension, a single crack typically forms, leading to failure. In fibre-reinforced concrete, however, the fibres usually remain intact after a crack forms. These fibres, which cross the crack, help to resist its widening and create what is known as a crack-closing or crack-bridging effect on the surfaces of the crack. Various failure modes may occur depending on how effectively the fibres provide crack bridging, see Figures 2.15a ,2.15b. If the fibres break or are pulled out during crack initiation, or if they are unable to carry additional load after the first crack forms, the initial cracking strength becomes the ultimate strength. Further deformation is then controlled by the opening of the single crack, with fibres either pulling out or breaking along its edges, as illustrated in Figure 2.15a. This type of behaviour is referred to as tension softening. On the other hand, if the fibres can withstand additional load after the initial crack forms, as illustrated in Figure 2.15b, this is referred as strain hardening behaviour.

In tension-softening FRC, the strength after cracking is lower than the matrix cracking strength, and typically, only a single crack forms in a specimen under direct tension. In this scenario, elongation is controlled by the crack opening (w). This behaviour is common in most FRC used for structural applications [47]. In this thesis only materials exhibiting the tension-softening behavoiur will be dealt with in detail.

In tension-hardening FRC, the strength after cracking surpasses the matrix cracking strength, leading to increased tensile strength without a dominant crack forming. During the hardening phase, multiple micro-cracks develop, and overall deformation or elongation is typically measured as strain for simplicity. Hardening behavior is uncommon in most FRC and is usually only achievable in certain UHPFRC with a high fiber content, where the fibers have high tensile strength and strong bonding properties [47].

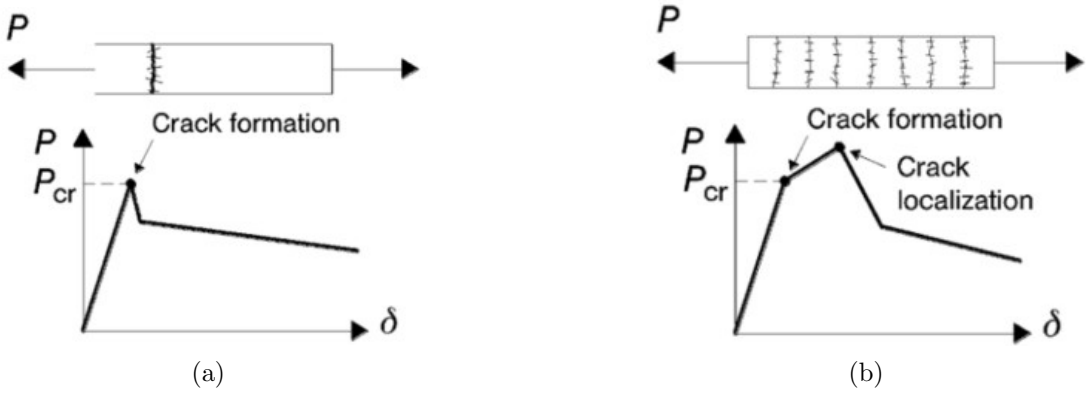

Figure 2.15: Softening (a) and Hardening (b) behaviour in axial tension [8].

2.1.5 Classification of Fibre Reinforced Concrete

Model Code 2020 [8] stated that "To classify the post cracking strength of FRC, a linear elastic behaviour can be assumed, by considering the characteristic flexural residual strength values that are significant for serviceability ($f_{R,1K}$) and ultimate ($f_{R,3K}$) conditions, and in particular, two parameters: f_{R1K} (representing the strength interval) and a letter a, b, c, d or e (representing the f_{R3K} / f_{R1K} ratio)."

The strength classes for f_{R1K} (characteristic value of f_{R1}) are defined by the following values: 1.0, 1.5, 2.0, 2.5, 3.0, **3.5**, 4.0, **4.5**, 5.0, 6.0, 7.0, 8.0, **10**, **12**, **14**

[MPa], the strength classes in Model code 2020 [8] updated compared to Model Code 2010 [1]. The bold numbers represent the updated classes.

$$\text{Class} = \begin{cases} a, & \text{if } 0.5 < \frac{f_{R,3k}}{f_{R,1k}} < 0.7 \\ b, & \text{if } 0.7 \leq \frac{f_{R,3k}}{f_{R,1k}} < 0.9 \\ c, & \text{if } 0.9 \leq \frac{f_{R,3k}}{f_{R,1k}} < 1.1 \\ d, & \text{if } 1.1 \leq \frac{f_{R,3k}}{f_{R,1k}} < 1.3 \\ e, & \text{if } 1.3 \leq \frac{f_{R,3k}}{f_{R,1k}} \end{cases} \tag{2.6}$$

Fibre reinforcement can substitute (also partially) conventional reinforcement at ultimate limit state, if the following relationships are fulfilled [1]. Alternatively, as described in the Model Code 2020 [8]: 'For the design according to the Model Code 2020, the following equations should be satisfied:'

$$\frac{f_{R,1k}}{f_{Lk}} > 0.4 \tag{2.7}$$

$$\frac{f_{R,3k}}{f_{1k}} > 0.5 \tag{2.8}$$

The classification according to EN 1992-1-1:2023 Annex L [9] is specified in terms of f_{R1K} and f_{R3K}, consistent with Model Code 2020 [8]. The values of f_{R1K} and f_{R3K} to use for design correspond to the values obtained from classifying the strength class and ductility class according to Table 2.2 respectively. Unlike Mode Code 2020, the ductility classes are not determined directly from the ratio of f_{R3K}/f_{R1K}. Instead, they are based on the ratio of f_{R3K}/SC (Strength Class), as shown in the Table 2.2. The values of characteristic residual flexural strength used correspond to those determined using EN 14651 [7] test methodology, as in Model Code 2020 [8].

Table 2.2: Performance classes for Steel Fibre Reinforced Concrete (SFRC) [MPa] [9].

Ductility Classes	**Strength Classes SC** ($f_{R1k} \geq SC$)												**Analytical Formula**
	1.0	1.5	2.0	2.5	3.0	3.5	4.0	4.5	5.0	6.0	7.0	8.0	
a	0.5	0.8	1.0	1.3	1.5	1.8	2.0	2.3	2.5	3.0	3.5	4.0	$f_{R3k} \geq 0.5SC$
b	0.7	1.1	1.4	1.8	2.1	2.5	2.8	3.2	3.5	4.2	4.9	5.6	$f_{R3k} \geq 0.7SC$
c	0.9	1.4	1.8	2.3	2.7	3.2	3.6	4.1	4.5	5.4	6.3	7.2	$f_{R3k} \geq 0.9SC$
d	1.1	1.7	2.2	2.8	3.3	3.9	4.4	5.0	5.5	6.6	7.7	8.8	$f_{R3k} \geq 1.1SC$
e	1.3	2.0	2.6	3.3	3.9	4.6	5.2	5.9	6.5	7.8	9.1	10.4	$f_{R3k} \geq 1.3SC$

2.1.6 Constitutive Laws

A stress-crack opening law in uniaxial tension is defined for the post-cracking behaviour of FRC. The post-cracking tensile behaviour can be derived through inverse analysis from the result of EN 14651 [7] test, as advised in the Model Code 2020 [8] and detailed in the numerical modelling chapter 5 of this PhD thesis.

Model Code 2020 [8] proposes two simplified stress-crack opening constitutive laws that can be deduced from the bending test results: a plastic rigid behaviour or a linear post-cracking behavior (hardening or softening), as shown in Figure 2.16. Where, f_{Fts} represents the serviceability residual strength, defined as the post-cracking strength for serviceability crack opening, and f_{Ftu} represents the ultimate residual strength. The two simplified models corresponding to LoA (Level of Approximation) I and II, cannot be used with Finite Element analyses, because they cannot reproduce crack localisation because they fully neglect the matrix behaviour and reproduce only the pull-out resistant mechanism exhibited in the post-cracking regime and, therefore, they risk introducing a significant spurious dissipated energy [8].

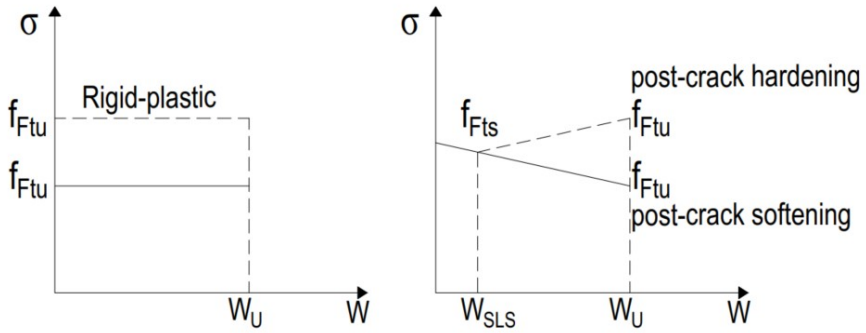

Figure 2.16: Simplified post-cracking constitutive laws: stress-crack opening (continuous and dashed lines refer to softening and hardening post-cracking behaviour, respectively) [8].

The rigid-plastic model, identifies a unique reference value, f_{Ftu}, based on the ultimate behaviour see Figure 2.16 a and Equation 2.9.

$$f_{Ftu} = \frac{f_{R,3k}}{3} \tag{2.9}$$

The linear model, a more advanced model, which identifies two reference values, namely f_{Fts} and f_{Ftu} as shown in the Figure 2.16 b. They have to be defined through residual values of flexural strength using the following equations:

$$f_{Fts} = 0.37 f_{R,1k} \tag{2.10}$$

$$f_{Ftu} = f_{Fts} - \frac{W_u - CMOD_1}{CMOD_3 - CMOD_1}(f_{Fts} - 0.57 f_{R,3k} + 0.26 f_{R,1k}) \geq 0 \tag{2.11}$$

Where W_u is the maximum crack opening accepted in structural design; its value depends on the ductility required.

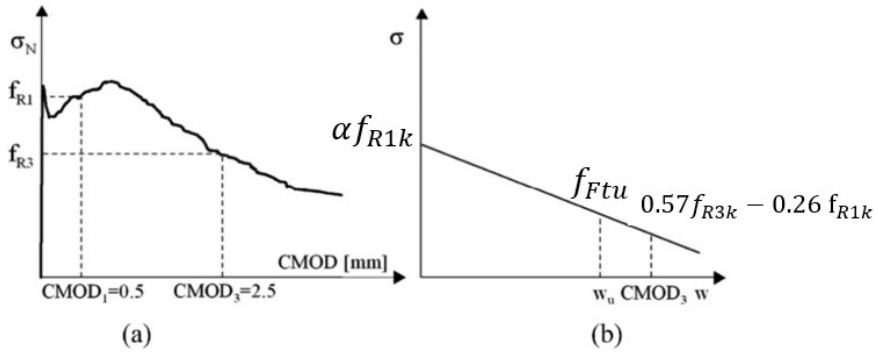

Figure 2.17: Typical results from a bending test on a softening material (a); linear post-cracking constitutive law (b) [8].

α is the coefficient corresponding to W = 0 and is computed from the linear post-cracking constitutive law at W = 0 as represented in the following equation.

$$\alpha = 0.52 - 0.15\frac{f_{R,3k}}{f_{R,1k}} \tag{2.12}$$

In both the rigid and linear models in Model Code 2010 [1], it was not specified the residual values were characterstics or not. In contrast, the Model Code 2020 [8] clearly defines the residual values of flexural strength as characterstic values.

In Model Code 2020 [8] it is advised that, for higher levels of approximation at the Ulitimate Limte State (ULS) and the Serviceability Limit State (SLS), more refined uniaxial stress-strain relationships in tension can be applied. At Level of Approximation III (LoA III), four cases are distinguished. In this thesis, we have discussed two cases that may be applicable to the softening FRC materials used in this thesis.

Case (I) For softening materials at SLS ($f_{Fts} \leq 0.8 f_{ctm}$), the same constitutive relationship adopted for plain concrete in uniaxial tension is used up to the peak strength f_{ctm}. In the post-cracking stage, a bilinear relation applies (Figure 2.18a). The post-peak propagation branch (see BC in Figure 2.18a) is analytically described as:

$$\frac{\sigma - f_{ctm}}{0.2 f_{ct} - f_{ctm}} = \frac{\varepsilon - \varepsilon_P}{\varepsilon_Q - \varepsilon_P}, \quad \text{for } \varepsilon_P \leq \varepsilon \leq \varepsilon_C \tag{2.13}$$

Where

$$\varepsilon_Q = \frac{G_F}{f_{ctm} l_{cs}} + \left(\varepsilon_P - \frac{0.8 f_{ctm}}{E_C} \right) \tag{2.14}$$

$$G_F = 73 \cdot f_{cm}^{0.18} \tag{2.15}$$

Point A in the curve of Figure 2.18a, 2.18b is defined in Figure 2.18 .

For softening materials, the residual strength (fourth branch) is defined by two points corresponding to (ε_{SLS} , f_{Fts}) and (ε_{ULS}, f_{Ftu}) where:

$$\varepsilon_{SLS} = \frac{\text{CMOD}_1}{l_{cs}} \tag{2.16}$$

$$\varepsilon_{ULS} = \frac{w_U}{l_{cs}} = \min \left(\varepsilon_{Fu}, \frac{2.5}{l_{cs}} \right) \tag{2.17}$$

with $\varepsilon_{FU} = 2\%$ for variable strain distribution along the cross-section and 1% for only tensile strain distribution along the cross-section.

Case (Il): materials characterised by a residual strength f_{Fts} larger than 0.8 f_{ctm}. In this case the cracking process shows localisation, but the residual strength on uniaxial tension at SLS strain remains close to the peak strength: a three-branch post-peak relation defines the constitutive relationship. The first branch in the post-peak remains that corresponding to plain concrete, while the second branch (C'V) is analytically described as:

$$\frac{\sigma - \beta f_{ct}}{\sigma_v - \beta f_{ct}} = \frac{\varepsilon - \varepsilon_{C'}}{\alpha_S \varepsilon_{SLS} - \varepsilon_{C'}} \quad \text{for } \varepsilon_C \leq \varepsilon \leq \alpha_S \varepsilon_{SLS} \tag{2.18}$$

Where:

β - tensile strength factor at the breakpoint of matrix crack (Figure 2.18bb)

α_S - peak strain factor of the hardening branch due to fibre residual strength (Figure 2.18bb)

σ_v - peak stress of the hardening branch due to fibre residual strength (Figure 2.18bb)

ε_{SLS} - limit strain at SLS (given in Equation 2.16)

ε_{ULS} - limit strain at ULS (given in Equation 2.17)

ε_Q - breakpoint strain of plain concrete (given in Figure 2.18a) computed as $\frac{w}{l_{cs}}$ (Figure 2.18a).

After having reached point V the material follows the pull-out branch characterised by softening with the slope or the branch (DE).

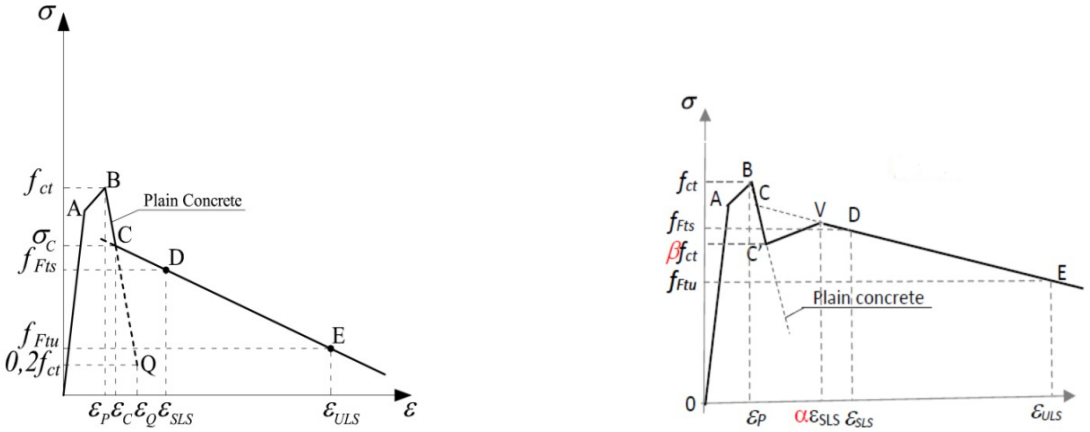

(a) (b)

Figure 2.18: Stress-strain relations at SLS for softening Case (I) $f_{FTs} \leq 0.8 f_{ctm}$ (a) and quasi-plastic Case (II) $f_{FTs} > 0.8 f_{ctm}$ (b) behaviour of FRC [8].

The values α_s and β can be identified by means of equilibrium equations: they may be assumed conservatively as $\alpha_s = 1$ and $\beta = 0.75$.

The constitutive law discussed in Eurocode 2 Annex L [9] is as depicted in Figure **??** and the parameters are determined as follows:

$$f_{Ft1,ef} = k_0 \cdot k_G \cdot 0.37 f_{R,1K} \tag{2.19}$$

$$f_{Ft3,ef} = k_0 \cdot k_G \cdot (0.57 f_{R,3K} - 0.26 f_{R,1K}) \tag{2.20}$$

$$\varepsilon_{Ftu} = \frac{w_u}{l_{cs}} \leq \frac{2.5\text{mm}}{l_{cs}} \leq \varepsilon_{Ftud} \tag{2.21}$$

$$l_{cs} = \begin{cases} \min\{h; s_{r,m,cal,F}\}, & \text{for members subjected to combined axial and bending} \\ S_{r,m,cal,F}, & \text{for members subjected to uniaxial tension} \end{cases} \tag{2.22}$$

$$S_{r,m,cal,F} = 1.5c + \frac{k_{f1}k_b}{7.2}\frac{\phi}{\rho_{p,eff}}(1-\alpha_f) \tag{2.23}$$

$$\alpha_f = \frac{0.37k_0k_Gf_{R1K}}{f_{ctm}} \leq 1.0 \tag{2.24}$$

$$\varepsilon_{ctm} = \frac{f_{ctm}}{E_{cm}}, \quad \varepsilon_{F,0} = 2\varepsilon_{ctm} \tag{2.25}$$

The simplified laws, the rigid plastic law and the linear law in Model Code 2020 [8], are the same as those in Eurocode 2 Annex L [9]. The difference lies the residual strength values, which are design values that have been factored.

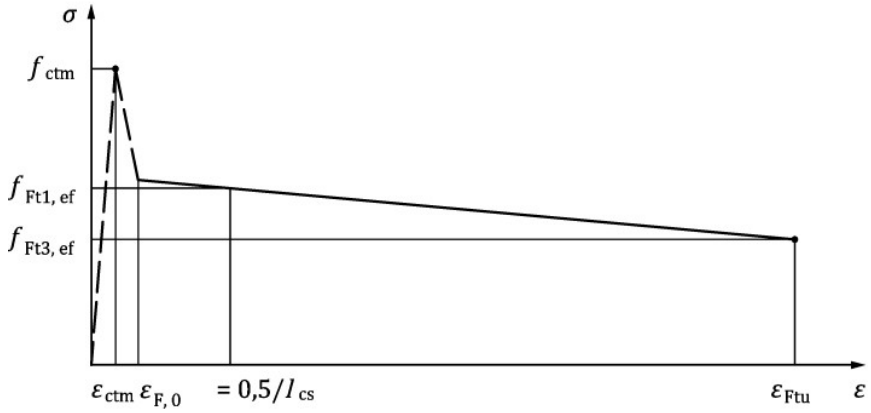

Figure 2.19: Constitutive law of SFRC in uniaxial tension for structural analysis [9].

The constitutive law described in Model Code 2020 [8] and Eurocode 2 Annex L [9] is nearly similar. However, the assumption regarding the pre-cracking and crack initiation stage is slightly different.

In addition, in Eurocode 2 Annex L [9], the residual values used in the constitutive law are factored by an orientation factor instead of the characteristic residual strength values used in the Model Code 2020 [8], as shown in Figure 2.20

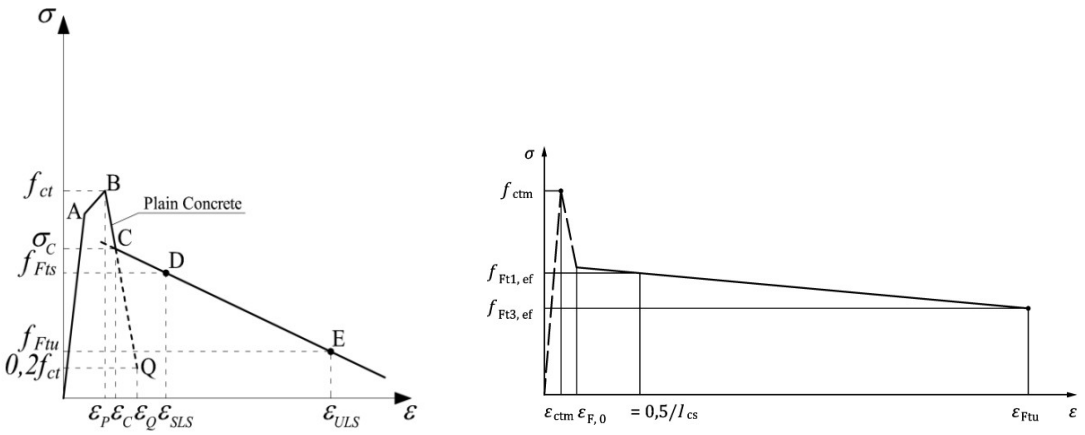

Figure 2.20: Stress-strain relations at SLS for softening Case I Model Code 2020 [8] (a) and Constitutive law in uniaxial tension Eurocode 2 Annex L [9] (b).

The post-cracking tensile behaviour is derived from the results of the notched beam and panel tests for different fibre types in this PhD thesis. The constitutive laws for these fibre types are proposed through inverse analysis, with details provided in Chapter 5 on numerical modelling.

To compare the constitutive laws in the Model Code and Annex L with the inverse analysis from the experiment results, the Stress vs. Strain representation should be changed to Stress vs. Crack-width.

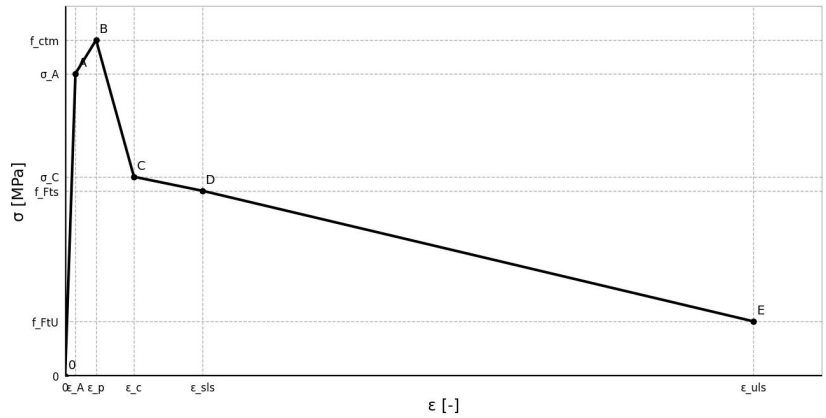

(a)

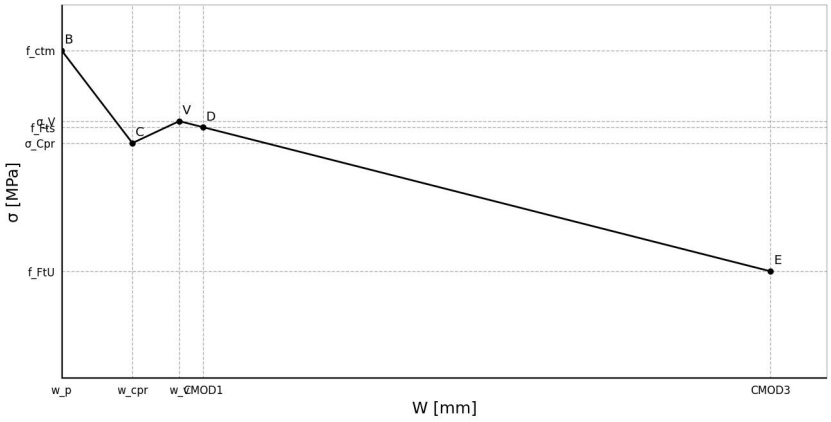

(b)

Figure 2.21: Stress-strain Case I Model Code 2020 (a) and Stress-crack width Case I (b) constitutive laws.

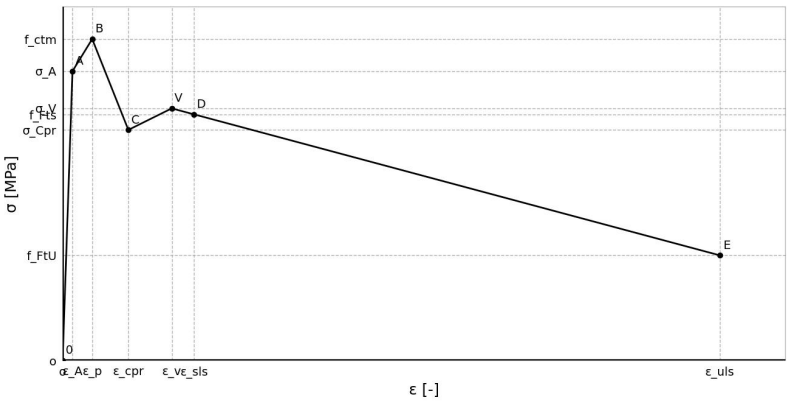

(a)

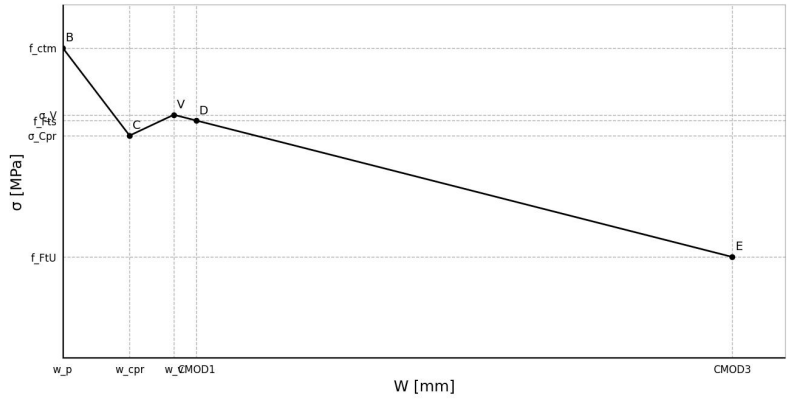

(b)

Figure 2.22: Stress-strain Case II Model Code 2020 (a) and Stress-crack width Case II (b) constitutive laws.

2.1.7 Fibre Distribution and Orientation

Fibres crossing the fracture surface significantly influence the performance of fibre reinforced concrete (FRC) and are crucial in determining fracture outcomes used to assess the structural integrity of the composite. Therefore, the post-cracking behaviour of FRC depends on the number of fibres engaged at the crack surface and their alignment. The position and orientation of the fibres are influenced by the pouring method, wall effects, formwork geometry and the concrete's rheological properties [21]. Some researchers argued, among the several aspects governing fiber orientation, the fresh state properties of and the wall effects introduced by the sides of the mold are most affecting [10, 48, 49].

The Fresh state properties of FRC are affected by fibre despression [50];fibres can be clumping when fibres are not randomly distributed throughout the matrix. They bundle together leaving some parts of the matrix unreinforced see Figure 2.23a. Fibres also segregate, fibre segregation is defined as the settling of fibres under gravitational forces (Figure 2.23b). Fibre segregation results in weakly reinforced upper sections of the components. Preferred orientation is as shown in the Figure 2.23c, the preferred alignment of fibres which may occur due to several reasons such as casting method, formwork restrictions, the flow-ability of the matrix, etc.

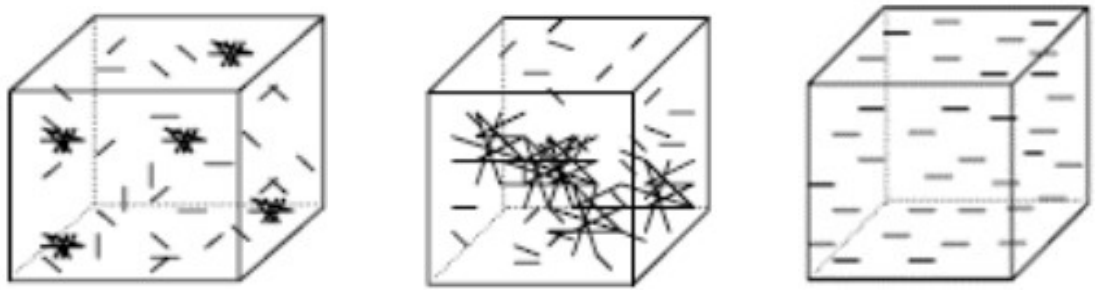

(a) (b) (c)

Figure 2.23: Fibre dispersion state; Fibre clamping (a), Fibre segregation (b) and Preferred orientation (c) [10].

In order to consider the orientation of fibres in a cracked concrete surface, several researchers have used the so-called fibre orientation factor. Among the many research works, a simple expression for estimating the fibre orientation factor with respect to a given direction of tensile stresses and thus to a given cross-section (the expected crack plane, perpendicular to the tensile stresses) was proposed by Krenchel [51]. Thus, the number of fibres (N) crossing a given section can be related to the fibre orientation factor (α), as follows:

$$N = \frac{\alpha V_f}{A_f} \tag{2.26}$$

where N is the number of fibres per unit surface, α is the fibre orientation factor, A_f is the cross-sectional area of one fibre, and V_f is the fibre volume fraction.

In relation to the structural design, the Model Code 2020 [8] and EN 1992-1-1:2023 Annex l [9], introduce an orientation factor, denoted as k_0, which adjusts both the serviceability and ultimate residual strengths by multiplying them by k_0. This factor can either reduce or increase these strength values as in Equation 2.28 and Equation 2.29. In short, the main goal is to consider within the design process the actual post-cracking behaviour exhibited by FRC belonging to a given structure by considering the actual orientation of fibres in the structure with respect to that exhibited in standard samples. In this regard, in the *fib* Model Code 2020, a factor k_0 corresponding to the ratio between the fibre orientation α_0 in the structure and the fibre orientation equal to 0.58 in the EN 14651 [7] standard specimen is introduced:

$$k_0 = \frac{\alpha_0}{0.58} \tag{2.27}$$

In the equations in Model Code 2020 [8] referred in this thesis Equation 2.28 and Equation 2.29, the values $f_{Fts,ef}$ and $f_{Ftu,ef}$ represent represent the residual tensile strength values identified by bending test according to EN 14651 [7] and corrected taking into account the manufacturing method and the concrete workability:

$$f_{Fts,ef} = k_0 f_{Fts} \tag{2.28}$$

$$f_{Fts,ef} = k_0 f_{Ftu} \tag{2.29}$$

For favourable effects, an orientation factor $k_0 > 1.0$ may be applied if experimentally verified. A maximum value of 1.5 may be assumed. When $k_0 > 1.0$ is applied in one direction, the k_0 in the orthogonal direction $k_{0,\perp}$ has to be considered lower than 1. For unfavourable effects, an orientation factor $k_0 < 1.0$ must be experimentally determined and applied. It is worth noticing that the orientation factor as intended by documents [8, 9], can also be considered as the ratio between the post-cracking strengths exhibited by FRC belonging to a given structure and the reference post-cracking performance (f_{Ri}), as retrieved by standard notched FRC samples tested according to EN 14651. Accordingly, in some research works [52, 53], small beam samples were saw-cut from real structures and tested to obtain the residual post-cracking strengths (f_{Ri}). The latter were compared to those obtained by standard samples cast-in-mould, the authors [52, 53] imply that these comparison can be considered as the orientation factors intended by standards, since they are experimentally determined. In these approaches, the fibre orientation factor is not estimated or measured; basically, the consequences of possible different fibre orientation are only evaluated in terms of post-cracking performance.

Table 2.3: Fibre orientation factor values provided by the models from various researchers [21].

Probabilistic Boundaries	**2-D**	**3-D**
[54, 55]	0.637	0.405
[21, 49, 56]	0.600	0.500
[57]	0.637	0.500
[58]	0.667	0.444

Due to the growing interest in developing techniques to identify the final orientation and distribution of fibres within hardened concrete, various advanced technologies have been employed. These range from expensive equipment to complex procedures and from destructive methods to post-test approaches, providing numerous ways to measure fibre positioning. The most straightforward technique involves counting the fibres on cut surfaces. After curing and testing the specimen, a grid is drawn on the sawn surface, and the fibres are counted. Afterwards, taking advantage of Equation 2.26, the fibre orientation factor (α) can be estimated for that given cut surface. It is a simple approach with less accuracy than other methods listed in Table 2.5, but it is aligned with the purpose of obtaining the orientation factor. In fact, Equation 2.26 is currently cited in the *fib* Model Code 2020 [8] for estimating α_0. This method has been utilized in this thesis. Additional methods for studying fibre orientation are presented in Table 2.5 as discussed in the paper [21].

Table 2.5: Methods to determine fibre orientation factor [21].

Method Type		**Technique**
Destructive	Indirect	Manual counting + theoretical expression
	Direct	Image analysis
		X-ray method (computerized tomography)
Non-destructive	Direct	Alternating current-impedance spectroscopy
		Translucent fluid
		Open coaxial transmission line
		Dielectric waveguide antennas
		Electrical resistivity methods
		Magnetic monitoring
		Electromagnetic and inductive methods

2.2 Sprayed Concrete

Sprayed concrete technology traces its origins and development to the early 20th century. Carl Ethan Akeley, an American taxidermist at the Field Museum of Natural History in Chicago, initially designed a device to create artificial landscapes using spray gypsum. He advanced this device around 1907 into a practical two-chamber system for applying cementitious materials. In 1911, Akeley received a patent for this device, known as the cement gun, marking the "birth" of sprayed concrete technology. Since then, shotcrete has evolved significantly, particularly in recent decades, into a high-performance construction technology that has greatly transformed underground construction [59].

Sprayed concrete, commonly referred to as shotcrete, is a type of concrete or mortar that is conveyed through a hose and pneumatically projected at high velocity onto a surface. The impact of this high-velocity application simultaneously compacts the material. Various standards describe this process similarly:

- **EN 14487-1 2022** [19]: defines sprayed concrete as concrete projected pneumatically onto a surface at high speed.
- **EFNARC** [60]: explains it as concrete conveyed through a hose and pneumatically projected at high velocity.
- **ASTM C1385 / C1385M − 10:2017** [61]: describes it as either concrete or mortar transported via hose and pneumatically applied at high speed onto a surface.
- **ACI 506R-16 Guide to Shotcrete** [62]: refers to shotcrete as mortar or concrete pneumatically projected at high velocity, often reinforced with steel rods, mesh, or fibres.
- **CSA A23.1-19** [63]: defines sprayed concrete as concrete or mortar conveyed through a hose and applied pneumatically at typically high velocity.

- **JSCE Guidelines for Concrete No.16** [64]: defines and emphasizes that the material can be applied in either wet or dry mix form and is compacted by the force of its application.

In general, sprayed concrete involves conveying the material under pressure and projecting it onto a surface at high speed, where it is compacted by the impact. Sprayed concrete is also refered to as 'shotcrete' and both terms are used in this PhD thesis.

2.2.1 Major Development in Sprayed Concrete

Major developments in sprayed concrete have significantly advanced the shotcrete industry over the decades. A major revolution occurred in the 1950s with the development of the wet-mix shotcrete process. In 1971, the Batelle Research Corporation in the United States first developed the concept of reinforcing shotcrete with discrete, discontinuous fibers [65].

Another significant milestone was achieved in 1975 in Norway, where condensed silica fume was first incorporated as a supplementary cementitious material in shotcrete mixtures [66]. This innovation brought major benefits, including enhanced adhesion and cohesion, reduced rebound and fallout in plastic shotcrete, and increased strength and durability in hardened shotcrete.

In the 1990s, the introduction of synthetic fibre-reinforced contributing to the continued evolution of sprayed concrete technology [67].

A significant advancement in shotcrete technology came in also in the 2000s with the introduction of "alkali-free" shotcrete accelerators [68]. These liquid accelerators, typically composed of aqueous solutions or suspensions of aluminum sulfate compounds, have a PH of around 3 and cause less negative impact on the compressive strength, permeability, and durability of shotcrete. They are also compatible with most hydration-controlling admixtures. Since the 1970s, Research and development have focused on creating accelerators and admixtures that provide higher early strengths with lower dosages, while maintaining the long-term strength. This also aimed to reduce dust and rebound during application. Additionally, advancements in spraying equipment

have enhanced the quality, quantity, and automation. As initial challenges were addressed, subsequent research shifted towards better understanding the durability and mechanical properties of sprayed concrete, leading to more refined design approaches and applications.

Critical to the use of sprayed concrete in underground support was the development of design methodologies that allowed engineers to replace conventional steel meshs and timber lagging-type designs or cast-in-place reinforced concrete lining designs with rock bolt and shotcrete designs. The innovation of the use of 3-D scanning survey equipment allows shotcrete lined tunnels to be constructed without lattice girders.

Spray applied waterproofing membranes (SAWMs) which are discussed in Section 2.4 and shown in Figure 2.32 allow concrete to be sprayed directly onto them, creating a bond between the primary and secondary linings. This development is linked to the advancements in sprayed concrete lining. The use of SAWMs facilitates the creation of composite action between the primary and secondary linings, leading to the development of composite tunnel lining designs, one of the most efficient tunnel lining design options, as it has been discussed in Section 2.4.1.

Finally, the use of fibre reinforced sprayed concrete for permanent tunnels, which is the key focus of this thesis, represents a major advancement resulting from the significance improvements listed above.

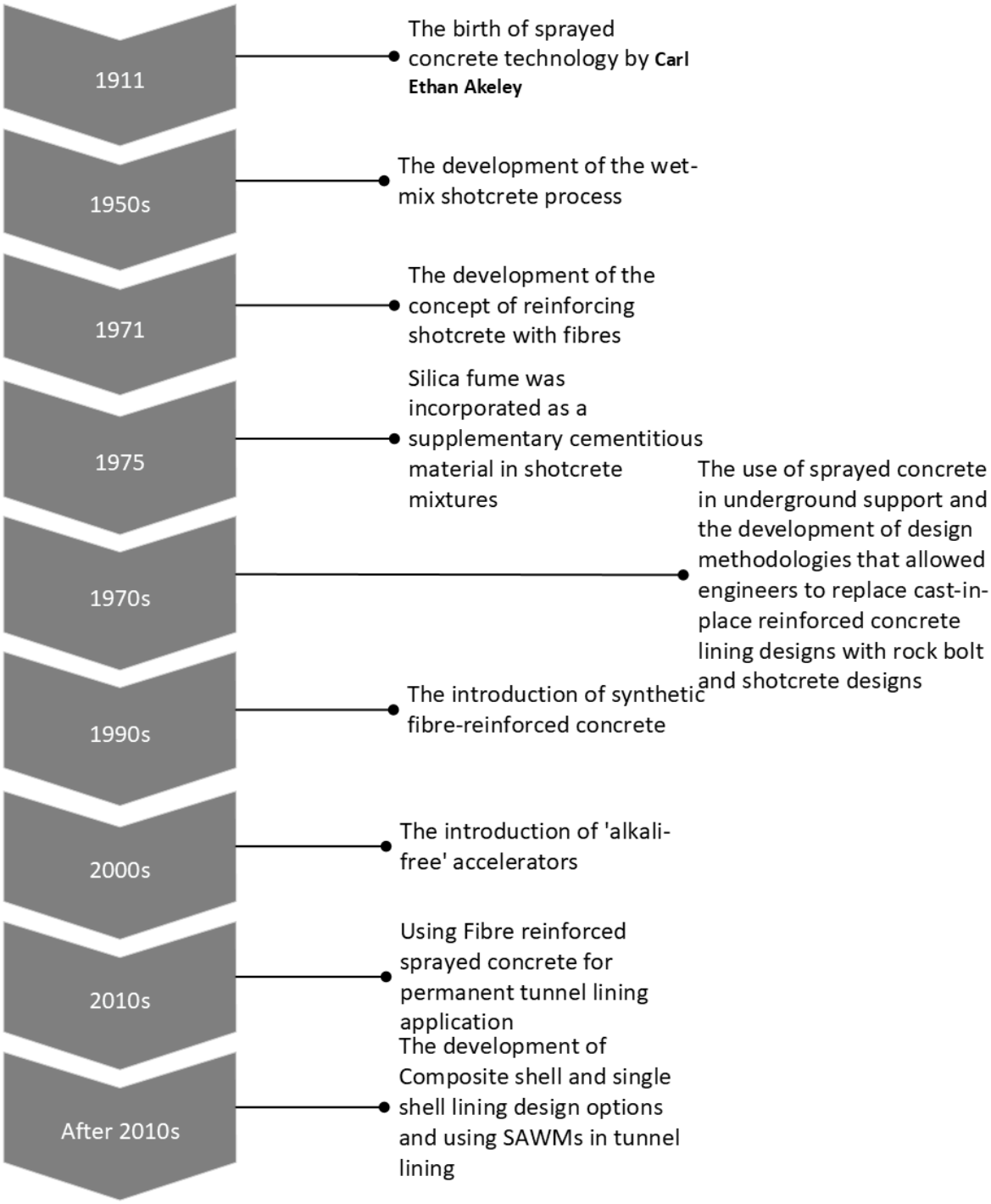

Figure 2.24: Major developments in sprayed concrete.

2.2.2 Spraying Method

Sprayed concrete is produced in two ways: the dry mix process and the wet mix process.

2.2.2.1 Dry Mix Sprayed Concrete

In this process, aggregate naturally moist or oven-dried, along with cement, and additives are transported by compressed air through a hose to a nozzle. At the nozzle, water and possibly a liquid accelerator is added to create a plastic material upon impact with the receiving surface (see Figure 2.25) [11]. The process involves five steps: first, thoroughly mixing all dry ingredients except water; second, feeding this mixture into delivery equipment; third, introducing it into the delivery hose via a metering device; forth, carrying it by compressed air to the nozzle; and finally, jetting the material at high velocity onto the target surface [11].

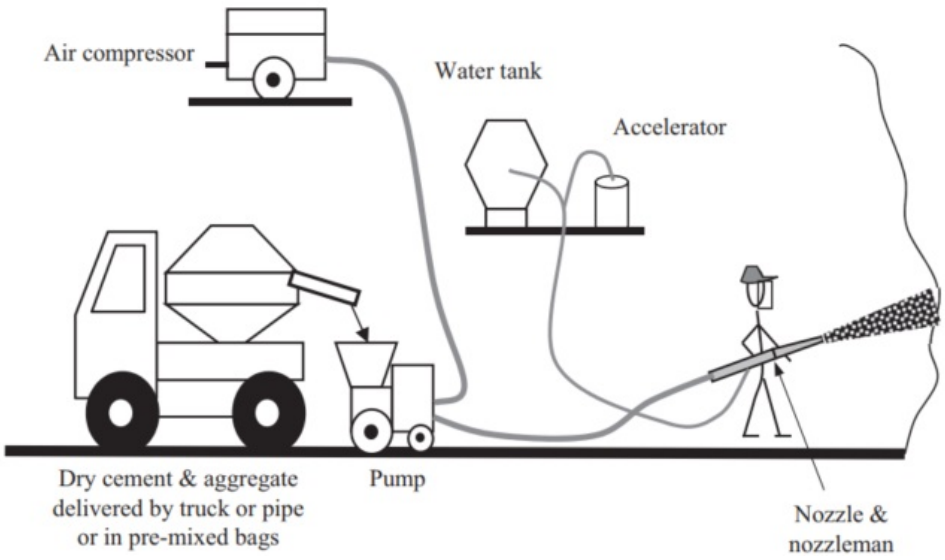

Figure 2.25: Dry mix process [11].

2.2.2.2 Wet-Mix Sprayed Concrete

Wet-mix sprayed concrete consists of cement, aggregates, water, and possibly admixtures, which are hydraulically pumped to a nozzle where compressed air is added to ensure high-velocity placement and consolidation on the target surface [11] (see Figure 2.26). The main advantage of the wet-mix method is that all ingredients are thoroughly mixed beforehand, for faster placement of larger volumes compared to the dry-mix process. This process involves five steps: fully mixing all ingredients, introducing the mixture into delivery equipment, metering it into a delivery hose, adding compressed air at the nozzle to increase velocity, and finally spraying the concrete at high velocity onto the receiving surface [11].

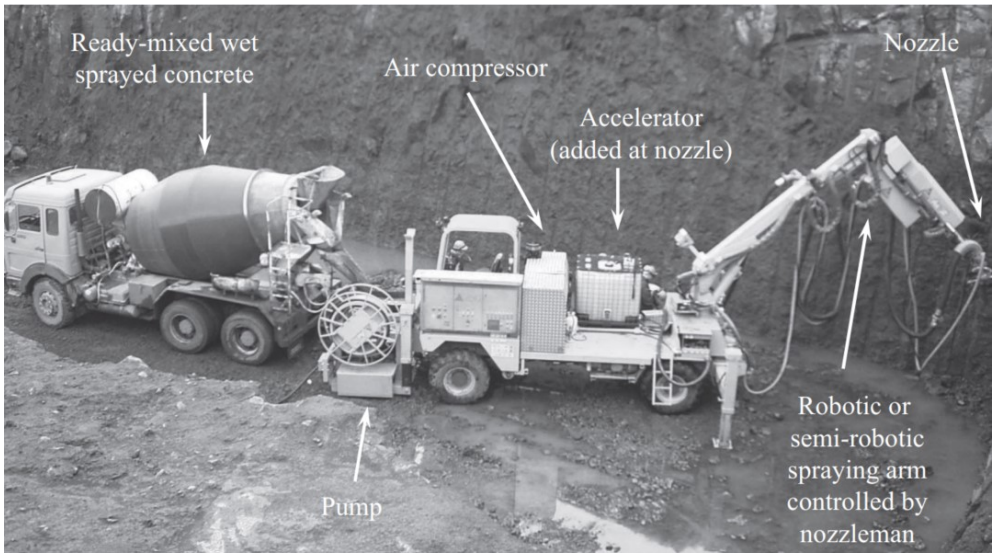

Figure 2.26: Wet mix process [11].

Table 2.7: Comparison of dry-mix and wet-mix processes.

Dry-Mix Process	**Wet-Mix Process**
Higher early age strength	Lower early age strength
Lower plant cost	Higher plant cost
Lower volume per hose size	Higher volume per hose size
Higher rebound	Lower rebound
Higher level of dust	Less dust
Variability due to nozzleman influence	Batched at a plant, fixed water–cement ratio
Three manual dry-mix sprayers match one wet-mix mechanized unit	Mechanized wet-mix spraying saves energy
More manpower required	Less manpower required
More rebound	Less rebound, reducing waste
Lower spraying output (3 m^3/hr)	Higher spraying output (18 m^3/hr)
More processing time	Time-saving process
More wear and tear	Less wear and tear

2.2.3 Mix Proportions of Sprayed Concrete

Sprayed concrete consists of water, cement and aggregate, together with various additives. Its mixture is formulated to ensure that it can be conveyed to the nozzle and sprayed with a minimum of effort, adhere effectively to the excavated surface, support its own weight as well as the ground loading as it develops and attain the strength and durability requirements for its purpose in the medium to long term [11]. The goal of mix proportioning is to reduce voids in the placed concrete by optimizing the grading of solid particles such as aggregates, cement, and mineral additives. This must be done while ensuring the concrete maintains the necessary rheological properties for effective pumping and spraying [69]. In recent decades, numerous institutions have established standards and guidelines for sprayed concrete, detailing procedures for proportioning, requirements, and recommendations. Refer to Table 2.6 for the standards and Table 2.7 for the technical guidelines. Compared to traditional cast concrete, the mix contains

more sand, a higher amount of cement, smaller aggregate particles size, and additional additives [70].

Table 2.9: Common standards related to sprayed concrete mix design.

Number	**Title**
EN 14487-1:2022	Sprayed concrete – Part 1: Definitions, specifications, and conformity
ACI 506R-16	Guide to shotcrete (Reported by ACI Committee 506)
SAS JGJ/T 372:2016	Technical specification for the application of sprayed concrete
ABNT NBR 14026:2023	Shotcrete – Specification

Table 2.11: Common technical guidelines related to sprayed concrete mix design.

Number	**Title**
EFNARC: 1996	European Specification for sprayed concrete
DIN 18, 551	Sprayed concrete - National application rules for series DIN EN 14,487 and rules for the design of sprayed concrete constructions.
OBV: 2013	Austrian Society for Construction Technology (OBV): OBV Guideline Sprayed Concrete
AFTES: 2000	AFTES recommendations for the design of sprayed concrete for underground support
NB: 2011	Sprayed Concrete for Rock Support
JSCE: 2007 (Chapter 8)	Standard specification for concrete structures

2.2.3.1 Aggregates

Most of the regulations and standards recommend maximum aggregate sizes to comply with the restraints imposed by the spraying equipment, layer thickness, and minimize the rebound. They suggest that the maximum particle size should be 1/3 to 1/5 of

the internal diameter of the spray hose and nozzle, with proposed maximum aggregate size between 8mm and 20mm [69]. In his book on sprayed concrete lined tunnels, Alun Thoma [11] recommends a maximum aggregate size of 10mm for sparyed concrete tunnel lining.

2.2.3.2 Binder

The binder type and content should be selected to meet the specified requirements for concrete pumpability, strength at early ages, durability, and proper compatibility with admixtures [69]. Commonly, sprayed concrete is produced with CEM I and CEM II Portland cement or equivalent classifications used in different regions. CEM I 52.5 R might be preferably adopted for applications where high strength at early ages is required. Although CEM I 52.5R SR a C3A content below 5%, is typically recommended for tunnel lining applications, spraying concretes with low C3A contents may present challenges in building up layers in overhead areas, particularly in cold climates [69].

Standards and guidelines set minimum requirements for cement (binder) content and sometimes recommended appropriate ranges depending on the spraying process (dry or wet), material type (mortar or concrete), target compressive strength and particular environmental exposure classification. Typically, the industry uses in spraying concrete in range between 300 kg/m^3 and 500 kg/m^3. European sprayed concrete standard EN 14487-1 [19] recommended on a minimum cement content in a basic mix shall be 300 kg/m^3. The ACI 506R-16 [62] guidelines suggest a cement content between 385 and 415 kg/m^3 for most wet applications, while early EFNARC [60] guidelines recommend a range of 400 to 500 kg/m^3 for wet spraying process. No direct correlation between cement content and f_{ck} must be assumed since the spraying process significantly influences the mechanical properties of the matrix [69].

Minerals are added in cement, the most commonly used mineral additions are fly ash, silica fume, and limestone filler. Additions of minerals effectively reduce permeability and rebound and improve the consistency and workability of fresh concrete [71–73]. The incorporation of these mineral additions is becoming more common, particularly

in tunnel lining applications. A typical mix might include 290 kg/m^3 of cement, 80 kg/m^3 of fly ash (20%) and 30 kg/m^3 of silica fume (7.5 %), totalling 400 kg/m^3 [69]. Standards and guidelines recommend limiting silica fume content between 12 and 15% of cement weight, with under 10% preferred for permanent structure. For fly ash, the maximum dosage range between 15% and 20% by cement weight.

The link between the target strength of the sprayed concrete and the cement content is not well established; this might be because the spraying process significantly influences the mechanical properties of the matrix. However, in some guidelines [74] proposes indicative cement content ranges based on the strengths required: 380–425 kg/m^3 for a target strength (f_{ck}) of 25–30 MPa, 400–450 kg/m^3 for 30–35 MPa, 425–475 kg/m^3 for 35–40 MPa, and over 450 kg/m^3 for f_{ck} exceeding 40 MPa.

2.2.3.3 Water

Ordinary water is used for sprayed concrete, and, in the same was as conventional concrete, the water–cement ratio has a large influence on the strength of the concrete. When determining the water demand of the sprayed concrete mix, the moisture content of the aggregates and water contained in admixtures should be considered. Furthermore, the water/cement or water/ binder ratio of the base mix must meet the requirements associated with the exposure classification. For the wet spraying method, w/c values reported are generally in the range between 0.35 and 0.60 [11, 69]. The lower values are usually adopted underground applications, tunnel lining applications (0.35–0.45) [11].

2.2.3.4 Accelerators

Accelerators are added to wet-mix sprayed concrete to promote rapid strength gian, enhance the maximum layer thickness and decrease the likelihood of early material fallouts. Currently, the most commonly used types of chemical accelerators are those based on alkaline aluminates and almunium sulfate or alkali-free. Alkali-free accel-

erators are the most widely used globally. In contrast, alkaline accelerators tend to significantly reduce long-term strength and pose health risks for workers [75–78]. The only drawback of the alkali-free accelerators is their slower setting time compared to the alkali one: initial set takes under 300 seconds and final set under 600 seconds, compared to alkaline accelerators, which set in under 60 seconds and 240 seconds, respectively [11]. The ideal dosage varies with spraying method, concrete mix, type and content of cement, spraying position, type of backing material, and presence of water in the substrate. Between 4 and 10% by weight of cement for alkali-free accelerators is recommended for tunnel lining application [11].

Studies have shown that sprayed concrete contains more embodied carbon per cubic meter compared to cast concrete because of its higher cement content. However, the overall carbon footprint of a project can be reduced when using sprayed concrete for tunnels, as it requires less material [79]. Unlike conventional concrete, there is no widely recognized procedure for selecting admixtures and determining mix proportions for sprayed concrete. In this PhD thesis, mix proportions for sprayed concrete have been gathered from various case studies, research studies, and experimental investigations and summarized Table 2.13.

Table 2.13: Summary of sprayed concrete mix proportions from case studies, research, and experimental investigations.

Case Study	**Cement**	**Sand**	**Agg**	**Fly ash**	**Micro silica**	**Acce**	**Plast**	**W/C**	**W/B**	**Max Agg Size**
[-]	[kg/m³]	[kg/m³]	[kg/m³]	[kg/m³]	[kg/m³]	[%]	[l/m³]	[-]	[-]	[mm]
[79]	425	-	-	-	20	-	-	-	-	-
	450	1240	413	50	50	7%	2.8	-	0.38	-
	513	343	1245	-	21	-	-	-	0.44	10
	419	860	860	-	54	-	71	0.39	-	-
	480	1120	480	-	30	-	5.8	0.43	-	9
	370	1100	520	100	30	-	4.8	-	0.43	10
	443	837	844	-	-	-	2.66	0.44	-	-
	430	1080	540	107.5	30.1	6-8%	5	0.44	-	-
[14]	355	1000	536	68	27	6%	-	0.72	0.57	10
	382	1075	576	73	29	0	-	0.53	0.42	10
	355	997	535	67	27	5%	-	0.72	0.57	10
	381	1072	575	72	29	0	-	0.53	0.42	10
[80]	382	1074	576	73	29	0	-	0.53	0.42	10
[15]	480	1160	510	-	-	8%	4.5	0.4	-	10
[81]	480	1160	510	-	-	7%	3.5	0.4	-	10
[82]	450	1600	-	-	-	5.50%	2.52	0.45	-	8
[83]	450	-	1595	-	-	4.5%	5.8	0.44	-	8
	450	-	1583	-	-	4.5%	6.1	0.44	-	8
	450	-	1583	-	-	4.5%	6.1	0.44	-	8
	454	-	1571	-	-	4.5%	6.1	0.44	-	8

Continued on next page

(Continued from previous page)

Case Study	**Cement**	**Sand**	**Agg**	**Fly ash**	**Micro silica**	**Acce**	**Plast**	**W/C**	**W/B**	**Max Agg Size**
[-]	[kg/m^3]	[kg/m^3]	[kg/m^3]	[kg/m^3]	[kg/m^3]	[%]	[l/m^3]	[-]	[-]	[mm]
	450	-	1583	-	-	4.5%	6.1	0.44	-	8
	420	-	1610	-	10	4.8%	5.8	0.46	-	8
	420	-	1605	-	10	4.8%	5.8	0.46	-	8
	420	-	1609	-	10	4.8%	5.8	0.46	-	8
[84]	400	889	840	-	-	5.1%	0.84	0.50	-	12.5
[85]	420	1655	331	-	2.94	-	2.10	0.37	-	10
[86]	420	1955	-	-	-	-	2.1	0.37	-	10
[87]	400	1320	-	-	40	-	3	0.5	-	8
	620	1025	620	40	40	0	-	-	-	10
	500	1190	500	-	40	0	-	-	-	10
[88]	550	1075	550	-	8	0	-	-	-	10
	550	1000	550	20	30	0	-	-	-	10
	500	1075	500	-	40	0	-	-	-	10
[89]	480	-	1620	-	-	0	4	0.45	-	8
	410	930	950	0	0	-	2	-	-	20
	390	950	950	0	0	-	1.5	-	-	20
	350	670	980	120	40	-	1	-	-	20
[90]	350	670	980	120	40	-	1	-	-	20
	360	690	1030	100	0	-	0	-	-	20
	360	690	1030	100	0	-	0	-	-	20
	360	690	1030	100	0	-	0	-	-	20

Continued on next page

(Continued from previous page)

Case Study	**Cement**	**Sand**	**Agg**	**Fly ash**	**Micro silica**	**Acce**	**Plast**	**W/C**	**W/B**	**Max Agg Size**
[-]	[kg/m³]	[kg/m³]	[kg/m³]	[kg/m³]	[kg/m³]	[%]	[l/m³]	[-]	[-]	[mm]
[91]	450	1300	550	0	0	6%	4.05	0.45	-	8
[92]	385	1092	600	-	-	4%	-	-	-	10
	425	1052	600	-	-	4%	-	-	-	10
	445	1030	610	-	-	4%	-	-	-	10
	495	970	620	-	-	4%	-	-	-	10
[93]	292	857	1052	125	-	-	-	0.57	-	-
[94]	410	1284	544	-	-	6.5%	4.62	0.50	-	8
[95]	500	489	1141	-	-	-	5	0.41	-	8
[43]	426	985	868	-	-	3.5%	-	0.43	-	9.5
[96]	396	874	840	-	34	-	-	0.52	-	-
[97]	400	1030	690	-	-	4%	3.2	0.48	-	12
[98]	430	365	1097	-	35	0	-	0.64	0.59	5
[99]	440	1281	548	-	-	4%	6.5	0.45	-	8
[100]	475	110	450	60	15	4%	-	0.48	0.42	9.5
	650	1310	0	0	0	0%	-	0.55	-	9.5

2.2.4 Mechanical Properties of Fibre-reinforced Sprayed Concrete

Compressive strength is a key performance indicator of sprayed fibre reinforced concrete, similar to its role in conventional fibre-reinforced concrete, as discussed in Section 2.1. According to the specification for sprayed concrete, EN 14487-1 [19], performance requirements include compressive strength. A persistent misunderstanding exists within both the research

and practitioner communities regarding the effects of the spraying process which do not occur in conventional FRC and can lead to a reduction in compressive strength. In addition, another misconception concerns the direct application of strength-development relationships established for conventional cast concrete when evaluating sprayed concrete.

Eurocode 2 (EN 1992.1.1:2004) [101], provides a widely used strength-development equation (2.30) originally developed for cast concrete. The applicability of this equation to sprayed concrete remains a subject of investigation.

$$f_{cm}(t) = \beta_{cc}(t) f_{cm} \tag{2.30}$$

$$\beta_{cc}(t) = \exp\left\{ s \left[1 - \left(\frac{28}{t} \right)^{\frac{1}{2}} \right] \right\} \tag{2.31}$$

f_{cm} Mean compressive strength at 28 days.
$\beta_{cc}(t)$ Coefficient depending on the age of the concrete t.
t Age of the concrete in days.
s Coefficient depending on the type of cement.

The modulus of elasticity is one of the fundamental parameters for the mechanical properties for sprayed fibre reinforced concrete, similar to its significance in conventional FRC, typically measured through the test of specimens subjected to uniaxial compressive loading, as discussed in 2.1.2. The equations available in the literature, including those in the Model Code 2020 [8] and Eurocode 2 [9], do not account for the distinct characteristics of sprayed concrete compared to conventional concrete. According to the experimental study [102], the predictions performed with the Model Code 2020 [8] and Eurocode 2 [9] lead to an overestimation of the modulus of elasticity of the sprayed concrete 24.22 % and 37.56 % respectively.

$$E_{cm,j} = 9.5 \cdot \sqrt[3]{f_{cm,j}} \tag{2.32}$$

$$E_{cm}(t) = \left(\frac{f_{cm}(t)}{f_{cm}} \right)^{0.3} E_{cm} \tag{2.33}$$

$$E_{cm} = E_{co} \cdot \alpha_E \cdot \left(\frac{f_{cm}}{10}\right)^{\frac{1}{3}} \tag{2.34}$$

$$E_{cm,j} = \sqrt{\exp\left\{s \cdot \left[1 - \left(\frac{28}{t}\right)^{0.5}\right]\right\}} \cdot E_{cm} \tag{2.35}$$

2.2.5 Fibre Content and Fibre Rebound

The post-cracking mechanical performance of fibre-reinforced sprayed concrete is primarily affected by the quantity, distribution, and orientation of the fibres, which are parameters that are influenced by the specific application technique, as discussed in detail in Section 2.2 of this thesis. Due to the relatively high impact velocity, the fibres do not fully adhere to the target surface, resulting in a significant quantity of fibres rebound. Note that the final fibre content of the in-place material is usually different from the initial fibre content. The rebound behaviour of macro-synthetic and steel fibres differs. In the experimental study by [103], the rebound of fibres of 25 to 44% was observed, the lowest rebound was found for macro-synthetic fibres. Another experimental study on fibre-reinforced sprayed concrete [104] reported fibre losses of 24% for steel fibres. According to the book Sprayed Concrete Lined Tunnel by Alun Thomas [11], the typical rebound for the sprayed process with wet mixture is around 16%. However, two additional experimental studies [15], [81] observed a fibre rebound 39-44%, which differ significantly from the results of two studies and the reference book mentioned.

Table 2.14: Fibre rebound percentages from various studies.

Studies	Fibre rebound percentage [%]
[103]	25-44
[104]	24
[11]	16
[15], [81]	39-44
[105]	12

2.3 Fibre Reinforced Sprayed Concrete in Tunnelling

Fibre-reinforced sprayed concrete (FRSC) is shotcrete containing dispersed, randomly oriented fibres. These fibres are incorporated into sprayed concrete almost for the same reasons they are used in conventional fibre-reinforced concrete which is discussed in detail Section 2.1. The main purpose is to offer reinforcement post cracking resistance, bridging tensile cracks, which helps to control the width of these cracks and adds durability to the material that would otherwise be brittle, and impact resistance. And one of the main reasons for including fibres in many ground support applications is to provide toughness [106]. Fibre reinforced sprayed concrete (FRSC) can be used in most situations where a sprayed concrete lining can be applied. This covers all types of ground conditions from soft ground to hard rock.

2.3.1 Fibre Reinforced Sprayed Concrete in Soft Ground Tunnelling

Soft ground tunnels generally are defined as those in which the ground may be excavated or dug by conventional means, as opposed to rock tunnels, soft ground tunnels require more or less immediate support to maintain the opening, when unsupported it has a stand-up time of less than a few hours [107].

Shotcrete is used in soft ground tunnelling primarily for two purposes, one is to provide a structural arch inside the tunnel to support the natural arch of the substrate. The other one is to seal the exposed ground surface immediately after excavation to protect the ground from the elements to avoid deterioration of the structural properties due to ravelling.

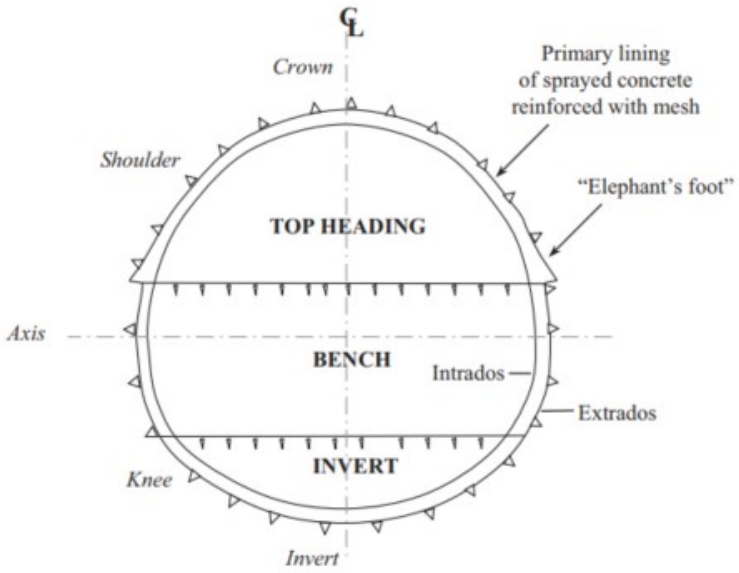

Figure 2.27: Cross-section of an SCL tunnel in soft ground [11].

2.3.2 Fibre Reinforced Sprayed Concrete in Hard Ground Tunnelling

Hard rock covers to strong, continuous rock mass with widely spaced joints, typically having strength above 50 MPa and a stress-strength ratio below one. Though block failure and plastic deformation can occur, the rock generally deforms elastically to tunnel excavation, with unsupported stand-up time lasting ranges days to years [11]. In rock tunnels, sprayed concrete often works in concert with rock bolts to support the rock. The structural behaviour of an excavated rock mass is difficult to predict due to the many uncertainties, such as the quality and orientation of the joints in the rock mass. The role of sprayed concrete is primarily to support isolated blocks, rather than the rock mass as a whole, the rock itself is often stronger than the sprayed concrete. Therefore, designing a suitable rock support is a complicated task. For these reasons, the design is often based on a combination of empirical methods and numerical analysis, and many countries have also developed individual strategies and empirical knowledge for the structural design of rock support [95]. Sprayed concrete is used in hard rock tunneling primarily for two purposes, one is to bridge the gap between rock bolts by building local arches from bolt to bolt. These arches are collecting the load locally and transferring it to the rock bolts. The second one is to seal of the exposed rock surface after excavation to protect it from the elements to avoid deterioration of the structural properties due to traveling of disturbed or weathered rock.

Note that for design options such as composite shell lining and single shell lining, which are discussed in detail in Section 2.4.1, fibre-reinforced sprayed concrete can be used without rock bolts or lattice girders, as the fibre sprayed concrete alone form a structural lining ring.

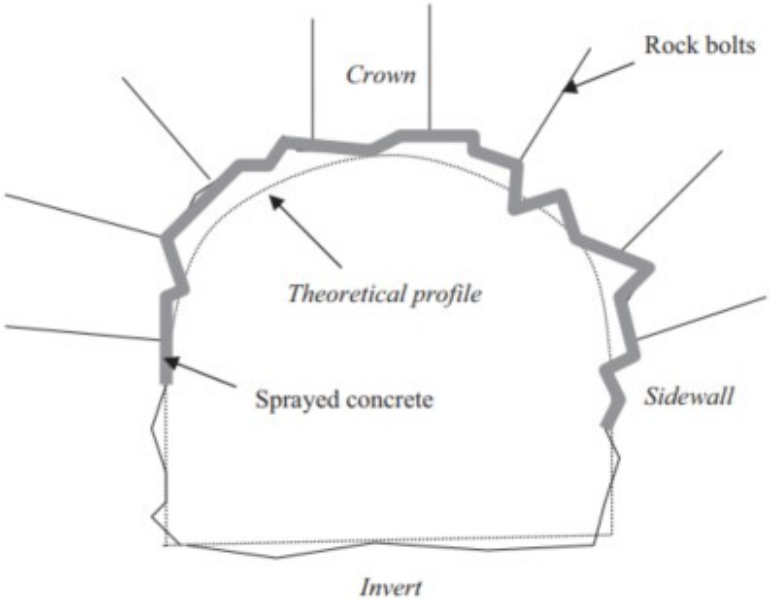

Figure 2.28: Cross-section of an SCL tunnel in hard rock tunneling sprayed concrete with rock bolts [11].

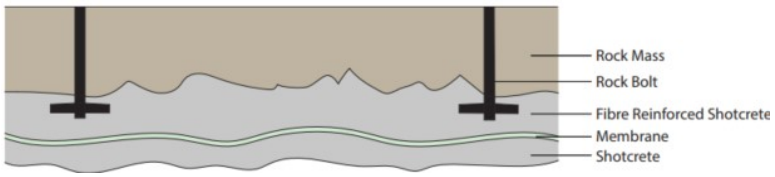

Figure 2.29: Sprayed concrete lining cross-section in hard rock tunneling [12].

2.3.3 Behaviour of Fibre Reinforced Sprayed Concrete Tunnel Linings

The behaviour of fibre-reinforced sprayed concrete (FRSC) linings is influenced by factors such as the age of the lining, the design's geometric characteristics, the ductility of the sprayed fiber-concrete mix, and the interaction with the surrounding ground [106]. As described in detail in Section 2.3.2, FRSC primarily supports hard ground by restraining its surface, stopping it from gradually deteriorating. In soft ground, it typically functions as a supporting arch as described in Section 2.3.1. The following sections discuss the behaviour of FRSC linings during early and matured stages under both hard and soft ground tunneling conditions.

2.3.3.1 Behaviour of Sprayed Fibre-Reinforced Concrete Lining at Early Age

The effect of fibres is significant in increasing of ductility of sprayed concrete lining right after placing, in spite of poor bond between fibres and hardening cement paste in young FRSC [108]. Bond strength development between an FRS lining and the underlying substrate progresses slowly from a non-zero starting point to a maximum value of no more than 0.2 MPa at 24 hours [109]. The capacity of an FRS lining to stabilize the ground in the early stages in the initial 24 hours depends on various factors, including the following.

The bond effect is crucial, as the early performance of FRSC relies on establishing a strong bond with the ground and developing strength in the freshly applied lining. Fibres do not influence bond strength at either early or later stages. In hard rock settings, the initial bond between the sprayed concrete and the substrate is typically influenced by the quality of the ground preparation. In certain types of soft ground, like sandy layers, it can be very challenging for sprayed concrete to adhere properly, as failures within these layers can cause sections to fall out.

The Strength effect is another important factor. The effectiveness of an early age lining in stabilizing the ground is highly dependent on the rapid development of compressive and shear strength within the initial hours [109]. Fibres offer minimal enhancement to the residual strength or energy absorption of sprayed concrete in its early stages [88].

The lining thickness effect is also significant, Fibre reinforced sprayed concrete linings in soft ground specially for permanent tunnel lining tend to be more than 200 mm thick so the sprayed concrete lining must be built up in several passes. Each layer must gain enough strength to support its own weight as well as any ground loading before the next layer is applied.

The ground conditions effect cannot be overlooked. Ground stresses from large-scale instability or squeezing conditions, inherent ground weakness, or excessive moisture from water ingress can make it extremely challenging for a newly sprayed lining to remain in place during hydration.

Finally, the load transfer effect is key. The main method for load transfer between the ground and the lining, particularly in soft ground, is the bond and ground pressure between the sprayed concrete and the ground. In rock tunnels, the load transfer between the bolts and the sprayed concrete lining is a crucial aspect of ground support design.

2.3.3.2 Hardened Reinforced Sprayed Concrete Lining Behaviour

As the sprayed concrete matrix hydrates, several changes in behaviour occur. The compressive strength increases rapidly. The shear resistance increases dramatically, thereby reducing the likelihood of shear failure. The bond to the rock also increases, but not at a dramatic rate. Most importantly, the fibres become more effective due to increased friction between each fibre and the concrete matrix during pullout. This last phenomenon has the effect of increasing post-crack performance in tension.

The impact of these changes on the behavior of an FRSC lining is evident in various aspects.

In terms of compressive capacity, the compressive strength of the sprayed concrete improves with time as the lining matures, and this increase is largely independent of the presence of fibres. The load resistance of the lining in compression grows significantly in the initial days after spraying, which is beneficial in cases of significant convergence or short stand-up times, as this enhanced support can facilitate compressive arching in the ground. In soft ground conditions, the lining frequently depends on quickly developing compressive strength to provide support, as the loads can increase rapidly as the tunnel progresses.

Regarding shear capacity, as FRSC ages, its shear resistance increases significantly. Load redistribution around shearing zones is inadequate because of the limited alternative load paths, so fibres are not an effective method for enhancing the shear resistance of a lining. Opportunely, concrete has significant shear resistance, particularly when a compressive membrane stress is applied, making shear failures uncommon in mature FRSC linings.

In terms of toughness, the fibres' post-cracking load-bearing capacity aids in redistributing load around unstable ground areas, while also restraining ground movement, thus enabling the ground to support itself more effectively. Fibres also help prevent fragments from falling out of a sprayed concrete lining if extensive cracking occurs. Bolts serve as the primary method of global ground support in underground hard rock excavations, while thin-walled FRSC linings in hard rock are designed to provide support between the bolts. Thus, most FRSC linings in hard rock should be regarded as providing only local ground support. But recently, thick, hard rock tunnels lined with permanently sprayed concrete, without anchor bolts, act as global ground support around an excavation. Some permanently sprayed hard rock tunnels are referred to in Table 2.19. In soft ground, where linings are sprayed as thick arches of suitable geometry, sprayed concrete can be considered to act as global ground support around an excavation.

Finally ground Interaction, the bond between the ground and the sprayed concrete and its progressively stiffer support offers an excellent form of support to both soft ground and hard rock.

2.3.4 Types of Fibres Used in Sprayed Concrete Lining

Fibres in sprayed concrete are generally classified by their material and size. They fall into two size-based categories: microfibers and macrofibre's. For structural purposes in sprayed concrete, steel and synthetic macrofibres are the most commonly utilized. Non-structural micro-synthetic fibres are typically used to control plastic shrinkage cracking, decrease rebound, and lessen the risk of spalling when sprayed concrete is exposed to high-intensity hydrocarbon-fuelled fires.

The maximum effectiveness of fibre reinforcement is constrained by several factors: the tensile strength of individual fibres, the bond between the fibres and the concrete, the dosage rate of fibres, the aspect ratio [67].

2.3.4.1 Steel Fibre

The mechanical properties have already been discussed in Section 2.1.1.1. This subsection focuses only on aspects of steel fibre relevant to sprayed concrete linings. The advantages of using steel fibres for concrete modification in tunnel lining are primarily evident in several ways: (1) enhancing the ductility, toughness, flexural strength, and shear strength of cementitious materials [110]; (2) absorbing energy, bridging cracks, transmitting loads, and preventing crack propagation and integration under external loads steel fibre reinforced concrete elements ; (3) improving fatigue, impact, and explosion resistance [111]; and (4) providing notable benefits in tunnel linings, such as higher early strength, lower rebound rates, and easier construction [112].

Steel fibres used in sprayed concrete typically range between 18 to 36 mm length and from 0.4 to 0.8 mm in equivalent diameter [113]. EN 14489-1 [114] and ASTM A820/A820M-22 [115] are the European and American standards, respectively, that specify the requirements for steel fibres used in concrete.

2.3.4.2 Macro-synthetic Fibre

Macro synthetic fibre is the standard solution for initial linings in the USA and Europe, and have been used for permanent tunnel linings in recent tunnel construction in Europe and other parts of the world. Macrosynthetic fibre used in shotcrete are generally between 40 to 65 mm in length, with equivalent diameters similar to those of the steel fibres [113]. EN 14489-2 [116] and ASTM D7508/D7508M [117], European and American standards for the Macro-synthetic fibre confirmation used in concrete respectively. Because of their flexibility, macro synthetic fibres are easier to handle, pump, and apply than steel fibres, as they are less likely to cause blockages and reduce wear on slick lines [118] . The tensile strength and the young's modulus are typically around 300 to 700 MPa and 5 to 14 GPa, respectively [103]. The physical characteristics of various macro synthetic fibers on the market differ widely. For tunnel applications, it is recommended to use only advanced macro synthetic fibers that have a tensile strength exceeding 600 MPa and a Young's modulus above 10 GPa [118].

Typical dosages for shotcrete used in primary ground support and initial tunnel linings range from 3 to 6 kg/m^3. For permanent sprayed tunnel linings, dosages generally range from 5 to 9 kg/m^3, according to the case studies collected in the Table 2.19.

Figure 2.30: Various types of macro-synthetic fibres (images sourced from manufacturer's data sheets).

2.3.4.3 Micro-synthetic Fibre

Microfibres are defined as fibres with an equivalent diameter less than 0.3mm for use in shotcrete and are normally polyolefin-based [113]. To address explosive spalling during fires by melting and creating void space, polypropylene microfibers should be used, with diameters less than 33 µm and lengths equal to or shorter than 12 mm, though they can range from 6 to 50 mm. Additionally, micro synthetic fibers are included to reduce plastic shrinkage cracks.

Figure 2.31: Micro-synthetic fibres (images sourced from manufacturer's data sheets).

2.4 Sprayed Fibre-Reinforced Concrete for Permanent Tunnel Linings

There are three types of sprayed concrete systems used in tunnelling or underground construction. Type 1 is used as a protective coating, functioning similarly to cement by binding ground particles or rock fragments together and preventing the ground from breaking apart. This type is typically applied in very thin layers, about a few millimetres in depth, and is not designed to bear any load [119]. Type 2 is a sprayed concrete system used as a structural layer. It functions as a composite structure that integrates reinforced ground with a sprayed concrete layer. This system supports the ground, maintains cohesion over a limited depth of several decimetres, and serves as a link between support elements such as rock bolts. It primarily handles shear forces and is reinforced with welded wire mesh or fibres [119]. Type 3 is a sprayed concrete system used as a structural ring, engineered to withstand normal forces and bending moments. These modes are not mutually exclusive or strictly defined. For instance, sprayed concrete intended as a structural layer may initially serve as a protective layer, while a structural layer can also function locally as a structural ring, offering some confining pressure [119]. When sprayed concrete

is used in either the second and the third type systems as permanent or designed to last equal to the design life of the underground structure or tunnel, the sprayed material is considered a permanent material.

Sprayed concrete lining tunnels are typically constructed by excavating the ground in short advances and progressively applying sprayed concrete to support the ground both temporarily and permanently [120], [121]. Permanent sprayed concrete lining is made of the same materials and applied in the same way as temporary sprayed concrete lining. In contrast to temporary sprayed concrete, permanent sprayed concrete must have the same service life as the tunnel or underground facility to which it is applied. Several advances have made the use of Sprayed concrete lining as a permanent structure possible: The shift in producing SCL from the dry-mix process to a wet-mix process, The adoption of alkali-free accelerators, The use of fibre reinforcement instead of mesh reinforcement eliminated the concern of "shadows", shortened construction programme and saved overall cost, The shift from hand spraying to robotic spraying speeded up progress and produced less material waste, The use of real-time surveying with total stations instead of lattice girders to ensure the correct profile of the tunnel excavation and control the lining thickness has accelerated construction and also removed a key durability concern [121].

Advancements in materials, equipment, testing, and quality assurance have made sprayed concrete a cost-effective alternative that matches the durability of conventional concrete. Compared to traditional lining methods, fibre-reinforced sprayed concrete can offer reduced capital and operational expenses, as well as a lower carbon footprint [79].

Permanent sprayed concrete, in conjunction with spray-applied waterproofing membranes, allows for the enhancement of tunnel size and shape beyond what traditional SCL methods offer [13]. When sheet membranes are used, it is assumed that there is no bonding across the waterproof membranes installed between the tunnel's primary and secondary linings. Additionally, any structural contribution of the primary lining is disregarded in the design of the secondary lining [122]. Spray-applied membranes enable partial bonding between the two linings, leading to a composite effect. Presumed stresses at the membrane-spraying interface sandwiched between the spray in Figure 2.32, the primary and secondary linings are displayed. The structural advantage of the primary lining is now recognized due to the composite action, which allows designers to consider the primary and secondary linings as a unified composite structure. The composite action creates the opportunity to reduce the thickness of the secondary lining, which can lead to a thinner overall lining thickness [123]. The primary factor

influencing the lining's performance is the long-term bond strength between the membrane and the shotcrete layers. However, there are no standard test results available to predict the lining's behaviour over time. All the available sprayed lining design options have been discussed in Section 2.4.1.

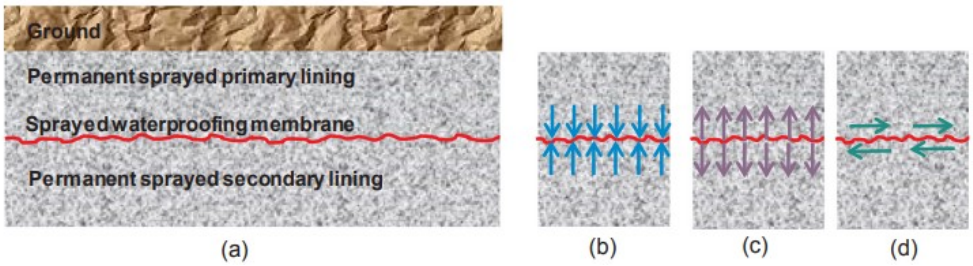

Figure 2.32: (a) Sprayed membrane interface and potential stresses: (b) Compression, (c) Tension and (d) Shear [13].

2.4.1 Types of Sprayed Concrete Tunnel Linings

The sprayed concrete linings can be broadly categorized into three types: Double shell linings (DSL), Composite shell linings and Single shell linings [11], [124].

2.4.1.1 Double Shell Linings (DSL)

Initially when using sprayed concrete linings, the primary lining was regarded as temporary due to worries about the long-term effects of some of the additives and the overall quality of the lining such as the embedding of steel mesh and arches in the concrete. A secondary lining was installed inside the primary lining to handle all permanent loads. However, the two issues mentioned above have been resolved with the availability of non-alkaline materials and advanced tunnel lining construction methods. This approach is still commonly used and is still referred to as a 'two-pass lining' or a double shell lining (DSL). In this method, a sacrificial primary lining is assumed to handle temporary loads from ground load (GL) and hydrostatic load (WL), while the secondary lining is designed to bear long-term water load (WL) and ground load (GL), [11, 13, 122, 124] as shown in Figure 2.33. Since the primary lining is treated as temporary, the secondary lining is engineered to support both long-term hydrostatic and ground loads, making it considerably thicker than other sprayed-concrete tunnel linings, despite having a robust design.

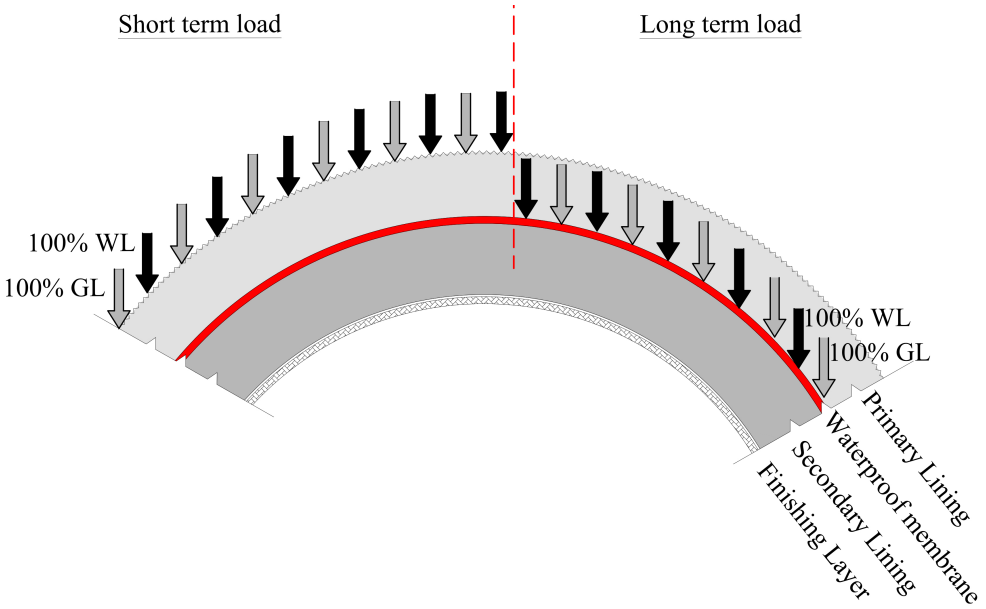

Figure 2.33: Typical Cross-section and loading configuration of a double shell lining.

2.4.1.2 Composite Shell Lining (CSL)

The use of sprayed waterproof membranes have given engineers an opportunity to explore the benefits of a composite shell lining, which includes a sprayed permanent primary lining, a sprayed waterproof membrane, and a sprayed secondary lining [11, 13, 122, 124]. Using sprayed applied waterproofing membranes between the linings create the potential for load sharing between the primary and secondary linings. Whether or not these benefits can be realised depends heavily on the design approaches. Early projects assumed zero bond in both shear and tension at the membrane such as the Crossrail project in London, UK [125]. In this setup, the primary lining works in concert with the secondary lining, sharing some of the long-term ground loads, as illustrated in Figure 2.34. This design methodology has resulted in some reductions to the thickness of secondary lining when compared to conventional Double Shell Lining.

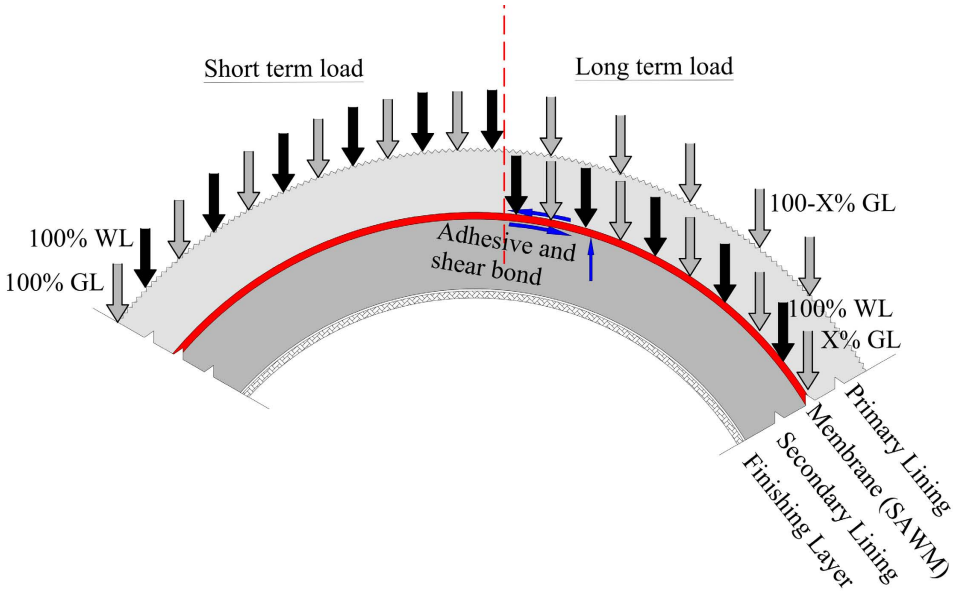

Figure 2.34: Typical cross-section and loading configuration of a composite shell lining.

By now in some studies have accepted that there is sufficient test data for some (Spray Applied Water Proofing Membrane) SAWMs to include meaningful values of bond at the interface of the membrane. Given that the bond and the membrane itself has finite properties which are lower than the concrete linings, the composite action is less than the ideal case. The effectiveness of a full composite lining, full transfer of shear, and bond strength at the interface of the spray-applied waterproofing membrane between the primary and secondary lining is still not confirmed. Research and testing are in progress to demonstrate the effectiveness of a fully composite lining, as refer in Figure 2.35. Still the meaningful bond reduce the thickness of the lining, if the composite action and the bond work fully, it may be possible to further reduce the thickness of the secondary lining.

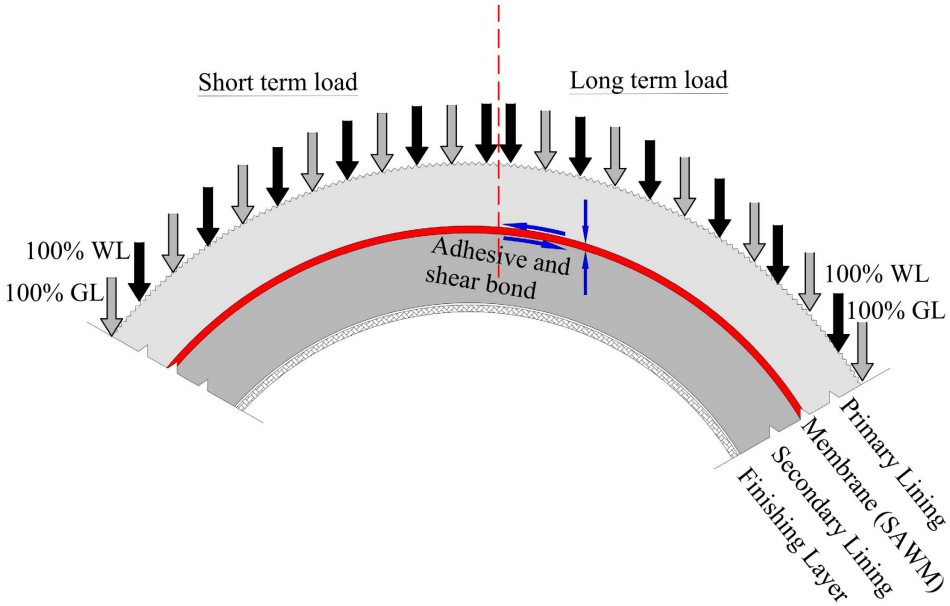

Figure 2.35: Typical cross-section and loading configuration of a fully composite shell lining.

The paper [22] discusses a modified composite shell lining, specifically designed for soft ground tunnelling. The proposal suggests that, in structural terms, the primary lining would work in conjunction with the bonded membrane. The secondary lining, positioned inside, would then becomes a non-structural element with a various potential function such as fire protection for the membrane, enhancing aesthetics, and supporting small fixing loads (see Figure 2.36) [22].

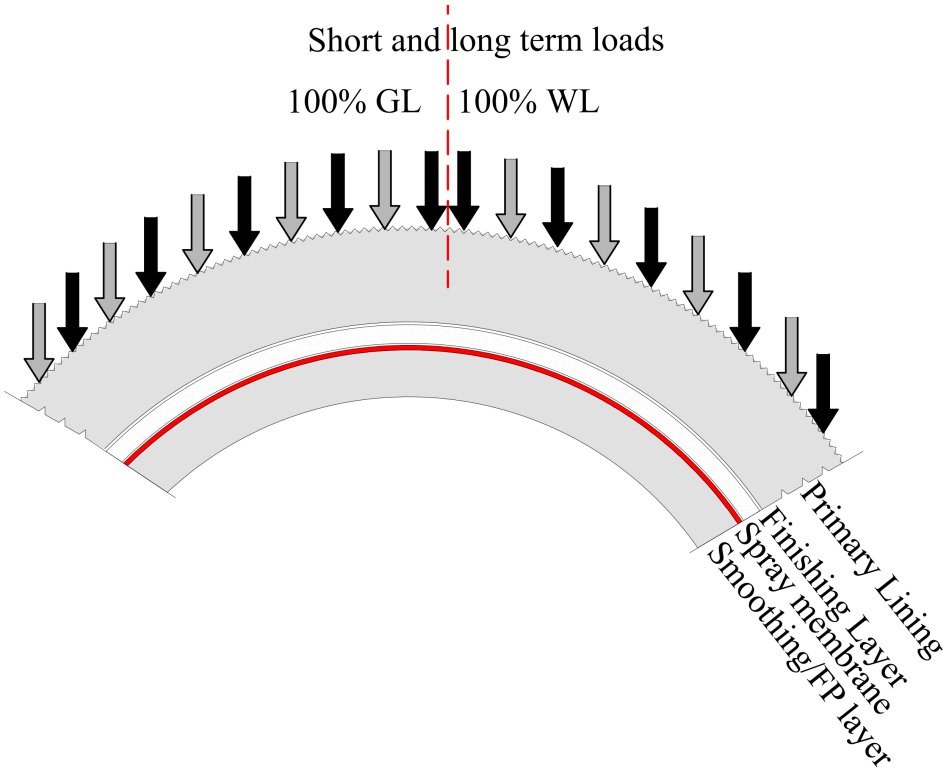

Figure 2.36: Typical cross-section and loading configuration of a modified composite shell lining (secondary lining non-structural).

Table 2.15: Comparison of modified composite shell lining vs composite shell lining (Crossrail tunnel) for a typical 10 m soft ground SCL [22]

Layers for PSCL	**Modified-composite shell lining**	**Composite shell lining (Crossrail)**
Sealing layer [mm]	50	75
Primary layer [mm]	325	325
Regulating layer [mm]	40	40
Membrane [mm]	4	4
Secondary layer [mm]	0	300
Fire protection layer [mm]	75	50
Total thickness [mm]	494	794

2.4.1.3 Single Shell Lining (SSL)

In fact, the "single shell" may consist of several layers of sprayed concrete, placed at different times. However, the underlying principle is that all the sprayed concrete carries load over the life of the tunnel, and the different layers normally act together as a composite structure. This approach is common in certain sectors – notably on hydroelectric power projects – and in certain ground conditions – such as dry hard rock. A single shell lining is installed as the excavation progresses, serving as both the initial support to stabilize the ground and as part of the final lining structure. Consequently, the quality of the installed lining material must be superior compared to the primary lining used in a double-shell lining system [70]. Single-shell linings are the most effective lining design (in dry or mostly dry ground) because they can withstand both short-term and long-term loads, and their construction takes much less time than that of double-shell or composite linings, which require separate stages for the primary and secondary linings [11, 122, 124].

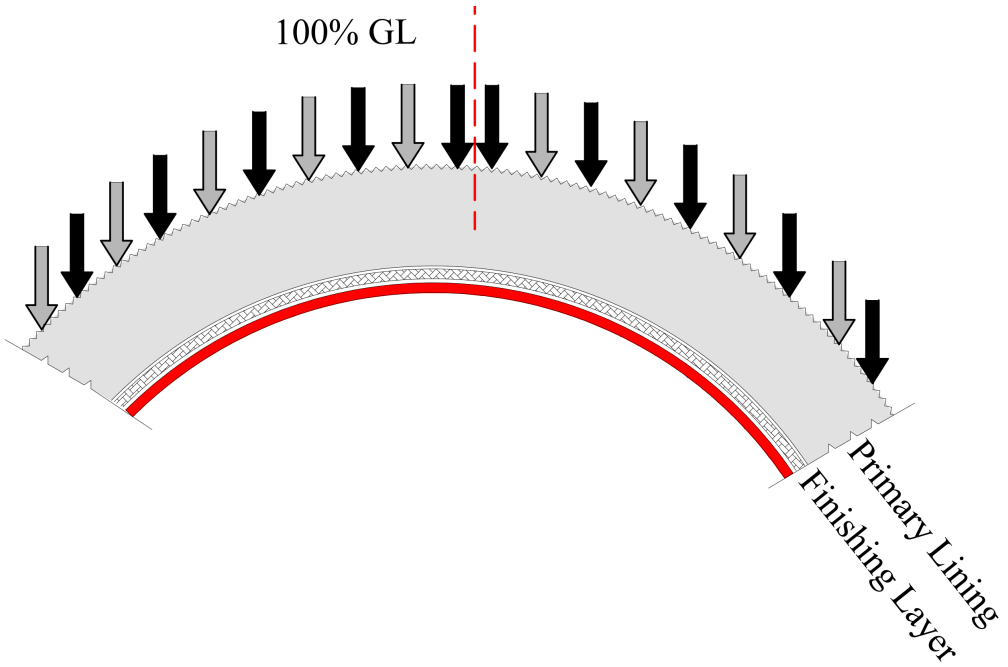

Figure 2.37: Typical cross-section and loading configuration of a single shell lining.

Table 2.17: Comparison of different types of lining systems [11]

Types of Lining	**Primary Lining**		**WP**	**Secondary Lining**	
	Type	**Existence**		**Type**	**Existence**
Double shell lining	SCL	Temporary	Sheet	Cast	Permanent
Partial composite shell lining	SCL	Permanent	Sprayed	SCL	Permanent
Full composite shell lining	SCL	Permanent	Sprayed	SCL	Permanent
Single shell lining	SCL	Permanent	None	-	-

2.4.2 Case Studies on Permanent Fibre-Reinforced Sprayed Concrete Linings

Over the last 30 years, fibre-reinforced sprayed concrete has been extensively used for tunnel lining applications. In this thesis, various case studies and research papers focusing on the application of fibre-reinforced sprayed concrete in tunnelling industry have been reviewed. Relevant data on materials and parameters were collected from these sources. The key materials and parameters analysed in the case studies and literature reviews include: data on material composition, thickness of the lining, type of fibre utilized, fibre dosage used, size and diameter of fibres (aspect ratio), tensile strength of fibres, and concrete strength. A summary of this information is presented in Table 2.19.

Table 2.19: Fibre-reinforced sprayed concrete tunnel lining experiences.

Case Studies [-]	Year [-]	Country [-]	Function [-]	Internal span [m]	Design option [-]	Ground [-]	Lining [-]	Lining thickness [m]	f_{ck} [MPa]	Fibre type [-]	Aspect ratio ($\frac{L_f}{\phi_f}$) [-]	Fibre Content [kg/m3]
[126]	2016	Pakistan	Hydropower	10	DSL	Rock-soil	SL	0.3	30	SF	64	40
[127]	2008	USA	Road	10	DSL	Soil	SL	0.35	38	SF	-	40
[128]	2000	Canada	Hydropower	6.7	SSL	Rock	PL	0.08-0.1	40	SF	60	57
[125]	2011	UK	Road	10	CSL	Soil	PL SL	0.325 0.3	32 32	SF SF	- -	45 45
[129]	2009	UK	Road	11.6	CSL	Rock	PL	0.2-0.3	32	SF	-	45
[130]	2004	Slovenia	Road	10	DSL	Rock	SL	0.2	20	SF	40	32
[131]	-	Luxembourg	Road	4	-	-	TPL	0.18	-	SF	47	40
[132]	2016	Chile	Road	-	SSL	Rock	PL	0.15	35	SF	64	35
[132]	2016	Chile	Road	-	SSL	Rock	PL	0.15	35	MSF	74	6
[133]	2012	Brazil	Mining	-	SSL	Rock	TPL	0.08	48	SF	70	25
[134]	2016	California	Road	-	-	Rock	TPL	-	20	MSF	60	6
[135]	2016	Canada	Service	5.5	-	Rock	PL	-	35	MSF	-	7

Continued on next page

Continued from previous page

Case Studies [-]	Year [-]	Country [-]	Function [-]	Internal span [m]	Design option [-]	Ground [-]	Lining [-]	Lining thickness [m]	f_{ck} [MPa]	Fibre type [-]	Aspect ratio ($\frac{L_f}{\phi_f}$) [-]	Fibre Content [kg/m3]
[136]	2003	USA	Road	5	DSL	Soil	SL	0.3	35	SF	-	40
[79]	1999	Switzerland	Road	7.6	DSL	Rock	SL	0.1-0.15	35	SF	-	47.5
[79]	2009	Norway	Railway	-	CSL	Soil	SL PL	0.06 0.07-0.1	- -	MSF MSF	- -	6 6
[137]	2015	Australia	Road	9	SSL	Rock	PL	0.25	40	MSF	60	6
[138]	2018	Chile	Service	8.05-8.40	SSL	Rock	PL	0.1-0.40	30	MSF	-	5
[79]	2020	Australia	Road	16.5-19	CSL	Rock	SL PL	0.2-0.3 0.3-0.35	40 40	SF SF	- -	40 37.5
[139]	2016	Czech	Road	-	SSL	Rock	PL	0.15-0.25	20	SF	-	35
[140]	2005	Iran	Road	-	DSL	-	SL	0.15	35	MSF	-	6

Continued on next page

Continued from previous page

Case Studies [-]	Year [-]	Country [-]	Function [-]	Internal span [m]	Design option [-]	Ground [-]	Lining [-]	Lining thickness [m]	f_{ck} [MPa]	Fibre type [-]	Aspect ratio ($\frac{L_f}{\phi_f}$) [-]	Fibre Content [kg/m3]
[141]	2008	Switzerland	Railway	7	CSL	Rock	SL	0.14	-	SF	-	-
							PL	0.25	-	SF	-	-
[142]	2019	China	Railway	20	CSL	Rock	SL	0.10	40	MSF	69	6
							PL	0.15	40	MSF	69	6
[143]	-	Mexico	Railway	11	-	Rock	TPL	0.2	25	SF	64	30
[144]	2001	Norway	Road	-	-	Rock	TPL	-	40	MSF	53	5 - 8
[145]	2001	China	Railway	-	-	Rock	TPL	-	35	SF	60	50
[146]	2003	Spain	Road	-	-	-	TPL	0.05-0.2	-	SF	-	-
[147]	-	France	Road	-	-	-	TPL	0.2-0.3	-	SF	-	-
[148]	2009	Italy	Road	-	-	-	TPL	0.05 - 0.25	-	SF	-	-
[149]	-	China	Road	-	-	-	TPL	0.2	-	SF	-	45
[150]	-	Germany	Road	-	-	-	TPL	-	-	SF	47	40
[151]	-	Canada	Railway	-	SSL	-	PL	0.25	-	SF	60	59
[152]	2020	China	Road	5	SSL	Rock	PL	0.25	40	SF	-	50

Continued on next page

Continued from previous page

Case Studies [-]	Year [-]	Country [-]	Function [-]	Internal span [m]	Design option [-]	Ground [-]	Lining [-]	Lining thickness [m]	f_{ck} [MPa]	Fibre type [-]	Aspect ratio ($\frac{L_f}{\phi_f}$) [-]	Fibre Content [kg/m3]
[153]	2023	Australia	Road	23	CSL	Rock	PL	0.11	40	SF	64	35
							SL	0.125	40	SF	64	35
[154]	2022	India	Railway	8-17	DSL	Rock	SL	0.3-0.45	32	SF	64	38
[155]	2024	Canada	Railway	14-16	CSL	Rock	PL	0.05	42	SF	64	-
							SL	0.05	42	SF	64	-

Note: PL = Primary Lining; TPL = Temporary Primary Lining; SL = Secondary Lining; DSL = Double Shell Lining; CSL = Composite Shell Lining; SSL = Single Shell Lining; SF = Steel Fibre; MSF = Macro Synthetic Fibre; mSF = micro Synthetic Fibre; f_{ck} = Characteristic compressive strength; L_f = Length of fibre; ϕ_f = Diameter of fibre;

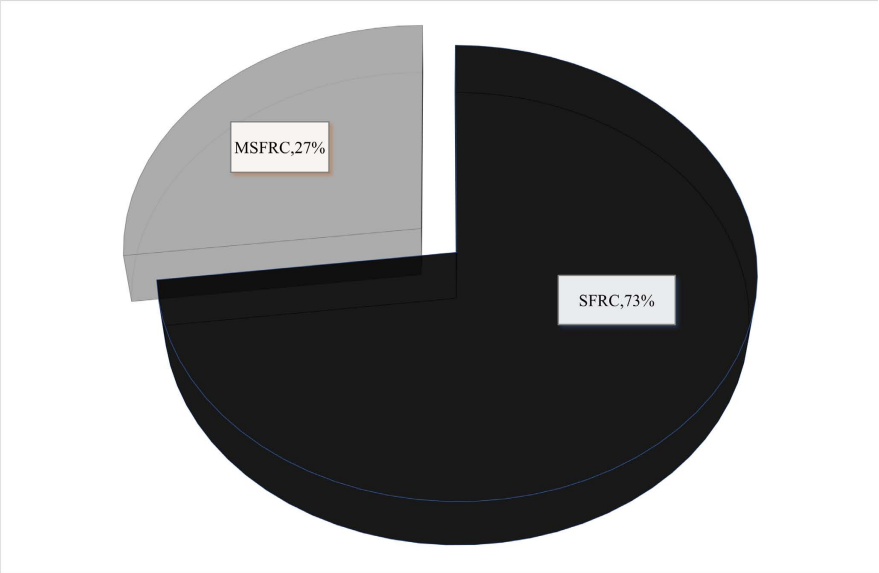

Figure 2.38: Percentage of fibre types used in the permanent sprayed concrete tunnel lining based on case studies from Table 2.19.

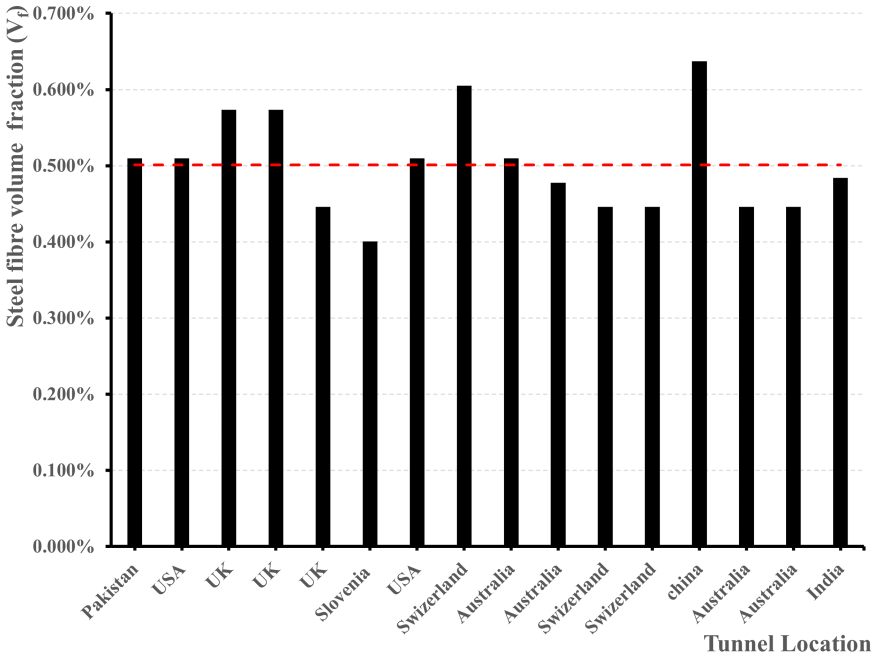

Figure 2.39: Steel fibre volume fractions used in the permanent sprayed concrete tunnel lining based on case studies from Table 2.19.

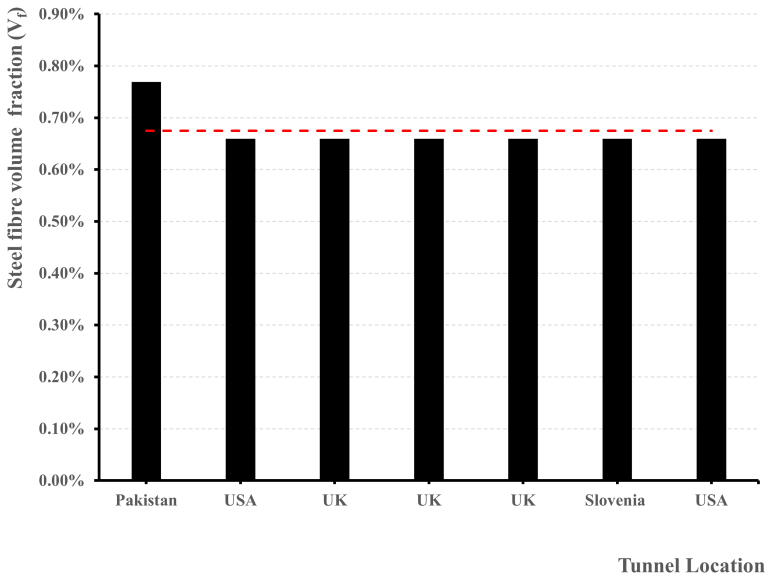

Figure 2.40: Macro synthetic fibres volume fractions used in the permanent sprayed concrete tunnel lining based on case studies from Table 2.19.

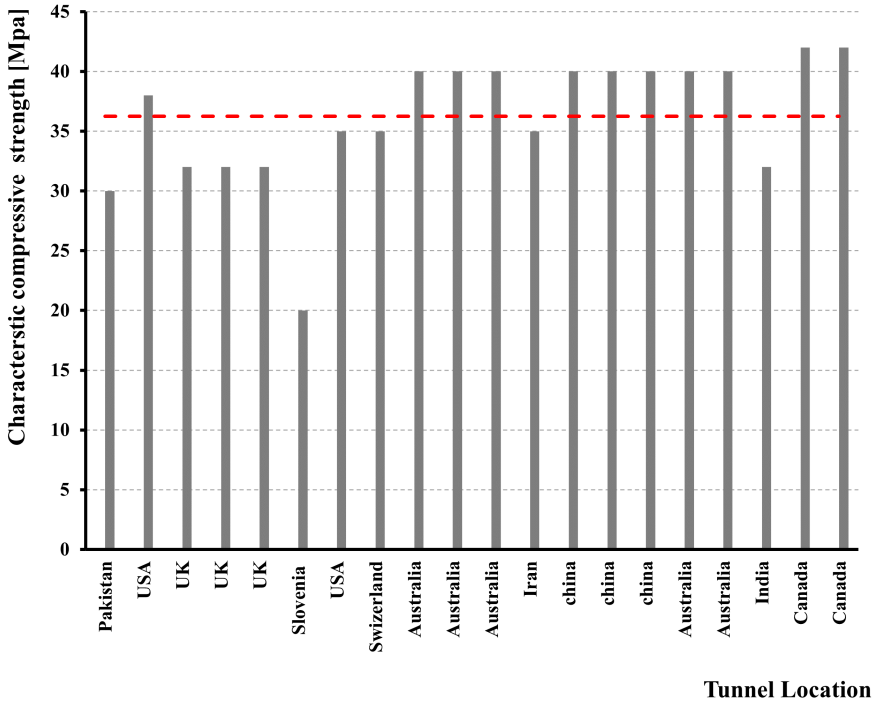

Figure 2.41: Concrete compressive strength used in permanent sprayed concrete tunnel lining based on case studies from Table 2.19.

2.5 Material Characterisation and Classification of FRC Sprayed Concrete

In all the design options mentioned in Section 2.4.1, sprayed concrete is used as a permanent material for either the secondary lining or for both primary and secondary linings. As long as sprayed concrete is used for permanent linings, study its mechanical properties is mandatory to develop the design process. The mechanical characteristics of uncracked sprayed fibre reinforced concrete can be evaluated through compression, bending, or shear tests, and elasticity is occasionally measured as well. Post-cracking performance is commonly assessed in terms of residual strength or energy absorption.

The typical test methods employed for characterising FRC materials mainly consist of beam bending tests, and more recently, there has been a growing use of panel bending tests, particularly for sprayed FRC. These tests include three-point and four-point bending for beams and three-point bending for panels. The main advantages of the three-point bending beam test are that it is well-established, relatively easy to perform, supported by an extensive database for comparative analysis, and alignment with existing tunnel design guidelines. However, this test is specifically designed for pure concrete as stated in the relavent standards. The four-point bending test involves the sawing beam of the panel, which introduces additional complexity compared to the three-point bending test for the panels, which maintains the same geometry as the energy absorption test. Furthermore, it is more appropriate to perform panels tests when dealing with tunnel lining, as they more closely simulate the actual conditions compared to the beam. The three-point panel test is the focus of this thesis and will be discussed in detail in the following section.

In general, testing the structural performance of FRC is essential to characterise its post-crack behaviour and to derive tensile strength parameters for use in design analysis [156]. Currently, numerous flexural test methods are available to assess the post-cracking performance of fibre-reinforced concrete elements, based on beam or panel tests, as listed in Table 2.20 and discussed above. This study provides an in-depth examination of the viable flexural test methods for characterizing and classifying sprayed fibre-reinforced concrete (FRC) materials for use in permanent tunnel linings.

Despite advances in the tunnel construction industry, current standards and research studies seem insufficient to fully convince the industry to adopt fibre-reinforced sprayed concrete for

permanent linings. The *fib* Model Code 2010 [1] is used as a reference document in tunnel lining design, the recommendations of the ITA Report and the fib Bulletin regarding the segmental linings of the FRC tunnels [157], [158] and suggests the three-point bending test EN 14651 [7] for the characterisation and classification of reinforced concrete material (FRC). This beam geometry and test are suitable for cast-in-situ or precast FRC structural applications but not for fibre-reinforced sprayed concrete. In fact, contrary to the *fib* Model Code 2010 [1], the European sprayed concrete standard EN 14487-1 2006 [159] described various methods for specifying the ductility of fibre-reinforced sprayed concrete in terms of residual strength according to EN 14488-3 2006 [160] and of energy absorption capacity through EN 14488-5 [18]. The energy values provided by tests carried out according to EN 14488-5 [18] are generally considered when designing a temporary sprayed FRC lining and are not generally used to characterise and classify the material for the design of a permanent tunnel lining. The residual strength four point bending test of EN 14488-3 [160] is incongruent with the MC 2010 [1] and testing on the saw cut beams from the panels was not feasible and easy. To be convenient with the MC 2010 [1], EFNARC produced a document [161] advising the use of three point bending tests on panels with notch having the same geometry as EN 14488-5 [18] and recommending a correlation between the EFNARC notched panel test and the EN 14651 [7] notched beam test. Despite this, most research and case studies were utilized EN 14651 [7] 3-point bending beam test for the characterization and classification of fibre-reinforced sprayed concrete. ITA Report 24 [79], published in 2020 by Working Group 12, comprehensively addressed the construction, application, and design aspects of sprayed fibre-reinforced concrete (FRC) for permanent tunnel lining applications. It endorsed the EN 14651 [7] three-point bending test (3PBT) for material characterization and classification of sprayed FRC. Conversely, the European sprayed concrete standard advocates for the use of the flexural test EN 14488-3 (four-point bending test) [160] on beams extracted from panels, for the purpose of specifying the ductility of sprayed concrete. The rationale behind the ITA Report 24's [79] 2020 exclusion of the EN 14488-3 [160] four-point bending test, despite its prescription in the European sprayed concrete standard, remains unclear.

Subsequently, the European sprayed concrete standard EN 14487-1 2022 [19] was recently updated to include the notched panel test. Consequently, the corresponding standard EN 14488-3 2023 [16] incorporates the test methods for the notched panel as Method B, along with the four-point bending test as Method A.

Although the EN 14487-1 [19] standard is specified for sprayed concrete, the frequent men-

tion of the EN 14651 [7] test methods, which are usually used to pour concrete, is not clearly explained in the EN 14487-1 [19]standard. Furthermore, the new standard states that the residual strength values at the respective CMOD of 0.5 mm, 1.5 mm, 2.5 mm and 3.5 mm of the EN 14651 [7] beam test are considered equal to the residual strength values obtained from the notched panel test at the same CMODs. However, this research analytically, experimentally, and numerically justifies that these values are not equal.

Subsequent to the incorporation of the notched panel test into the European standard for sprayed concrete, two experimental studies [15] and [81] have been published, examining the consistency of the Model Code 2010 classification when using both notched panel and notched beam tests. Furthermore, a thorough investigation performed by Laval University in collaboration with Bekaert [14] evaluated and compared the residual strength values derived from the results of both the panel and beam tests. The findings indicated substantial discrepancies in the classification and post-crack strength variations of FRC-sprayed concrete in most types of fibres. However, for specific steel fibres, the results of the notched beam and the notched panel did not show significant differences, as depicted in Figures 2.42, 2.43, and 2.44. The reasons for these inconsistencies were not fully explained in the studies. Earlier research [162] found that the residual strength ratio of the FRC's notched beam and panel tests was almost one, but both were cast, not sprayed. This Ph.D. study investigates the relationship and correlation between the performance of sprayed fibre-reinforced concrete (FRC), evaluated using the referenced sprayed notched panel test (EN 14488-3, Method B [16]) and the notched beam test (EN 14651 [7]), and their consistency with the constitutive models, the characterization and classification specified in the Model Code 2020 [8] and Euro Code 2 [9], through combined experimental and numerical analyses.

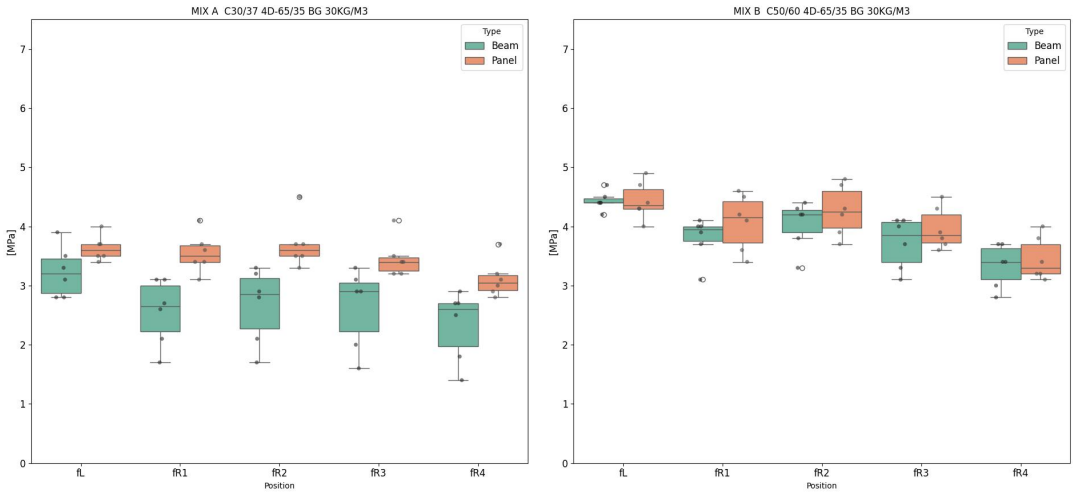

Figure 2.42: Comparison of residual strength results for EN 14651 beam and EN 14488-3 Method B panel tests using 4D-65/35 steel fibre in C30/37 concrete grades (a) and in C30/37 concrete grades (b) at 30 kg/m³ fibre dosage [14].

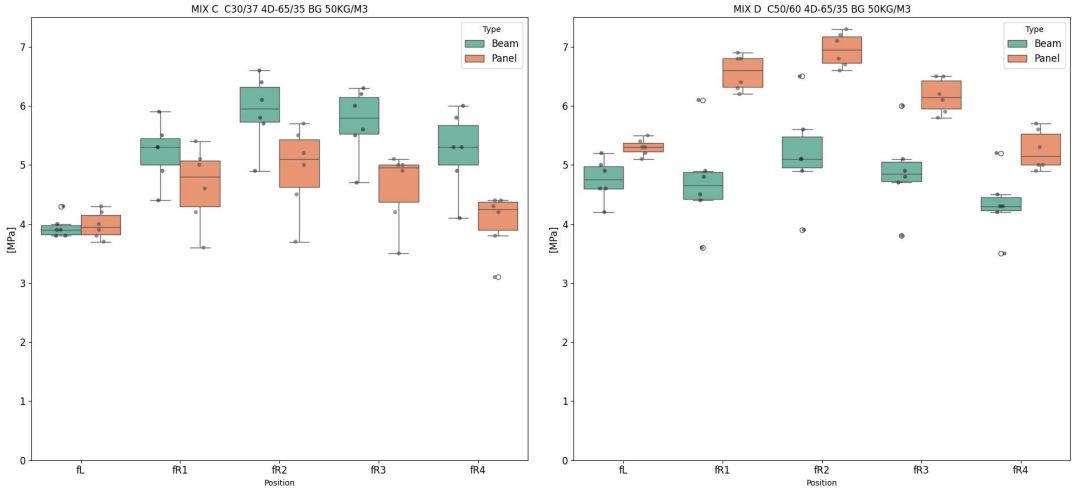

Figure 2.43: Comparison of residual strength results for EN 14651 beam and EN 14488-3 Method B panel tests using 4D-65/35 steel fibre in C30/37 concrete grades (a) and in C50/60 concrete grades (b) at 50 kg/m³ fibre dosage [14].

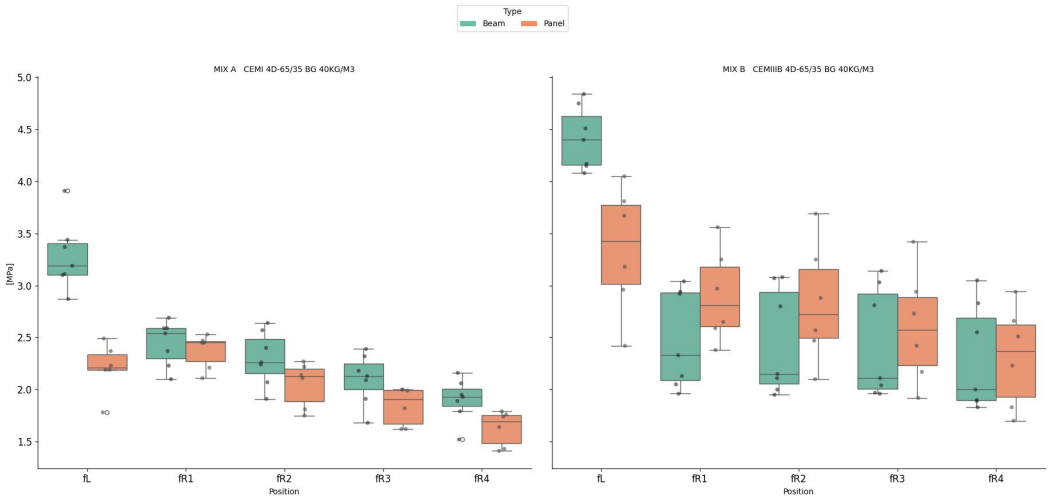

Figure 2.44: Comparison of residual strength results for EN 14651 beam and EN 14488-3 Method B panel tests using 4D-65/35 steel fibres at 40 kg/m^3 dosage [15].

Structural design of FRC elements is based on the post-cracking residual strength provided by fibre reinforcement. Instances like early age crack-control or fire resistance, are considered non-structural use of FRC. Fibres can enhance performance at SLS by reducing crack spacing and width, which in turn increases durability, and they can improve performance at ULS by partially or totally substitute conventional reinforcement [1]. The addition of fibres alters the mechanical properties of a cementitious matrix. However, the fibres do not significantly affect the elastic properties or compressive strength unless they are added in high percentage [8].

The characterisation and classification of the material of the FRC sprayed concrete for the tunnel lining is mainly concerned with the post-cracking performance of the material. As mentioned above, post-cracking performance is typically evaluated in terms of residual strength and energy absorption. Residual strength can be used for material classification purposes and the design of the lining, while energy absorption capacity provides insights into the behaviour of the FRC-sprayed lining under significant deformation. The residual strength and energy absorption, including the testing methods, are discussed in the following sections.

Table 2.20: Common standard flexural test methods for post-cracking performance of FRC and sprayed FRC.

Test Methods	**Europe**	**USA**	**Japan**
Testing sprayed concrete – Part 3:Flexural strengths of fibre-reinforced beam specimens	EN 14488-3 Method A	-	-
Testing sprayed concrete – Part 3: Flexural strengths of fibre-reinforced panel specimens	EN 14488-3 Method B	-	-
Testing sprayed concrete – Part 5: Determination of energy absorption capacity of fibre-reinforced slab specimens	EN 14488-5	-	-
Test method for metallic fibre concrete measuring the flexural tensile strength	EN 14651	-	JSCE-G552
Method of tests for flexural strength and flexural toughness of steel FRC	-	-	JSCE-G552
Standard test methods for flexural toughness FRC (using centrally loaded round panel)	-	ASTM C1550	-
Standard test method for flexural performance of FRC	-	ASTM C1609	JSCE-G552

2.5.1 Residual Strength of FRC Sprayed Concrete

Generally, fibres do not affect the properties of concrete before it develops cracks. However, once cracks form, fibres become essential by bridging these cracks and supporting the tensile stresses. This capability allows fibre-reinforced concrete (FRC) to retain load-bearing capacity even after cracking, a characteristic commonly referred to as "residual strength" or post-crack strength.

The magnitude of this residual strength is influenced by several factors, including the type of fibre used, their inherent properties, size, shape, bonding characteristics, the quantity of fibres added and, most importantly, the combined influence of these factors on hardened concrete.

As described in the previous section, the European sprayed concrete standard EN 14487-1 [19] recommends using the four-point unnotched beam test EN 14488-3 Method A and Method B three-point notched panel test methodologies to determine the residual strength of FRC-sprayed concrete for the characterisation and classification of the material. The small-scale, nonstandard indirect tensile tests discussed in Section 2.1.3.1 as conventional FRC test methodologies have been used by some researchers [43] to study post-crack performance of sprayed FRC concrete. However, these tests have not been validated by international standards organisations. The following sections describe the EN 14488-3 Method B panel test and the EN 14651 notched beam test.

2.5.1.1 EN 14488-3 Method B (Three-Point Bendig Notched Panel Test)

This test is a method of measuring the flexural tensile strength of the sprayed FRC on the panel. The flexural strengths are determined on notched panels with dimensions of 600 mm (width) x 600 mm (length) x 100 mm (height) in a three-point bending test (Figure 2.45 and Figure 2.46). As described in the above section, this test is included in EN 14488-3 [16] as Method B in 2024. The test method is almost the same as the EFNARC 3PBT [161] three-point bending test.

The test specimens shall be panels that comply with EN 14488-1 [163] with nominal dimensions of 600 mm in width, 600 mm in length, and 100 mm in thickness as shown in Figure 2.46, and shall be sprayed in compliance with the same standard. The notch depth is 10 mm and the corresponding effective cross-section in the mid-span (h_{sp}) is 90 mm. The distance between the support rollers is 500 mm (Figure 2.46). Usually, the applied load and the displacement in the crack mouth opening (Crack Mouth Opening Displacement [CMOD]) are measured. Alternatively, the deflection can be measured in the mid-span and converted using the CMOD-deflection relation according to Equation 2.36. In case of a testing machine that controls the rate of increase of CMOD, the machine shall be operated so that CMOD increases at a constant rate of 0.05 mm/min. When CMOD = 0.2 mm, the machine must be operated so that CMOD increases at a constant rate of 0.2 mm/min.

The test shall be terminated at a CMOD value not less than 5mm, and the tests advised by EN 14488-3 [16] during which the crack starts outside the notch shall be rejected.

$$CMOD_S = \frac{4 \cdot \delta_{FLs} \cdot h_{sp}}{l} \tag{2.36}$$

Where:
$CMOD_S$ is the CMOD value, in mm, measured at the bottom of the notch;
δ_{FLs} is the deflection, in mm;

The test results which need to be expressed are the limit of proportionality (LOP) and the residual flexural strength. The limit of proportionality $f^f_{\mathrm{cts,Ls}}$ is calculated as Equation 2.37. The load value F_{Ls} shall be determined by drawing a line at a distance of 0.05 mm and paralled to the load-CMOD diagram and taking as F_{Ls} the highest load value in the interval [0 mm : 0.05 mm].

$$f^f_{\mathrm{cts,Ls}} = \frac{3F_{\mathrm{Ls}} \cdot l}{2bh^2_{\mathrm{sp}}} \tag{2.37}$$

Where:
$f^f_{\mathrm{cts,Ls}}$ is the LOP (limit of proportionality) in Mpa; F_{Ls} is the load corresponding to the LOP, in N;

The residual flexural tensile strength needs to be evaluated at four different displacements CMOD = $CMOD_{js}$ (j=1,2,3,4), as shown in the Table 2.22 and Equation 2.38, with the load $F_{J,S}$ corresponding to the displacements measured as shown in Figure 2.47. After obtaining the residual strengths, the material can be classified according to the EN 14487-1 standard [19] for a further design process. To classify and characterise the material according to Model Code 2010 and Eurocode 2, since the classification is based on the EN 14651 [7] beam test methodology, the correlation between the panel and beam test methodologies is required and have been discussed and advised in detail in the Chapter 6 of this thesis.

$$f_{\mathrm{R,js}} = \frac{3F_{\mathrm{j,s}} \cdot l}{2bh^2_{\mathrm{sp}}} \tag{2.38}$$

Where:
$f_{R,js}$ is the residual flexural tensile strength corresponding with CMOD = $CMOD_{js}$ or δ_{js}

(j=1,2,3,4), in Mpa;

$F_{j,s}$ is the load corresponding with CMOD = $CMOD_{js}$ orδ_{js} (j=1,2,3,4), in N;

l is the span length, in mm;

b is the width of the specimen, in mm;

h_{sp} is the distance, in mm, between the tip of the notch and the top of the beam (equal as the unnotched height);

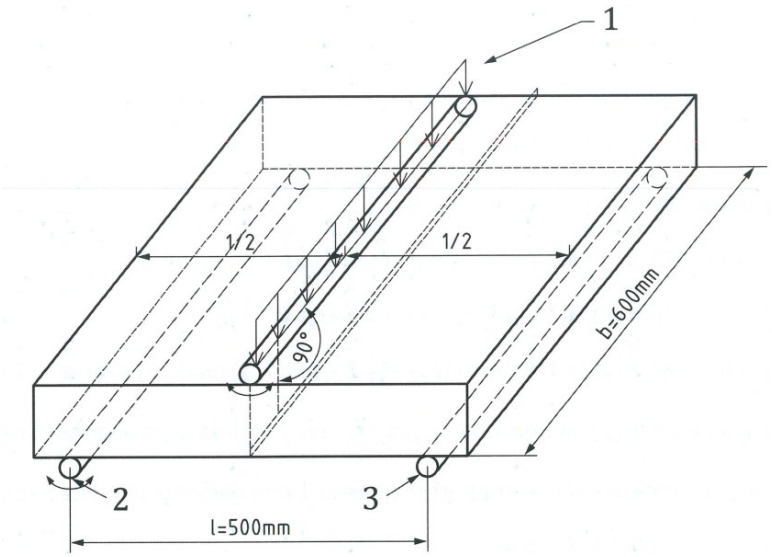

Key
1. Loading roller (capable of rotation and of being inclined)
2. Supporting roller (capable of rotation and of being inclined)
3. Stationary supporting roller

Figure 2.45: EN 14488-3 Method B (3PB notched panel test) arrangement of loading of test specimen [16].

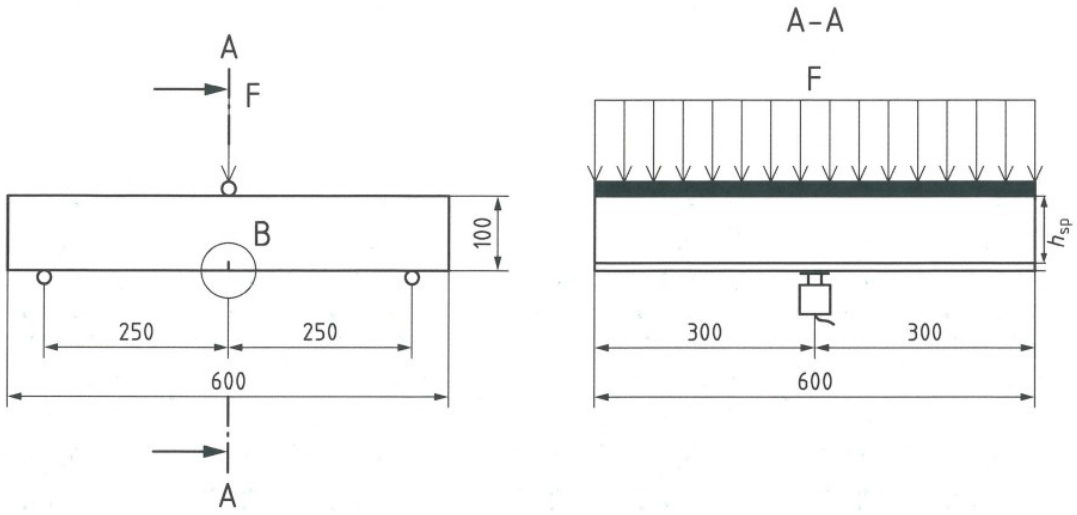

Figure 2.46: EN 14488-3 Method B (3PB notched panel test) test set-up (dimensions in mm) [16].

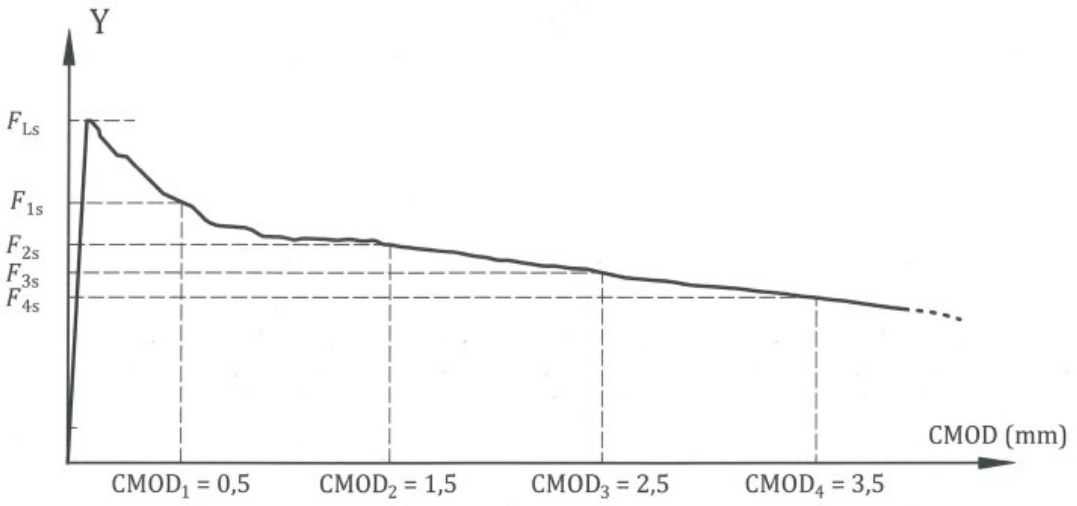

Figure 2.47: EN 14488-3 Method B Load – CMOD diagram [16].

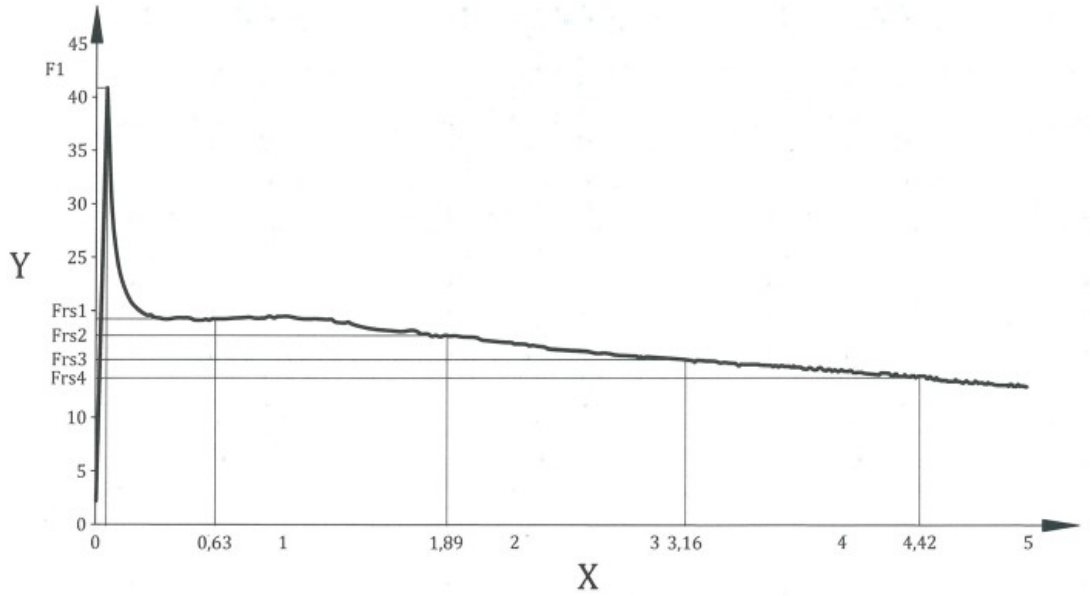

Figure 2.48: EN 14488-3 Method B Load–Deflection diagram [16].

Table 2.22: LOP (Limit of Proportionality) and residual strength of EN 14488-3 Method B with respective to CMOD and deflection values [16].

LOP / Residual flexural strength	**CMOD (mm)**	**Deflection (mm)**
$f^{f}_{\mathrm{cts,Ls}}$	0.05	0.063
$f_{R,1s}$	0.5	0.631
$f_{R,2s}$	1.5	1.894
$f_{R,3s}$	2.5	3.156
$f_{R,4s}$	3.5	4.420

Table 2.23: Definition of class of ductility according to EN 14487-1 [19].

Class of ductility	**Ductility requirement**	**Crack control requirement**
Class 1	$f_{R_{s3k}}/f_{R_{s1k}} > 0.5$	$f_{R_{s1k}}/f_{R_{lsk}} > 0.4$
Class 2	$f_{R_{s3k}}/f_{R_{s1k}} > 0.7$	$f_{R_{s1k}}/f_{R_{lsk}} > 0.5$
Class 3	$f_{R_{s3k}}/f_{R_{s1k}} > 0.9$	$f_{R_{s1k}}/f_{R_{lsk}} > 0.6$

Note: Class 1 for ductility and crack control requirements meets the requirement of the Model Code 2010

For permanent sprayed fibre reinforced concrete linings, the minimum performance level for the strength ratio (R_d) and ductility ratio (R_s) recommended in *fib* Bulletin 116 [164] are:

$$R_S = \frac{f_{R_{s1k}}}{f_{R_{lsk}}} > 0.8 \tag{2.39}$$

$$R_d = \frac{f_{R_{s1k}}}{f_{R_{lsk}}} > 0.9 \tag{2.40}$$

a minimum level of residual stress $f_{R_{lsk}}$ shall be greater than 2 MPa [164].

2.5.1.2 EN 14651 (Three-Point Bendig Notched Beam Test)

The EN 14651 3PB test was initially recommended for the characterisation and classification of conventional (cast) FRC, all relevant methodologies and tests are discussed in the FRC Section 2.1.3.3. However, this test specified in Model Code 2020 [8] and Eurocode 2 Annex N [9] refers to poured concrete (cast in-mould concrete), even though it is also mentioned in the European sprayed concrete standard EN 14487-1 [19]. Consequently, in this thesis, the test is used for the performance evaluation of both sprayed and cast-in-place FRC, as well as to establish a relationship between them.

2.5.2 Energy Absorption Capacity

The measurement of energy absorption capacity on panel specimens constitutes a fundamental requirement for fibre-reinforced shotcrete, as it provides vital information regarding performance at large deformations. Moreover, this metric is predominantly employed in the design of temporary primary linings. In the context of sprayed concrete linings, panel tests that quantify energy absorption prove to be a more suitable method to describe the performance and failure mechanisms of sprayed tunnel linings. These tests exhibit static indeterminacy, similar to the lining itself, thereby allowing for stress redistribution and the development of multiple cracks.

The energy absorption test necessitates the application of a central load on a panel, which may be square or circular, and is uniformly supported along all four edges or its outer boundary. This setup replicates the typical punching effect of a rock bolt on the shotcrete lining. The hyperstatic configuration of the test facilitates stress redistribution, enabling the formation of

multiple cracks depending on the performance of the fibres. In contrast to beam tests and the 3pbt panel test, the energy absorption panel tests accommodate larger deformations, reaching up to 25 mm, thus providing a better representation of the actual behaviour of shotcrete linings. In addition, energy panel tests demonstrate significantly lower variability due to the extension of longer cumulative crack lengths from multiple cracking, resulting in decreased coefficients of variation. However, these tests are inadequate for the characterisation or classification of the material properties of sprayed fibre-reinforced concrete for the design of permanent sprayed concrete tunnel linings, necessitating further material characterisation tests. The widely recognised standards are ASTM C1550-20 [17] in the USA and EN 14488 5 [18] in Europe, respectively.

2.5.2.1 ASTM C1550-20 Energy Absorption Centrally Loaded Round Panel Test

ASTM C1550-20 [17], This test method covers the determination of the flexural toughness of fibre-reinforced concrete expressed as energy absorption in the post-crack range using a round panel supported on three symmetrically arranged pivots and subjected to a central point load as shown in Figure 2.49. The performance of the samples tested by this method is quantified in terms of the energy absorbed between the beginning of loading and the selected values of central deflection.

Circular panels, either moulded or sprayed, undergo a central point loading while being supported on three symmetrically positioned pivots. The load is administered via a steel piston with a hemispherical end, advanced at a predetermined displacement rate. The resultant load and deflection are simultaneously documented until reaching a specified central deflection. The energy absorbed by the panel up to this point is indicative of the flexural toughness of the fibre-reinforced concrete panel. The ASTM C1550-20 [17] standard, while acknowledged, is not elaborated upon in this research; greater emphasis is placed on the European standard EN 14488-5 [18].

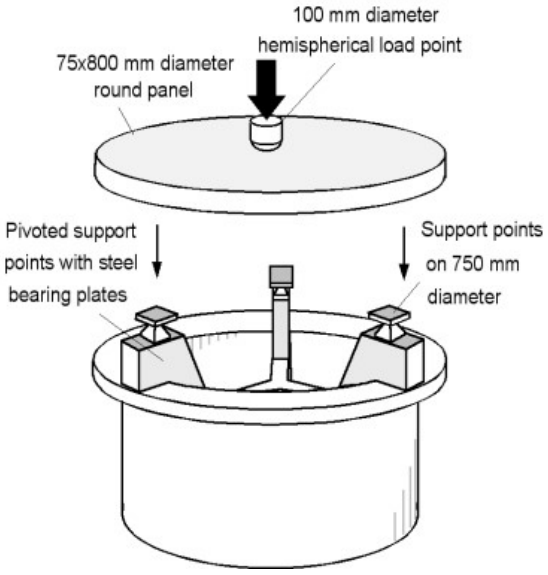

Figure 2.49: Round derminate panel test setup ASTM C1550 [17].

2.5.2.2 EN 14488-5 Energy Absorption Panel Test

This test is the square slab flexural-punching test, which simulates very effectively the behaviour of a tunnel lining under rock pressure around an anchor bolt. In this test, a fibre-reinforced slab specimen is subjected to a load, under deflection control, through a rigid steel block positioned in the centre of the slab. A square specimen shall be produced from a panel, sprayed and cured in a mould, according to EN 14488-1 [163], with dimensions of 600 mm x 600 mm and trimmed to a thickness of 100^{+5}_{0} mm immediately after spraying as shown in Figure 2.50. The prepared slab must be cured under conditions according to EN 12390-2, for a minimum of 3 days immediately before testing, and kept moist until testing.

According to EN 14488-5 [18], the specimen testing shall normally be performed at 28 days on a machine that can test in a displacement controlled way and has a minimum stiffness of at least 200 kN / mm (including the frame, load cell, load block, and support frame). The support is a 20mm thick rigid square frame with inner dimensions of 500 x 500mm as shown in Figure 2.50.

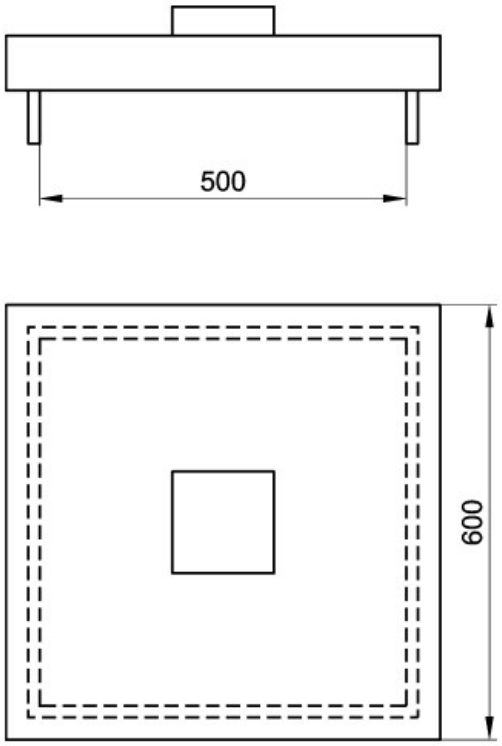

Figure 2.50: Arrangement of loading of test specimen for energy absorption test [18].

The test shall be displacement controlled, with a constant rate of 1 mm/min in the centre of the slab. The load and deflection shall be continuously recorded with the XY-plotter data logger until a deflection of at least 30 mm is obtained. From this curve, a second curve is calculated, which gives the energy as a function of the deflection. The result that needs to be expressed is the energy until a deflection of 25 mm is obtained, which can be calculated as the area under the load deflection curve between the 0 and 25 mm deflection range; see Figure 2.51 and Equation 2.41.

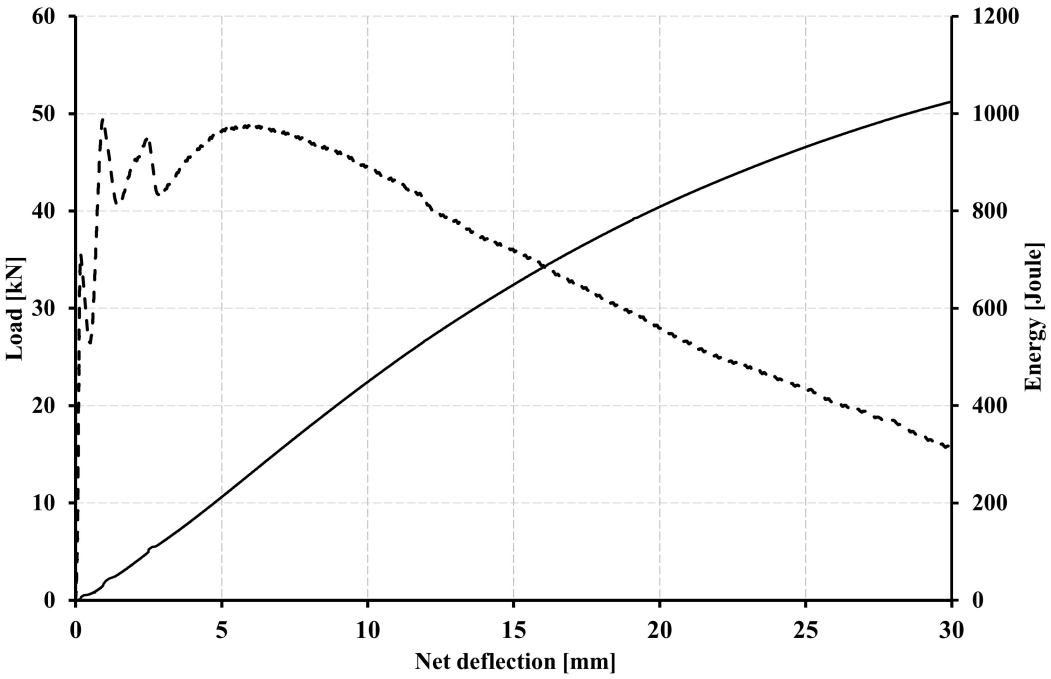

Figure 2.51: Load vs. Deflection and Energy vs. Deflection graph for EN 14488-5 energy absorption capacity test.

Some requirements for this test are added in the new version of the European sprayed concrete standard [19];

1. F_{el-max} is the maximum load value of the elastic part of the load-deflection curve, and $F_{post-crack}$ is the maximum load value between F_{el-max} and the load value at 5 mm deflection;

2. Each load-deflection curve shall fulfil the criteria: F_{el-max} shall be reached for a deflection lower than 2 mm; $F_{post-crack}$ shall be higher than 70% of F_{el-max};

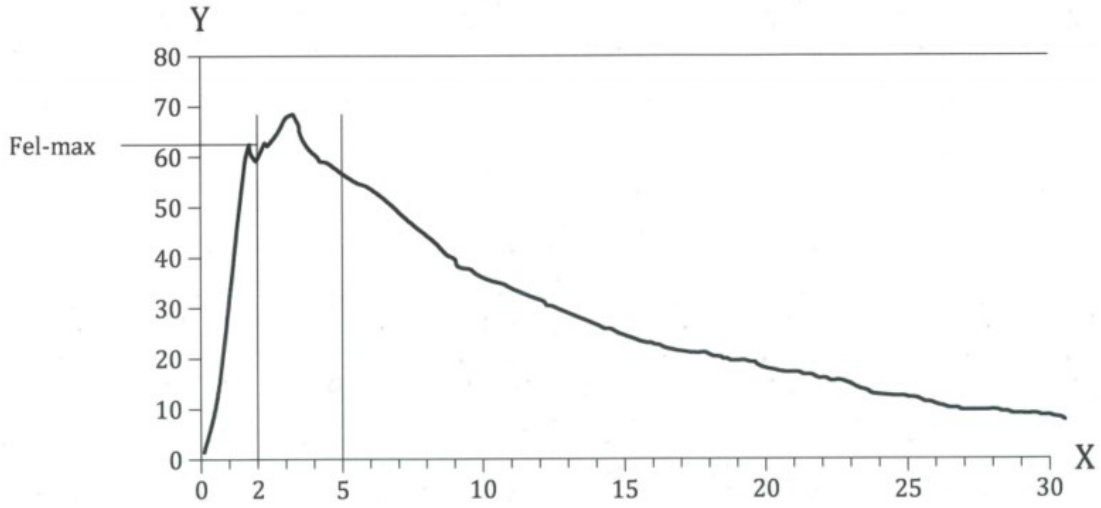

Figure 2.52: Typical Load vs. Deflection curve for EN 14488-5 energy test [19].

Key: X deflection [mm], Y load [kN]

The energy absorption capacity, $E(\delta)$ is the area under load-deflection curve until a deflection $\delta = 25$ mm, and can be calculated using the expression below

$$E_{25} = \int_0^{25} F(\delta)\, d\delta \tag{2.41}$$

Where; $F(\delta)$ is load as function of deflection;
After evaluating the energy absorption capacity of FRC sprayed concrete the classification the material followed according to the standard EN 14487-1 [19], the energy absorption class is as in the Table 2.24.

Table 2.24: Definitions of energy absorption classes EN 14487-1 [19].

Energy absorption class	**Energy absorption in J for deflection up to 25 mm**
E500	500
E700	700
E1000	1000

This chapter has presented a comprehensive review of the state of the art related to fibre-reinforced concrete (FRC) and its application in sprayed concrete for permanent tunnel linings. It first examined the general mechanical properties of FRC, the available testing methodologies, and the main approaches to classifying FRC. It then reviewed key developments in sprayed concrete technology, including spraying techniques and mix design considerations for fibre-reinforced sprayed concrete, with particular attention to previous studies on mix proportions and the collection of relevant data sets.

The review also analysed the behaviour of sprayed fibre-reinforced concrete in tunnel lining applications, assessing its mechanical response and post-cracking performance. Available design approaches for sprayed concrete tunnel linings were discussed, together with over 40 case studies on the use of Sprayed FRC in permanent tunnel linings illustrating practical experiences with permanent fibre-reinforced sprayed concrete linings.

From this critical review, several principal research gaps were identified: the lack of a well-accepted procedure to classify sprayed FRC for use in permanent tunnel linings; the absence of comprehensive design guidelines for such applications; and limited confidence in current methodologies for the post-cracking mechanical characterization of sprayed FRC. More generally, there remains insufficient understanding and a lack of standardized procedures for evaluating the mechanical properties of sprayed FRC in permanent tunnel lining applications. These identified gaps form the basis for the experimental, numerical, and analytical investigations presented in the subsequent chapters.

Chapter 3

Research Significance

This PhD research addresses a critical gap in the existing literature regarding standards related to the use of fibre-reinforced sprayed concrete for permanent tunnel lining applications. The study combines an extensive experimental campaign with complementary numerical analysis to provide comprehensive insights into the mechanical behaviour, post-cracking properties and mechanical characterisation of fibre-reinforced sprayed concrete. This research contributes to advancing the understanding and application of sprayed fibre-reinforced concrete (Steel Fibre Reinforced Concrete) in permanent tunnel linings.

There is considerable gap in existing standards and design practices regarding the post-cracking tensile properties and corresponding design procedures for sprayed concrete. Current design guidelines do not clearly include specific procedures applicable to sprayed FRC, and as a result, researchers and practitioners in the tunnelling industry often rely on design methodologies typically developed for conventional cast FRC and, as a consequence, to corresponding conventional test methods. However, the mechanical properties of sprayed FRC differ significantly from those of cast FRC, meaning that the direct adoption of existing test methodology mainly conceived for traditionally cast FRC for determining the residual strengths of sprayed FRC may not accurately represent the material's true behaviour.

Existing classification and characterisation frameworks, such as those outlined in the *fib* Model Code 2020 and Eurocode 2 Annex L, were primarily developed for conventional cast FRC. Their effectiveness in accurately describing the unique mechanical response of sprayed FRC remains uncertain. This research therefore evaluates the applicability of FRC classification proposed by these guidelines to sprayed FRC.

This research establishes a clear distinction between the test methodologies appropriate for

permanent sprayed linings and those suited to temporary support applications. In addition, the study investigates the relationships between mechanical post-cracking performance obtained from sprayed and cast-in-mould FRC test methodologies.

Through experimental and numerical evaluation of the post-cracking properties of sprayed FRC, the study demonstrates that sprayed FRC can meet the performance requirements for permanent tunnel linings. The findings confirm its potential as a reliable, efficient, and sustainable material for tunnel infrastructures, especially short and irregular tunnels. This research therefore contributes both to scientific understanding and to improved engineering practice, promoting the wider acceptance and standardisation of sprayed FRC for permanent tunnel lining applications in the construction industry.

3.1 Thesis Outline

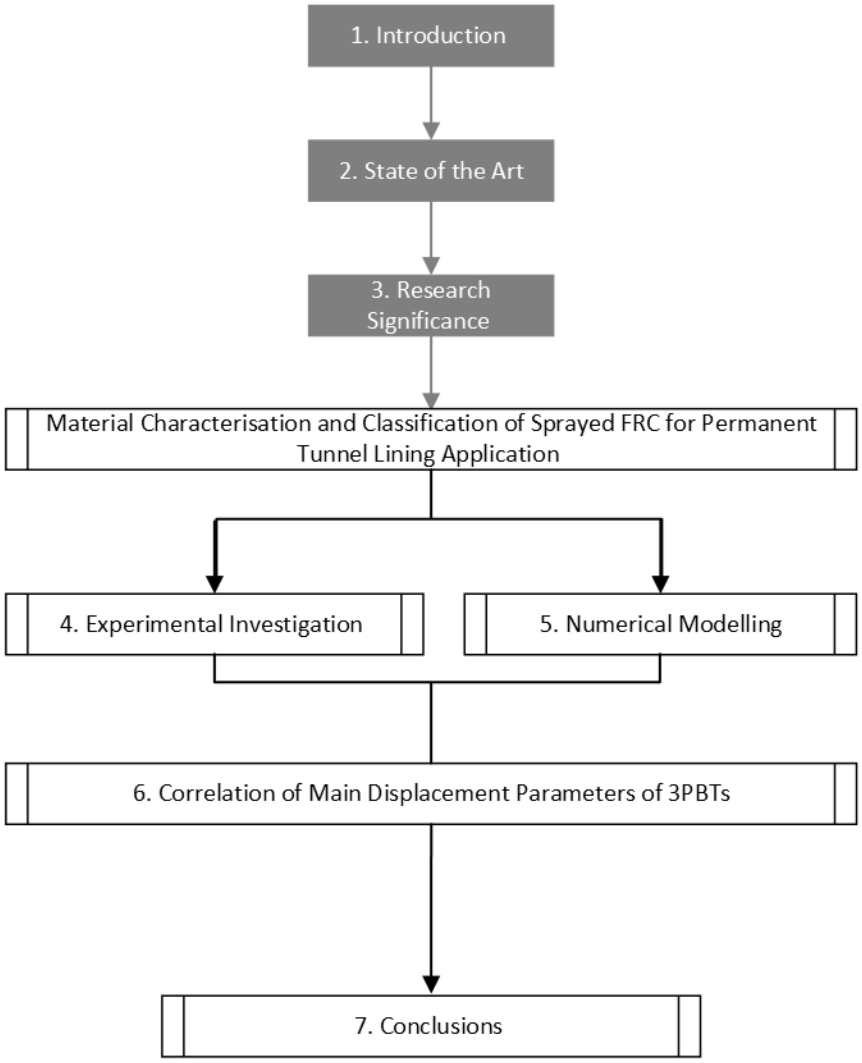

Figure 3.1: Structure of the thesis.

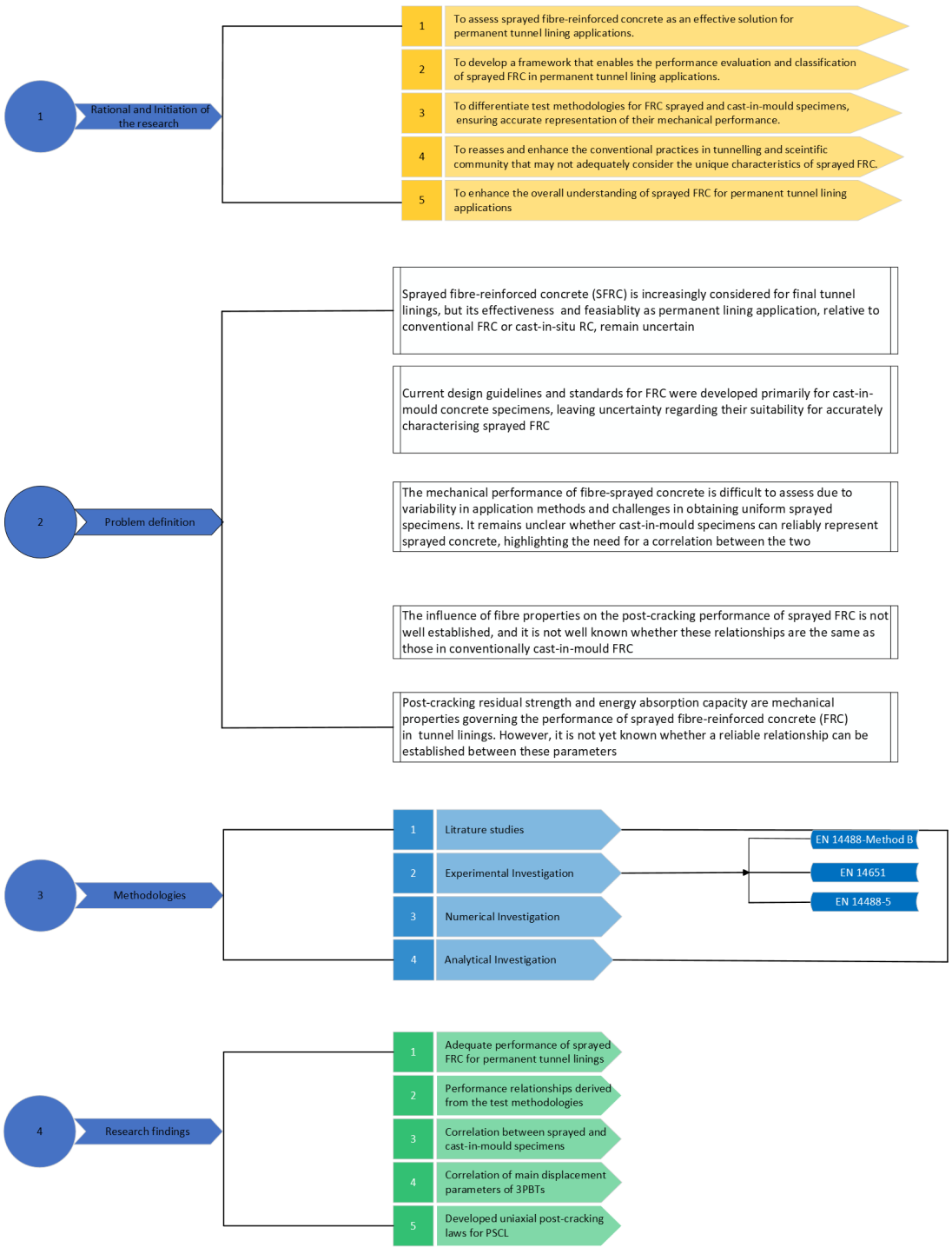

Figure 3.2: Summary of the research flow path.

Chapter 4

Experimental Investigation

This chapter covers the experimental investigation conducted as part of the thesis. Describes the experimental programmes, test methods, and laboratory setups employed in the study. All test methodologies for both sprayed and cast samples previously introduced in the state-of-the-art chapter are described here in detail, together with the experimental setup and procedures followed in the laboratory.

The sample preparation process for all test methodologies, covering both spray and casting techniques, is explained in detail. The fibre materials used in the research are described, including details of the concrete mix design. The results for each series of materials are presented, and their mechanical performance and residual strength are compared.

Detailed material characterisation and classification have been carried out and are discussed in this chapter. Comparative analyses are provided between the different material series and test methodologies. The classification of fibre-reinforced concrete (FRC) is also included based on the Model Code 2020 [8], the Eurocode 2 Annex L [9] and EN 14487-1 [19]. Furthermore, a comparative analysis of the mechanical characterisation and classification between sprayed FRC and conventional FRC is presented.

4.1 Experimental Programme

The main experimental tests carried out in this Ph.D. thesis are summarized in Table 4.1, together with the corresponding number of tests for each testing method and specimen type (sprayed and cast).

Table 4.1: Experimental program.

Test Methods	Casting	Number of tests at 1,3,7,10,14	Number of tests at 28 days	Number of tests at 90 days
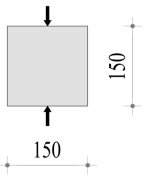 Compressive strength	Cast	3,3,3,3,3 SFRC25	3 SFRC25	3 SFRC25
		3,3,3,3,3 SFRC40	3 SFRC40	3 SFRC40
		3,3,3,3,3 MSFRC7	3 MSFRC7	3 MSFRC7
	Sprayed	3,3,3,3,3 SFRC25	3 SFRC25	3 SFRC25
		3,3,3,3,3 SFRC40	3 SFRC40	3 SFRC40
		-	-	-
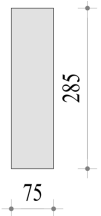 Shrinkage	Cast	3,3,3,3,3 SFRC25	3 SFRC25	3 SFRC25
		3,3,3,3,3 SFRC40	3 SFRC40	3 SFRC40
		3,3,3,3,3 MSFRC7	3 MSFRC7	3 MSFRC7
	Sprayed	-	-	-
		-	-	-
		-	-	-
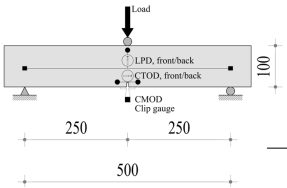 EN 14488-3 Method B	Cast	-	3 SFRC25	-
		-	7 SFRC40	-
		-	9 MSFRC7	6 MSFRC7
	Sprayed	-	9 SFRC25	6 SFRC25
		-	9 SFRC40	6 SFRC40
		-	-	-
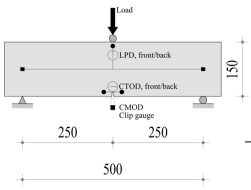 EN 14651	Cast	-	12 SFRC25	-
		-	12 SFRC40	6 SFRC40
		-	12 MSFRC7	6 MSFRC7
	Sprayed	-	13 SFRC25	13 SFRC25
		-	13 SFRC40	13 SFRC25
		-	-	-
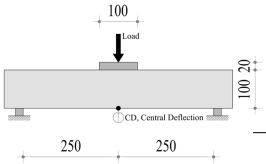 EN 14488-5	Cast	-	3 SFRC25	-
		-	3 SFRC40	-
		-	9 MSFRC7	3 MSFRC7
	Sprayed	-	6 SFRC25	-
		-	6 SFRC40	-
		-	-	-

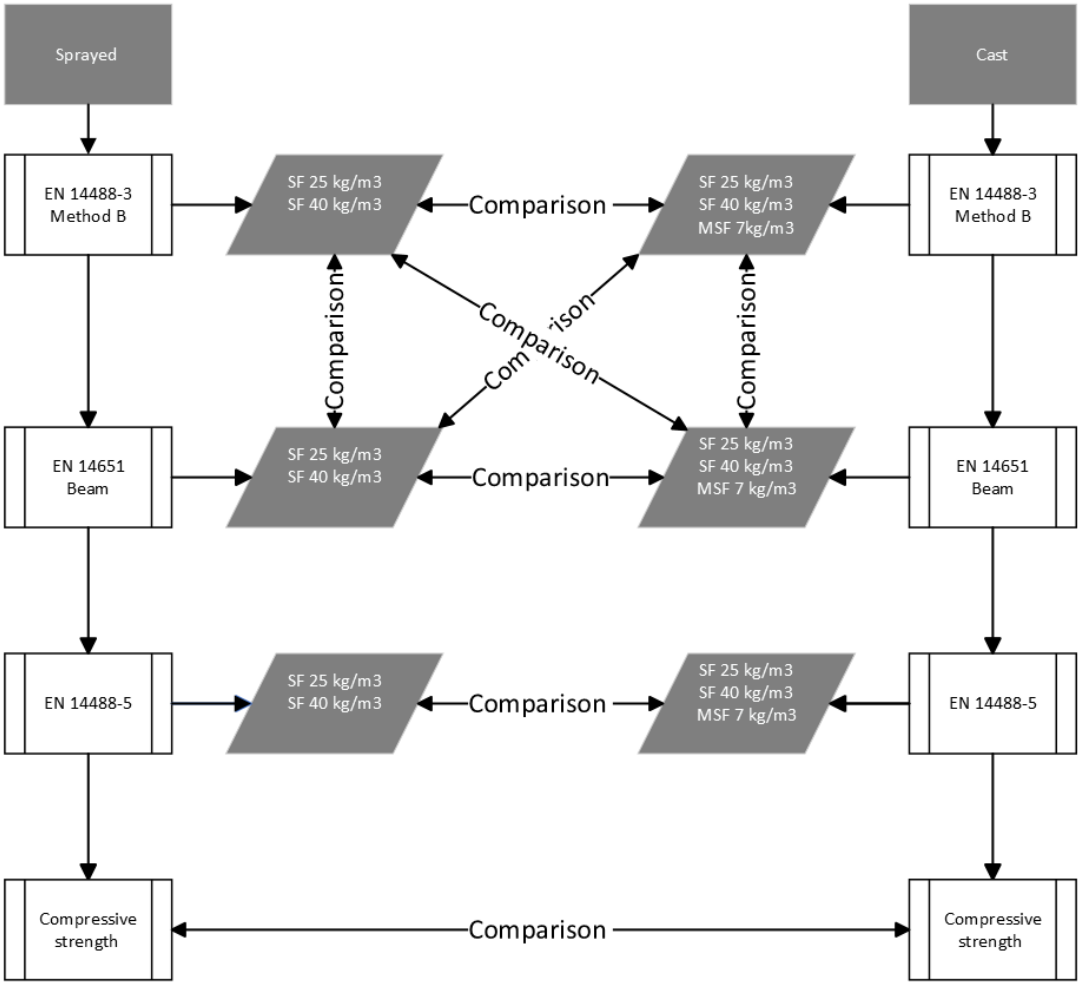

Figure 4.1: Overview of the experimental program comparing sprayed and cast fibre-reinforced concrete using EN 14488-3 Method B [16], EN 14651 [7], and EN 14488-5 [18] test methodologies, including compressive strength evaluation.

4.2 Materials and Mixture Proportion

In the experimental campaign presented herein a commercially produced concrete was used with all mixtures prepared from the same pre-bagged base mix of sand, aggregate, cement and superplasticizer. The concrete mix proportions are given in Table 4.2 and a target a strength class of C35, in according with *fib* Model 2010 [1], was adopted.

The maximum aggregate size used in this study was 6 mm, due to specific choices within mix proportions made by the concrete supplier, even though it is smaller than that reported in the case studies summarized in Table 2.13, 'Mix Proportion of Sprayed Concrete,' and in typical practices for sprayed fibre-reinforced concrete. Generally, an aggregate size of 8-10 mm is recommended for sprayed fibre-reinforced concrete tunnel linings. Furthermore, the maximum size was limited to 6 mm because the pumping hose of the spraying equipment was made of flexible plastic rather than the steel hoses typically used in robotic spraying systems. The flexible hose would not operate effectively if the aggregate size exceeded 6 mm.

Accelerators were injected into the nozzle during concrete spraying. Thus, the exact amount injected during the spraying process is unknown as it depends on the nozzle-man. Based on technical sheet, the accelerator adopted can be used within a typical range suggested for spraying process with respect to cement content (4 to 6%). Alkali accelerators were used, even though non-alkali accelerators are more effective and now more commonly adopted as discussed in detail in Section 2.2.3.4 of this PhD thesis. Nevertheless, the available nozzle operators are not yet familiar with their use. Therefore, alkali accelerators were used for this investigation, and their effects were duly considered in the study.

A superplasticiser was also used to regulate the rheology and improve the workability of the concrete, facilitating the spraying of high-fibre-content mixes. It is a water solution with modified acrylic polymers. The dosage adopted is about 1% with respect to cement content, leading to 5.5 l/m^3. The concrete was designed to get a concrete consistency class S5, according to EN 206 [165].

The water-to-cement ratio used was 0.37, which falls within the range of values found in the collected case studies, as shown in Table 2.13 and is expected to fit the proposed concrete class.

After establishing the base concrete mix composition, the selection of fibre type and dosage was made considering practical experience from permanent tunnel lining applications, as sum-

marised in the case studies presented in Table 2.19. The fibres were manually weighed and added directly into the mixing drum at the concrete batching plant.

The steel fibres used were a commercially supplied type, featuring a hooked-end geometry, a length of 30 mm, a diameter of 0.38 mm, an aspect ratio of approximately 80, a declared filament tensile strength of 3070 MPa, and a declared elastic modulus of 210 GPa. These fibres were at dosages of 25 kg/m^3 and 40 kg/m^3 , corresponding to a fibre volume content of 0.32% and 0.51%.

The macro-synthetic fibres were commercially available virgin polypropylene fibres with a length of 48 mm, a continuous embossing surface texture providing mechanical anchorage, a declared filament tensile strength of 640 MPa, and a declared Young's modulus of 12 GPa. These fibres were used at a dosage of 7 kg/m^3, corresponding to a fibre volume content of 0.78%.

Based on the fibre type and dosage, the fibre-reinforced concretes are designated as SFRC-25 and SFRC-40 for the steel fibre-reinforced concretes with 25 kg/m^3 and 40 kg/m^3 dosages, respectively, and MSFRC-7 for the macro-synthetic fibre-reinforced concrete with 7 kg/m^3, as detailed in Table 4.1.

The details of concrete mix design and the fibres properties are presented in Table 4.2 and Table 4.3, respectively.

Table 4.2: Mix Proportions of concrete.

Igredient	**Mix**
Aggregate (sand,gravel) [kg/m^3]	1494
Sand 0/2 [kg/m^3]	1089
Aggregate 2/6 [kg/m^3]	405
Maximum aggregate size [mm]	6
Cement type	CEM II/A-LL 42.5
Cement content [kg/m^3]	550
Water–cement ratio [-]	0.37
Superplasticizer [l/m^3]	5.5

Table 4.3: Fibre properties.

Fibre name	**Material**	**Length** (L_f)	**Dia** (Φ_f)	**Aspect ratio** (L_f/Φ_f)	**Fibre dosage**	**Elastic Modulus** (E_m)	**Filament tensile strength** (T_s)
		[mm]	[mm]	[-]	[kg/m^3]	[GPa]	[MPa]
S-0.38-80	Steel	30	0.38	80	25	210	3070
S-0.38-80	Steel	30	0.38	80	40	210	3070
MS 48	MS	48	-	-	7	12	640

4.3 Preparation of Specimens

The specimens were prepared at the Structural Laboratory of the University of Brescia. All specimens were produced over three production cycles. A single type of concrete mix, as discussed in Section 4.2 and detailed in Table 4.2 was used across all cycles, with different types of fibre and dosages of fibre. In the first cycle, a macro-synthetic fibre dosage of 7 kg/m^3 (MSFRC-7) was used. In the second cycle, 25 kg /m^3 of steel fibres (SFRC-25) were incorporated, and in the third cycle, the steel fibre dosage was increased to 40 kg /m^3 (SFRC-40).

Panels for the 3PB test on notched panels (EN 14488-3, Method B [16]) and for the energy absorption test in accordance with EN 14488-5 [18], as well as beams for the three-point bending test (3PBT) in accordance with EN 14651 [7], were prepared using the wet-mix spraying process and conventional casting in moulds.

4.3.1 Preparation of Moulds

The spraying and casting processes was carried out according to EN 14488-1 [163]

4.3.1.1 Sprayed and Cast Square Panels

Nine Large moulds with dimensions of (100 mm x 640 mm x 1880 mm) were prepared for panel spraying and casting. Each mould was configured to produce three square panels measuring (100 x 600 mm x 600 mm), separated by a 40 mm thick wooden divider, as shown in Figure

4.2. In total, these moulds yielded 27 panels.

The panels were grouped according to their intended use. A set of 15 square panels was designated to spray according to EN 14488-1 [163] to perform the 3PBT EN 14488-3 Method B test [16], while three square panels were used to cast to perform the same test. Another 6 panels were also sprayed according to EN 14488-1 [163] to perform energy absorption tests according to EN 14488-5 [18], along with three square panels (100 x 600 mm x 600 mm) cast for the same test. All the panels were used over three cycles of the spraying and casting process.

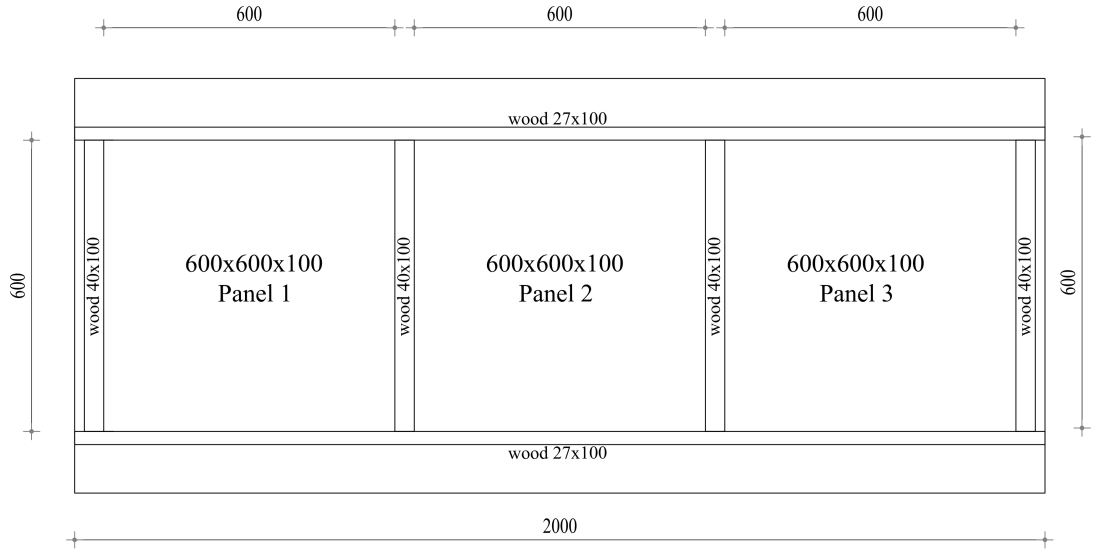

Figure 4.2: Square panels (600 mm x 600 mm x 100 mm) and wood moulds for sprayed and cast panels, dimensions in [mm].

4.3.1.2 Large Panels for Beam Saw Cutting

A large mould with a dimension of (150 mm x 2000 mm x 800 mm) was prepared for the spraying of the panels. From each sprayed in this mould, eight beams measuring (150 mm x 150 mm x 600 mm) were cut along the longer dimension, and five beams were cut along its shorter dimension (see Figure 4.3) for the subsequent test in accordance with EN 14651 [7]. As it will discussed in Section 4.5.3, the main goal was to test samples according to the experimental set-up provided by EN 14651 but with a fibre orientation and distribution well representative of a permanent sprayed concrete lining (PSCL). Furthermore, beams were saw-cut in two directions, make possible to investigate the post-cracking performance exhibited by sprayed FRCs related two positions of possible crack planes in the PSCL.

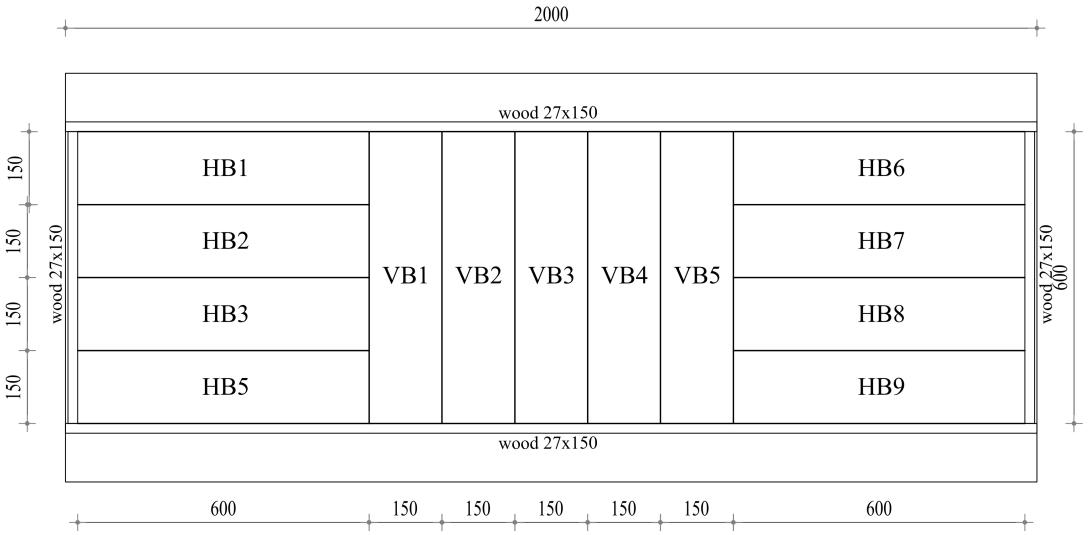

Figure 4.3: Large sprayed panel (2000 mm x 800 mm x 150 mm) for beam EN 14651 saw cut, dimensions in [mm].

4.3.2 Preparation of Sprayed Samples and Spraying Procedure

The plywood formworks panels, which prepared with the required dimensions shown in the Figure 4.2 and Figure 4.3 were positioned at approximately 20 degree with the vertical plane, as recommended in EN 14488-1 [163].

The spraying was carried out using the wet-mix process, in which ready-mixed concrete is conveyed hydraulically through pumping to the nozzle, where compressed air is added to ensure high velocity and a liquid accelerator was added at the nozzle to promote rapid setting and adhesion on the target surface. The concrete was then sprayed at high velocity onto the inclined panels.

All spraying processes were carried out outdoors. The wet-mix shotcrete mixtures was produced with shotcrete pump (Figure 4.6) connected to a long rubber delivery hose having a 50 mm internal diameter. For the spraying operation, the hose outlet was fitted with a nozzle (Figure 4.6b), through which compressed air is introduced via air ring. The diameter of the nozzle was 36 mm. During application, the distance between the nozzle and the panels was approximately 1.5 m. The accelerator was opportunely adjusted by the nozzle-man, with the amount reduced for the last layer of the panel to slow the concrete setting, making it easier to screed and achieve a uniform thickness and smooth surface. Both aspects are fundamentals for getting consistency results from experimental tests.

The freshly sprayed panels were covered with a plastic sheeting for a period of 24 hours to prevent moisture loss. Then, the samples were transferred to the laboratory and demoulded. After demolding the specimen were cured under moisture condition for 3 days. After the week the large panels intended for saw-cut beam specimens were cut to the required dimensions. In the following days, the beams prepared for the EN 14651 flexural test and the panels for EN 14488-3 Method B were notched using a water-cooled diamond circular table saw (Figure 4.15). The specimens were kept at room temperature for the remaining 7 days before testing. This curing sequence was done due to the large number of specimens involved in the experimental program.

(a) (b)

Figure 4.4: Outdoor panel layout prior to spraying: (a) Overall 20°-inclined layout of panels; (b) Detail view showing the 20° inclination of the plywood formwork.

Figure 4.5: Outdoor spraying of the panels using the wet mix spraying process.

(a)

(b)

Figure 4.6: Spraying process equipment: (a) Wet-mix process shotcrete pump; (b) Nozzle and hose detail.

Figure 4.7: Sprayed panels prepared for the EN 14488-3 Method B 3PBT notched panel test [16], along with the large panels intended for sawn-cut beams for the EN 14651 3PBT notched beam test [7].

4.3.3 Casting Sample Preparation (Panels and Beams)

In each cycle of the casting process, three panels were prepared for each of EN 14488-3 Method B [160] and the energy absorption test [18] see Figure 4.27. No mechanical vibration was applied during casting. Compaction was achieved by manual external hammering of the moulds along all sides taking advantage from the good workability of concrete (consistency class, S5). The panels were cast from the centre by means of a concrete bucket with side opening system which probably induced a preferable casting flow direction due to the rather good concrete flowability. Note that it was decided to initially plan the notch direction perpendicular to this preferable direction, the casting direction was opposite to the planned notch direction to consider the effect of fibre orientation with fibres likely aligning preferentially in the direction of flow. For the cast panel belonging to series SFRC40, the notch direction and the casting process were more investigated with respect to SFRC25, as described in Section 4.5.6.2.

A set of 12 beams (150 mm x 150 mm x 600 mm) was prepared in steel formwork. The procedure of filling the mould was as per section 7.2 of EN 14651 [7]. The central increment had twice the volume of the increments placed on the left and right. The moulds were filled to approximately 90% of the specimen height prior to compaction. External mechanical vibration

was then applied using a vibrating table, as shown in Figure 4.9a.

(a)

(b)

Figure 4.8: Panel casting procedure for the EN 14488-3 Method B [16] test methodology: (a) Moulds used for casting the panels; (b) Cast panel specimen.

(a)

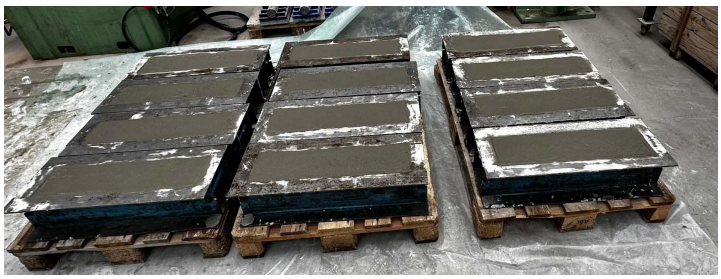

(b)

Figure 4.9: Casting procedure for EN 14651 [7] three-point bending test (3PBT) beams: (a) Beam casting using an external vibrating table; (b) Cast beam specimens.

4.3.3.1 Specimen Preparation for Compressive-Strength and Elastic-Modulus Tests

Cubes for compressive strength testing and cylinders for elastic modulus evaluation were cast in accordance with their respective standards. A total of 24 cubes for each cycle were prepared and tested at 1, 3, 7, 10, 14, 28, 56, and 90 days. Additionally, six cylinders were also cast to determine concrete's elastic modulus (Figure 4.10).

The compressive strength of sprayed concrete was also evaluated on sprayed elements, in accordance with the recommendations of EN 14487-1 [19]. Accordingly, cores samples were extracted from the sprayed concrete panels and tested for compressive strength at the same

interval as the cast specimens. These cylinders were obtained using a coring extraction machine equipped with a 100 mm diameter drill bit, as shown in the Figure 4.11.

(a) (b)

Figure 4.10: Specimen preparation for compressive strength and elastic modulus tests: (a) Steel moulds for casting concrete cubes and cylinders; (b) Cast cube and cylinder specimens.

(a) (b)

Figure 4.11: Compressive strength testing of cored cylinders extracted from sprayed panels: (a) Cored cylinders obtained from the sprayed panels ; (b) Compressive strength test set-up for the cored cylinders.

4.3.4 Preparation of Test Specimens

The beams and panels, after notching and final preparation, were stored in a climate chamber set at a temperature of 25 °C and a relative humidity of 80-90%. Prior to testing, the specimen were cleaned, surface dried, and measured. The specimens were tested at an age between 26 and 32 days. Although the plan was to test them exactly at 28 days according to the standard, logistical constraints prevented strict adherence to this schedule. The sprayed panels and beams were tested according to EN 14488-3 Method B [16] and EN 14651 [7], respectively, at 90 days, as specified in the experimental programme (Table 4.1).

4.3.4.1 Preparation of Saw-Cut Beams from sprayed panels for EN 14651 Testing

Two large panels, shown in Figure 4.3, were sprayed in each cycle of casting process. From each panel, 13 Beams were saw-cut (Figure 4.12), yielding a total of 26 beams per cycle. These beams were then used carry out the EN 14651 [7] three-point bending test (3PBT) at 28 and 90 days.

After saw-cutting, the beams were notched to a depth of 25 mm as per the standard requirements. The notching layout is shown in the Figure 4.13. Care was taken to ensure that the notches were not cut at the same longitudinal position on adjacent beams to better investigate the fibre orientation and distribution. In fact, two adjacent standard beams with notch cut in the same longitudinal position are expecting to have the same fibres distribution and orientation on the bending side in tension, resulting in similar post-cracking residual strengths. A minimum spacing of 150 mm was maintained between notch locations, as illustrated in Figure 4.13.

(a) (b)

Figure 4.12: Saw-cut layout and resulting beams for the EN 14651 [7] 3PBT: (a) Saw-cut layout of the large sprayed panel; (b) Saw-cut beam specimens.

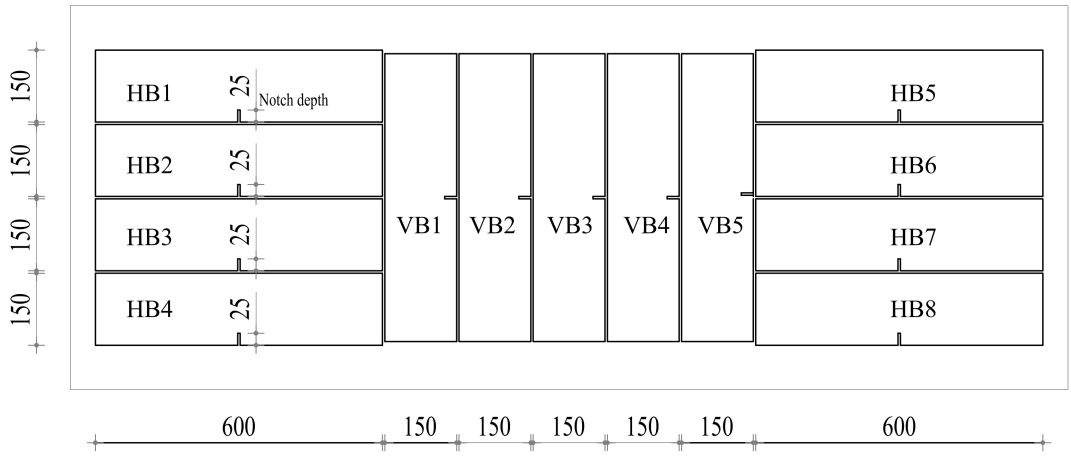

Figure 4.13: Saw cut and notched layout of sprayed beams for EN 14651 [7] 3PBT.

The geometry illustrated in Figure 4.14 was adopted for all beam tests in accordance with EN 14651 [7]. however all saw-cut beams specimens were individually measured prior to testing, and the actual dimensions were used in subsequent data analysis.

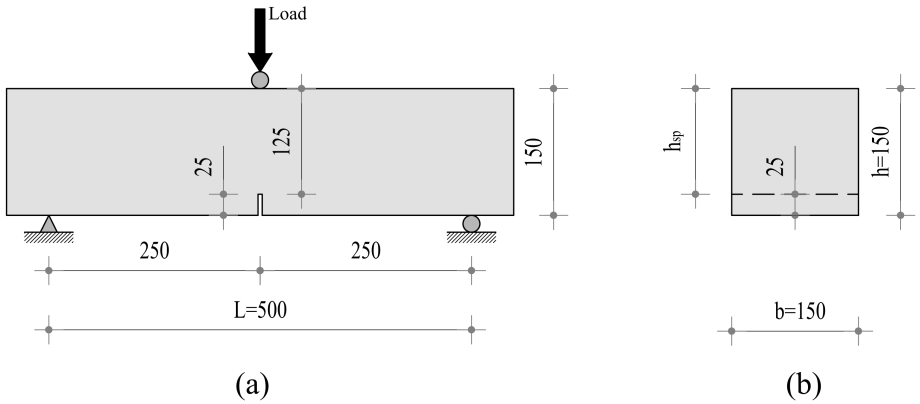

Figure 4.14: Specimen geometry for EN 14651 [7] test methodology: (a) Front view of the beam specimen; (b) Cross section of beam specimen (dimensions in mm).

4.3.4.2 Preparation of Test Specimens for EN 14488-3 Method B Testing

The spraying processes was carried out according to EN 14488-1 [163] and as described in Section 4.3. The geometry of the specimen for all panels is as depicted in Figure 4.16. As mentioned above EN 14488-3 Method B [16] test methodology performed on both the sprayed and cast panels. As per the standard EN 14488-3 Method B [16] a 10 mm notch was provided at the mid-span on the bottom face of the panel as shown in the Figure 4.16 using concrete blade as shown in the Figure 4.15. For the sprayed panels, the notch oriented perpendicular to the gravitational direction or to the horizontal of the spraying plane. For the cast panels, the notch was provided perpendicular to the probable preferable induced casting direction (flow direction). Specifically for the SFRC40 cast series, the prepared samples were notched parallel to the expected concrete flow direction and also some samples perpendicular to the expected concrete flow direction, in order to examine the relationship between the residual flexural strength of the FRC panel and the probable concrete flow direction 4.5.6.2.

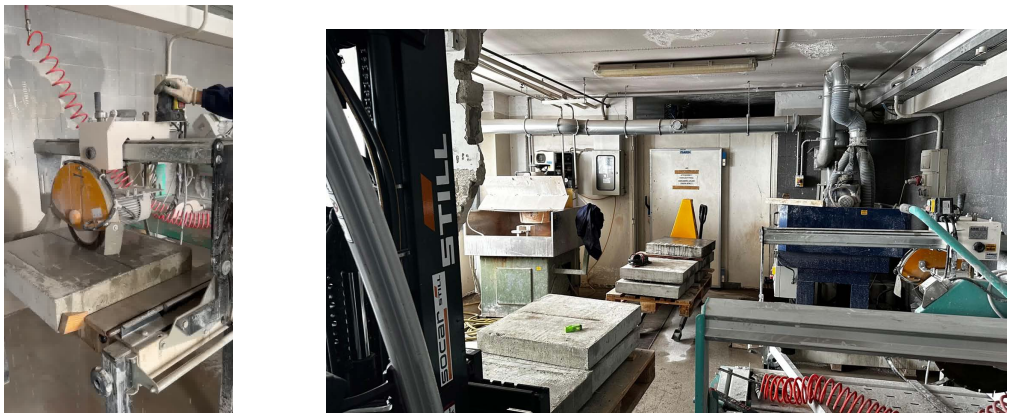

(a) (b)

Figure 4.15: Test panel preparation for EN 14488-3 Method B Panel: (a) Notching panel; (b) Prepared notched panel.

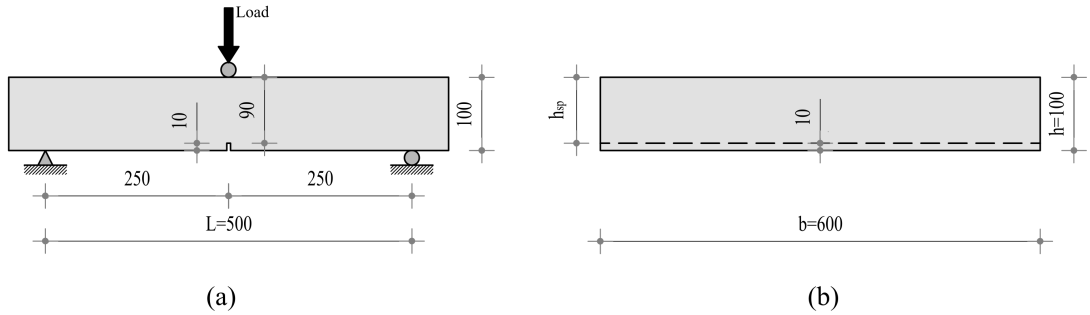

Figure 4.16: Specimen geometry for the EN 14488-3 [16] test methodology: (a) Front view of the panel specimen; (b) Panel cross section of the specimen (dimensions in mm).

4.4 Experimental Test Set-up

4.4.1 Three-point Bending Notched Panel Test (EN 14488-3)

The specimen geometries and test configurations followed the guidelines specified in the relevant standards EN 14488-3 [16] and EN 14487-1 [19], as detailed in Section 2.5.1.1. Figure 4.17 and 4.18a show the test set-up adopted for all panel specimens, while Figure 4.18b presents the instrumentation details. All tests were conducted using an INSTRON 1274 closed-loop servo-hydraulic testing machine with a load capacity of 500 kN, as shown in Figure 4.17. The experiments were carried out under displacement (CMOD) control, as described in Section 2.5.1.1.

The Crack Mouth Opening Displacement (CMOD) was measured using a clip gauge (Figure 4.18b) in strict compliance with the standard. In addition to the standard requirements, further measurements were carried out to obtain a more comprehensive understanding of crack development, structural response at larger deformations, and the correlation between the response parameters. Specifically, the Load Point Displacement (LPD) was measured using two LVDTs positioned at mid-span on the front and rear faces of the specimen, and the recorded values were averaged to obtain the representative LPD. Similarly, the Crack Tip Opening Displacement (CTOD) at the notch tip was measured on both faces using a pair of LVDTs, with the averaged values taken as the representative CTOD (Figure 4.18). Linear Variable Differential Transducers (LVDTs) with a measuring range of 10 mm were used to record the CTOD and LPD measurements.

The experiments were conducted with CMOD as the controlling parameter, reaching up to 5.0 mm. Two displacement rates were used: 0.05 mm/min up to a CMOD of 0.2 mm, followed by 0.2 mm/min up to a CMOD of 5.0 mm. After this point, the loading mode was changed to LPD control and the tests were continued until the load decreased to approximately 1% of the peak load or the mean CTOD (obtained by averaging the front and rear measurements) reached approximately 8.5 mm. Data acquisition was performed at a rate of 5 Hz for the first two minutes and then reduced to 2 Hz for the remainder of the test.

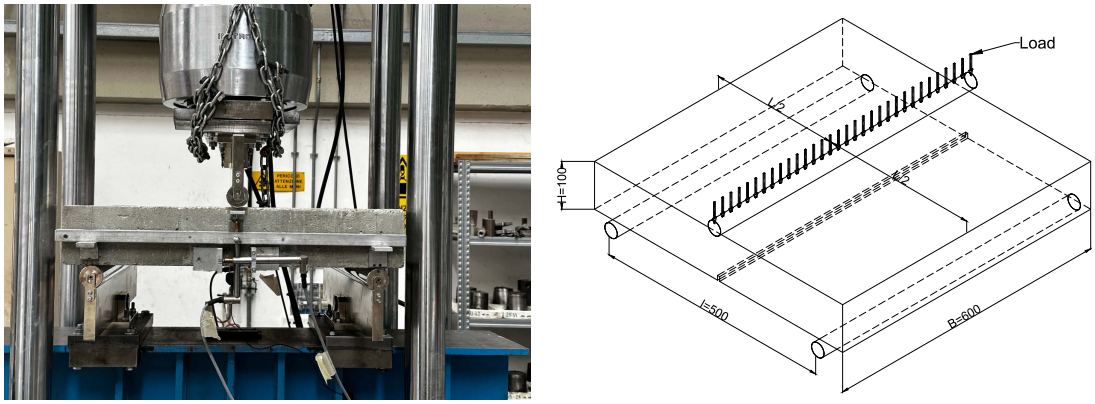

(a) (b)

Figure 4.17: Set-up for EN 14488-3 test methodology [16]: (a) INSTRON 1274 closed-loop servo-hydraulic machine (b) Arrangement of load application on the test specimen.

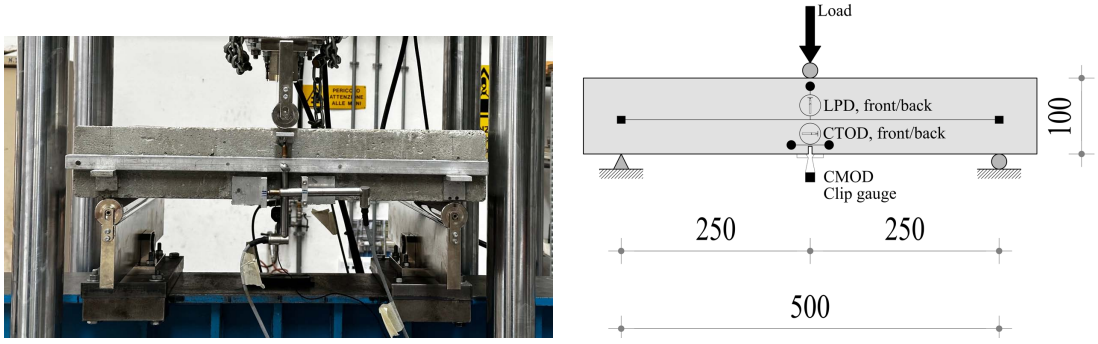

(a) (b)

Figure 4.18: Square panels with notch tested according to EN 14488-3 [16]: (a) Test set-up; (b) Instrumentation details (dimensions in mm).

Figure 4.19: EN 14488-3 Method B notched sprayed panel after testing, showing crack formation and panel deformation [16].

4.4.2 Three-Point Bending Notched Beam Test (EN 14651)

The specimen geometries and the test setup were followed in accordance with the requirements of the relevant standard EN 14651 [7], as thoroughly detailed in Section 2.1.3.3. The geometry illustrated in Figure 4.21 was used consistently for all beam tests; however, the cross section of each individual beam was measured prior to testing, and the measured dimensions were used in the analysis in accordance with EN 14651 [7].

The testing procedure for the beams followed the same principles applied to the panel tests,

ensuring consistency in instrumentation and control methodology. Figure 4.22a presents the test setup adopted for all beam specimens, while Figure 4.22b illustrates the instrumentation detail. All experiments were conducted using an INSTRON 1274 closed-loop servo-hydraulic testing machine with a loading capacity of 500 kN, as shown in Figure 4.22a. The tests were carried out under CMOD control as described in Section 2.1.3.3.

Linear Variable Differential Transducers (LVDTs) were used to measure the load point displacement (LPD) and the crack tip opening displacement (CTOD) on both the front and rear faces of the beam, with the averaged readings used as the representative LPD and CTOD. The Crack Mouth Opening Displacement (CMOD) was measured using a clip gauge in strict compliance with the requirements of the relevant standard (Figure 4.22). The experiments were performed under CMOD as the controlling parameter up to a value of 5.0 mm. Two displacement rates were used: 0.05 mm/min up to a CMOD of 0.1 mm, followed by 0.2 mm/min until reaching a CMOD of 5.0 mm.

After reaching the target CMOD, the control mode was switched to LPD control, and the tests were continued until the load decreased to approximately 1% of the peak value or until the mean CTOD (obtained by averaging the front and rear measurements) reached approximately 8.50 mm. Data acquisition was performed at a rate of 5 Hz during the first two minutes of testing and then reduced to 2 Hz for the remainder of the experiment.

Figure 4.20: Set-up for EN 14651 [7] with INSTRON 1274 closed-loop servo-hydraulic testing machine.

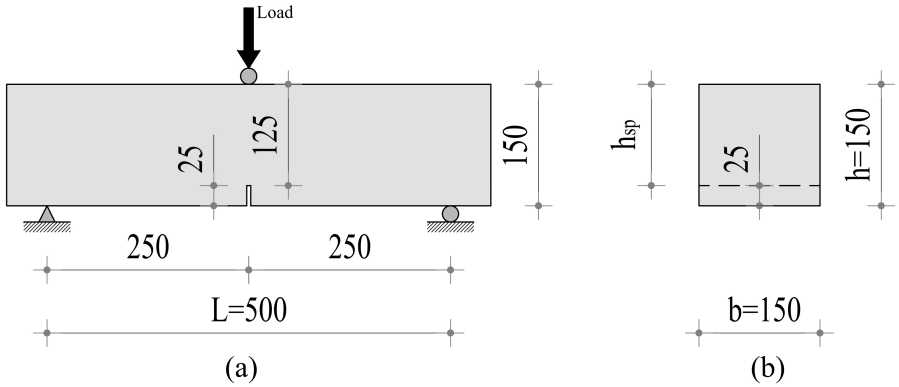

Figure 4.21: EN 14651 [7] test methodology: (a) Front view of the beam specimen; (b) Cross section of beam specimen (dimensions in mm).

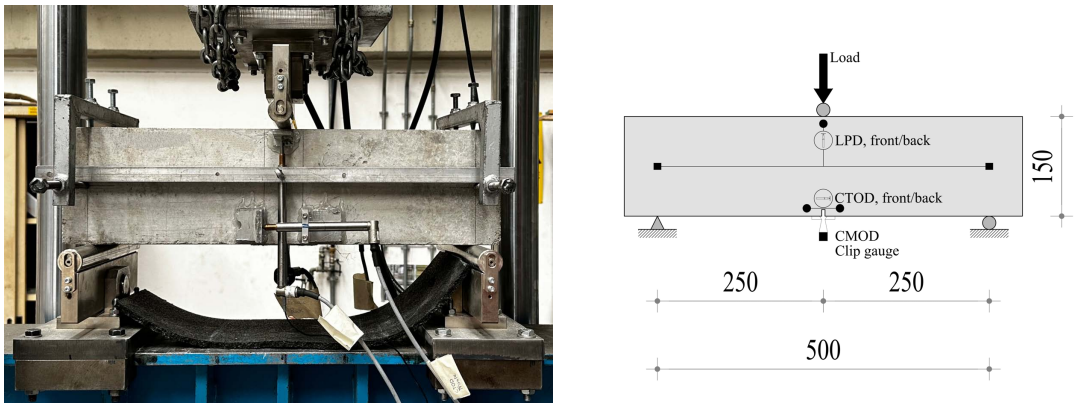

Figure 4.22: Three-point bending notched beam test according to EN 14651 [7]: (a) Test set-up; (b) Instrumentation details (dimensions in mm).

Figure 4.23: EN 14651 saw-cut notched beam specimen after testing, showing crack formation and beam deformation.

4.4.3 Energy Absorption Capacity Test (EN 14488-5)

The energy absorption capacity test is a deflection-controlled test conducted on a square panel measuring 600 × 600 × 100 mm, in accordance with the standards EN 14487-1 [19] and EN 14488-5 [18], as detailed in Section 2.5.2.2. The specimen geometry follows the respective standards and is further described in Section 2.5.2. All the panels tested the experiment campaign adopted the geometry depicted in Figure 4.25. The spraying and casting processes were carried out according to EN 14488-1 [163] and the procedures described in Section 4.3 of this thesis.

The specimen was placed on a square steel frame with a width of 20 mm and internal dimensions of 500 x 500 mm, as shown in the Figures 4.24 and 4.25. A steel plate measuring 100 × 100 mm with a thickness of 20 mm was positioned between the upper surface of the panel and the loading cell to ensure a uniform distribution of the load across the panel, as illustrated in Figure 4.25.

The load application system consisted of an electromechanical screw jack with a maximum capacity of 500 kN, used to apply the load under displacement-control conditions. Load measurement was obtained using A 200 kN load cell connected to a data acquisition system (Figure 4.24).

The central deflection at the midpoint of the specimen was measured using a Linear Displacement Transducer (LDT) with a measuring range of 50 mm, positioned on the underside of the specimen, as schematically illustrated in Figure 4.24 and Figure 4.25. Additionally, four LDTs with a measuring range of 20 mm were installed on the upper surface of the panel, one on each side, to record the displacements at the supports (Figures 4.24 and 4.25).

These measurements were used to generate the load-net deflection curve and energy-net deflection curve, as described in detail in Section 2.5.2.2. The energy absorption capacity was determined as the area under the load–deflection curve up to a net deflection of 25 mm, in accordance with the requirements of EN 14488-5 [18].

(a) (b)

Figure 4.24: Energy absorption test according to EN 14488-5 :(a) Electromechanical screw jack and rigid foundation support set-up; (b) Detail test setup.

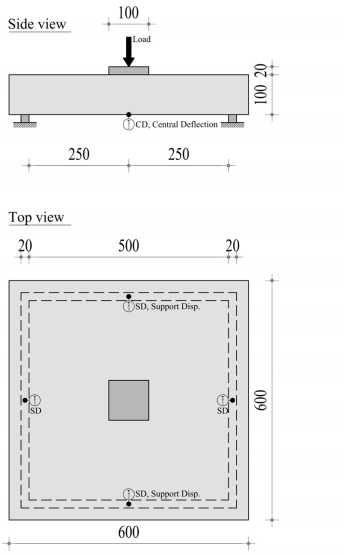

Figure 4.25: Instrumentation and specimen detail for the energy absorption capacity test (EN 14488-5) methodology.

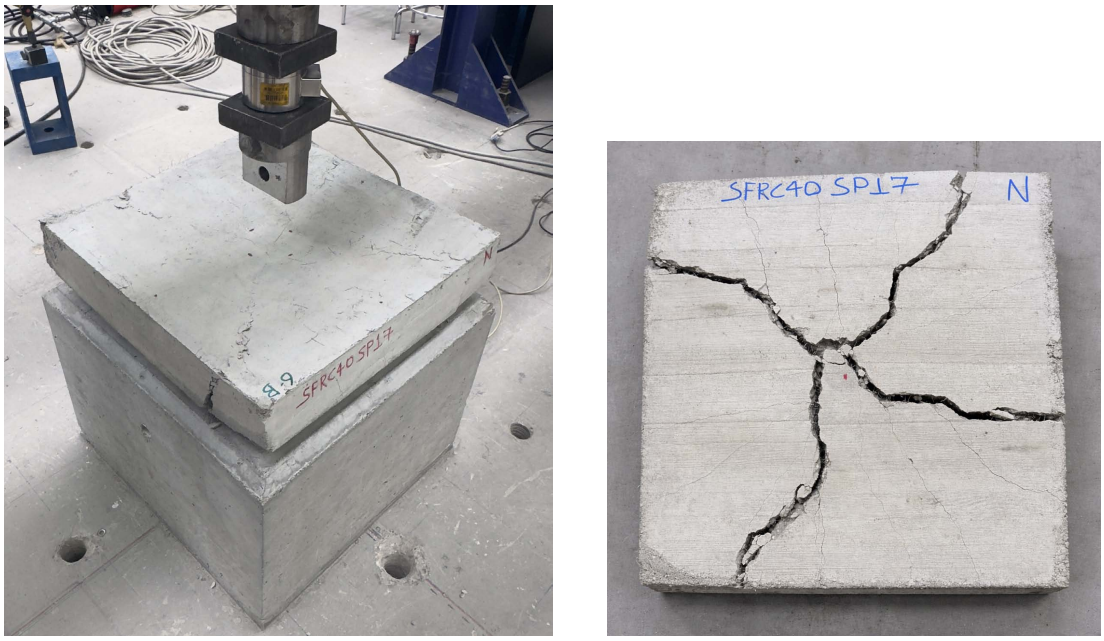

(a) (b)

Figure 4.26: Energy absorption test (EN 14488-5) after testing :(a) Test set-up and panel specimen ; (b) Crack pattern observed on the bottom surface of the panel.

4.5 Experimental Results and Discussions

4.5.1 Compressive Strength and Elastic Modulus

According to the specification for sprayed concrete, EN 14487-1 [19], the performance requirements include compressive strength. The compressive strength of the sprayed concrete was expressed and defined in accordance with EN 206 [165], while its sampling and testing were conducted following the procedure specified in EN 12504-1 [166]. The letter refers to EN 12390-3 [167] for testing in compression drilled core concrete samples. Hence, cylindrical samples having a diameter of ≈ 100 mm and a height of ≈ 100 mm samples were drilled from a panel ($1050 \times 750 \times 250$ mm) specifically sprayed for this purpose. Conventional concrete cubic samples (150×150 mm), cast-in-moulds, were also prepared for testing in accordance with EN 12390-3 [167]. Compressive strength tests were performed at the interval specified in Table 4.1 for both sprayed and cast specimens.

(a) (b)

Figure 4.27: Experimental setup: (a) Compressive strength test using a 3000 kN hydraulic press; (b) Elastic modulus test with displacement transducers.

It is worth noting that the compressive strength obtained from drilled-core samples taken from the large sprayed panels is hereafter referred to as the cubic compressive strength of

sprayed concrete, since the diameter and height of the cylindrical samples were in a 1:1 ratio as stated by EN 13791 [168], which clearly stated testing a core with equal length and a nominal diameter of 100 mm gives a strength value equivalent to the strength value of a 150 mm cube manufactured and cured under the same conditions.

The target compressive strength class C_{35} as defined in the Model Code 2010 [1] was achieved for both SFRC-25 and SFRC-40 with a mean cubic compressive strength values ($f_{cm,\text{cubic}}$) of 49.4 MPa and 52.1 MPa, respectively,determined on cast specimens. The evolution of concrete compressive strength over time is illustrated in Figure 4.28. At 7 days the mean compressive strength ($f_{cm,7}$), were 43.9 MPa and 47.5 MPa for SFRC-25 and SFRC-40, respectively, corresponding to approximately 87-91% of the 28-day strength. Beyond 28 days, the strength development tends to stabilize, with only a marginal increase observed at 90 days, where the mean values $f_{cm,90}$ reached 51.23 MPa and 54.48 MPa for SFRC-25 and SFRC-40, respectively.

In comparison the mean cubic compressive strength ($f_{cm,\text{cubic}}$) values for the sprayed specimens were 42.9 MPa and 43.5 for SFRC-25 and SFRC-40, respectively. At 7 days, the mean compressive strength ($f_{cm,7}$, were 32.60 MPa and 35.30 MPa for SFRC-25 and SFRC-40, respectively, corresponding to approximately 76-80% of the 28-day strength. Beyond 28 days, the strength development of the sprayed concrete also tends to stabilize, with only a marginal increase observed at 90 days, where the mean compressive strength $f_{cm,90}$ reached 45.4 MPa for SFRC-25 series.

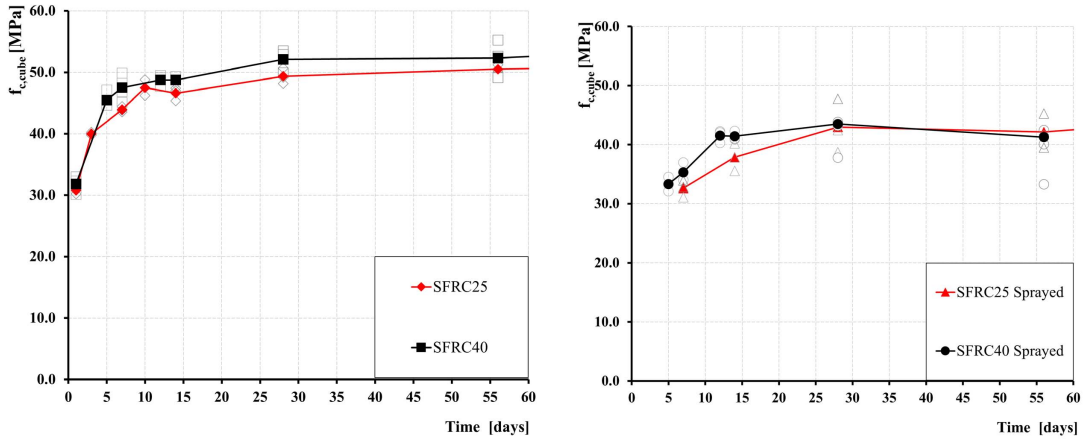

(a) (b)

Figure 4.28: Compressive strength results with respect to concrete ageing: (a) Cast specimens; (b) Sprayed specimens.

In the investigation, as shown in Figure 4.28 and Table 4.4, a clear difference observed in the compressive strength between the cast and sprayed specimens (drilled core from a sprayed panel). The compressive strength was tested at different ages ranging from 3 to 90 days. At approximately 28 days, the cubic compressive strength of the sprayed concrete ($f_{cm,\text{sprayed}}$) is about 0.87 times that of cast ones for SFRC-25 and 0.83 times for SFRC-40, thus on average $f_{cm,sprayed}$ reached about 85% of the corresponding cast concrete strength (Equation 4.1).

The lower compressive strength of the sprayed concrete might be attributed to several factors. Unlike cast-in-mould cubes, sprayed concrete is not subjected to vibration, which may result in less uniform compaction and a more porous internal structure. By considering all samples utilized for determining the compressive strengths, the density of sprayed specimens resulted -5.2% lower relative to the density of cast cube samples for SFRC-25; however, this difference was not observed in the SFRC-40 series, where a difference of -0.9% was obtained.

In addition, since the sprayed samples were cored from sprayed panels, part of the strength reduction may be attributed to micro-defects and microcracking induced by the drilling process. In this regard, a unique damage factor 1.06 has been suggested in ACI PRC-214.4-21 [169] and proposed by [170]. A damage factor is also suggested by Italian Explanatory Circular update of the Technical Standard for Construction, NTC 2018 [171], ranging from 1.10 to 1.00 depending on the concrete strength class.

In general, it seems that the dominant contribution is associated with the spraying process itself. The observed reduction in bulk density indicates an increase in void content due to the spraying mechanism. Additionally, the process alters the pore structure, induces microcracking, and modifies the characteristics of the interfacial transition zone (ITZ), the interface between coarse aggregate and cement paste, thereby influencing the overall microstructural integrity of the hardened concrete.

$$f_{cm,\text{Sprayed}} = 0.85\, f_{cm,\text{Cast}} \tag{4.1}$$

The modulus of elasticity is one of the fundamental mechanical properties of fibre-reinforced concrete. The parameter is typically determined through tests performed on specimens subjected to uniaxial compressive loading. In this thesis, the secant elastic modulus was evaluated for each series according with EN 12390-13 [172] (Figure 4.27b). Comparable results were obtained within each series, as presented in the mechanical properties of cast and sprayed concrete in Table 4.5.

Table 4.4: Summary of measured compressive strength and spray/cast ratio for all SFRC mixes.

Mix ID	**Age (days)**	**Cast (MPa)**	**Spray (MPa)**	$k = f_{\mathbf{spray}}/f_{\mathbf{cast}}$	$k(28)$	**Relationship at 28 days**
SFRC-25	7	43.93	32.60	0.74	0.87	$f_{\text{spray}}(28) = 0.87\, f_{\text{cast}}(28)$
	14	46.58	37.86	0.81		
	28	49.35	42.97	0.87		
	56	50.51	42.13	0.83		
	91	51.23	45.42	0.89		
SFRC-40	5	45.46	33.32	0.73	0.83	$f_{\text{spray}}(28) = 0.83\, f_{\text{cast}}(28)$
	7	47.51	35.30	0.74		
	12	48.75	41.52	0.85		
	14	48.75	41.42	0.85		
	28	52.11	43.49	0.83		
	56	52.33	41.26	0.79		

The elastic modulus results obtained from cast-in-mould samples were lower than those of ordinary concrete of the same concrete class, as currently estimated by the typical relationships proposed in Eurocode 2 [9] and *fib* Model Code 2010 [8]. This can be due to the lower maximum aggregate size used in the concrete and the cementitious property of the concrete. The elastic modulus of sprayed SFRC-25 is about 3.6% lower than that of cast specimens (assumed as the reference), while in case of SFRC-40 this percentage reduction is 8.5%.

Table 4.5: Mechanical properties of cast and sprayed concrete.

Parameters	**Cast**			**Sprayed**	
	SFRC-25	**SFRC-40**	**MSFRC-7**	**SFRC-25**	**SFRC-40**
$f_{cm,\text{cube}}$ (MPa)	49.4	52.1	40.0	43.0	43.5
	(0.03)	(0.04)	(0.02)	(0.11)	(0.01)
f_{cm} (MPa)	41.0	43.3	33.2	35.7	36.1
E_c (MPa)	24100	26300	21400	23200	24000
	(0.01)	(0.03)	(0.02)	(0.06)	(0.07)

4.5.2 Shrinkage Test

The test setup and the procedure followed according to the standard EN 12390-16 [173]. Prismatic specimens with nominal dimensions of 75 × 75 × 285 mm were used for the shrinkage test. Steel gauge studs were embedded at both ends along the longitudinal axis to allow precise length-change measurements using a mechanical comparator. For each specimen tested as per the schedule in Table 4.1, the total shrinkage strain, expressed as 10^{-6} (micro-strain), is calculated at time t from:

$$\varepsilon_{cs}(t, t_0) = \frac{l(t_0) - l_{cs}(t)}{L_0} \tag{4.2}$$

where L_0 is the gauge length (specimen length), in mm; $l(t_0)$ is the initial length at time t_0, in mm; $l_{cs}(t)$ is the length at time t, in mm; and $\varepsilon_{cs}(t, t_0)$ is the total shrinkage strain of the specimen at time t.

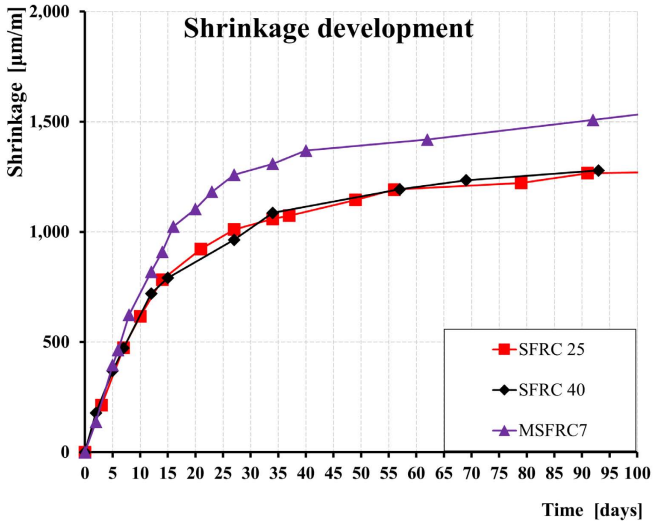

Figure 4.29: Shrinkage results for SFRC-25, SFRC-40, and MSFRC7 up to 100 days.

Figure 4.29 outlines the shrinkage development of SFRC-25, SFRC-40, and MSFRC-7 series over more than 90 days. All series show a rapid increase in shrinkage within the first 28 days, followed by a gradual stabilization thereafter. Increasing fibre dosage from 25 to 40 provides only a marginal additional reduction in shrinkage. At 28 days, the shrinkage strains were 1011 µm/m, 964 µm/m, and 1259 µm/m for SFRC-25, SFRC-40, and MSFRC-7, respectively. The relatively high shrinkage may be attributed to the cementitious matrix and the 6 mm maximum

aggregate size, which implies a less stiff aggregates' skeleton to counteract the shrinkage of cement paste. It is worth noticing that free shrinkage vs. time curves as plotted in Figure 4.29 provide important information for modelling the interaction between permanent sprayed linings in case of Composite Shell Lining (CSL) and Double Shell Lining (DSL) solutions 2.4.1.

4.5.3 Fibre Distribution and Orientation

The fibre distribution and orientation of FRC in general are discussed in detail in the state-of-the-art section of this thesis (Section 2.1.7). By using the simple approach briefly described in Section 2.1.7, differences in fibre distribution and orientation are observed between sprayed and cast beams, sprayed and cast panels, sprayed panels and beams, and cast beams and panels, due to their respective underlying factors influencing each element.

Generally speaking, it is of paramount importance to evaluate the possible effects of spraying process (sprayed panels and saw-cut beams from sprayed panels) on fibre orientation and distribution. The latter can be also strongly influenced by the casting process, as in the case of cast panels (see Section 4.5.6.2 about different possible directions considered).

Table 4.6: Measured fibre density (fibres/cm^2) and fibre orientation factor from the cracked cross-sectional plane of beams and panels after testing according to EN 14651 and EN 14488-3 standards, respectively.

Series	**Mean [fibres/cm^2]**	**α_0 Mean orientation factor**
SFRC-25 SB	1.01	0.36
SFRC-25 CB	1.41	0.50
SFRC-40 SB	1.60	0.36
SFRC-40 CB	2.48	0.55
SFRC-25 SP	1.01	0.36
SFRC-25 CP	1.10	0.39
SFRC-40 SP	1.50	0.33
SFRC-40 CP$\perp$	1.95	0.43
SFRC-40 CP+	1.69	0.38
SFRC-40 CP$\parallel$	1.19	0.26
MSFRC-7 CB	1.00	0.74
MSFRC-7 CP	0.75	0.55

After completing the flexural tests, the number of fibres bridging the notch or crossing the crack plane was manually counted for each panel, as illustrated in the cross-section layout in

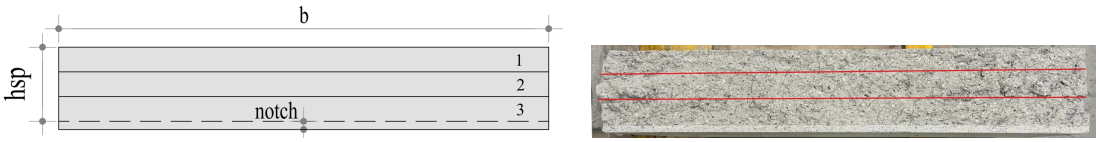

(a) (b)

Figure 4.30: Fibre density measurement layout after the EN 14488-3 Method B notched panel test: (a) Schematic layout and (b) Cross-section photo showing fibre-density regions.

Figure 4.30. The same cross-sectional layout was adopted for the beams. In total, the manual counting was performed on 63 x 2 beam crack faces and 38 x 2 panel crack faces. In the case of steel fibres, a complete debonding mechanism was evidenced by examining both faces of the crack in a given specimen. The fibre densities observed in the three stripes (top, middle, bottom) indicated in the layout shown in Figure 4.30 were rather similar. Thus, the results are presented in terms of average fibre density globally evidenced along the crack-surface.

Moreover, these data constitute the input required for evaluating the fibre orientation factor (Section 2.1.7). The fibre orientation factors determined for SFRC-CB 25 and SFRC-CB 40 cast beam series were 0.50 and 0.55, respectively, which are rather consistent with the value (0.58) reported in the *fib* Model Code 2020 [8] for elements cast and tested according to EN 14651.

The number of fibres per square centimetre (N_f/cm^2, average values) in the SFRC-40 cast beams was higher than in SFRC-25 cast beams. As expected, all series showed that a higher fibre volume fraction resulted in a higher N_f/cm^2. The number of fibres per square centimetre (N_f/cm^2) and orientation factors obtained from both the sprayed and cast series are presented in the Table 4.6.

The results indicate that the sprayed series exhibited lower fibres per square centimetre and consequently lower fibre orientation factors compared with the cast beams. This confirms that fibre orientation and distribution are probably major contributors to the differences in residual strength observed between the cast and sprayed series. Furthermore, based on the established relationship between the residual strength of the standard sprayed panels and that of the standard cast beams, the results presented in Table 4.6 can be used to interpret and compare their mechanical behaviour.

Since the thesis focuses on the relationship of those parameters which discussed and referred on *fib* Model Code [8] and Eurocode 2 [9] for conventional cast-in-mould FRC elements related

with sprayed FRC ones, the results obtained for the standard cast beams align well with the reference values reported in these documents. Although further data would be required to fully validate these findings, the ratios presented in Table 4.6 can be a reference for the design process of sprayed fibre reinforced concrete linings. The relationship between the number of fibres per square centimetre (N_f) and the residual strength for each series is presented in Figures 4.31 and 4.32.

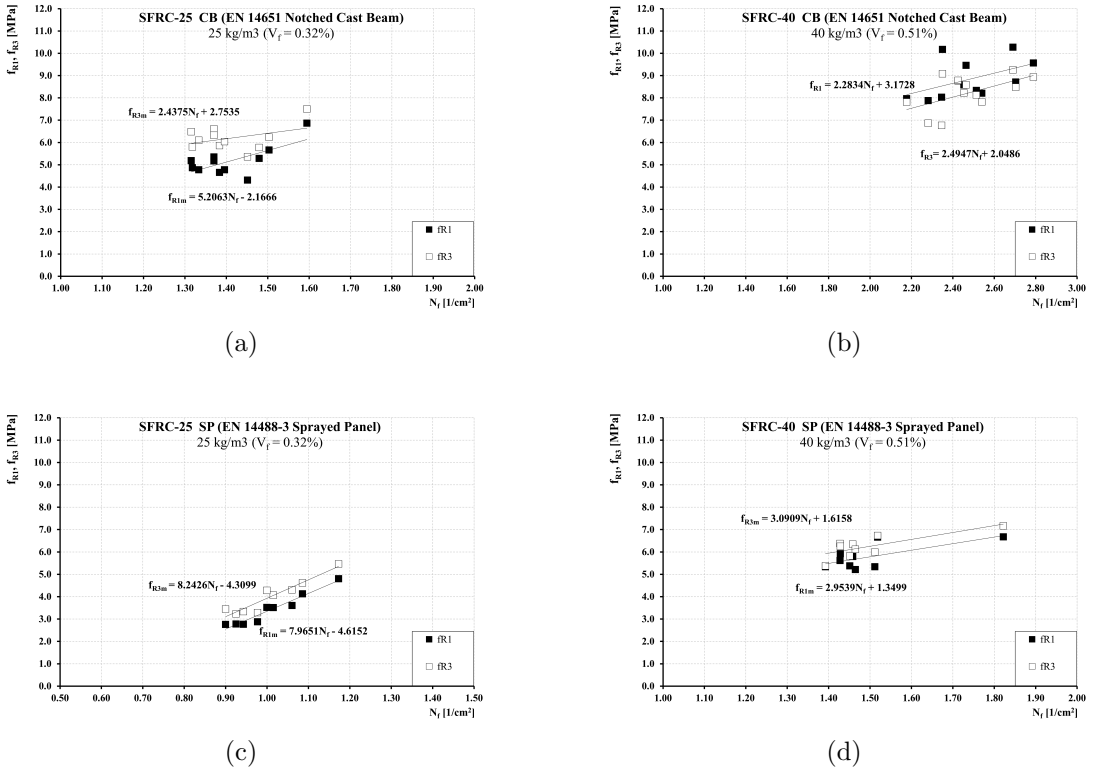

Figure 4.31: Relationship between the number of fibres (N_f/cm^2) and residual strength for SFRC-25 CB (a), SFRC-40 CB (b), SFRC-25 SP (c) and SFRC-40 SP (d).

In addition to the global effect of fibre orientation, this thesis includes an analysis of fibre orientation and distribution specifically within sprayed saw-cut beams. Flexural testing according to EN 14651 (3-point bending test) was performed on notched sprayed beams, as described in Section 4.3.4.1. A total of 52 beams were tested—13 beams per series at 28 and 90 days—comprising 20 vertical beams (with saw-cuts aligned with the direction of gravity) and 32 horizontal beams (with saw cuts oriented perpendicular to gravity). By considering these set of samples, it is possible to investigate the effect of fiber orientation according different directions of investigation and thus, different crack planes possibly occurring in the permanent

sprayed linings. In this regard, in the study by Hung et al. [174], the average number of fibres in the gravity direction was 1.4 and 5.6 times higher than in the lateral and spray directions, respectively, indicating a planar fibre orientation. In the study by A. Blanco et al. [175], the fibres oriented equally for the two directions perpendicular to the spraying direction on the spraying plane.

For the sprayed saw-cut beams tested in this study, the number of fibres per square centimetre (N_f) for the SFRC-25 series was 0.95 in the horizontal beams and 1.10 for the vertical beams. For the SFRC-40 series, the number of fibres per square centimetre (N_f) was 1.61 and 1.60 in the horizontal and vertical orientation, respectively. The corresponding residual strength results are summarised as follows. For SFRC-25 at 28 days, the average flexural strength of the horizontal beams was approximately 9% lower than that of the vertical beams. However, at 90 days, the horizontal beams exhibited a strength of about 15%. For SFRC40 at 28 days, the horizontal (lateral) beams demonstrated approximately 15% higher strength compared to the vertical beams, which is consistent with the 90-day results observed for SFRC-25. At 90 days, the SFRC-40 beams showed only a 3–4% difference in strength between the orientations.

Overall, the horizontal beams generally demonstrated slightly higher residual strengths. This trend was consistent across three of the four large panels, corresponding to 39 of the 52 beams tested. However, the differences between horizontal and vertical orientations of fibres remained relatively small. Therefore, based on both the residual strength results and the fibre-orientation analysis, this study did not observe the pronounced orientation-related effects reported in [174], demonstrating that tendencies about this topic strongly depends on the type of fibres, fibre content and concrete matrix in terms of class of consistency, amount of cement for a given w/c ratio and maximum diameter of aggregates. Since the study presented herein regards two steel fiber content of a typical fiber length used for sprayed concrete adopted in a concrete with a typical target compressive strength for use in sprayed permanent lining, the tendencies stemming out seems useful for the scientific community and among practitioners.

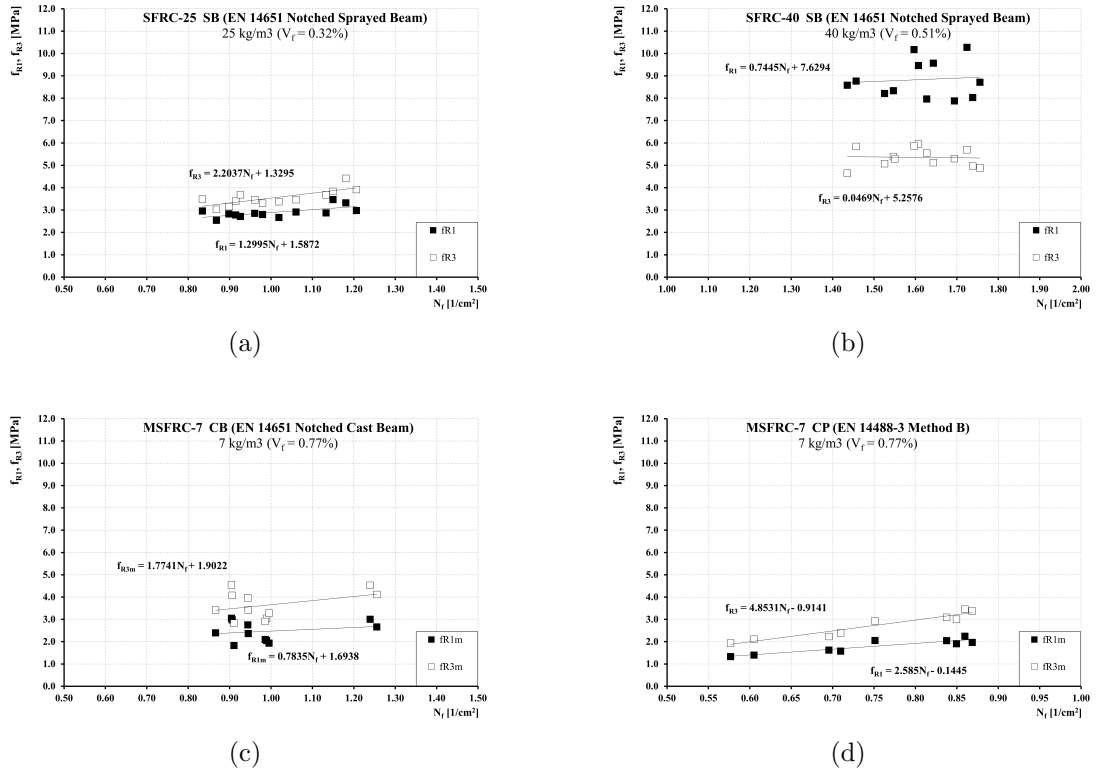

Figure 4.32: Relationship between the number of fibres (N_f/cm^2) and residual strength for SFRC-25 SB (a), SFRC-40 SB (b), MSFRC-7 CB (c) and MSFRC-7 CP (d).

4.5.4 Fibre Rebound

Section 2.2.5 of the state-of-the-art chapter presents a detailed discussion on fibre rebound, and the fibre rebound percentages reported in previous experimental studies are summarised in Table 2.14. The fibre rebound results obtained in the present study are discussed in this section.

In this Ph.D. study, the fibre content of the sprayed concrete was determined from hardened concrete samples in accordance with EN 14488-7 [159] Method A, for the FRC-25 and SFRC-40 series.

Cylinder cores with dimensions of 95 mm in diameter and 100 mm in height were extracted from the test panels after completion of the 3PBT. One core was taken from each panel at alternating locations among panels demoulded from the same mould to ensure representative sampling of a larger area, as illustrated in the figure below (Figure 4.33). To determine the fibre content in the beams, half of each test beam (150 × 150 × 270 mm) was cut and crushed

following the 3PBT, and the fibre content was subsequently quantified. For this purpose, three beams from the cast series and four beams from the sprayed saw-cut beams (two vertical and two horizontal) were examined for each of the SFRC-25 and SFRC-40 series. Totally, 14 half beam portions and 28 drilled core samples were crushed to investigate fibre-rebound effects due to spraying process.

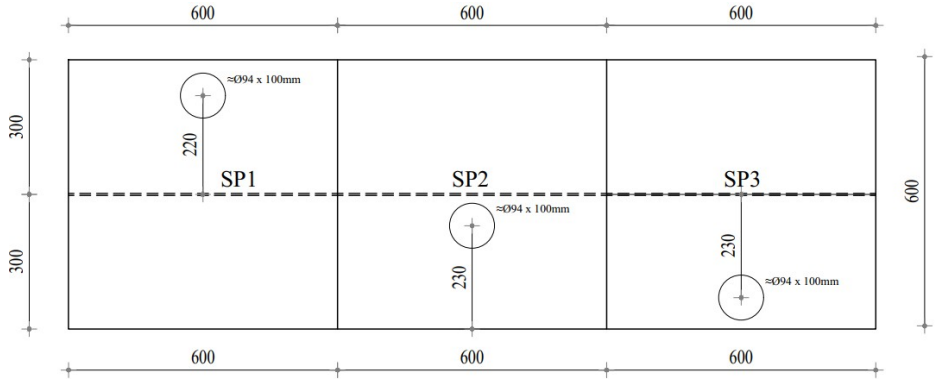

Figure 4.33: Layout of fibre coring for fibre content evaluation.

The percentage of fibre rebound was determined by comparing the fibres added in the fresh state with the actual fibres present in the prepared sprayed samples and was quantified as:

$$C_f = \frac{m_f/1000}{V_d} \tag{4.3}$$

Where:

C_f is the actual fibre content in kg/m^3
m_f is the mass of fibres extracted from the sample in g
V_d is the volume of the sample in m^3

The actual fibre content determined from the core cylinders (Table 4.7) shows that the mean measured fibre content is nearly identical to the design fibre dosage introduced during mixing, indicating that the average fibre rebound is negligible for both SFRC-25 and SFRC-40 series. In contrast, the fibre content determined from the cut beams (150 mm × 150 mm × 270 mm), also presented in Table 4.7, indicates a difference between the design fibre dosage and the measured fibre content. The actual fibre content in the sprayed, saw-cut beams was approximately 6% and 16% lower than the design fibre dosage for the SFRC-25 and SFRC-40

series, respectively, leading to an average rebound values of 11% in case of beam saw-cut from a sprayed panel having a thickness of 150mm. To the contrary, in case of sprayed panels 600 x 600 mm having a thickness of 100 mm, the fibre-rebound is almost negligible. Globally, it seems that fibre-rebound values retrieved are lower than those reported in the literature (Table 2.14).

In summary, on average, no significant percentage of fibre rebound was observed in the study that would adversely affect the post cracking performance of sprayed fibre reinforced specimens compared to the cast-in-mould specimens. This fibre-rebound tendency observed can be related to the type of steel fibres adopted together the cement concrete matrix used.

Table 4.7: Actual average fibre content (from crushed samples) and fibre rebound percentage of sprayed fibre-reinforced concrete.

FRC sprayed series	**Specimen type**	**Design fibre dosage (kg/m^3)**	**Mean measured fibre content (kg/m^3)**	**Fibre rebound (%)**
SFRC-25 SP	Drilled core	25	25.39	–
SFRC-40 SP	Drilled core	40	40.68	–
SFRC-25 SB	Saw-cut beam	25	23.45	6
SFRC-40 SB	Saw-cut beam	40	33.58	16

4.5.5 Flexural Tensile Strength

The mechanical properties of the concrete are summarised in Table 4.5. This section presents and discusses the results obtained from the flexural tensile test EN 14651 [7]. For each series, for both cast and sprayed saw-cut beams were tested as detailed in Section 4.1, the nominal stress-CMOD response along with the corresponding residual flexural tensile strength values (f_{Ri}) were analysed. The nominal stress-CMOD response and the nominal stress-CTOD response for the SFRC-25 and SFRC-40 series for both cast and sprayed saw-cut beams are presented in Figures 4.34, 4.35, 4.39. As detailed in Section 4.5.5 Crack Mouth Opening Displacement (CMOD), Crack Tip Opening Displacement (CTOD) and Load Point Displacement

(LPD) were measured during the experiments to capture the flexural tensile response over a wider crack range since the CMOD measurement was limited to approximatly 5mm. In addition to that recording all three parameters was essential to experimentally establish the relationships among them.

The limit of proportionality (f_{L}) and the residual flexural tensile strengths (f_{R1}, f_{R2}, f_{R3}, and f_{R4}) corresponding to CMOD values of 0.5, 1.5, 2.5, and 3.5 mm, respectively, were calculated from the experimental load–CMOD data and the measured cross-sectional dimensions of each beam, according to Equation 2.4 and Equation 2.5 presented in the State of Art of the thesis.

Referring to Figures 4.34 and 4.35, The cast beam results show that most specimens exhibited flexural hardening behaviour, with post-cracking residual strengths ($f_{\mathrm{R}i}$) higher than the limit of proportionality (f_L) after the initial peak. Except for a slight initial softening observed after the first peak in the SFRC-25 CB series, the SFRC-40 CB specimens continued to exhibit hardening from the first peak.

Considering the mean curve, it can be observed that at large cracks (around 8 mm) the post-cracking strength remains relatively high approximately 44% and 33% of the mean maximum residual strength for the SFRC-25 and SFRC-40 cast beams respectively. Similarly, the retained strengths were approximately 48% and 42% for the SFRC-25 and SFRC-40 sprayed beams,respectively.

The high fibre content and high aspect ratio allowed effective control of crack propagation at the initial stage, resulting in better ductility even at large crack width. Overall, cast beams exhibited higher residual strength and greater ductility compared to sprayed beams.

The difference in the limit of proportionality (f_{L}) between the SFRC-25 and SFRC-40 series was approximately 15% for both sprayed and cast beams. This relatively small variation indicates that the (f_{L}) is primarily governed by the concrete matrix strength rather than the fibre content difference between the two series.

For the series of cast beams, the residual flexural tensile strengths (f_{R1}, f_{R2}, f_{R3} and f_{R4}) increased by 76%, 49%, 36% and 30%, respectively, when comparing SFRC-40 to SFRC-25. In the case of sprayed beams, the corresponding increases were approximately 56%, 55%, 50% and 44%, respectively. The relative difference in residual strength between the two series was observed to decrease as the crack width increased. In Tables 4.9 and 4.10 the mean flexural tensile strength and the coefficient of variation (COV) are summarised for each series.

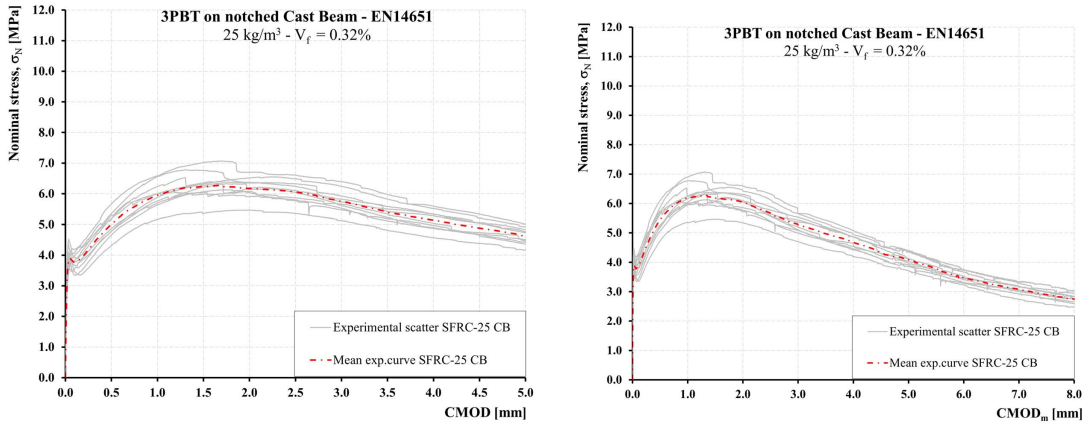

(a) (b)

Figure 4.34: Experimental flexural tensile strength results of SFRC-25 Cast Beams (CB) (EN 14651 [7] with mean curves: nominal stress σ_N vs. CMOD (a) and nominal stress σ_N vs. $CTOD_m$ (b).

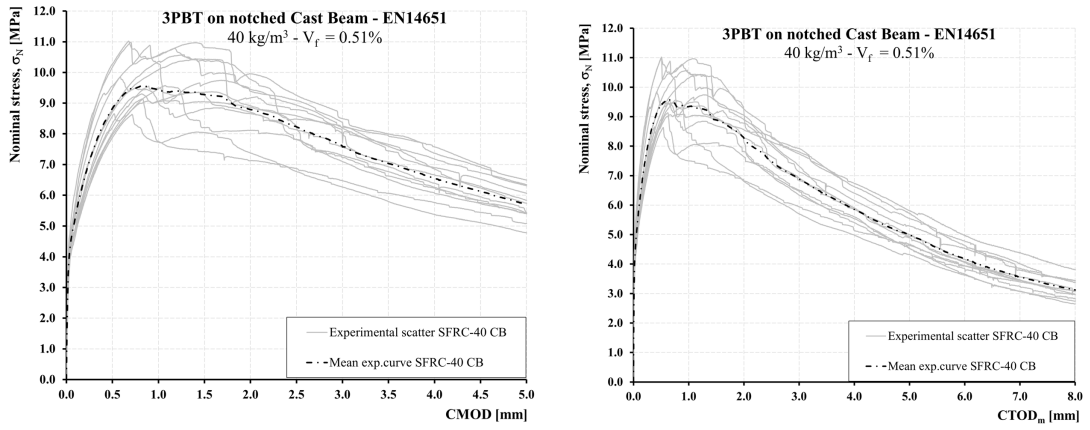

(a) (b)

Figure 4.35: Experimental flexural tensile strength results of SFRC-40 Cast Beams (CB) (EN 14651 [7] with mean curves: Nominal stress σ_N vs. CMOD (a) and Nominal stress σ_N vs. $CTOD_m$ (b).

Table 4.9: Mean flexural tensile strength of cast beam based on the EN 14651 notched beam test [7].

Parameter	f_L(MPa)	f_{R1}(MPa)	f_{R2}(MPa)	f_{R3}(MPa)	f_{R4}(MPa)
SFRC25	3.98	5.01	6.24	6.06	5.40
	(0.08)	(0.08)	(0.07)	(0.06)	(0.06)
SFRC40	4.55	8.83	9.28	8.23	7.03
	(0.07)	(0.10)	(0.11)	(0.10)	(0.10)
MSFCR7	2.87	2.44	3.29	3.60	3.57
	(0.10)	(0.18)	(0.18)	(0.17)	(0.16)

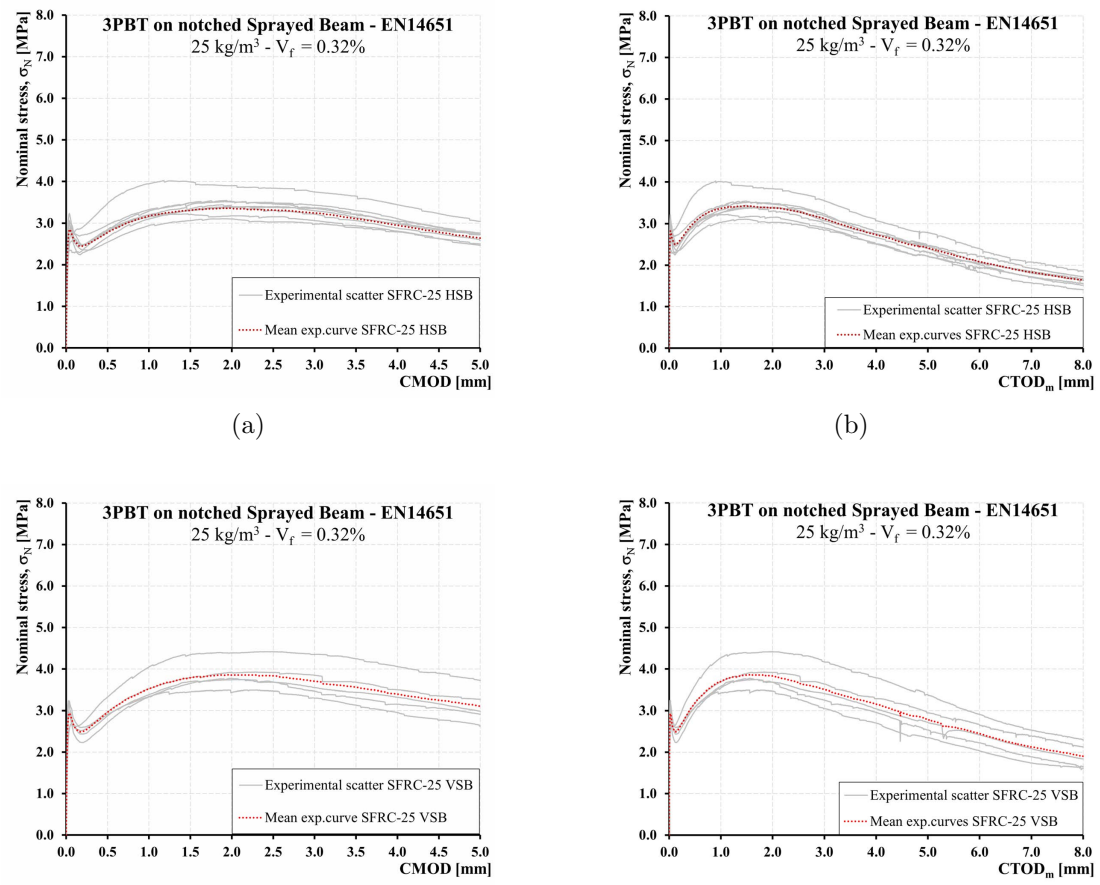

Figure 4.36: Experimental flexural tensile strength (EN 14651 [7]) results of SFRC-25 Sprayed Beams with mean curves: Nominal stress σ_N vs. CMOD (HSB) (a) and Nominal stress σ_N vs. $CTOD_m$ (HSB) (b), Nominal stress σ_N vs. CMOD (VSB) (c) and Nominal stress (VSB) σ_N vs. $CTOD_m$ (d).

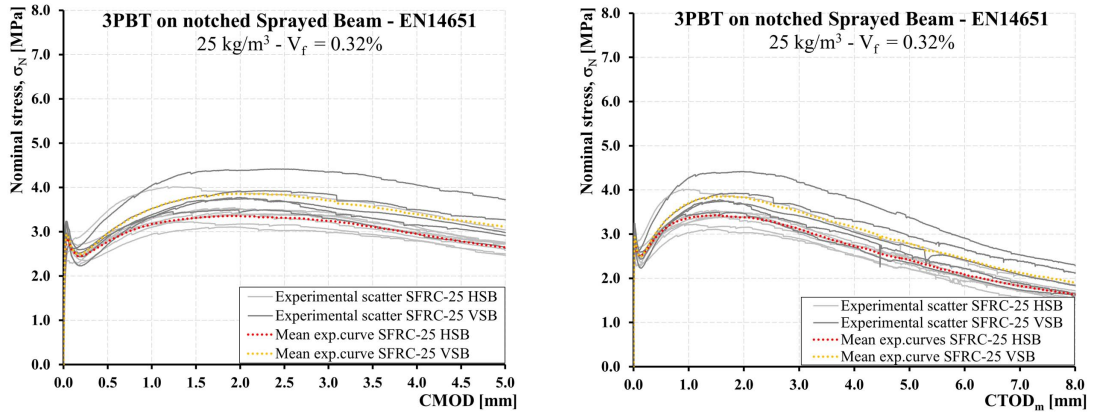

(a) (b)

Figure 4.37: Experimental flexural tensile strength (EN 14651 [7]) results of SFRC-25 sprayed beams (SB) with mean curves: Nominal stress σ_N vs. CMOD (a) and Nominal stress σ_N vs. $CTOD_m$ (b).

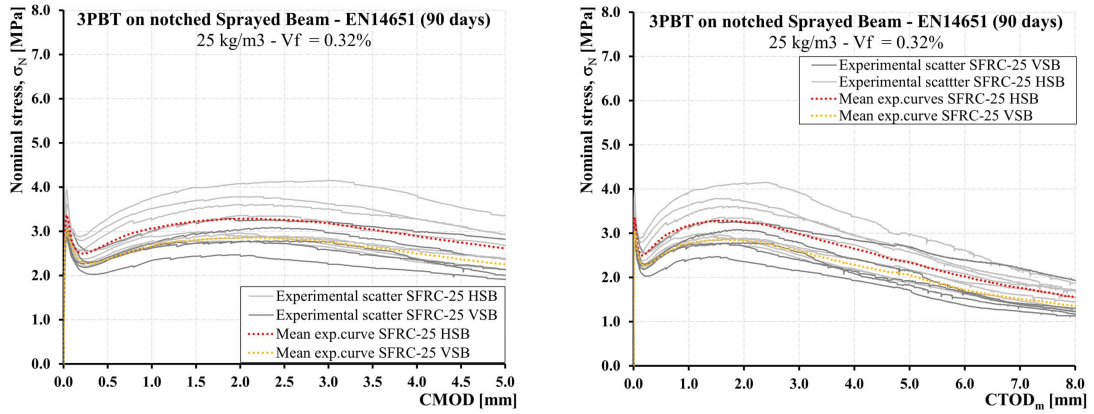

(a) (b)

Figure 4.38: Experimental flexural tensile strength (EN 14651 [7]) results (90 days) of SFRC-25 sprayed beams (SB) with mean curves: Nominal stress σ_N vs. CMOD (a) and Nominal stress σ_N vs. $CTOD_m$ (b).

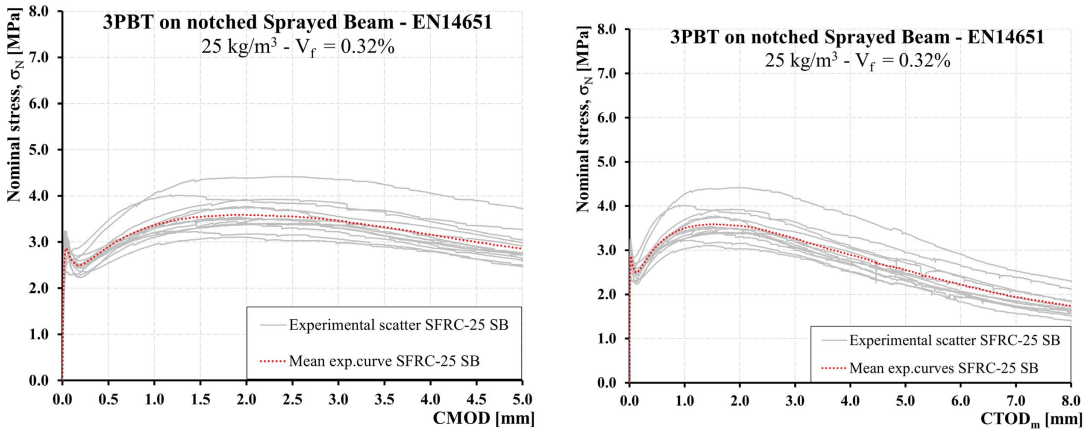

(a) (b)

Figure 4.39: Experimental flexural tensile strength (EN 14651 [7]) results of SFRC-25 Sprayed Beams (SB) with mean curves: Nominal stress σ_N vs. CMOD (a) and Nominal stress σ_N vs. $CTOD_m$ (b).

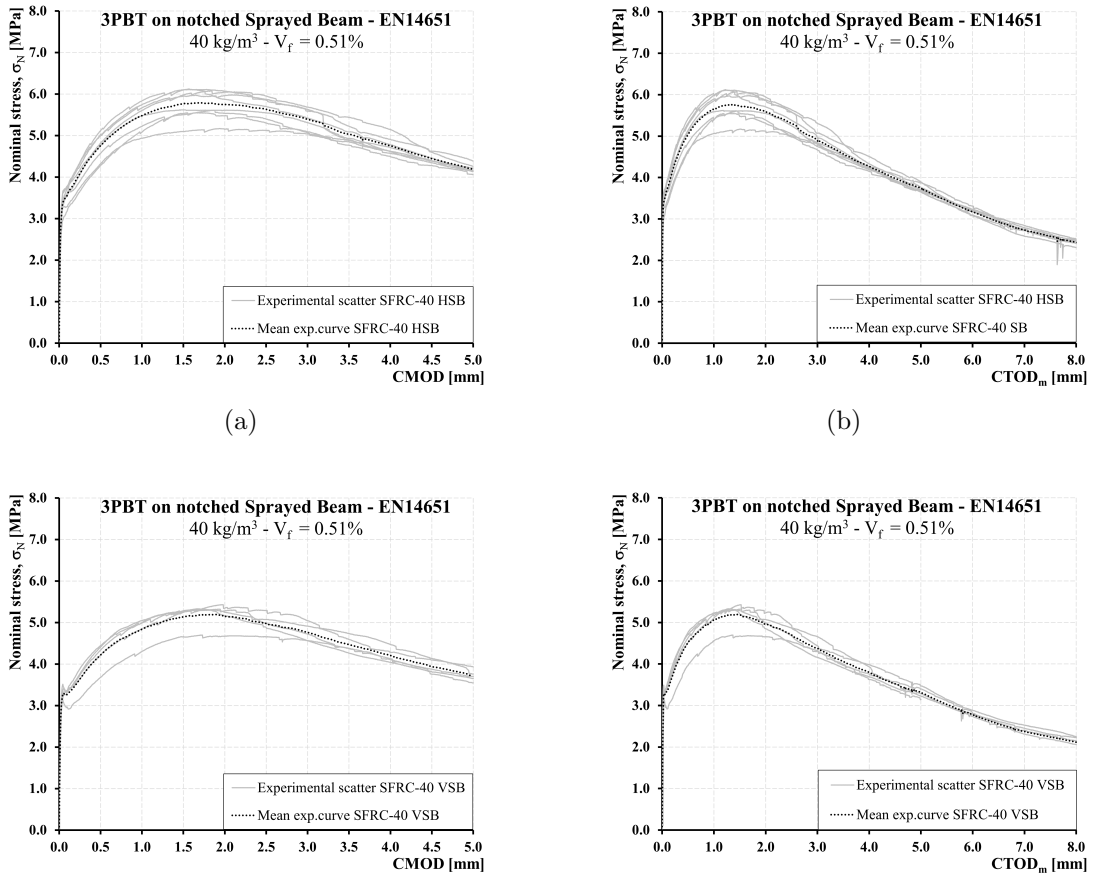

Figure 4.40: Experimental flexural tensile strength (EN 14651 [7]) results of SFRC-40 Sprayed Beams (SB) with mean curves: Nominal stress σ_N vs. CMOD (HSB) (a) and Nominal stress σ_N vs. $CTOD_m$ (HSB) (b), Nominal stress σ_N vs. CMOD (VSB) (c) and Nominal stress (VSB) σ_N vs. $CTOD_m$ (d).

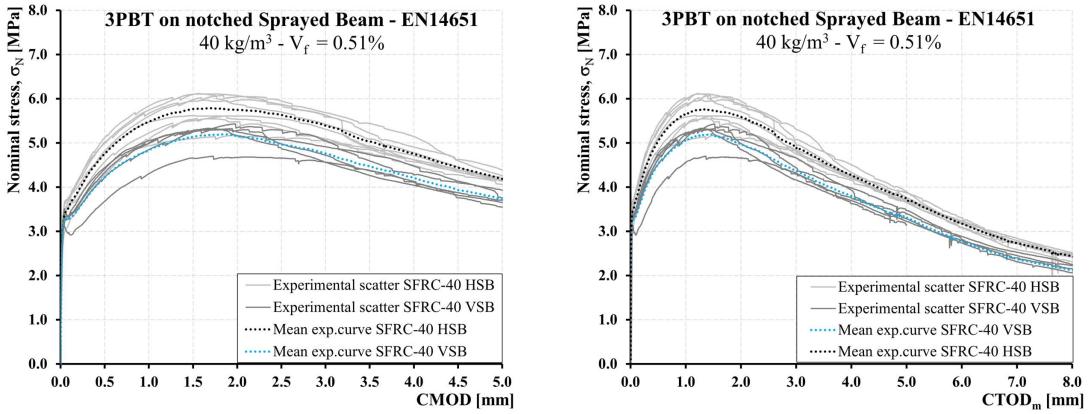

(a) (b)

Figure 4.41: Experimental flexural tensile strength results of SFRC-40 sprayed beams (EN 14651 [7]) with mean curves: Nominal stress σ_N vs. CMOD (a) and Nominal stress σ_N vs. $CTOD_m$ (b).

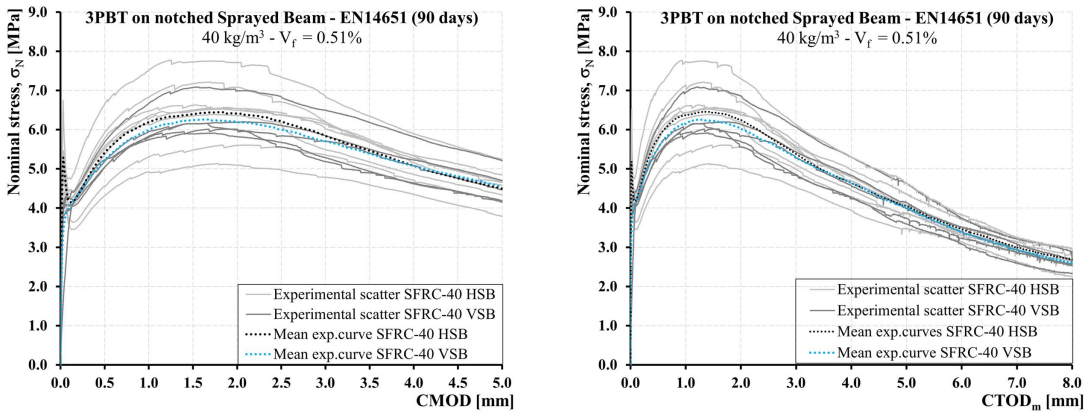

(a) (b)

Figure 4.42: Experimental flexural tensile strength results (90 days) of SFRC-40 sprayed beams (EN 14651 [7]) with mean curves: Nominal stress σ_N vs. CMOD (a) and Nominal stress σ_N vs. $CTOD_m$ (b).

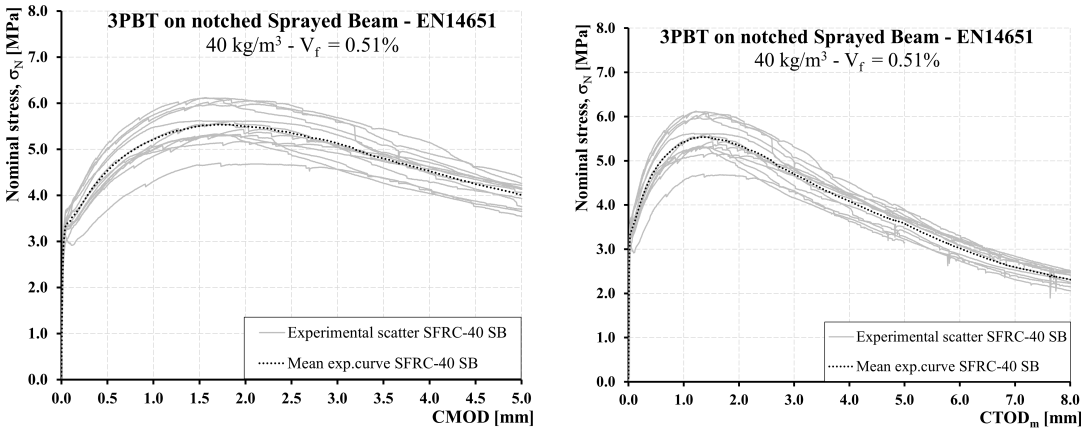

(a) (b)

Figure 4.43: Experimental flexural tensile strength results of SFRC-40 Sprayed Beams (CB) (EN 14651 [7] with mean curves: Nominal stress σ_N vs. CMOD (a) and Nominal stress σ_N vs. $CTOD_m$ (b).

4.5.5.1 Flexural Tensile Strength (Beams Sawn-cut from Sprayed Panels)

As described in the sample preparation and experimental setup subsection, the EN 14651 three-point bending (3PB) test was performed on sprayed beams. The saw-cut beams were section in two directions (Figures 4.12 and 4.13): (i)beams cut on the spraying plane in the vertical direction (parallel to gravity), referred to in this thesis as vertical sprayed saw-cut beams; and (ii) beams cut on the spraying plane in the horizontal direction (perpendicular to gravity) referred to in this thesis as horizontal sprayed saw-cut beams. This was done to determine whether differences in fibre orientation between the two cutting directions result in variations in residual strength.

In the Figures 4.37,4.41,4.38 and 4.42 show the experimental scatter curves for each sample, including the mean curves for both horizontal and vertical sprayed beams. Figure 4.44 presents the mean residual strength values of horizontal and sprayed beams for the SFRC-25 and SFRC-40 series at 28 and 90 days.

Out of the 52 beams tested (8 horizontal and 5 vertical for each of the SFRC-25 and SFRC-40 series at both 28 and 90 days), only one case, SFRC-25 at 28 shows higher results for vertical beams. In all other cases, the horizontal beams exhibit higher residual strengths, as indicated by the percentage differences shown in the graphs (Figure 4.44).

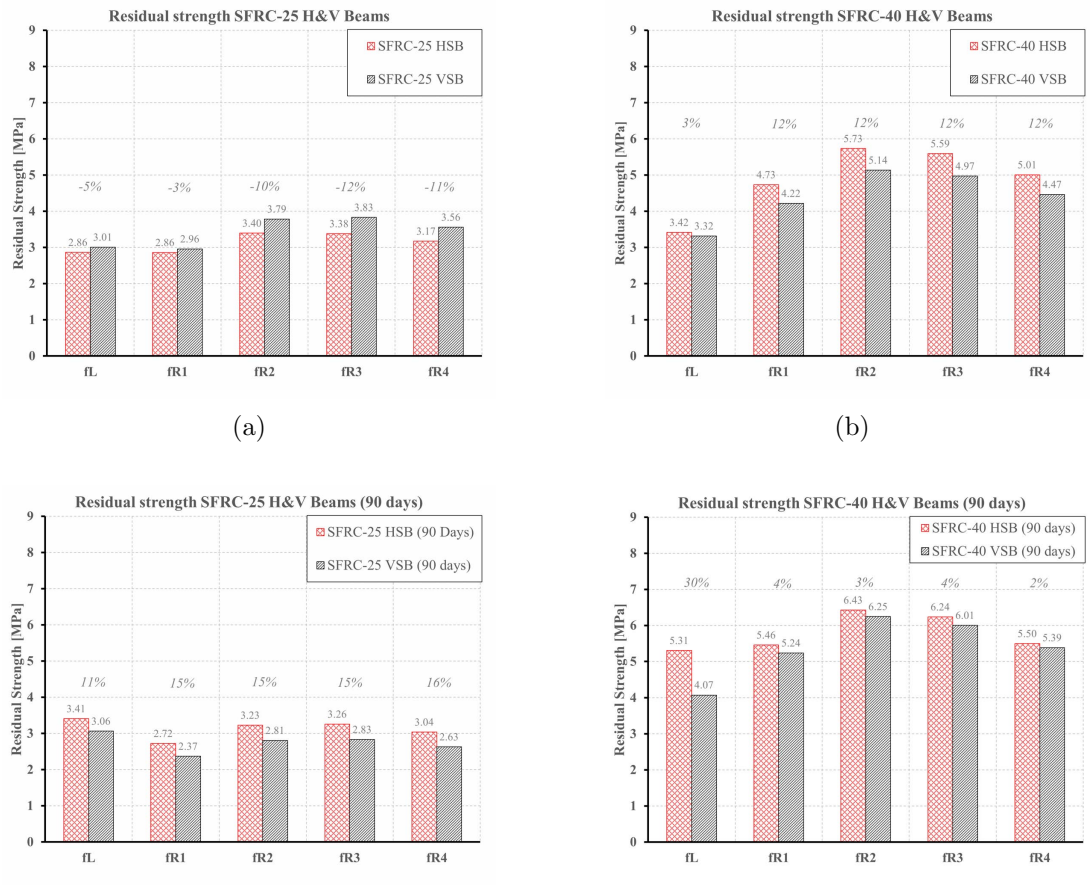

Figure 4.44: Residual strength difference between horizontal and vertical sprayed beam: (a) SFRC-25 HSB SFRC-25 VSB, (b) SFRC-40 HSB SFRC-40 VSB, (c) SFRC-25 HSB (90 days) SFRC-25 VSB (90 days), and (d) SFRC-40 HSB (90 days) SFRC-40 VSB (90 days).

Table 4.10: Mean flexural tensile strength of sprayed beam based on the EN 14651 notched beam test [7].

Parameter	f_L(MPa)	f_{R1}(MPa)	f_{R2}(MPa)	f_{R3}(MPa)	f_{R4}(MPa)
SFRC25	2.92	2.90	3.55	3.56	3.32
	(0.10)	(0.09)	(0.10)	(0.10)	(0.11)
SFRC40	3.38	4.54	5.50	5.35	4.80
	(0.06)	(0.09)	(0.08)	(0.08)	(0.07)

The box plots in Figures 4.45 and 4.46 show the interquartile range (IQR) with the median

(horizontal line), mean (red diamond), and individual results (black points). As shown in the box plots and Tables 4.9 and 4.10 highlight consistent trends between cast and sprayed samples, with cast beams showing higher mean residual strengths, sprayed beams results lower results and narrower statistical dispersion, showing slightly lower variability $COV \leq 0.10$.

No outlier values were identified within the SFRC-40 series, while a few were detected in SFRC-25 series. When comparing the two series, the SFRC-40 series is statistically better, however, both cast and sprayed samples of SFRC-25 and SFRC-40 show statistically reliable results, as all coefficients of variation (COV) remain below 10%.

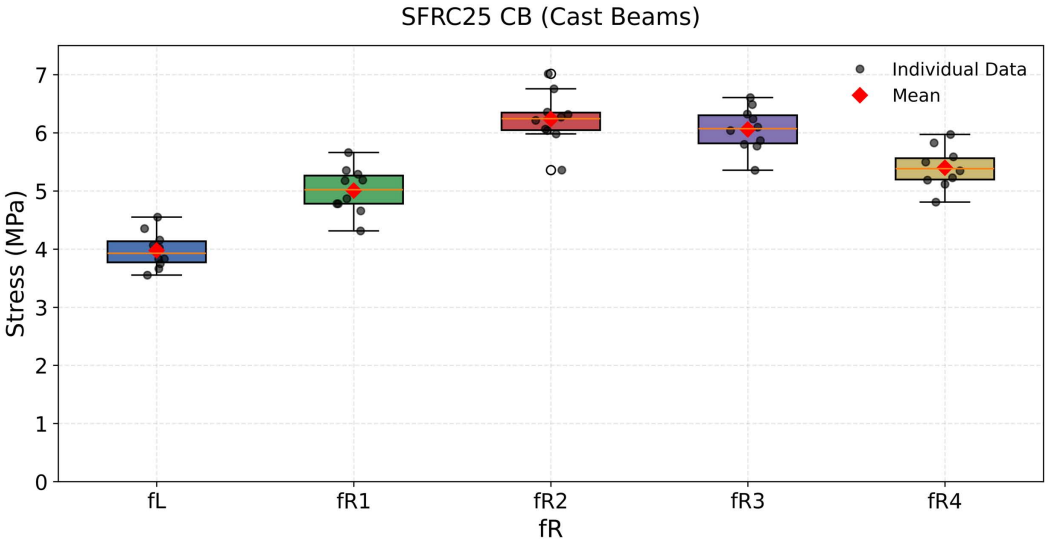

(a)

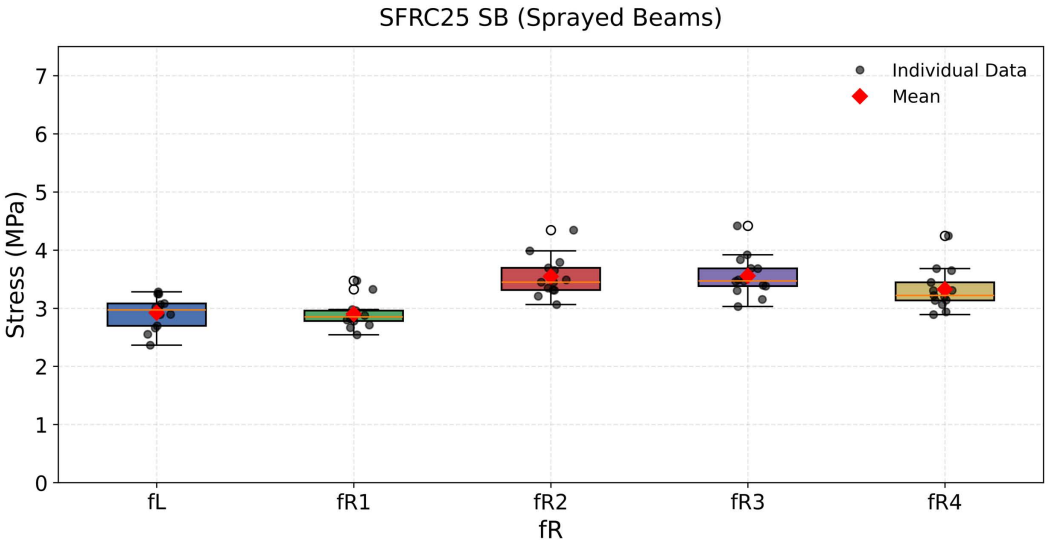

(b)

Figure 4.45: Box plots of residual strength values (f_L, f_{R1} - f_{R4}) for:(a) SFRC25 CB (Cast Beam) and SFRC25 SB (Sprayed Beam) (b).

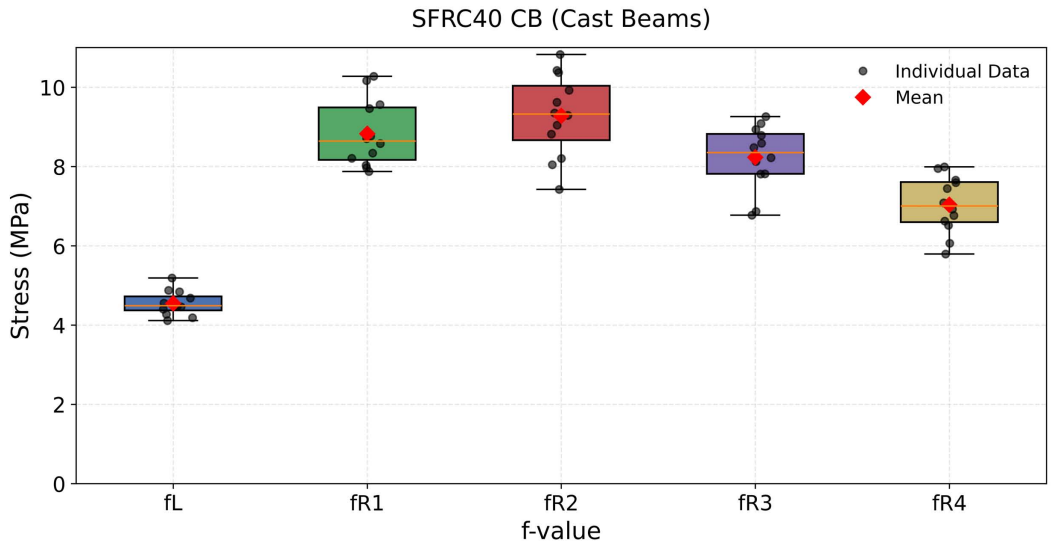

(a)

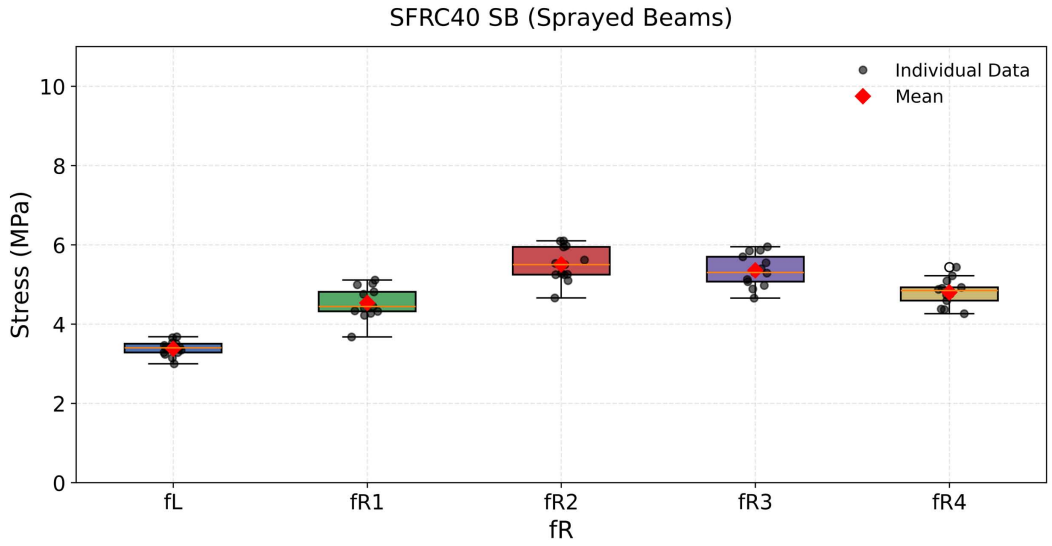

(b)

Figure 4.46: Box plots of residual strength values (f_L, f_{R1} - f_{R4}) for:(a) SFRC40 CB (Cast Beam) and SFRC40 SB (Sprayed Beam) (b).

4.5.6 Flexural Tensile Strength (EN 14488-3 Method B)

This section presents and discusses the results obtained from the flexural tensile test of the sprayed and cast panels according to EN 14487 -1 [19] and EN 14488-3 [16]. For each series, both cast and sprayed panels were tested as detailed in Section 4.1, the nominal stress-CMOD response along with the corresponding residual flexural tensile strength values (f_{R}) were analysed. The nominal stress-CMOD response and the nominal stress-CTOD response for the SFRC-25 and SFRC-40 sprayed panel series are presented in Figures 4.47 and 4.48. As detailed in the Section 4.4 CMOD, CTOD and LPD were measured during the experiment for the notched panel test in the same manner as in the notched beam test.

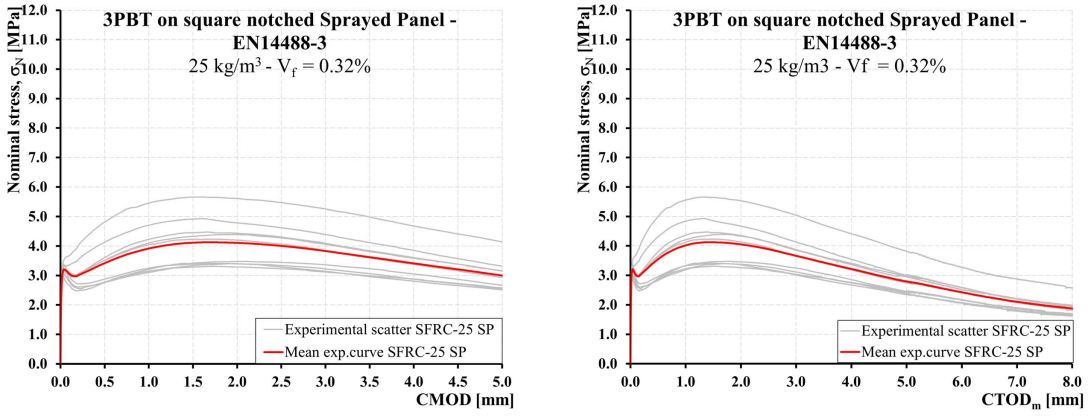

(a) (b)

Figure 4.47: Experimental flexural tensile strength results of SFRC-25 Sprayed Panels (SP) (EN 14488-3 Method B [16] with mean curves: Nominal stress σ_N vs. CMOD (a) and Nominal stress σ_N vs. $CTOD_m$ (b).

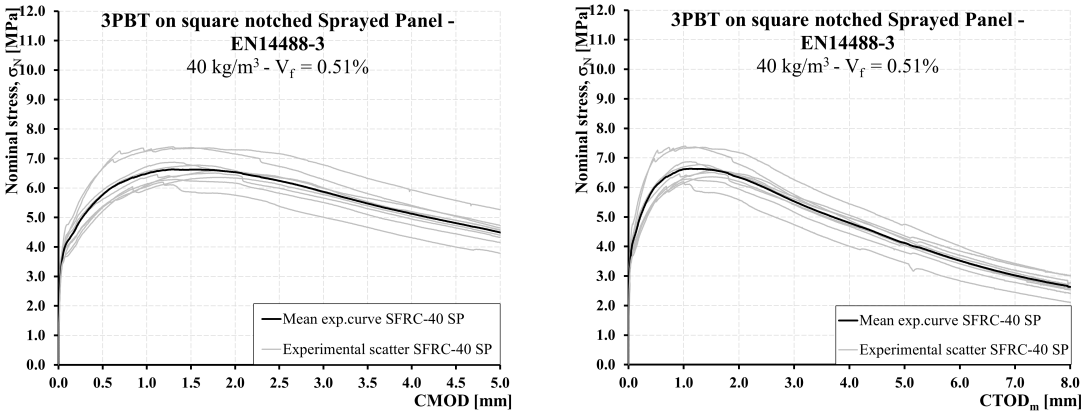

(a) (b)

Figure 4.48: Experimental flexural tensile strength results of SFRC-40 Sprayed Panels (SP) (EN 14488-3 Method B [16] with mean curves: Nominal stress σ_N vs. CMOD (a) and Nominal stress σ_N vs. $CTOD_m$ (b).

Table 4.11: Mean flexural tensile strength of sprayed panel based on the EN 14488-3 Method B [16].

Parameter	f_L(MPa)	f_{R1}(MPa)	f_{R2}(MPa)	f_{R3}(MPa)	f_{R4}(MPa)
SFRC25	3.25	3.42	4.11	4.00	3.62
	(0.05)	(0.21)	(0.20)	(0.19)	(0.18)
SFRC40	3.72	5.77	6.62	6.24	5.47
	(0.06)	(0.10)	(0.08)	(0.08)	(0.08)

Table 4.12: Mean flexural tensile strength of cast panels based on the EN 14488-3 Method B [16].

Parameter	f_L(MPa)	f_{R1}(MPa)	f_{R2}(MPa)	f_{R3}(MPa)	f_{R4}(MPa)
SFRC25	3.52	4.39	5.50	5.27	4.76
	(0.05)	(0.06)	(0.06)	(0.05)	(0.05)
SFRC40	5.38	9.66	9.50	8.28	7.13
	(0.03)	(0.02)	(0.05)	(0.02)	(0.03)
MSFCR7	2.76	1.79	2.49	2.72	2.65
	(0.05)	(0.18)	(0.20)	(0.21)	(0.21)

In Tables 4.11 and 4.12 the mean flexural tensile strength is summarised for the sprayed and cast series. The limit of proportionality (f_{L}) and the residual flexural tensile strengths (f_{R1}, f_{R2}, f_{R3}, and f_{R4}) corresponding to CMOD values of 0.5, 1.5, 2.5, and 3.5 mm, respectively, were calculated from the experimental load–CMOD data and the measured cross-sectional dimensions of each panel, according to Equation 2.37 and Equation 2.38 presented in the State of Art of the thesis. The sprayed panels exhibit slightly lower strengths but higher variability as shown the results in Tables 4.11 and 4.12 and the nominal stress vs.CMOD/CTOD responses in the Figures 4.47 and 4.48.

Based on the mean response curve, it can be observed that at large crack openings (approximately 8 mm), the post-cracking strength remains relatively high approximately 45% and 40% of the mean maximum residual strength for the SFRC-25 and SFRC-40 sprayed panels, respectively. Similarly, the retained strengths for the cast panels were approximately 47% and 34% for the cast panels SFRC-25 and SFRC-40, respectively. For the MSFRC-7 cast panels, the retained strength at CTOD of 8 mm was round 68%. It should be noted that, however, that the maximum residual strength of the MSFRC-7 was lower compared to that of the SFRC series.

The difference in the limit of proportionality (f_{L}) between the SFRC-25 and SFRC-40 series was approximately 14% and 50% for sprayed and cast panles respectively. This relatively small variation indicates that (f_{L}) is primarily governed by the strength of the concrete matrix rather than the difference in fibre content between the two series compared to other residual strength values.

For the series of sprayed panels, the residual flexural tensile strengths (f_{R1}, f_{R2}, f_{R3} and f_{R4}) increased by 69%, 61%, 56% and 51%, respectively, when comparing SFRC-40 to SFRC-25. In the case of cast panels, the corresponding increases were approximately 120%, 73%, 57% and 50%, respectively. The relative difference in residual strength between the two series was observed to decrease as the crack width increased.

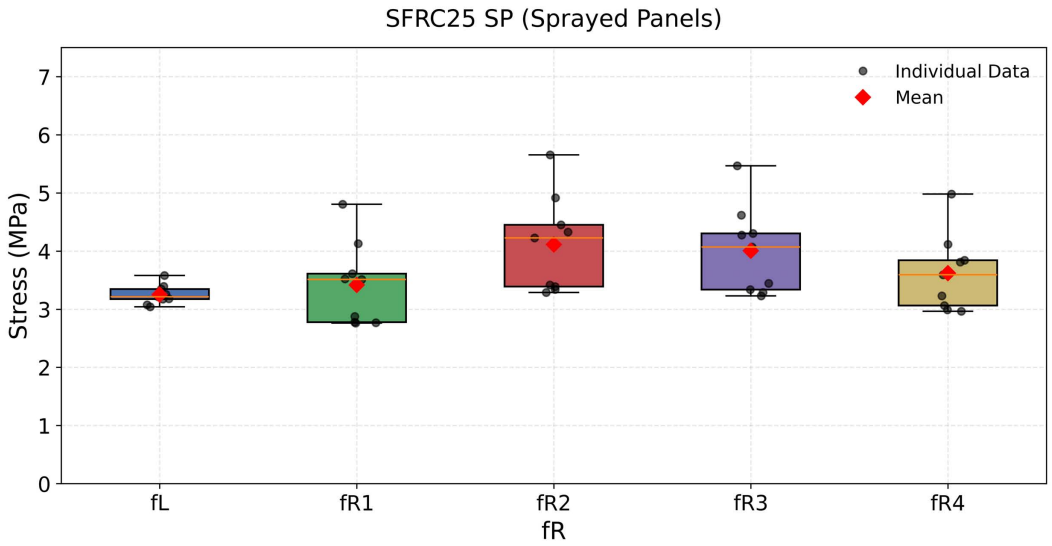

(a)

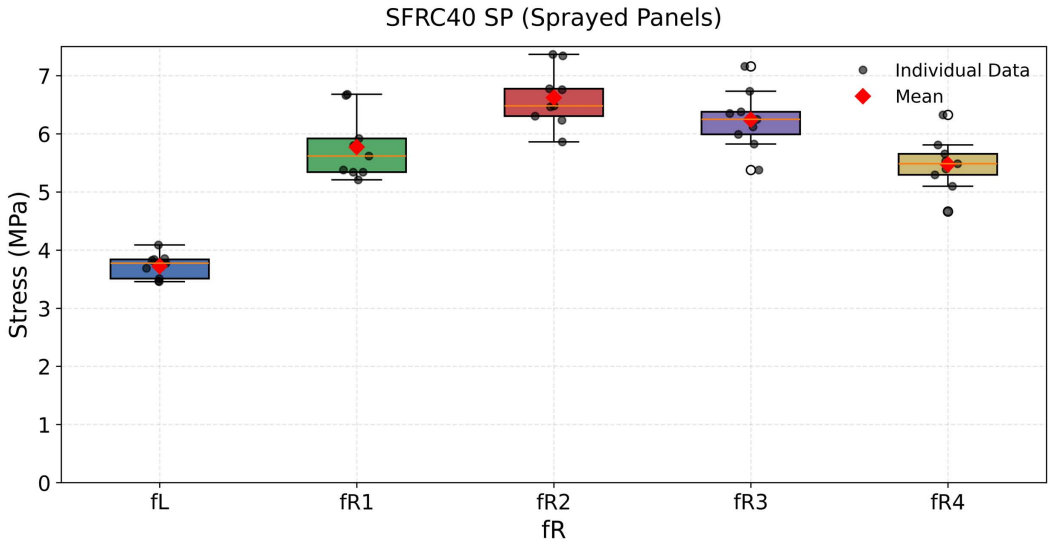

(b)

Figure 4.49: Box plots of residual strength values (f_L, f_{R1} - f_{R4}) for:(a) SFRC25 SP (Sprayed Panel) and SFRC40 SP (Sprayed Panel) (b).

The box plots in Figures 4.49 summarize the statistical distribution of the residual strength for SFRC 25 and SFRC 40 (f_{L}, f_{R1}, f_{R2}, f_{R3}, f_{R4}). Noted that the boxes are smaller in SFRC-40 which indicate less variability, however, few outliers observed. In SFRC-25 SP, the mean and median are fairly close for most residual strength results, indicating reasonably symmetric distribution. As shown also in the Tables 4.11 and 4.12, when comparing sprayed and cast panels cast panel result are less variable with 10% COV for SFRC-25 and SFRC-40 and 20% for MSFRC-7.

4.5.6.1 Overall Comparison of Flexural Tensile Strength Results

The flexural tensile strength results, obtained in accordance with EN 14651 [7] and EN 14488-3 Method B [16] test methodologies, in terms of the nominal stress versus CMOD (Crack Mouth Opening Displacement) and the mean residual strength (f_{Ri} values) are presented in the Figure 4.50 for the SFRC-25 series.

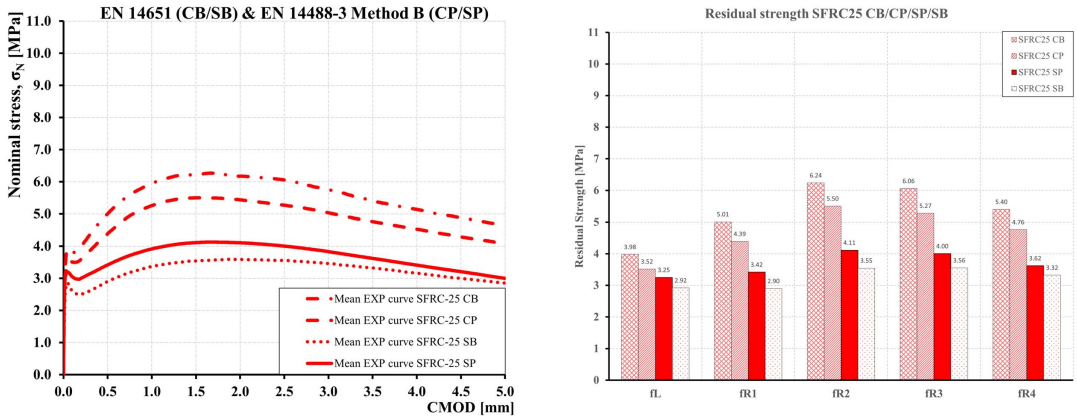

(a) (b)

Figure 4.50: Mean experimental flexural tensile strength results (EN 14488-3 [16] and EN 14651 [7]) for SFRC-25 (SP,CP,CB, and SB): (a) Mean nominal stress (σ_N) vs. CMOD and (b) Mean residual strength values (histogram).

The mean curves for both the beam and panel specimens, and for both cast and sprayed samples, are shown in Figure 4.50. The results indicate that magnitudes follow the order: SFRC-25 cast-in-mould beam > SFRC-25 cast-in-mould panel > SFRC-25 sprayed panel > SFRC-25 sprayed beam. It can be observed that the cast elements exhibit a higher flexural tensile strength compared to the sprayed elements.

In the case of the SFRC-40 series, the results indicate that the magnitudes follow the or-

der: SFRC-40 cast-in-mould panel > SFRC-40 cast-in-mould beam > SFRC-40 sprayed panel > SFRC-40 "sprayed beam". From the graphs in Figure 4.51, it can be observed that the cast elements exhibit a higher flexural tensile strength compared to the sprayed elements, the same as the trend observed in the series SFRC-25. However, the order of SFRC-40 cast-in-mould panel > SFRC-40 cast-in-mould beam differs from that of the SFRC-25 series, where SFRC-25 cast-in-mould beam > SFRC-25 cast-in-mould panel. This variation may be attributed to the lower fibre content in SFRC-25, which increases the influence of vibration on the orientation of the fibre. As a result, improved fibre alignment in the SFRC-25 cast-in-mould beam could explain the higher results of the cast beam.

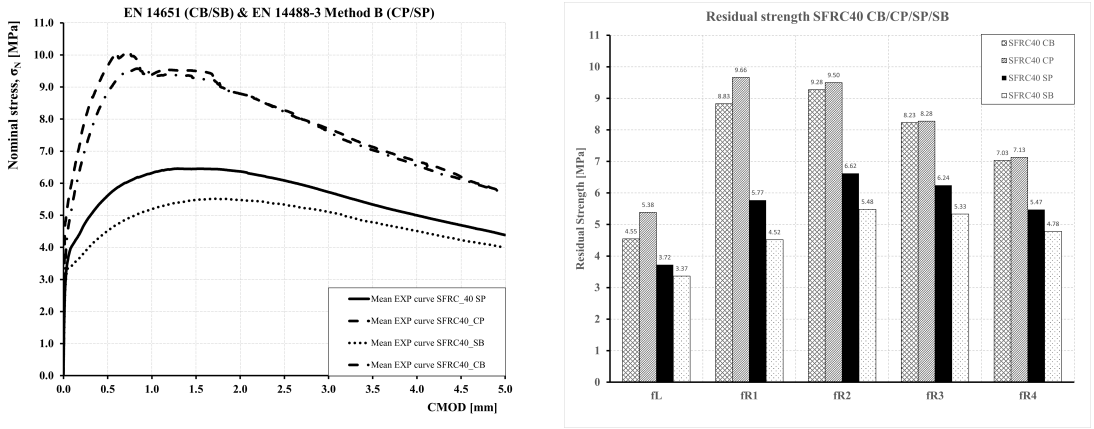

(a) (b)

Figure 4.51: Mean experimental flexural tensile strength results (EN 14488-3 [16] and EN 14651 [7]) for SFRC-40 (SP,CP,CB, and SB): (a) Mean nominal stress (σ_N) vs. CMOD and (b) Mean residual strength values (histogram).

Regarding the effect of fibre content, for the series of cast-in-mould beams, the residual flexural tensile strengths (f_{R1}, f_{R2}, f_{R3} and f_{R4}) increased by 76%, 49%, 36% and 30%, respectively, when comparing SFRC-40 to SFRC-25. In the case of "sprayed beams", the corresponding increases were approximately 56%, 55%, 50% and 44%, respectively. For the sprayed panels, the residual flexural tensile strengths (f_{R1}, f_{R2}, f_{R3} and f_{R4}) increased by 69%, 61%, 56% and 51%, respectively, when comparing SFRC-40 to SFRC-25. In the case of cast-in-mould panels, the corresponding increases were approximately 120%, 73%, 57% and 50%, respectively. In both sprayed and cast-in mould specimens, an increase in an fibre content resulted in an increase the residual strength as discussed. However as shown in the Figure (4.52, the residual strength f_{R3} is greater than f_{R1} in both sprayed panel and sprayed saw-cut beam. In contrast, for cast-in-mould specimens, the residual strength f_{R3} is lower than f_{R1} in both the cast-in-mould

beam and the cast-in-mould panel.

Table 4.13: Pairwise one-way ANOVA results between SFRC-40 Series (SP = Sprayed Panel, SB = Sprayed Beam, CP = Cast Panel, CB = Cast Beam).

Comparison	f_L	f_{R1}	f_{R2}	f_{R3}	f_{R4}
Sprayed Panel vs Sprayed Beam	0.0006 (S)	0.0000 (S)	0.0000 (S)	0.0002 (S)	0.0008 (S)
Cast Panel vs Cast Beam	0.0036 (S)	0.2027 (NS)	0.7792 (NS)	0.9382 (NS)	0.8588 (NS)
Sprayed Panel vs Cast Panel	0.0000 (S)	0.0000 (S)	0.0000 (S)	0.0005 (S)	0.0010 (S)
Sprayed Beam vs Cast Beam	0.0000 (S)	0.0000 (S)	0.0000 (S)	0.0000 (S)	0.0000 (S)
Sprayed Panel vs Cast Beam	0.0000 (S)	0.0000 (S)	0.0000 (S)	0.0000 (S)	0.0000 (S)
Cast Panel vs Sprayed Beam	0.0000 (S)	0.0000 (S)	0.0000 (S)	0.0000 (S)	0.0000 (S)

(S) = Significant at $p < 0.05$, (NS) = Not significant

Table 4.14: Pairwise one-way ANOVA results between SFRC-25 series (SP = Sprayed Panel, SB = Sprayed Beam, CP = Cast Panel, CB = Cast Beam).

Comparison	f_L	f_{R1}	f_{R2}	f_{R3}	f_{R4}
Sprayed Panel vs Sprayed Beam	0.0050 (S)	0.0241 (S)	0.0380 (S)	0.0499 (S)	0.1885 (NS)
Cast Panel vs Cast Beam	0.0339 (S)	0.0292 (S)	0.0236 (S)	0.0064 (S)	0.0136 (S)
Sprayed Panel vs Cast Panel	0.0378 (S)	0.0476 (S)	0.0201 (S)	0.0195 (S)	0.0173 (S)
Sprayed Beam vs Cast Beam	0.0000 (S)	0.0000 (S)	0.0000 (S)	0.0000 (S)	0.0000 (S)
Sprayed Panel vs Cast Beam	0.0000 (S)	0.0000 (S)	0.0000 (S)	0.0000 (S)	0.0000 (S)
Cast Panel vs Sprayed Beam	0.0037 (S)	0.0000 (S)	0.0000 (S)	0.0000 (S)	0.0000 (S)

(S) = Significant at $p < 0.05$, (NS) = Not significant

However, the differences within the SFRC-25 and SFRC-40 series arise from the casting methods and the test methodologies discussed and analysed above. In addition, a one-way ANOVA was performed for both the SFRC-25 and SFRC-40 series, and a statistically significant difference was observed between the groups for the f_{Ri} values (Figure 4.13 and 4.14). This indicates that the variability between the groups is substantially greater than the variability within each group.

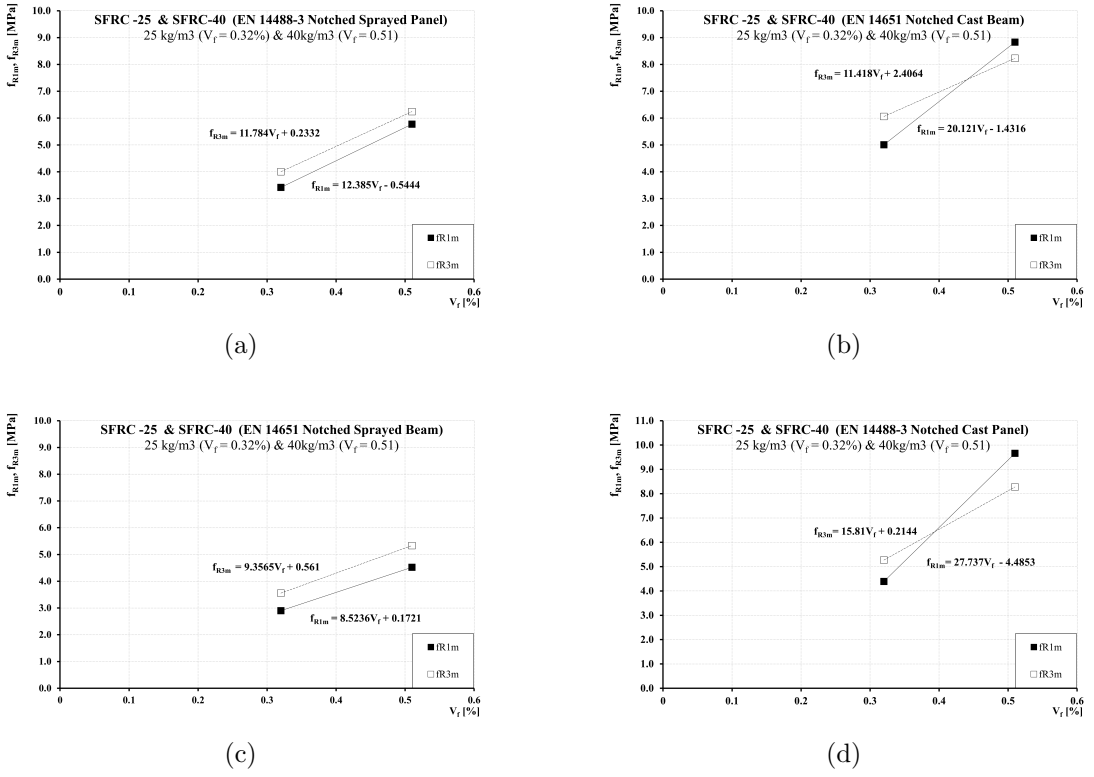

Figure 4.52: Influence of fibre content: (a) SFRC -25 SFRC-40 (EN 14488-3 Notched Sprayed Panel), (b) SFRC -25 SFRC-40 (EN 14488-3 Notched Cast Panel), (c) SFRC -25 SFRC-40 (EN 14651 Notched Cast Beam), and (d) SFRC -25 SFRC-40 (EN 14651 Notched Sprayed Beam).

In tunnelling practice, and among some researchers within scientific community is often performed EN 14651 [7] on cast beams to represent the residual strength for PSCL (Permanent Sprayed Concrete lining). However, as discussed earlier, the residual strength values obtained from the EN 14651 differ from those derived from sprayed panel results (EN 14488-3), as well as from EN 14651 tests conducted on sprayed beams. The ratios between these results almost consistent for SFRC-25 and SFRC-40 series, as shown in the Figure 4.53.

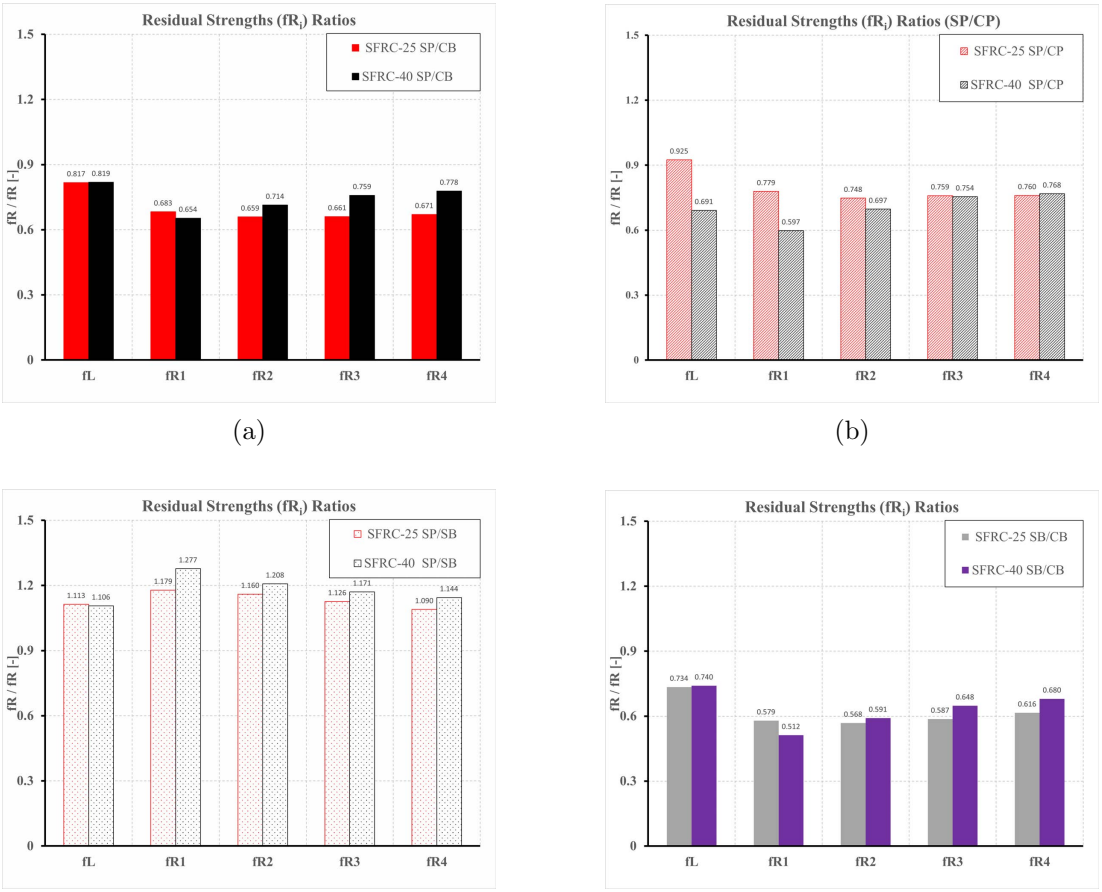

Figure 4.53: Residual strength ratios between series: (a) SFRC-25 and SFRC-40 (SP/CB), (b) SFRC-25 and SFRC-40 (SP/CP), (c) SFRC-25 and SFRC-40 (SP/SB), and (d) SFRC-25 and SFRC-40 (SB/CB).

Considering the effect of concrete strength, the residual strength of both sprayed and cast series were normalized by by the square root of their corresponding compressive strengths $\left(\frac{f_{Ri}}{\sqrt{f_{cmi}}}\right)$. As shown in the Figure 4.54, this normalization did not significantly alter the ratios, indicating that while concrete strength contributes to the difference in residual strength between sprayed and cast specimens, it is not the governing factor.

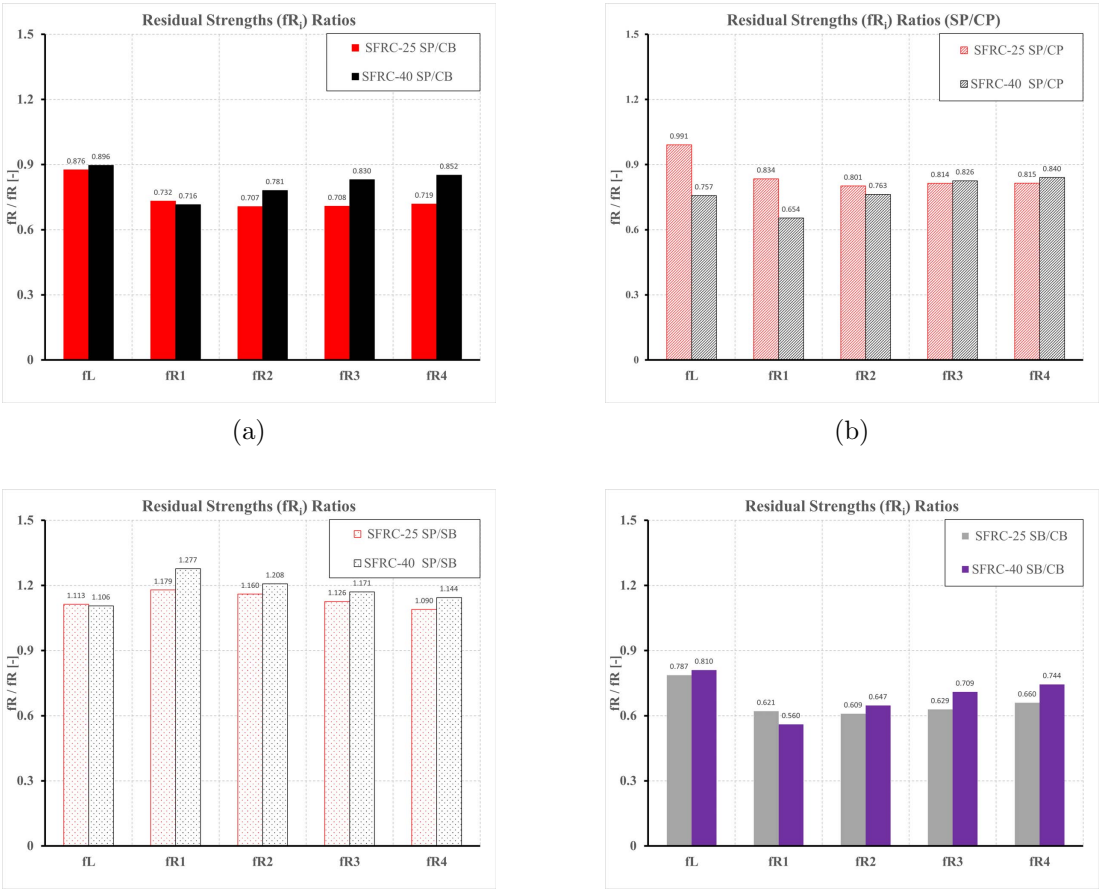

Figure 4.54: Residual strength ratios between series (normalised by compressive strength): (a) SFRC-25 and SFRC-40 (SP/CB), (b) SFRC-25 and SFRC-40 (SP/CP), (c) SFRC-25 and SFRC-40 (SP/SB), and (d) SFRC-25 and SFRC-40 (SB/CB).

4.5.6.2 Influence of possible induced Concrete Flow Direction on Residual Strength

For SFRC 40 series, to see the effect of possible induced concrete flow direction during the casting process of panels on the fibre orientation as a result also on the effect on the flexural tensile results, the panels were notched in two ways, as shown in the Figure 4.55 to perform the test EN 14488-3 [16], so the notch was provided in two orientations one is parallel to the possible induced concrete flow and one perpendicular. In addition a third scenario was also considered for SFRC40 cast-in-mould panels by forcing with an opportune concrete bucket the casting process exactly from the centre in approximately all direction. The orientation factor

was measured after the flexural tests from the cracked plane of the Panels and was found 0.43, 0.38 and 0.26, for the perpendicular, outward from the centre in all directions, and Parallel scenarios, respectively.

In expectation of a larger number of fibres aligning in the concrete flow direction, allowing more fibres to contribute to the fibre bridging effect in the perpendicular direction of the concrete flow, and thus increasing the residual strength of the FRC series in this case, the notch was provided perpendicular to the concrete flow direction (Figure 4.55a).

In the other case, the notch was provided parallel to the concrete flow direction (4.55b), expecting less fibres aligned perpendicular to the concrete flow direction resulting in fewer fibres working in the bridging effect, as fewer fibres were oriented perpendicular to the notch. consequently, lower residual strength. As shown in the Figure 4.56 the mean flexural tensile strength results for the two orientation, the effect is very significance almost double.

Regarding the casting configuration in which the concrete flow from the centre in all direction (4.55c), the mean flexural stress vs CMOD response curve lies between the two cases discussed above. As shown in the Figure 4.56, the difference compared to the first scenario is, on average, approximately 40%.

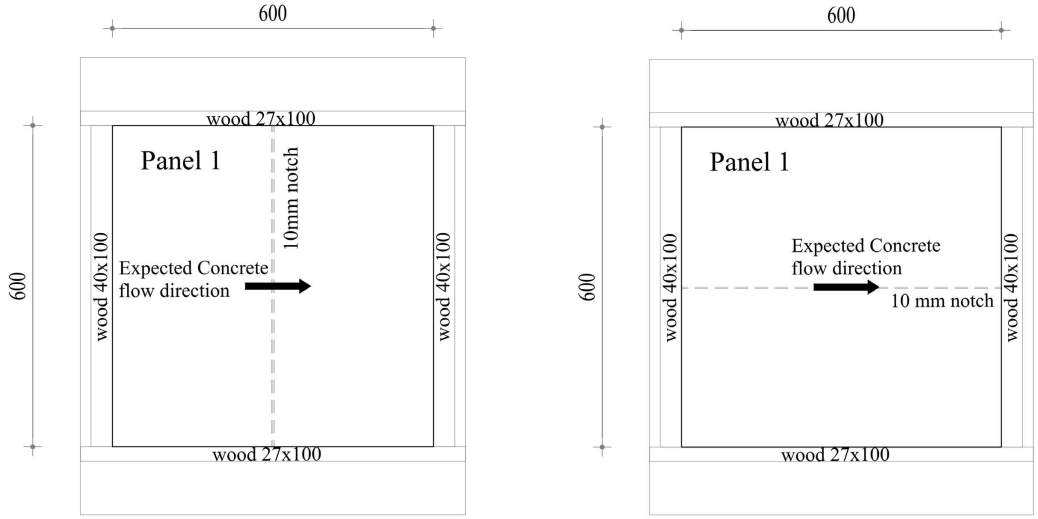

(a)

(b)

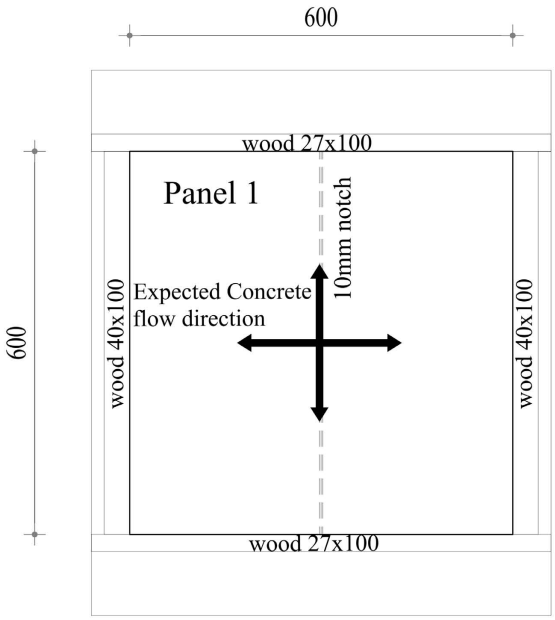

(c)

Figure 4.55: Concrete flow direction and notching direction: Expected concrete flow direction perpendicular to the notch direction (a), Expected concrete flow parallel to the notch (b), and Expected concrete flow from the centre to all directions(c).

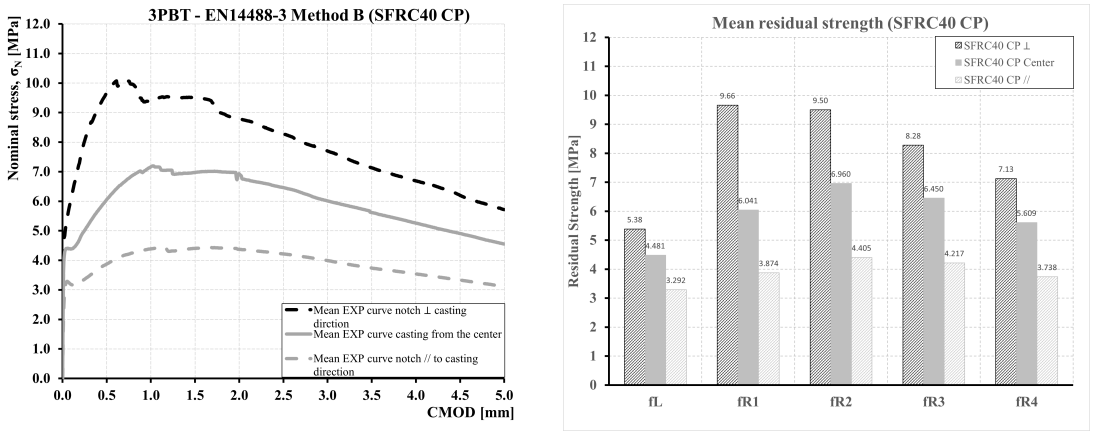

(a) (b)

Figure 4.56: Flexural tensile strength results: Nominal stress (σ_N) vs. CMOD (a) and Residual strength (b) for SFRC40 CP notched perpendicular and parallel to the casting direction, cast from the centre.

4.5.6.3 Comparison of Flexural Tensile Strength of Sprayed FRC at 28 and 90 Days

The flexural test on the sprayed panels and beams were also conducted at 90 days to evaluate the effect on age on the post cracking strength, and to compare the results with those obtained at 28 days, with a methodologies EN 14488-3 Method B [16] and [7], respectively.

Table 4.15: Mean flexural tensile strength results (EN 14488-3 Method B and EN 14651 notched beam) at 90 Days.

Parameter	f_L (MPa)	f_{R1m} (MPa)	f_{R2m} (MPa)	f_{R3m} (MPa)	f_{R4m} (MPa)
SFRC-25 SP	4.03	3.33	4.06	4.06	3.66
	(0.13)	(0.14)	(0.15)	(0.15)	(0.15)
SFRC-40 SP	4.40	5.93	6.73	6.26	5.43
	(0.09)	(0.10)	(0.11)	(0.10)	(0.10)
SFRC-25 SB	3.28	2.59	3.07	3.10	2.88
	(0.09)	(0.13)	(0.14)	(0.16)	(0.17)
SFRC-40 SB	4.90	5.37	6.36	6.15	5.45
	(0.17)	(0.11)	(0.11)	(0.10)	(0.09)
SFRC-40 CB	5.52	7.62	9.34	8.70	7.77
	(0.03)	(0.14)	(0.13)	(0.14)	(0.14)
MSFRC-7 CB	4.29	2.40	3.29	3.63	3.65
	(0.02)	(0.05)	(0.08)	(0.09)	(0.11)
MSFRC-7 CP	4.29	2.34	3.43	3.73	3.58
	(0.09)	(0.11)	(0.10)	(0.10)	(0.09)

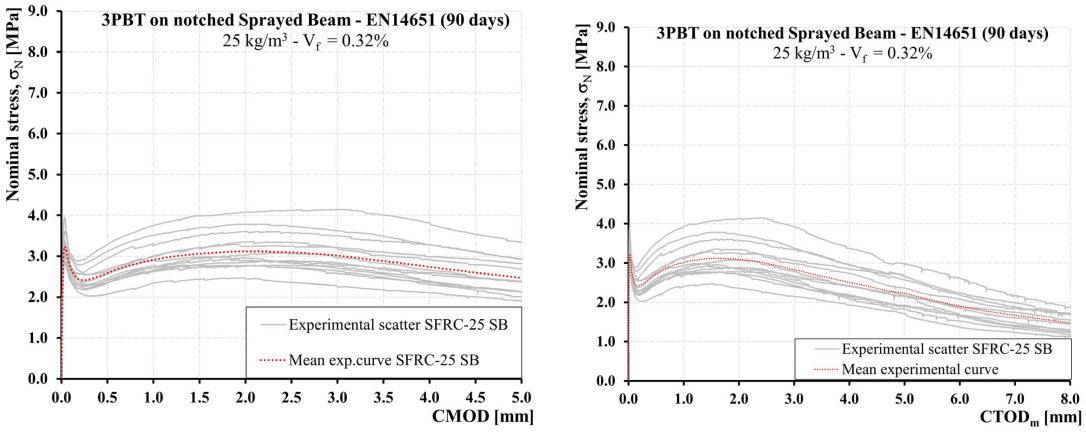

(a) (b)

Figure 4.57: Experimental flexural tensile strength (EN 14651 [7]) results (90 days) of SFRC-25 Sprayed Beams (SB) with mean curves: Nominal stress σ_N vs CMOD (a) and Nominal stress σ_N vs $CTOD_m$ (b).

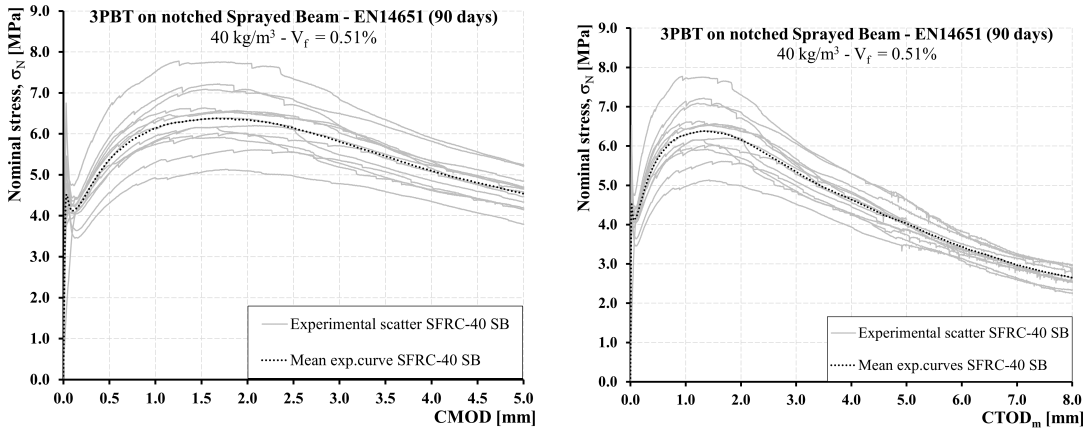

(a) (b)

Figure 4.58: Experimental flexural tensile strength (EN 14651 [7]) results (90 days) of SFRC-40 Sprayed Beams (SB) with mean curves: Nominal stress σ_N vs CMOD (a) and Nominal stress σ_N vs $CTOD_m$ (b).

Across all series, the limit of proportionality (f_L) values increased considerably by approximately 33%, which can be attributed to the strong influence of compressive strength of the concrete on f_L compared to the residual strength parameters (f_{R1}, f_{R2}, f_{R3} and f_{R4}) see Figure 4.59 and 4.60 .

For the other residual strength parameters (f_R values), the increase was less pronounced than that of f_L, however, but an upward trend was still observed (Figure 4.59 and 4.60).

In detail, for the SFRC-40 series, the residual strength values of the sprayed beam increased approximately 16%, while the sprayed panels showed a more moderate increase of 4%. For the sprayed panel SFRC-25 with a difference of 1–3%. In contrast for the SFRC-25 series sprayed beam, the residual strength values of the sprayed beams at 90 days were on average 14% lower than those at 28 days.

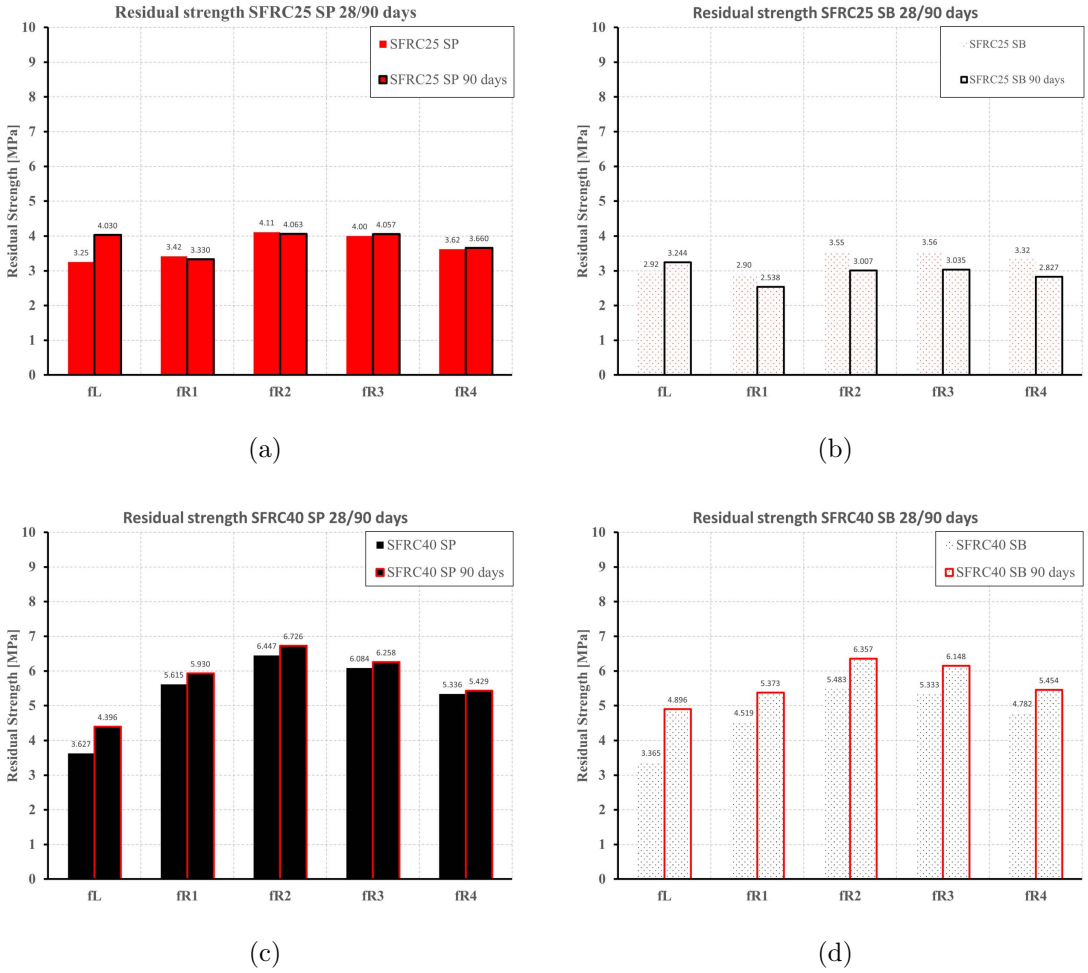

Figure 4.59: Comparison of residual strength results of FRC sprayed concrete at 28 and 90 days (a) SFRC25 SP, (b) SFRC25 SB, (c) SFRC40 SP, and (d) SFRC40 SB.

Regarding the series of cast elements (Figure 4.60, the SFRC-40 cast beams (SFRC-40 CB) showed a 8% increase in the values of f_{R3} and f_{R4}. The MSFRC7 cast beams showed a minimal variation, with 1% and 2% differences in f_{R3} and f_{R4}, respectively, indicating a negligible change over time. However, MSFRC7 cast panels exhibited a significant increase of approximately 35%.

From the above discussion,it can be summarised that, considering the consistent results observed in the SFRC-40 sprayed series, there was an overall 4- 16% increase in residual strength at 90 days compared to the results at 28 days.

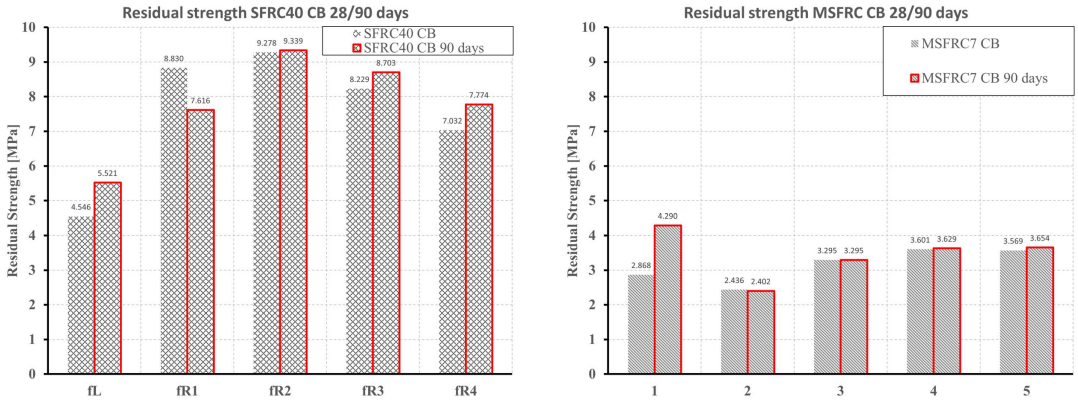

(a) (b)

Figure 4.60: Comparison of residual strengths for FRC cast seriesat 28 and 90 days: (a) SFRC40 CB, (b) MSFRC7 CB.

4.5.7 Energy Absorption Capacity (EN 14488-5)

As mentioned in Section 2.5.2, the European sprayed standard EN 14488-7 [19] it is advised to specify the ductility of fibre reinforced sprayed concrete, EN 14488-5 [18] energy absorption test should be performed in addition to the residual strength test EN 14488-3 [18]. The tests were carried out on sprayed specimens of SFRC-25 and SFRC-40; additionally, the test also performed on cast specimens of SFRC-25, SFRC-40 and MSFRC-7.

In the Figure 4.61a, the load–net deflection response up to 30 mm net deflection from the energy absorption capacity test is presented. The cumulative energy corresponding to each net deflection is plotted separately in the energy graph shown in Figure 4.61b. The cumulative energy at 25 mm referred to as the energy absorption capacity class E_{25} of the series, is indicated on the graph by a dot. The same type of response is presented in Figures 4.62 and 4.63 for SFRC-

40 SP and MSFRC-7 CP series, respectively. In both the (a)and (b) graphs, the experimental scatter is shown in grey, while the mean responses are highlighted in bold red, black, and blue for SFRC-25, SFRC-40, and MSFRC-7, respectively. All series are above the minimum class according to EN 14487-1 [19] sprayed concrete standard (4.16. The summary results for each series and the energy class are shown in Table 2.24.

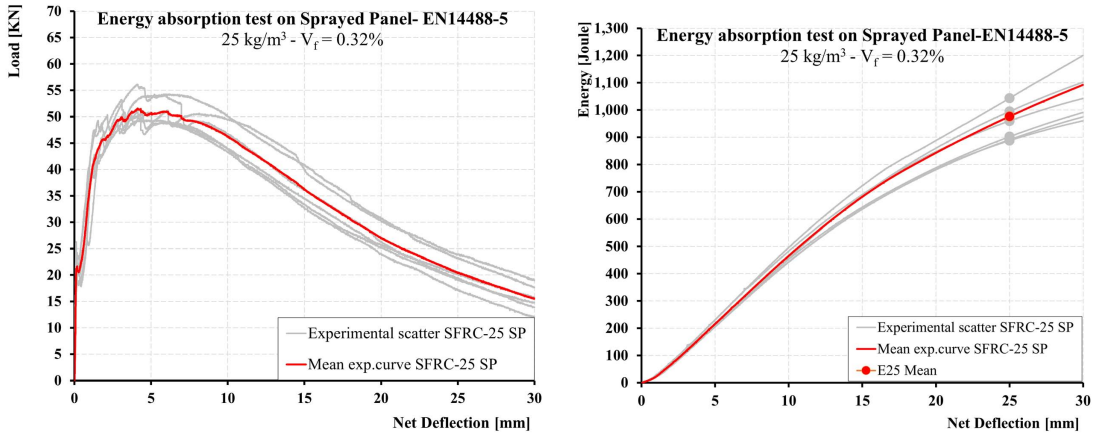

(a) (b)

Figure 4.61: Energy absorption capacity results SFRC-25 SP series: Load vs. Net deflection (a) and Energy vs. Net deflection (b).

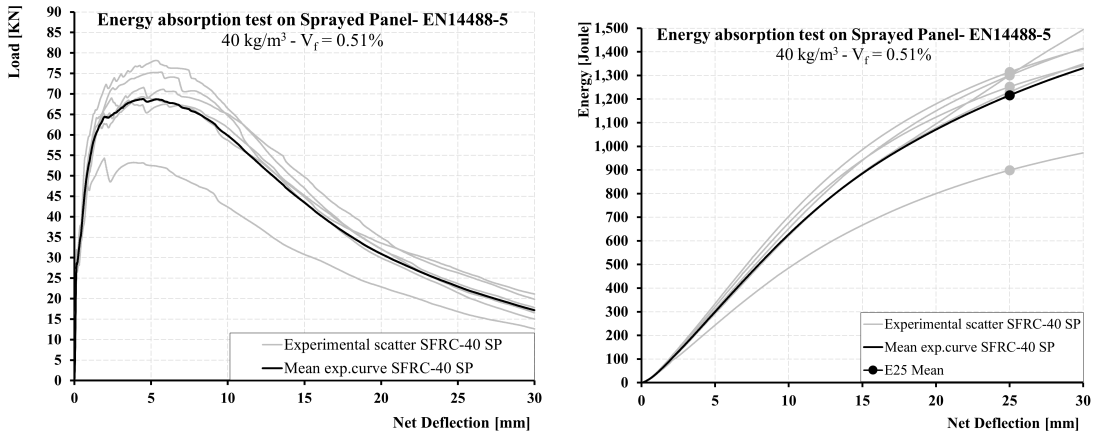

(a) (b)

Figure 4.62: Energy absorption capacity results of SFRC-40 SP series: Load vs. Net deflection (a) and Energy vs. Net deflection (b).

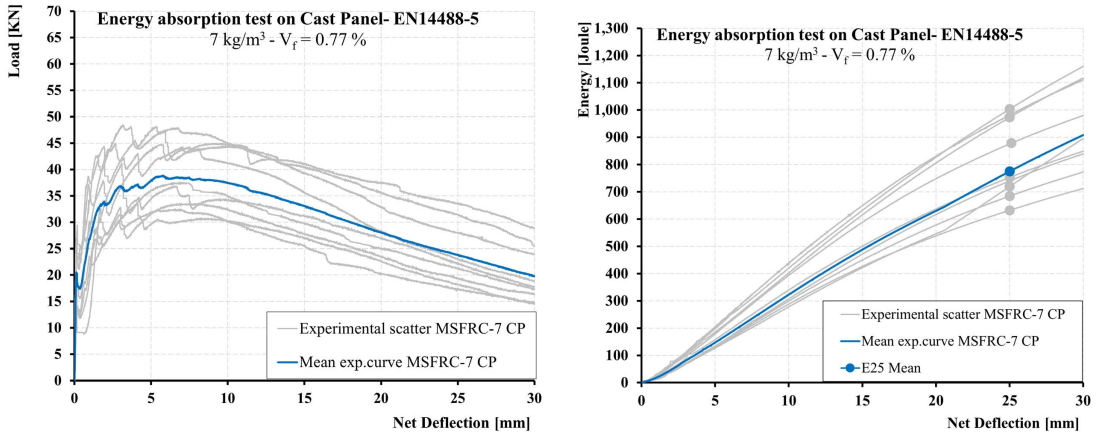

(a) (b)

Figure 4.63: Energy absorption capacity results of MSFRC-7 CP series: Load vs. Net deflection (a) and Energy vs. Net deflection (b).

The energy absorption capacity or toughness of the sprayed FRC lining increases with increasing fibre dosage. In this research, when the fibre content increase by 60%, 25 kg/m^3 to 40 kg/m^3, the energy absorption capacity increased by 28% and 21% for the sprayed and cast series, respectively. Compared to the variation in residual strength, this increase is relatively moderate. Regarding the difference between the sprayed and cast series, with the 25 kg/m^3 fibre dosage the difference is 5.90%, while at 40 kg/m^3 fibre dosage, the energy absorption capacity of the cast and sprayed series is nearly identical.

Therefore, in terms of toughens, the use of cast specimens to represent the sprayed linings less sensitive than when evaluating residual flexural strength (Table 2.24 and Figure 4.65).

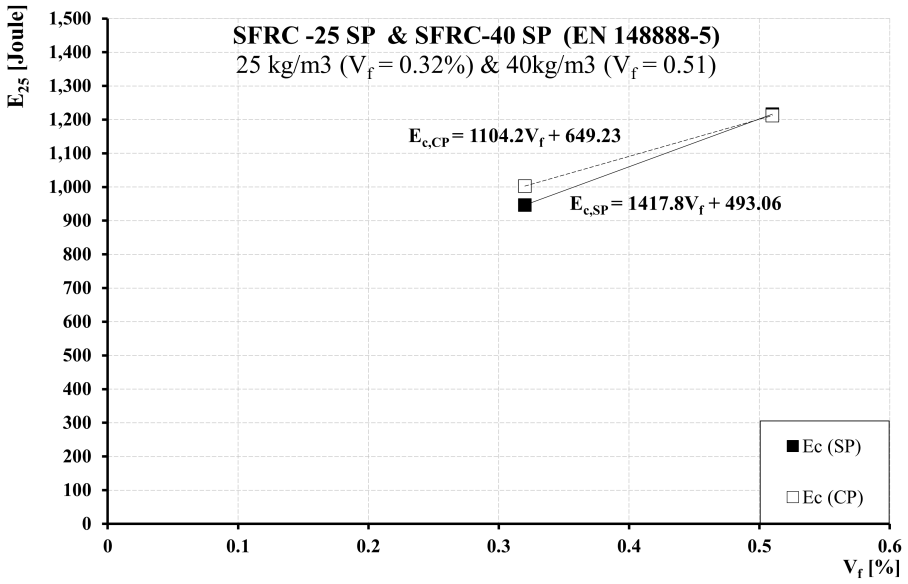

Figure 4.64: Fibre content effect on energy absorption capacity (E_25).

Table 4.16: Definitions of energy absorption classes based on EN 14487-1 [19].

Energy absorption class	**Energy absorption in J for deflection up to 25 mm**
E500	500
E700	700
E1000	1000

Table 4.18: Energy absorption class based on EN 14488-5 [18] test methodology and sprayed concrete standard EN 14487-1 [19].

Parameter	**Mean energy absorption capacity (E_{25}) (Joule)**	**Energy absorption class**
SFRC25_SP	947 (0.07)	E700
SFRC25_CP	1003	E1000
SFRC40_SP	1216 (0.13)	E1000
SFRC40_CP	1212	E1000
MSFRC7_CP	818 (0.17)	E700

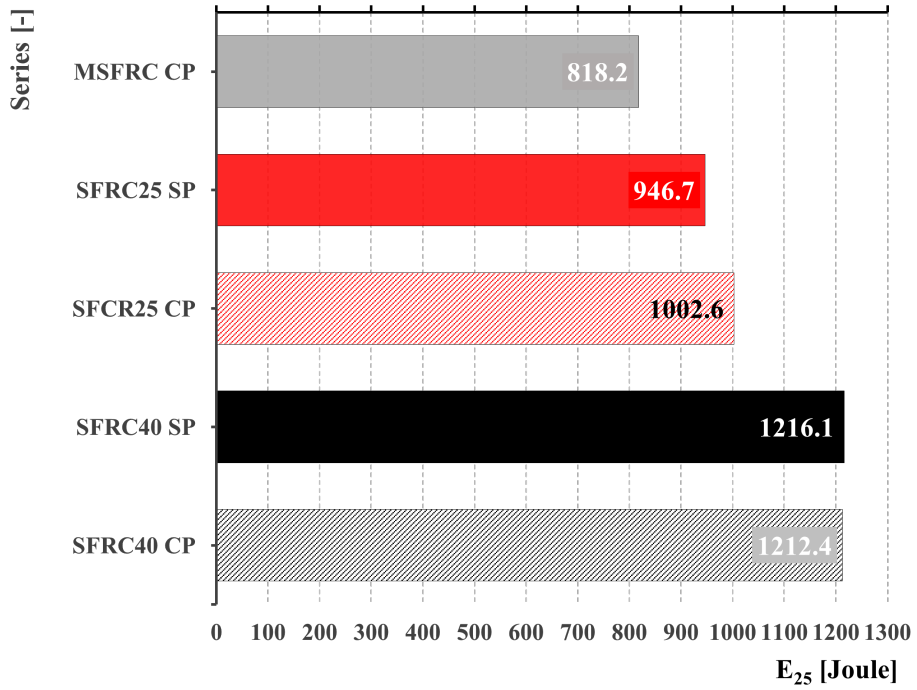

Figure 4.65: Energy absorption capacity (E_25) for all series.

As clearly stated in the relevant standard [19] and detailed in Section 2.5 of this thesis, the residual flexural strength and toughness are not directly comparable, as they are derived from different experimental setups, distinct loading configurations, and are designed to assess different material responses.

4.6 Material Characterisation and Classification

Material characterisation and classification for sprayed FRC and conventional FRC have been discussed in the state-of-the-art of this thesis, specifically in Sections 2.5 and 2.1.5, respectively.

The classification of the beam series follows the guidelines of Model Code 2020 [8] and Eurocode 2 Annex L [9], as detailed in Section 2.1.5. Both standards classify the performance of FRC solely on the basis of the residual flexural strength values. The strength class (SC) is determined by the characteristic value f_{R1k}, while the ductility class is defined by the ratio f_{R3k}/f_{R1k} according to Model Code 2020 [8]. In Eurocode 2 Annex L [9], ductility is instead defined by the ratio f_{R3k}/SC (Strength Class).

The characteristic values were quantified using normal distribution and log-normal distribution, in accordance with the recommendations of the Model Code 2020 [8] and Eurocode 2 Annex L [9], respectively. The k_n values were selected based on the number of samples, as shown in Table 4.20, and as noted in the reference, these values apply to normal distribution. In addition, characteristic values computed using k_n with a quantile factor 5% for the normal distribution were also determined and classified accordingly.

The procedure adopted for calculating the standard deviation follows the method suggested in EN 1990:2023 [176].

$$s_x = \sqrt{\frac{\sum_{i=1}^{n}(x_i - x_m)^2}{n-1}} \tag{4.4}$$

where:
s_x = standard deviation,
x_m = mean value of the test results,
x_i = individual test result,
n = number of tests.

$$x_k = x_m - k_n\, s_x \tag{4.5}$$

where k_n is a parameter depending on the number of tests as per Table 4.20.

Table 4.20: Parameters for determining the characteristic strength (Model Code 2020 [8]).

Parameter	**3**	**4**	**5**	**6**	**8**	**10**	**12**	**20**	**30**	**40**
k_n (known)	1.89	1.83	1.80	1.77	1.74	1.72	1.71	1.68	1.67	1.64
k_n (unknown)	3.37	2.63	2.33	2.18	2.00	1.92	1.87	1.76	1.73	1.64

Table 4.21: Classification at 28 days based on characteristic values computed using the normal distribution approach, employing the k_n factors proposed in Model Code 2020 [8], as provided in Table 4.20.

Parameter	f_{Lk} **(MPa)**	$f_{R,1k}$ **(MPa)**	$f_{R,3k}$ **(MPa)**	$f_{R,3k}/f_{R,1k}$	$f_{R,1k}/f_{Lk}$	**Class (MC2020)**
SFRC25_CB	3.38	4.25	5.34	1.26	1.26	4d
SFRC25_SB	2.39	2.43	2.88	1.19	1.02	2d
SFRC40_CB	3.97	7.25	6.72	0.93	1.83	7c
SFRC40_SB	3.02	3.79	4.59	1.21	1.26	3.5d
MSFCR7_CB	2.31	1.61	2.44	1.52	0.70	1.5e

Table 4.22: Classification at 28 days based on characteristic values computed using the normal distribution approach, employing the k_n factor (with $k_n = 1.645$, corresponding to the 5% lower quantile).

Parameter	$\mathbf{f_{Lk}}$ (MPa)	$\mathbf{f_{R,1k}}$ (MPa)	$\mathbf{f_{R,3k}}$ (MPa)	$\mathbf{f_{R,3k}/f_{R,1k}}$	$\mathbf{f_{R,1k}/f_{Lk}}$	**Class (MC2020)**
SFRC25_CB	3.46	4.36	5.46	1.25	1.26	4d
SFRC25_SB	2.45	2.48	2.96	1.19	1.01	2d
SFRC40_CB	4.04	7.44	6.90	0.93	1.84	7c
SFRC40_SB	3.06	3.88	4.68	1.21	1.27	3.5d
MSFCR7_CB	2.38	1.71	2.58	1.51	0.72	1.5e

Table 4.23: Classification based on characteristic values computed using the normal distribution approach, employing the k_n factor (with $k_n = 1.645$, corresponding to the 5% lower quantile) at 90 days.

Parameter	$\mathbf{f_{Lk}}$ (MPa)	$\mathbf{f_{R,1k}}$ (MPa)	$\mathbf{f_{R,3k}}$ (MPa)	$\mathbf{f_{R,3k}/f_{R,1k}}$	$\mathbf{f_{R,1k}/f_{Lk}}$	**Class (MC2020)**
SFRC25_SB	2.80	2.02	2.29	1.14	0.72	2d
SFRC40_SB	3.55	4.39	5.11	1.16	1.24	4d
MSFRC7_CB	4.15	2.18	3.07	1.40	0.53	5d

Determination of characteristic values using log-normal distribution considering 5% lower quantile and a 75% confidence level, as advised by EN 1990:2023 [176] and Eurocode 2 Annex L [9].

$$m_y = \frac{1}{n}\sum_{i=1}^{n} \ln x_i, \tag{4.6}$$

$$s_y = \sqrt{\frac{1}{n-1}\sum_{i=1}^{n} (\ln x_i - m_y)^2}, \tag{4.7}$$

$$X_k = \exp\left(m_y - k_n\, s_y\right) \tag{4.8}$$

where:

m_y = mean of the natural logarithm of the experimental values ($\ln x_i$);

s_y = standard deviation of the natural logarithm of the experimental values;

n = total number of samples;

x_i = individual experimental value;

X_k = characteristic value corresponding to the 5% quantile of the log-normal distribution;

k_n = statistical factor corresponding to the 5% lower fractile (95% probability of exceedance), equal to 1.645.

As representative log-normal probability density functions (PDFs) of residual flexural tensile strengths for SFRC-40 CB (Figure 4.66), showing the 5% lower quantile (characteristic value) and the 75% confidence level (CL). The figure illustrates the log-normal distribution fitted to the experimental data, with individual test results indicated by orange markers. For the SFRC-40 CB series, all data points lie above the 5% lower quantile, confirming the consistency and reliability of the experimental measurements.

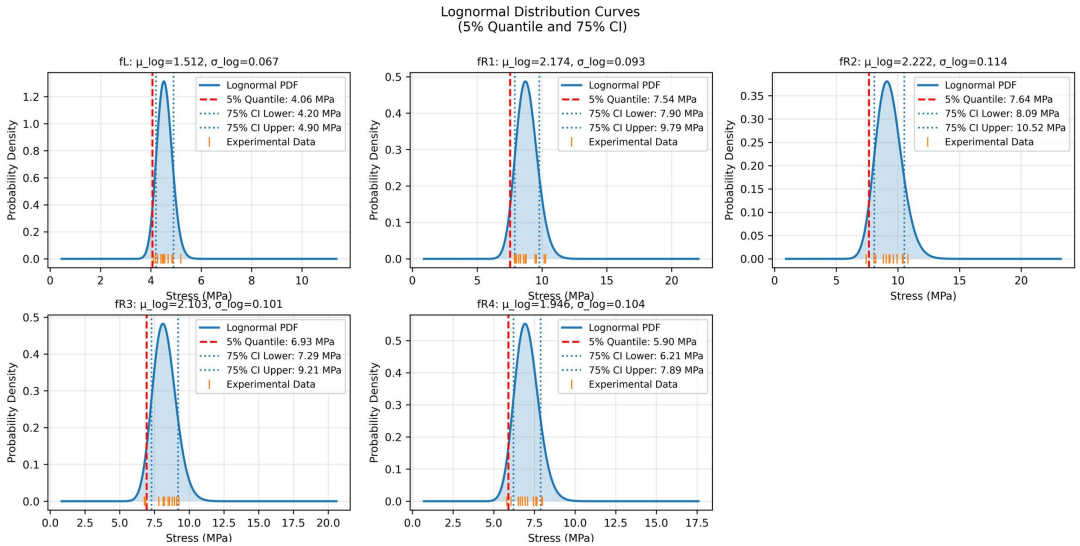

Figure 4.66: Log-normal probability density functions (PDFs) of residual flexural tensile strengths for SFRC-40 CB series.

Table 4.24: Classification at 28 days based on characteristic values computed using the log-normal distribution approach.

Parameter	$\mathbf{f_{Lk}}$ (MPa)	$\mathbf{f_{R,1k}}$ (MPa)	$\mathbf{f_{R,3k}}$ (MPa)	$\mathbf{f_{R,3k}/f_{R,1k}}$	$\mathbf{f_{R,1k}/f_{Lk}}$	**Class (Eurocode 2 Annex L)**
SFRC25_CB	3.49	4.38	5.46	1.25	1.25	4e
SFRC25_SB	2.47	2.52	3.01	1.20	1.02	2.5d
SFRC40_CB	4.06	7.54	6.93	0.92	1.86	7d
SFRC40_SB	3.07	3.89	4.70	1.21	1.27	3.5e
MSFCR7_CB	2.41	1.78	2.69	1.51	0.74	1.5e

Table 4.25: Classification based on characteristic values computed using the log-normal distribution approach at 90 days.

Parameter	$\mathbf{f_{Lk}}$ (MPa)	$\mathbf{f_{R,1k}}$ (MPa)	$\mathbf{f_{R,3k}}$ (MPa)	$\mathbf{f_{R,3k}/f_{R,1k}}$	$\mathbf{f_{R,1k}/f_{Lk}}$	**Class (Eurocode 2 Annex L)**
SFRC25_SB	2.84	2.08	2.38	1.15	0.73	2d
SFRC40_SB	3.70	4.44	5.16	1.16	1.20	4d
MSFRC7_CB	4.15	2.19	3.11	1.42	0.53	2e

The characteristic values obtained from the normal and log-normal statistical models show slight differences.

The performance differences between 28 days and 90 days, as discussed in Section 4.5 are consistent with the expected changes in the characteristic residual strength values. The variation in ductility class with ageing between 28 and 90 days is minimal; the only observed change is a slight shift in the SFRC-40 series from Class 3.5d to Class 4d.

For the sprayed FRC Panels, the classification is not explicitly defined in the Model Code [8] or EN 1992 Annex L, as both documents address conventional or cast FRC. Moreover, neither the Model Code [8] nor Eurocode 2 Annex L clarified whether this classification is intended to apply to sprayed FRC. However, the European standard for sprayed concrete [19] introduces a ductility classification (Table 4.26).

Table 4.26: Definition of class of ductility EN 14487-1 [19].

Class of Ductility	**Ductility Requirement**	**Crack Control Requirement**
Class 1	$f_{\mathrm{R3}k}/f_{\mathrm{R1}k} > 0.5$	$f_{\mathrm{R1}k}/f_{\mathrm{L}sk} > 0.4$
Class 2	$f_{\mathrm{R3}k}/f_{\mathrm{R1}k} > 0.7$	$f_{\mathrm{R1}k}/f_{\mathrm{L}sk} > 0.5$
Class 3	$f_{\mathrm{R3}k}/f_{\mathrm{R1}k} > 0.9$	$f_{\mathrm{R1}k}/f_{\mathrm{L}sk} > 0.6$

Table 4.27: EN 14487-1 classification [19] at 28 days based on characteristic values computed using the normal distribution approach, employing the k_n factors proposed in Model Code 2020 [8], as provided in Table 4.20.

Parameter	$\mathbf{f_{Lk}}$ (MPa)	$\mathbf{f_{R,1k}}$ (MPa)	$\mathbf{f_{R,3k}}$ (MPa)	$\mathbf{f_{R,3k}/f_{R,1k}}$	$\mathbf{f_{R,1k}/f_{Lk}}$	**Classification (EN 14487-1)**
SFRC25_SP	2.92	2.03	2.52	1.25	0.69	Class 3
SFRC40_SP	3.19	4.70	4.98	1.06	1.47	Class 3
SFRC25_SB	2.39	2.43	2.88	1.19	1.02	Class 3
SFRC40_SB	3.02	3.79	4.59	1.21	1.26	Class 3

Table 4.28: EN 14487-1 classification at 28 days based on characteristic values computed using the normal distribution approach, employing the k_n factor (with $k_n = 1.645$, corresponding to the 5% lower quantile).

Parameter	$\mathbf{f_{Lk}}$ (MPa)	$\mathbf{f_{R,1k}}$ (MPa)	$\mathbf{f_{R,3k}}$ (MPa)	$\mathbf{f_{R,3k}/f_{R,1k}}$	$\mathbf{f_{R,1k}/f_{Lk}}$	**Classification (EN 14487-1)**
SFRC25_SP	2.98	2.25	2.76	1.23	0.76	Class 3
SFRC40_SP	3.37	4.85	5.39	1.11	1.44	Class 3
SFRC25_SB	2.45	2.48	2.96	1.19	1.01	Class 3
SFRC40_SB	3.06	3.88	4.68	1.21	1.27	Class 3

Table 4.29: EN 14487-1 classification [19] at 28 days based on characteristic values computed using the log-normal distribution approach.

Parameter	$\mathbf{f_{Lk}}$ (MPa)	$\mathbf{f_{R,1k}}$ (MPa)	$\mathbf{f_{R,3k}}$ (MPa)	$\mathbf{f_{R,3k}/f_{R,1k}}$	$\mathbf{f_{R,1k}/f_{Lk}}$	**Classification (EN 14487-1)**
SFRC25_SP	2.99	2.42	2.92	1.21	0.81	Class 3
SFRC40_SP	3.38	4.93	5.43	1.10	1.46	Class 3
SFRC25_SB	2.47	2.52	3.01	1.20	1.02	Class 3
SFRC40_SB	3.07	3.89	4.70	1.21	1.27	Class 3

Table 4.30: EN 14487-1 classification [19] based on characteristic values computed using the normal distribution approach, employing the k_n factor (with $k_n = 1.645$, corresponding to the 5% lower quantile) at 90 days.

Parameter	$\mathbf{f_{Lk}}$ (MPa)	$\mathbf{f_{R,1k}}$ (MPa)	$\mathbf{f_{R,3k}}$ (MPa)	$\mathbf{f_{R,3k}/f_{R,1k}}$	$\mathbf{f_{R,1k}/f_{Lk}}$	**Classification (EN 14487-1)**
SFRC25_SP	3.17	2.55	3.03	1.19	0.80	Class 3
SFRC40_SP	3.73	4.91	5.18	1.05	1.32	Class 3
SFRC25_SB	2.80	2.02	2.29	1.14	0.72	Class 3
SFRC40_SB	3.55	4.39	5.11	1.16	1.24	Class 3

Table 4.31: EN 14487-1 classification based on characteristic values computed using the log-normal distribution approach, employing the k_n factor (with $k_n = 1.645$, corresponding to the 5% lower quantile) at 90 days.

Parameter	$\mathbf{f_{Lk}}$ (MPa)	$\mathbf{f_{R,1k}}$ (MPa)	$\mathbf{f_{R,3k}}$ (MPa)	$\mathbf{f_{R,3k}/f_{R,1k}}$	$\mathbf{f_{R,1k}/f_{Lk}}$	**Classification (EN 14487-1)**
SFRC25_SP	2.99	2.42	2.92	1.21	0.81	Class 3
SFRC40_SP	3.38	4.93	5.43	1.10	1.46	Class 3
SFRC25_SB	2.47	2.52	3.01	1.20	1.02	Class 3
SFRC40_SB	3.07	3.89	4.70	1.21	1.27	Class 3

According to the definitions of ductility classes in EN 14487-1 [19] both SFRC-25 and SFRC-40 sprayed panels fall within Ductility Class 3,which the ductility requirement is $f_{\mathrm{R1}k}/f_{\mathrm{R3}k} > 0.9$ and the crack control requirement is $f_{\mathrm{R1}k}/f_{\mathrm{L}k} > 0.6$. The classification was also performed at 90 days. Although a slight increase in the characteristic residual strength values was observed, no change in ductility class occurred between 28 and 90 days.

Since the Model Code 2020 [8] and Eurocode 2 Annex L [176] classify FRC based on the characteristic residual strengths $f_{R,ki}$ corresponding to CMOD values of 0.5, 1.5, 2.5, and 3.5 mm obtained from cast-in-mould beam tests (EN 14651), the post-cracking residual strengths $f_{R,ki}$ retrieved from tests carried out according to EN 14488-3-Method B on notched-panels were used to determine the sprayed-panel classification. By using normal distribution approach, the classification at 28 days of notched sprayed panels result 2d and 4.5d for SFRC-25 and SFRC-40, respectively. Referring to the same PDF, experimental results at 90 days lead to a classification equal to 2.5d and 4.5d. In the case of log-normal distribution approach the same classifications are retrieved.

Based on the mean values, the performance of the sprayed FRC and cast FRC was compared, and the corresponding strength ratios were established in Section 4.5.6.1. This section discusses the strength class and ductility class for each series. The results demonstrate clear differences in class between the sprayed and cast series. Considering the post-cracking properties at 28 days, for the SFRC25 series, the sprayed panels (SFRC25-SP) correspond to Class

2d, whereas the cast beams (SFRC25-CB) correspond to Class 4d. Similarly, for the SFRC40 series, the sprayed panels (SFRC40-SP) fall into Class 4.5d, while the cast beams (SFRC40-CB) fall into Class 7c. A comparable trend is observed in beam tests: the sprayed beam SFRC25-SB corresponds to Class 2d compared with SFRC25-CB at Class 4d, and the sprayed beam SFRC40-SB corresponds to Class 3.5d compared with SFRC40-CB at Class 7c.

Chapter 5

Numerical Modelling

5.1 Introduction

The post-cracking behaviour or properties of concrete materials, whether plain or fibre-reinforced, can be predicted using a stress versus crack-opening displacement (σ-w) relationship. As discussed in detail in the state of the art of this thesis (Section 2.1.2), the σ-w diagram is considered the characteristic material property of FRC materials. For plain concrete, this behaviour is typically characterised by its tensile strength and fracture energy, as the shape of the σ-w curve doesn't vary for plain concrete.

A bilinear σ-w relationship generally provides a reliable estimation of the post-cracking performance of plain concrete [20]; see Figure 5.1 and corresponding Equations 5.1,5.2 and 5.3. In contrast, for fibre-reinforced composites, the shape of the σ-w curve varies significantly based on the type of fibre, its content and properties, and the type of concrete matrix and its quality. As a result, for each specific FRC composition, it is essential to establish the σ-w relationship that most accurately reflects the tensile behaviour of the composite.

Ideally, a direct tension test should be performed to establish the σ-w relationship. However, this test is complicated, as described in detail in Section 2.1.3. An alternative approach, currently under extensive investigation, involves using the load-displacement response from the 3PB tests to drive the σ-w curve of the material through inverse analysis. Most researchers have focused on the behaviour of notched beams under three-point bending loads, while inverse analysis using 3PBT notched panel tests, which is the test methodology for characterising FRC sprayed concrete, has been scarcely addressed in the literature.

Consequently, this thesis aims to propose the inverse analysis procedure to drive uniaxial

post-cracking laws from the EN 14488-3 Method B [16] sprayed panel test. In addition inverse analysis are performed on notched cast beams and saw-cut sprayed beams to determine the σ-w relationships for steel fibre content of 25 and 40 kg/m^3 ,up to distinct ultimate crack widths, and to investigate the post-cracking behaviour of sprayed fibre-reinforced concrete.

Through this numerical method approach, the characteristic material properties of sprayed fibre-reinforced concrete are investigated, based on the experimental results in Chapter 4. A comparison of main displacement parameters of 3PBTs, analysed experimentally in Chapters 4 and analytically in Chapter 6, is provided. In Addition, uniaxial post-cracking constitutive laws are developed for different fibre contents and casting methods.

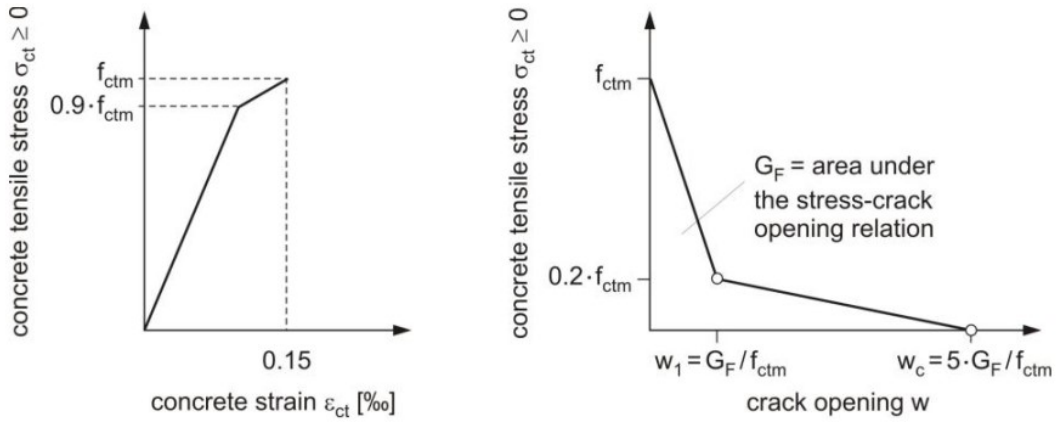

Figure 5.1: Stress-strain and stress-crack opening diagram of plain concrete for uniaxial tension [20].

$$\sigma_{ct} = E_{ci} \cdot \varepsilon_{ct}, \quad \text{for } \sigma_{ct} \leq 0.9 f_{ctm} \tag{5.1}$$

$$\sigma_{ct} = f_{ctm} \cdot \left(1 - 0.1 \cdot \frac{0.00015 - \varepsilon_{ct}}{0.00015 - \frac{0.9 f_{ctm}}{E_{ci}}}\right), \quad \text{for } 0.9 f_{ctm} < \sigma_{ct} \leq f_{ctm} \tag{5.2}$$

$$G_F = 73 \cdot f_{cm}^{0.18} \tag{5.3}$$

5.2 Description of the Finite Element Model (FEM)

The numerical model was created using a commercially available finite element program [177]. A two-dimensional finite element model (FEM) of EN 14488-3 [16] test methodology and EN 14651 [7] test methodology has been developed for FRC panels and FRC beams, respectively, with different fibre contents and casting methods.

A 2D plane stress element was utilized for the numerical modelling of the EN 14488-3 method B [16] 3-point bending panel test methodology; although a preliminary evaluation of mesh reliability was necessary. In fact, the geometrical dimensions of the notched panels do not strictly correspond to those of a 2D plane stress condition and are probably closer to those of a thin-slab condition. Nevertheless, during tests, a simple support condition is adopted, corresponding to a statically determinate scenario in terms of boundary conditions. Furthermore, when carrying out tests, it was clear that the notch depth in the cracking stage determined a flexural behaviour dominated by bending behaviour in the direction governed by the position of line supports. This tendency is clearly confirmed in terms of kinematic behaviour through the correlation between CMOD and CTOD experimental measurements and those obtained from the 2D plane stress models, as will be described later in detail.

To evaluate the impact of these aspects, a 3D solid element mesh (shown in Figure 5.2) was implemented, and a finite element model was developed for one series of the panels. The mesh is characterised by 3D solid elements and interface elements (adequate for considering the post-cracking non linear behaviour, discrete crack approach) along the central expected crack plane over the central notch. In this regard, a mesh division of 44 elements was adopted along the 90 mm of height above the notch (element size of approximately 2 mm), while along the 600 panel width, 60 elements were used, leading to an element size of 10 mm in this direction.

It is worth noting that only half of the panel was modelled, taking advantage of the symmetry of the loads and boundary conditions along the 600 mm width direction. It was not possible to model one quarter of the panel due to numerical instability (difficulties in convergence) when applying symmetric constraints to the interface elements. For the same reason, the 2D plane stress element mesh of the notched panel does not take advantage of the only possible exploitable symmetry of loads and supports. In the case of 3D solid elements mesh, an imposed displacement is applied along the line corresponding to the central roller used in test to apply the load. A constitutive uni-axial tensile post-cracking law representative of concrete reinforced by macro-synthetic fibre was used.

The results from the 3D and 2D models are compared in terms of residual strengths versus CMOD in Figure 5.3. It can be noted that, a very good agreement can be observed, proving the reliability and consistency of the 2D model. The 2D model runs on a standard computer in about 6 minutes, whereas the 3D model requires about 12 hours, making the 2D model the best choice for the inverse analysis procedure.

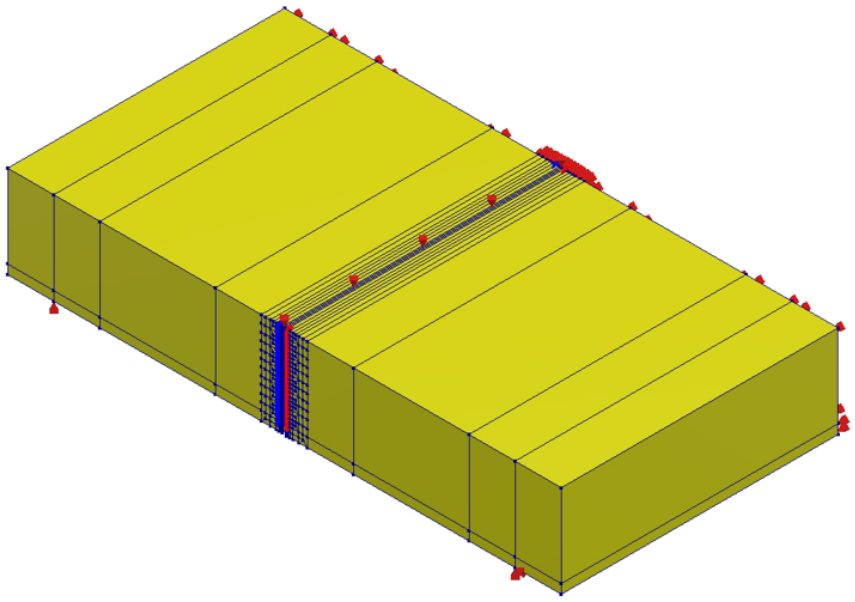

Figure 5.2: EN 14488-3 Method B [16] 3PBT finite element modelling (3D geometry with half symmetry).

Thus, the 2D mesh model was adopted for the thesis. This approach was used for the numerical modelling of both the EN 14488-3 method B [16] 3-point bending panel test and the EN 14651 [16] 3-point bending beam test. It is worth noting that also in the case of the geometrical configuration of standard beam (150 x 150 x 550 mm) according to EN 14651 [7], the beam width (150 mm) is not negligible, strictly speaking, with respect to the other two dimensions, leading to a perfectly ideal 2D plane stress condition. Nevertheless, the boundary conditions together with the governing crack phenomenon at midspan described by interface elements (adequate for considering the post-cracking non-linear behaviour, discrete crack approach), make the adoption of the 2D model adequate as proven by a broad literature in this regard.

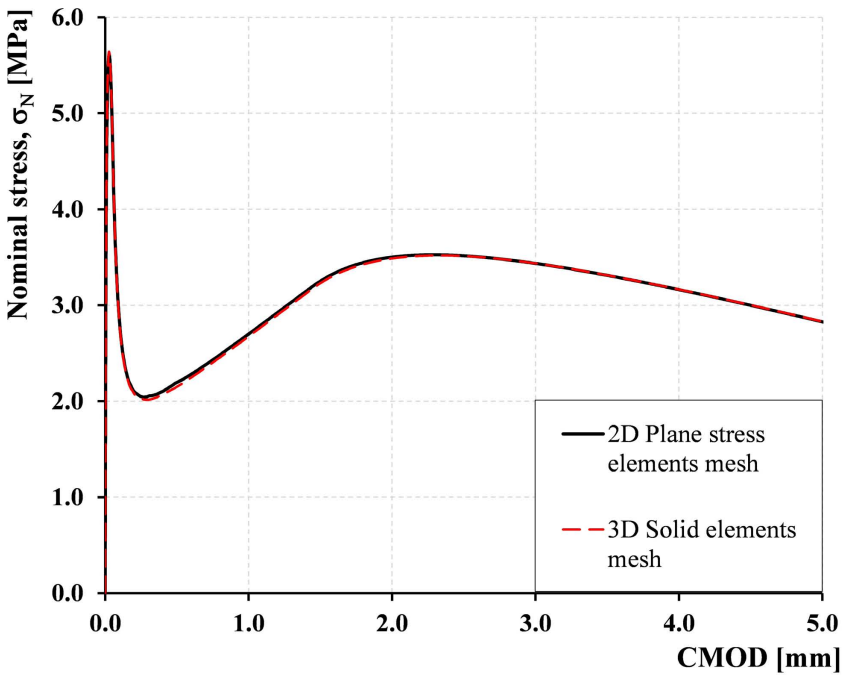

Figure 5.3: Comparison of inverse analysis results using 2D plane-stress element mesh and 3 D solid element mesh for the EN 14488-3 Method B notched panel test.

As discussed above, the numerical modelling involved the EN 14488-3 Method B [16] 3-point bending panel test methodology and EN 14561 [16] 3-point bending beam test methodology. A notched panel was supported by a roller at one end and a pin at the other, with a loading roller at the top. Similar boundary conditions were applied to the FEM model, with roller support at one end and pin support at the other opposite side, as shown in Figure 5.4. A coarse mesh was selected for the left and right sides, while a finer mesh was applied in the middle to achieve greater accuracy in the results. To capture non-linear post-cracking phenomena, proper mesh refinement was implemented at mid-span, as shown in the Figure 5.5.

In this regard, 46 interface elements (which entirely describe the non-linear post-cracking behaviour) are used for the 2D mesh depicted in Figure 5.4 (3PBT on notched panels), while 36 are used for the numerical model illustrated in Figure 5.6 and 5.6 (3PBT on notched beams). The latter meshing division were calibrated in previous research works [178, 179]. In particular, within the discrete approach, it was demonstrated that moving from 36 divisions to 64 divisions the average absolute percentage difference between the numerical curves was about 0.7% to 0.8% within a CMOD range of 0.05-5 mm.

The verification was carried out with 2D triangular elements as well as with quadrilateral elements. The coarse mesh on the other sides was chosen because of the linear elastic behaviour of these parts of the mesh and the tendency of the standard notched beam to behave as two rigid blocks with a crack at the centre, as proven by kinematic relationships between CTOD and CMOD reported in Section 6.

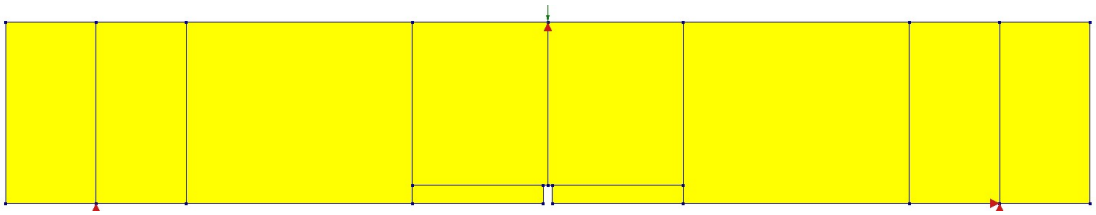

Figure 5.4: A two-dimensional numerical modelling of EN 14488-3 Method B [16] 3PBT test methodology (2D geometry model).

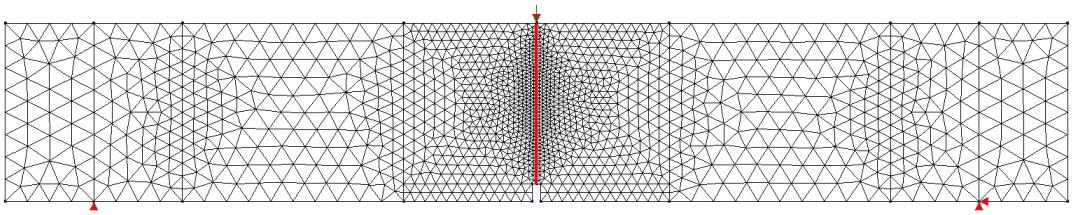

Figure 5.5: Plain stress-mesh configuration of the panel and interface elements used to represent the discrete mid-span crack (EN 14488-3 Method B Panel).

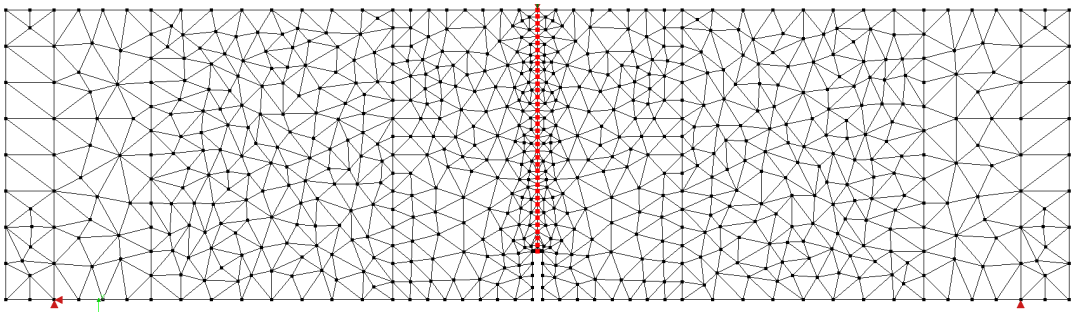

Figure 5.6: Plain stress-mesh configuration of the beam and interface elements used to represent the discrete mid-span crack (EN 14651 Beam).

The FRC panels and beams were modelled with a regular plane stress element type. Specifically, a 2D plane stress, denoted as T6MEM, was utilized. T6MEM (Figure 5.7a) is a triangular isoparametric plane stress element with three nodes [177], based on linear interpol-

ation and area integration. The the displacement field, defined by the components μ_x and μ_y is expressed in Equation 5.4.

The crack propagation was modelled as a discrete crack using interface elements, and the fictitious crack model (FCM) is applied to describe the softening behaviour within the fracture process zone. The interface line element L8IF was employed, with 46 interface elements used along h_{sp} for the EN 14488-3 Method B notched panel, highlighted in red in Figure 5.5 and 36 interface elements used for the EN 14651 notched beam, also highlighted in red in Figure 5.6. These elements were introduced to represent the discrete mid-span crack above the notch. The L8IF element is an interface element between two lines in a two-dimensional configuration (Figure 5.7b [177]. It consists of four nodes Node 1 to Node 4 in sequence, as shown in Figure 5.7b. Nodes 1 and 3 may overlap as may nodes 2 and 4. The local xy axes for the displacements are evaluated in the first node with x from Node 1 to Node 2. The kinematic variables of two-dimensional structural line interface are oriented in the local xy axes (Equation 5.5). The element is based on linear interpolation.

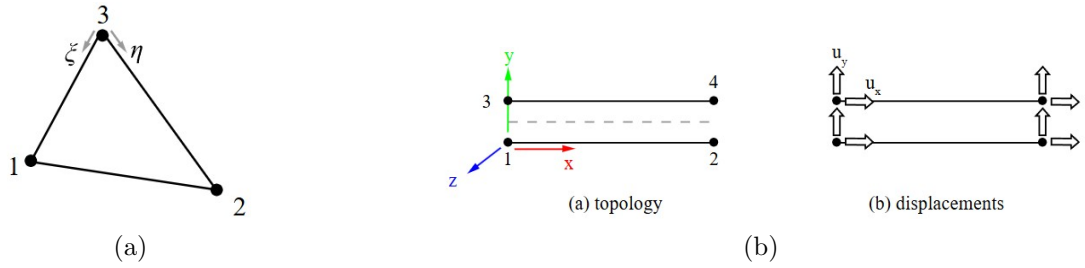

(a) (b)

Figure 5.7: (a) Element type, T6MEM, 2D plane stress, 6-noded triangular isoparametric elements and (b) L8IF structural interface elements, interface line elements.

$$\mu_i(\xi, \eta) = a_0 + a_1\xi + a_2\eta + a_3\xi\eta \tag{5.4}$$

The normal traction t_{ny} is perpendicular to the interface; the shear traction t_{sx} is tangential to the interface (Figure 5.8).

$$\mu_e = \begin{Bmatrix} \mu_x \\ \mu_y \end{Bmatrix}, \quad \Delta\mu = \begin{Bmatrix} \Delta\mu_{sx} \\ \Delta\mu_{ny} \end{Bmatrix}, \quad t = \begin{Bmatrix} t_{sx} \\ t_{ny} \end{Bmatrix} \tag{5.5}$$

As stated above and as illustrated in Figures 5.6 and 5.5, cracking is modelled using a

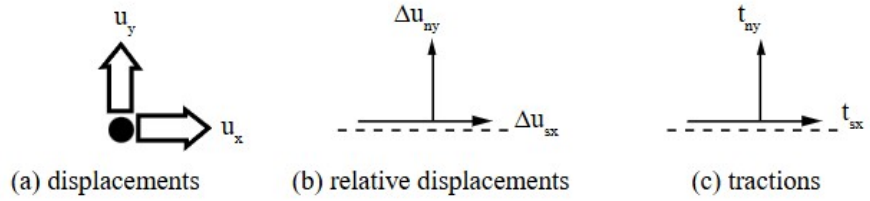

Figure 5.8: Variables of two-dimensional line interfaces.

discrete crack approach and the Fictitious Crack Model (FCM) [180], [181], [182] is applied to describe the softening behaviour within the fracture process zone. In the fictitious crack model, the material response is governed by or the main parameters are the tensile strength, the modulus of elasticity, the fracture energy G_f, and the shape of the stress-crack opening (σ–w) relationship. The tensile fracture behaviour of a concrete is therefore characterized by the relationship between tensile stress and crack opening, which forms the basis of fictitious crack model proposed by Hillerborg and others [180] and [183].

The fracture energy can be experimentally obtained from uni-axial tension tests or flexural tests, as described in Section 2.1.3, which provide the full σ–w curve. In cases where experimental data are not available, the *fib* Bulletin 42 [20] and *fib* Model Code 2020 [8] provides recommended expressions for fracture energy of plain concrete, as given in Equation 2.15. In this section, the fracture energy derived from the uniaxial tensile laws obtained through inverse analysis are discussed.

Thus, a discrete crack approach models a crack as a geometrical discontinuity [184] to simulate failure in 3PBT of FRC notched sprayed panels, cast-in-mould notched panels and notched sprayed saw-cut beams as well as notched cast-in-mould beams. Using a concept of predefined locations of potential cracking, since there is already a notch at the bottom of beams and panels. For this purpose, interface elements are embedded within the original mesh along the expected crack path. These elements are first given a high stiffness value to represent the uncracked condition with a rigid connection between overlapping nodes. When a condition for crack initiation is breached, such as exceeding maximum stress levels, the stiffness of the elements is altered, and a constitutive model for discrete cracks is activated. This model relates the traction vector t^{cr} acting along the crack interface to the relative displacement vector u^{cr} over the crack through C^{cr} a traction-separation relationship, which illustrates phenomena such as tension-softening and aggregate interlock [184].

$$\Delta t^{cr} = C^{cr} \Delta \mu^{cr} \tag{5.6}$$

Prior to cracking, concrete is assumed to behave as an isotropic, linear-elastic material, characterized by Young's modulus E and Poisson's ratio υ. Up on crack initiation, the total strain increment ($\Delta\varepsilon$) decomposed according to Equation 5.7, into a contribution associated with the crack (($\Delta\varepsilon^{cr}$)) and a contribution of the bulk concrete (($\Delta\varepsilon^{co}$)). The bulk concrete continues to be modelled using linear elasticity, while Equation 5.6 is inserted for the crack behaviour.

$$\Delta\varepsilon = \Delta\varepsilon^{cr} + \Delta\varepsilon^{co} \tag{5.7}$$

In the FCM a material point on the crack extension path is assumed to be in one of three possible states: an undisturbed elastic state (no fracture, no lack of compatibility), a fracture state in which the material is softened by microcracking (the fictitious crack), and a state of a fully cracked state, in which no stress transmission across the crack and the point lies on a free surface [181], as illustrated in Figure 5.9.

For all material points outside the fracture process zone, the mechanical response is described by the linear theory of elasticity, corresponding to the pre-cracked state (Equation 5.8). The separation of points in the fracture zone is governed by traction-separation relationship, defined by a multilinear tension-softening criterion expressed in terms of the stress-crack opening displacement relationship (σ–w relation) given by the Equation 5.8.

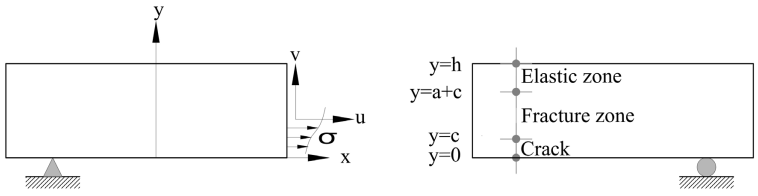

Figure 5.9: Fictitious crack modelling for the discrete crack approach, considered with crack, fracture zone and elastic zone of a given length.

$$\sigma = \begin{cases} \varepsilon E, & \text{pre-crack state} \\ \sigma_w(w), & \text{cracked state} \end{cases} \tag{5.8}$$

5.3 Inverse Analysis

Figure 5.12 shows a schematic representation of the inverse analysis procedure, based on the methodology proposed in [185], [186] for the EN 14651 3PB notched beam test and adopted in this thesis for EN 14488-3 Method B sprayed notched panel test. This process is subdivided into four steps.

The first step is the input stage, where the specimen geometries and boundary conditions are defined, and initial assumptions are made regarding the uniaxial tensile behaviour of the the fibre reinforced concrete. The concrete pre-cracking behaviour is linear elastic and defined by concrete elastic modulus and mean tensile strength (f_{ctm}), as generally adopted by numerous authors [186, 187]. The experimental values of concrete elastic modulus reported in Table 4.5 (Section 4.5.1) were adopted. As mentioned in Section 4.5.1, the experimentally measured values of elastic modulus result lower than those of ordinary concrete with the same class of strength as can be estimated according to current Eurocode 2 [9] and *fib* Model Code 2010 [1]. Therefore, it would have been reasonable to expect a lower concrete mean tensile strength value (f_{ctm}) than that exhibited by ordinary concrete, but it was not possible to develop experimental direct tensile tests. Accordingly, the f_{ctm} was evaluated by initially applying the relationship based on compressive strength proposed by *fib* Model Code 2010 [1] and by apply to the such f_{ctm} an opportune reduction factor for getting a good matching between the numerical curves and experimental ones exhibited in 3PBTs. In this regard, for cast-in-mould concrete a reduction 20% was adopted, while for sprayed concrete 30%.

The second stage is the numerical analysis stage, in which multilinear tension softening laws (see Figure 5.11) are implemented in the model, and the fracture response is analysed. The Non-linear Finite Element Analyses (NLFEA) are performed under displacement-controlled loading by prescribing a total vertical displacement 1 mm at the loading node in the negative Y-direction. The prescribed displacement is applied incrementally using a user-defined load-step scheme.

The third stage involves verifying the accuracy of the numerical stress-crack mouth opening displacement (CMOD) response. At this stage, the deviation between the numerical nominal stress-CMOD curve and the corresponding experimental nominal stress-CMOD results is evaluated. Based on this deviation and the prescribed allowable error, the analysis is repeated using a modified tension-softening diagram until the error falls below the predefined accuracy threshold, as defined in Equation 5.9.

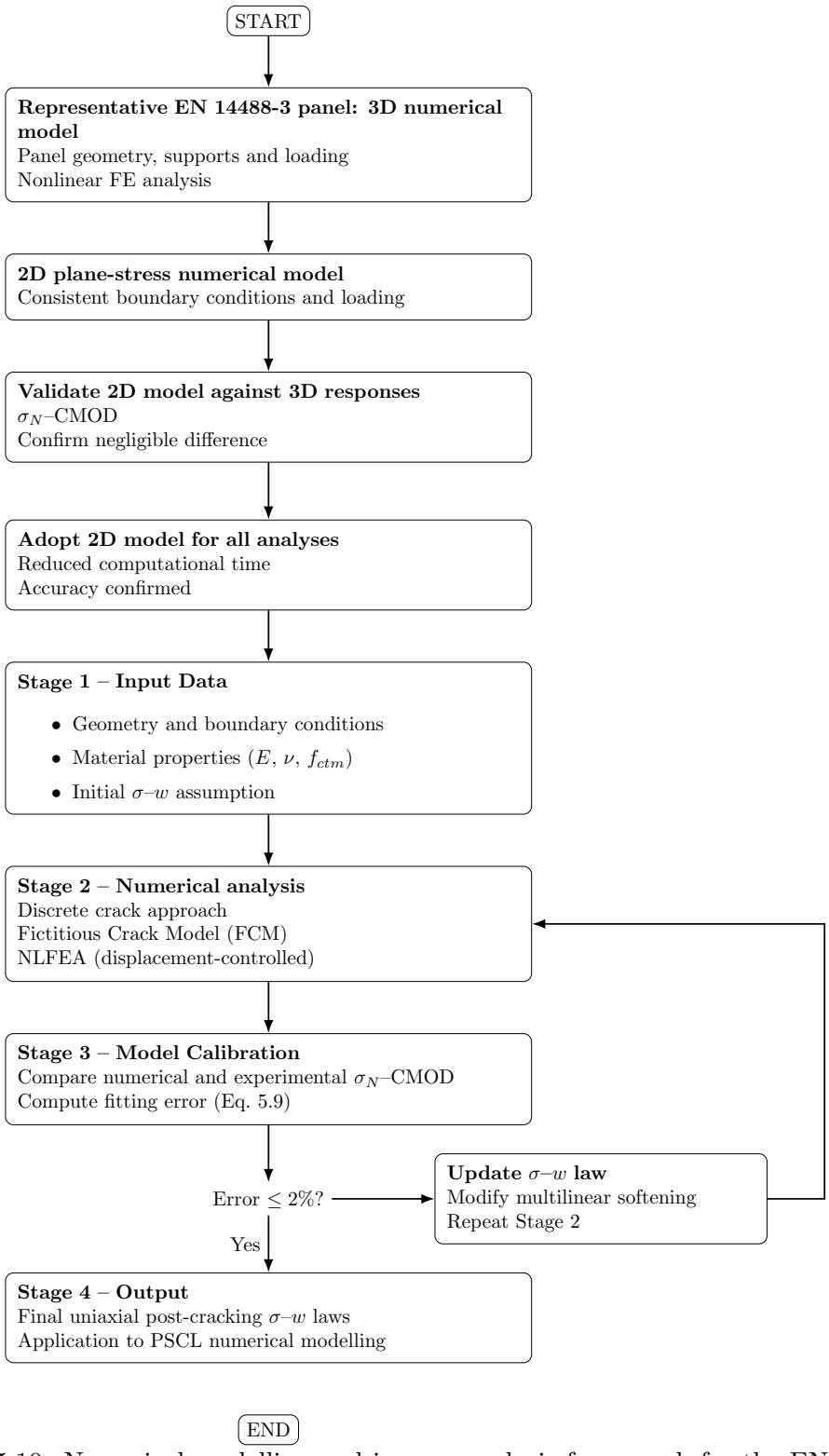

Figure 5.10: Numerical modelling and inverse analysis framework for the EN 14488-3 Method B 3PB sprayed notched panel test.

Finally, the fourth stage is the output stage, in which the final uniaxial post-cracking constitutive laws are identified for each series. Once the numerical response satisfies the predefined accuracy criteria, the corresponding tension-softening σ–w relationships are extracted and adopted as the representative series laws. These laws characterize the post-cracking behaviour and are subsequently used to compare different fibre contents and evaluate the post-cracking performance for the sprayed notched panels and cast-in-mould beams. Moreover, the identified uniaxial post-cracking laws for fibre reinforced sprayed concrete are intended for use in the numerical modelling of permanent sprayed concrete lining (PSCL).

The inverse analyses are performed for each test series, considering different fibre types and fibre contents for sprayed panels and cast-in-mould panels, as well as for cast-in-mould beams and sprayed saw-cut beams.

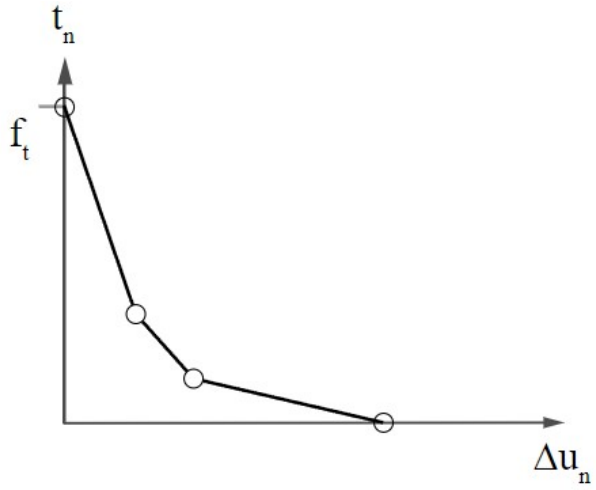

Figure 5.11: Multilinear diagram.

$$\int_0^{\mathrm{CMOD}_i} |\sigma_{\mathrm{Numerical}} - \sigma_{\mathrm{Experimental}}| \ \mathrm{dCMOD} < \mu \tag{5.9}$$

where:

$\sigma_{\mathrm{Numerical}}$ = numerical nominal stress obtained from the FEA,

$\sigma_{\mathrm{Experimental}}$ = experimental nominal stress,

CMOD = crack mouth opening displacement,

CMOD_i = maximum CMOD value considered in the comparison,

μ = prescribed allowable error.

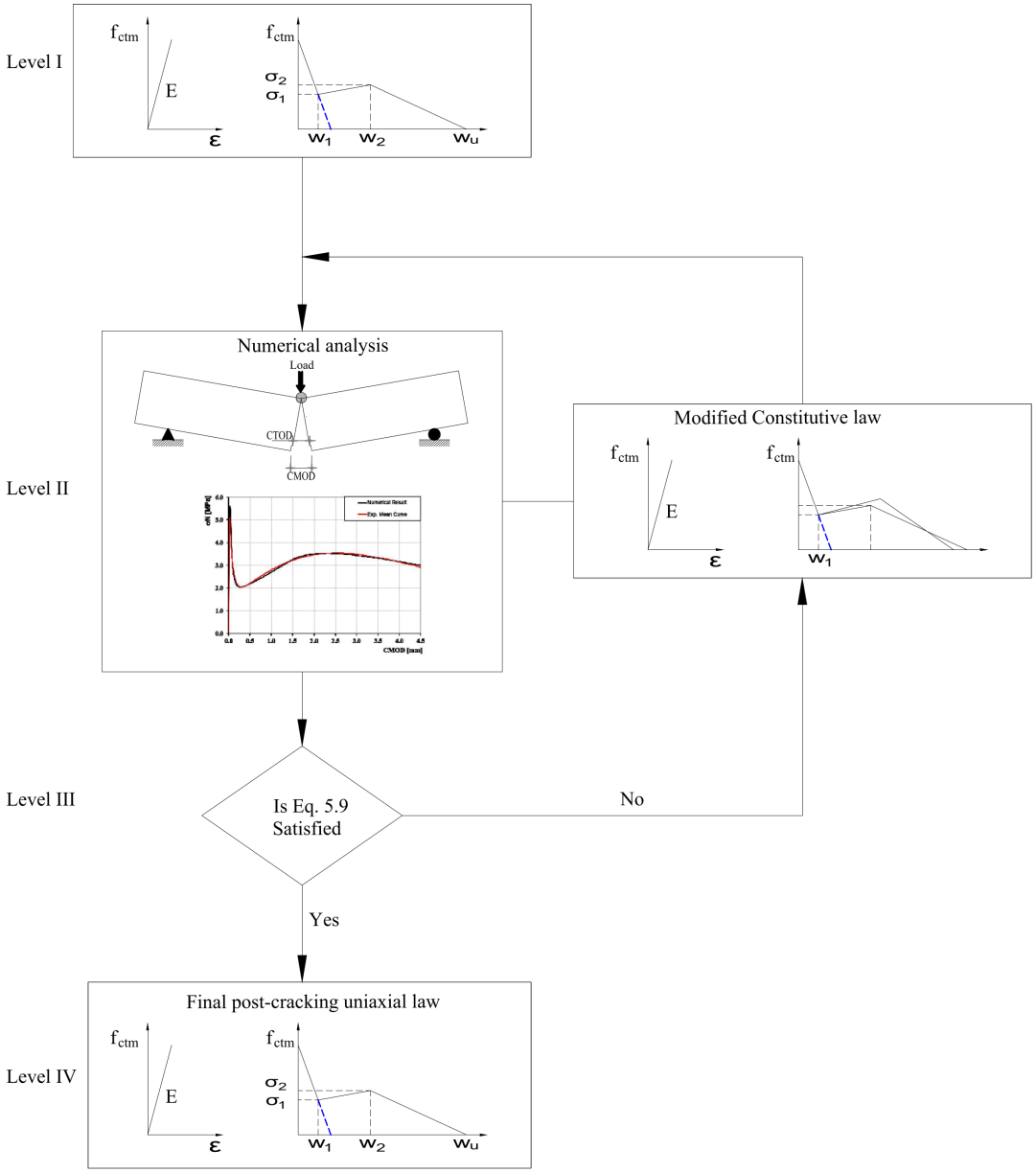

Figure 5.12: Inverse analysis procedure.

5.4 Post-Cracking Uniaxial Constitutive Laws

The stress-crack width (σ–w) uniaxial constitutive laws of the SFRC-25 and SFRC-40 series, including both sprayed and cast panels (EN 14488-3 Method B [16]) as well as sprayed saw-cut beams and cast beams (EN 14651 [7]), were retrieved through an inverse analysis procedure (Section 5.3), based on a Finite Element Modelling (FEM) framework described in detail in Section 5.2.

To identify the uniaxial stress-crack width (σ–w) constitutive laws by means of inverse analysis, the numerical response in terms of nominal stress σ_N versus CMOD was fitted to the corresponding mean experimental curve by minimizing the fitting error, as described in Section 5.3. The representative best-fitting numerical curve, compared with the corresponding mean experimental responses, are reported in Figures 5.13, 5.14 and 5.15 for the sprayed panel, cast beam and saw-cut beam series, respectively, showing a consistent level of agreement. A very good correlation between trend lines is observed; with the mean absolute percentage difference is below 2% for CMOD values ranging from 0.5 mm to 5 mm, thereby confirming the accuracy and reliability of the adopted finite element model.

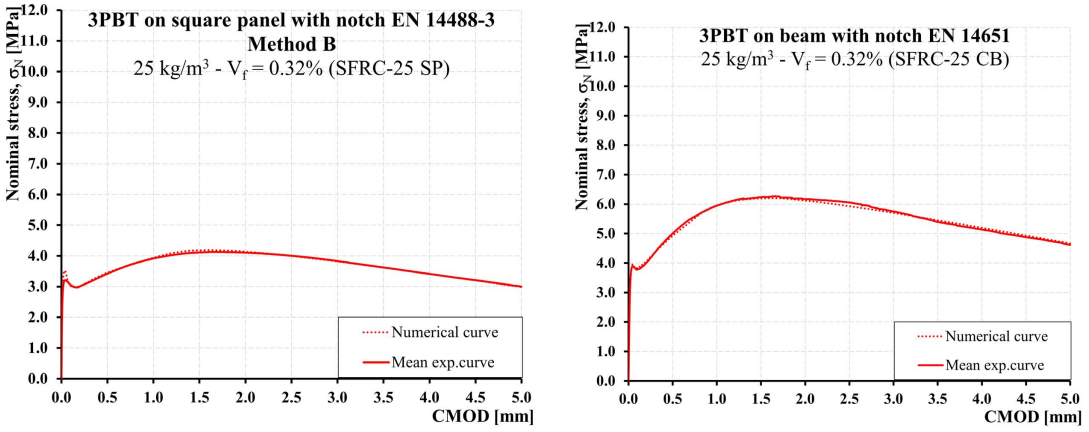

(a) (b)

Figure 5.13: Mean experimental and numerical nominal stress-CMOD curves (σ_N–$CMOD$) obtained through inverse analysis for SFRC-25 SP (EN 14488-3 Method B 3PB notched panel test) (a) and SFRC-25 CB (EN 14651 3PB notched beam test) (b).

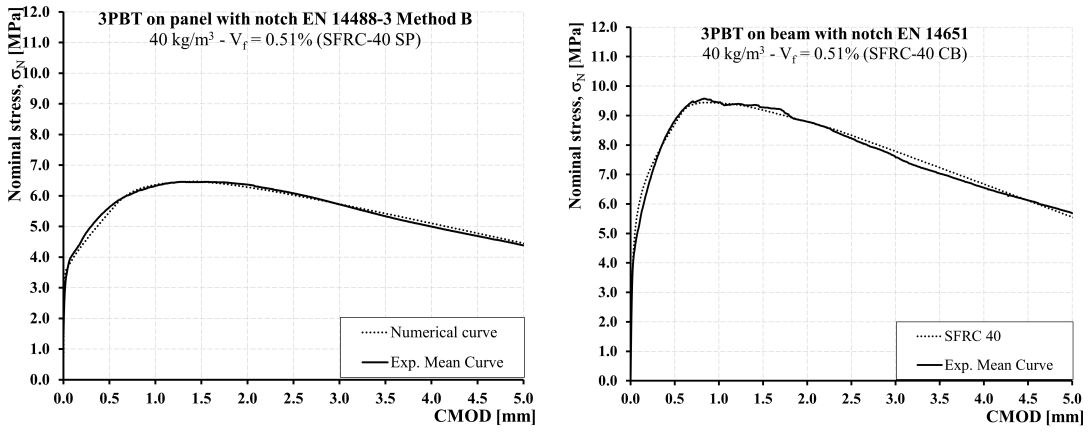

(a) (b)

Figure 5.14: Mean experimental and numerical nominal stress-CMOD curves (σ_N–$CMOD$) obtained through inverse analysis for SFRC-40 SP (EN 14488-3 Method B 3PB notched panel test) (a) and SFRC-40 CB (EN 14651 3PB notched beam test) (b).

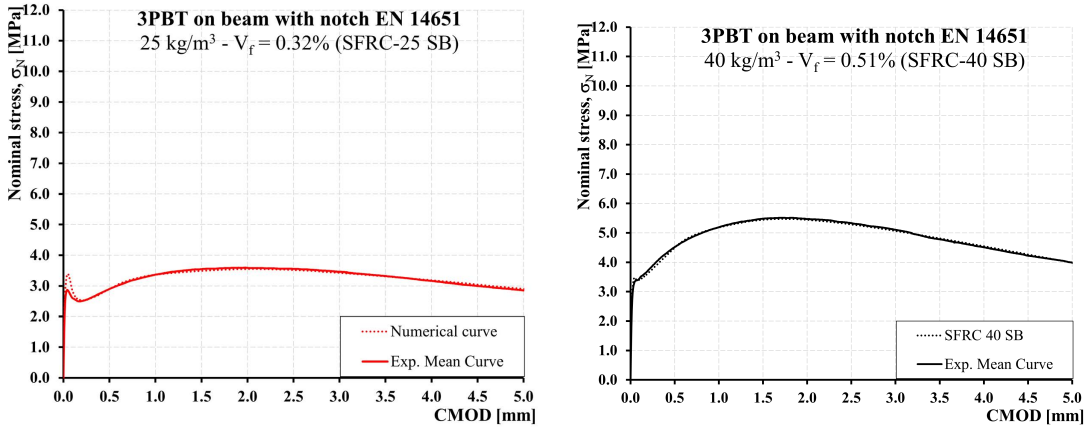

(a) (b)

Figure 5.15: Mean experimental and numerical nominal stress-CMOD curves (σ_N–$CMOD$) obtained through inverse analysis for SFRC-25 SB (EN 14651 3PB notched beam test) (a) and SFRC-40 SB (EN 14651 3PB notched beam test) (b).

To further validate the reliability of the numerical model adopted, the experimental results from all tested notched panels and beams were used to drive the corresponding CMOD-CTOD, CMOD-DEF and CTOD-DEF correlation curves (Figure 5.16 and Figure 5.17). Based on these experimental relationships, experimental trend lines were obtained and are shown as solid

red line in Figures 5.16 and 5.17. The corresponding numerical trend lines, derived from the FEM simulations, are also reported in the same figures as red dashed lines. A good agreement between the experimental and numerical trend lines is observed, confirming the reliability of the numerical model.

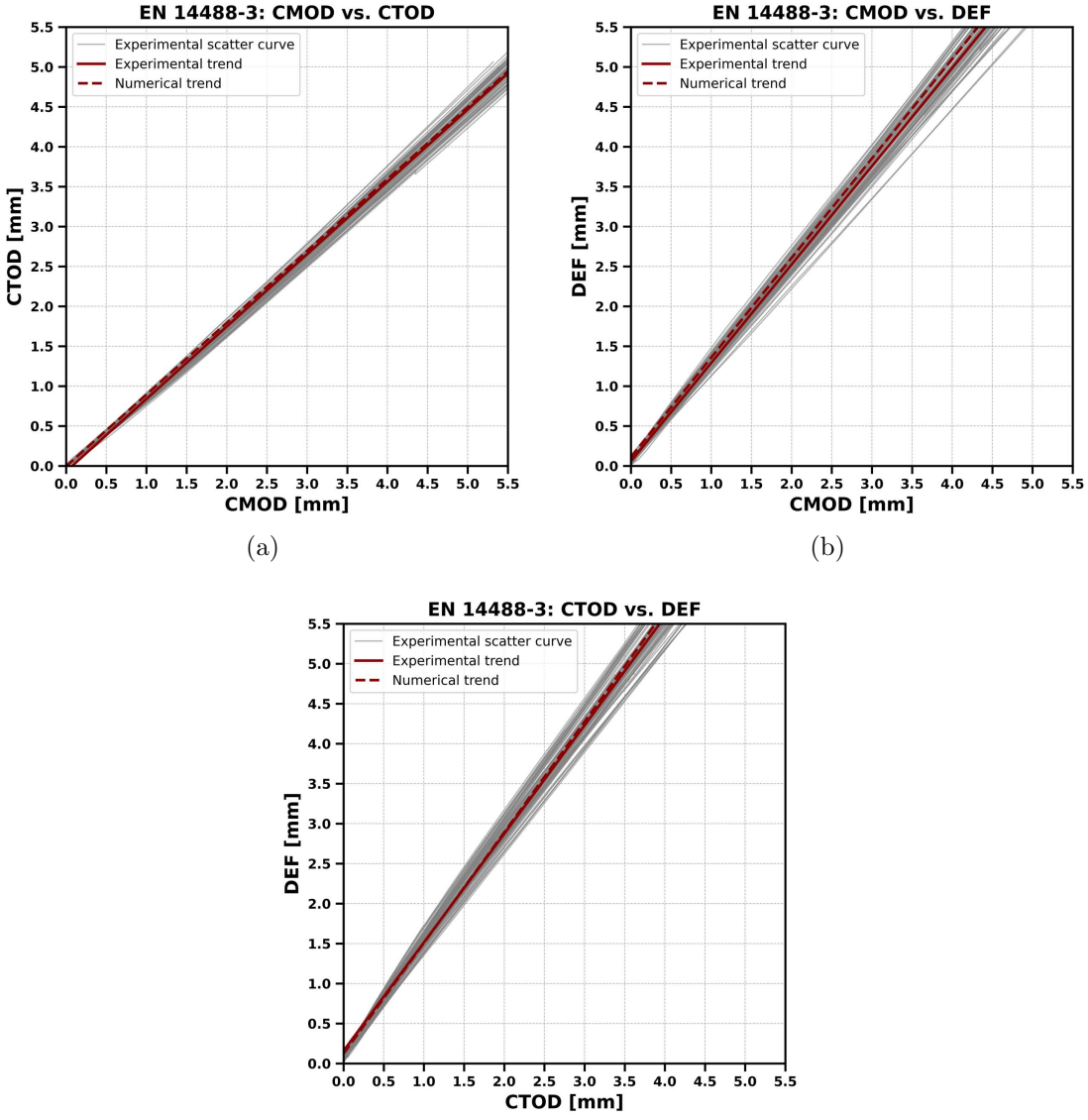

Figure 5.16: Comparison between experimental and numerical correlations (EN 14488-3 Method B): (a) CMOD vs. CTOD, (b) CMOD vs. DEF, and (c) CTOD vs. DEF, showing the agreement between experimental and numerical trend lines.

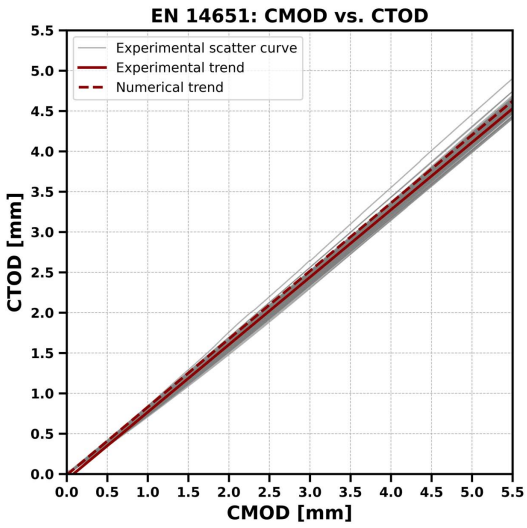

(a)

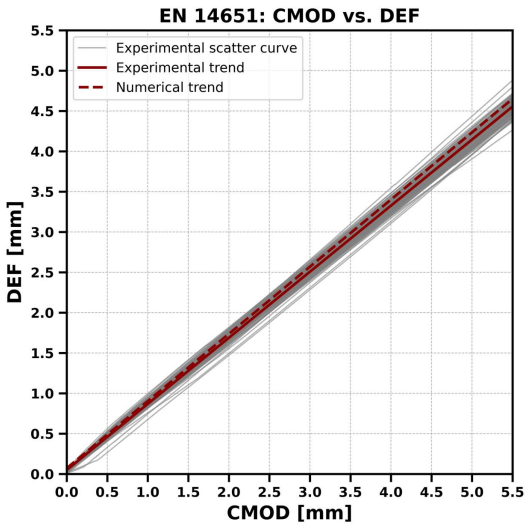

(b)

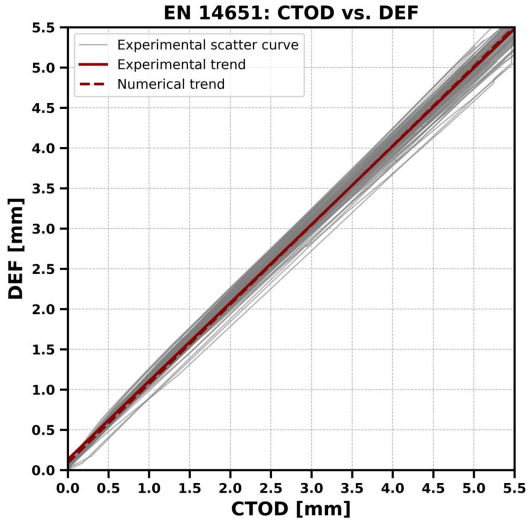

(c)

Figure 5.17: Comparison between experimental and numerical correlations (EN 14651): (a) CMOD vs. CTOD, (b) CMOD vs. DEF, and (c) CTOD vs. DEF, showing the agreement between experimental and numerical trend lines.

It is worth noting that, together with the robust numerical model adopted, a proper shape of uniaxial constitutive law was selected to start the numerical analysis (Section 5.3). In this context, a four-branch linear post-cracking law was used to capture the typical behaviour exhibited by steel fibre-reinforced concrete. Subsequently, through the inverse analysis procedure, the uniaxial post-cracking laws for each series were determined.

The SFRC post-cracking uniaxial laws of all series investigated are shown in Figure 5.18, and their main parameters are summarised in Table 5.1 and Table 5.2. It can be noticed that for all uniaxial laws the ultimate crack width (wc) is close to typical values cited in literature in case of complete steel fibre debonding [186, 188].

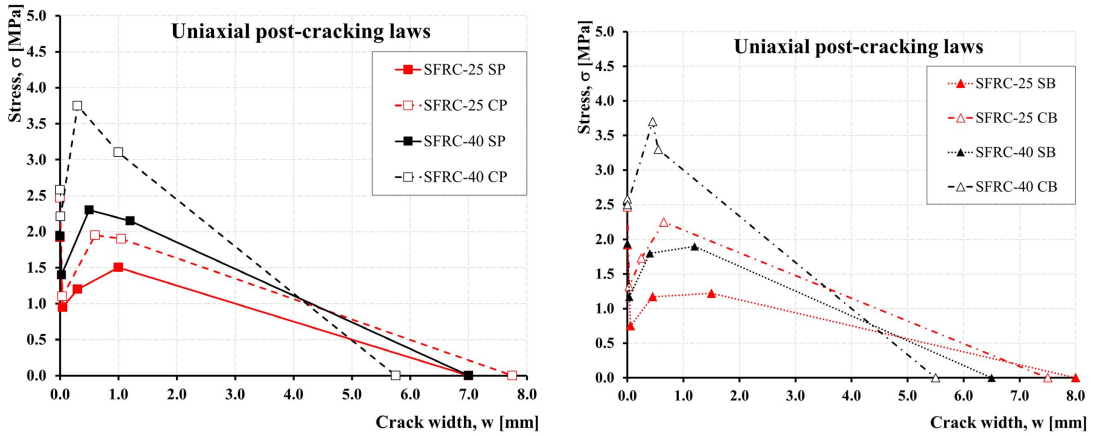

(a) (b)

Figure 5.18: Post-cracking uniaxial constitutive laws: SFRC-25 SP/CP, SFRC-40 SP/CP (EN 14488-3 Method B) (a) SFRC-25 CB/SB, SFRC-40 CB/SB (EN 14651) (b).

Table 5.1: Main parameters of the σ–w laws obtained from inverse analysis of EN 14488-3 Method B 3PB notched panel tests.

Series	f_{ctm} [MPa]	σ_1 [MPa]	**W1** [mm]	σ_2 [MPa]	**W2** [mm]	σ_3 [MPa]	**W3** [mm]	**WC** [mm]	$G_{f,0.5}$ [N/mm]	$G_{f,2.5}$ [N/mm]	$G_{f,tot}$ [N/mm]
SFRC-25 SP	1.921	0.95	0.0457	1.20	0.30	1.5025	1.00	7.00	0.588	3.257	5.792
SFRC-25 CP	2.467	1.10	0.0400	1.95	0.60	1.90	1.05	7.75	0.738	4.248	8.157
SFRC-40 SP	1.941	1.40	0.0250	2.30	0.50	2.15	1.20	7.00	0.921	4.960	8.713
SFRC-40 CP	2.580	2.21	0.0100	3.75	0.30	3.10	1.00	5.75	1.620	7.201	10.648

Table 5.2: Main parameters of the σ–w laws obtained from inverse analysis of EN 14651 3PB notched beam tests.

Series	f_{ctm} [MPa]	σ_1 [MPa]	**W1** [mm]	σ_2 [MPa]	**W2** [mm]	σ_3 [MPa]	**W3** [mm]	**WC** [mm]	$G_{f,0.5}$ [N/mm]	$G_{f,2.5}$ [N/mm]	$G_{f,tot}$ [N/mm]
SFRC-25 CB	2.467	1.32	0.0335	1.73	0.25	2.25	0.65	7.50	0.867	4.790	8.896
SFRC-25 SB	1.921	0.75	0.0551	1.17	0.45	1.22	1.50	8.00	0.511	2.834	5.672
SFRC-40 CB	2.580	2.50	0.00216	3.70	0.45	3.30	0.55	5.50	1.574	6.911	9.911
SFRC-40 SB	1.941	1.17	0.0356	1.80	0.40	1.90	1.20	6.50	0.777	4.244	7.112

To ensure appropriate assessment of the post-cracking performance, the fracture energy $G_f(w)$ derived from the uniaxial constitutive law was also considered. These parameter represents the area under the multi-linear curve up to the given crack width (w). The evolution of $G_f(w)$ is plotted in Figure 5.19 for the sprayed and cast panels series (EN 14488-3 Method B) and in Figure 5.20 for saw-cut sprayed and cast beam series (EN 14651). The fracture energies corresponding to fundamental levels of crack widths of 0.5 mm, 1.5 mm, 2.5 mm and 3.5 mm (i.e., $G_{f,0.5}$, $G_{f,1.5}$, $G_{f,2.5}$ and $G_{f,3.5}$) were also computed, while the total fracture energy ($G_{f,total}$) was evaluated at the ultimate crack opening (w_c). The corresponding values are reported in Table 5.3.

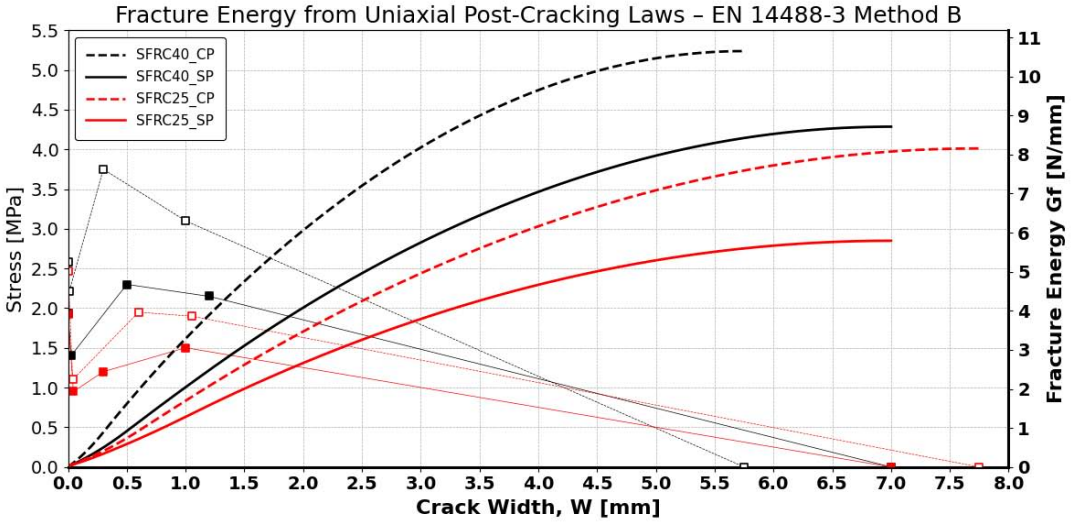

Figure 5.19: Fracture energy from uniaxial constitutive laws: SFRC-25 SP/CP, SFRC-40 SP/CP (EN 14488-3 Method B).

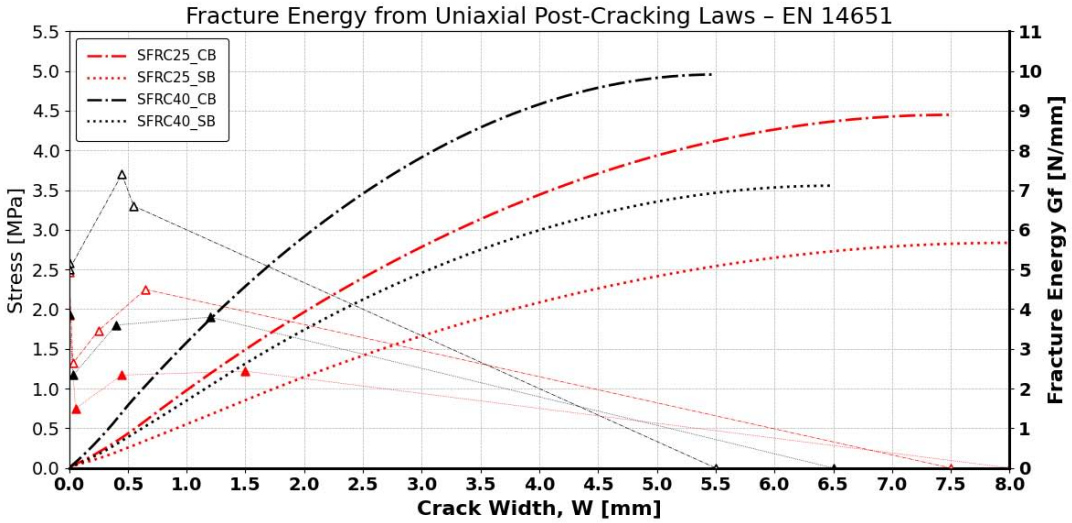

Figure 5.20: Fracture energy from uniaxial constitutive laws: SFRC-25 CB/SB, SFRC-40 CB/SB (EN 14651).

Table 5.3: Computed fracture energy G_f from uniaxial post-cracking laws for each investigated series.

Series	G_f **@ 0.5 mm [N/mm]**	G_f **@ 1.5 mm [N/mm]**	G_f **@ 2.5 mm [N/mm]**	G_f **@ 3.5 mm [N/mm]**	G_f **Total [N/mm]**
SFRC40 CP	1.62	4.75	7.20	9.00	10.65
SFRC40 SP	0.92	3.11	4.96	6.44	8.71
SFRC25 CP	0.74	2.62	4.25	5.59	8.16
SFRC25 SP	0.59	2.01	3.26	4.26	5.79
SFRC25 CB	0.87	2.98	4.79	6.27	8.90
SFRC25 SB	0.51	1.71	2.83	3.77	5.67
SFRC40 CB	1.57	4.58	6.91	8.58	9.91
SFRC40 SB	0.78	2.63	4.23	5.45	7.11

Similar tendencies to those observed in the flexural response discussed in Section 4.5.6 and 4.5.5 can be identified from the uniaxial post-cracking laws obtained through the inverse analysis procedure. The corresponding uniaxial post-cracking laws for each series are illustrated (Figure 5.18) while the associated fracture energy distributions are presented in (Figure 5.19 and 5.20). In all cases, consistent with the flexural response, the uniaxial post-cracking response of the sprayed elements derived from the numerical modelling exhibited lower values compared to the cast elements Figure 5.21.

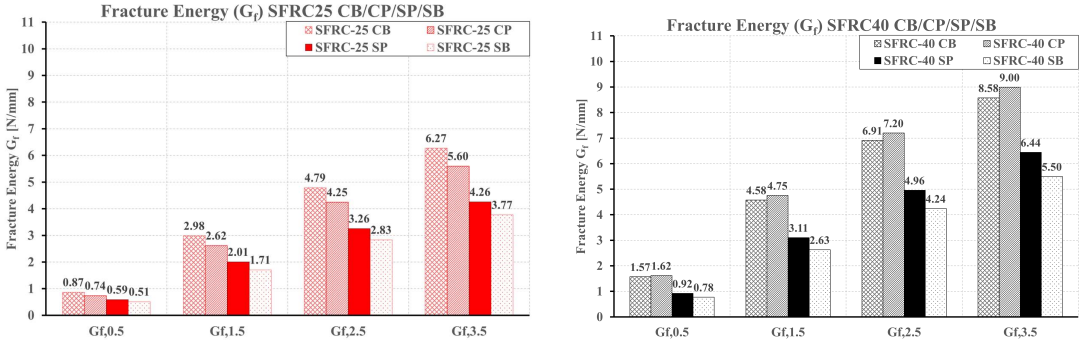

(a) (b)

Figure 5.21: Fracture energy (G_f) for: (a) SFRC25 CB/CP/SP/SB; (b) SFRC40 CB/CP/SP/SB.

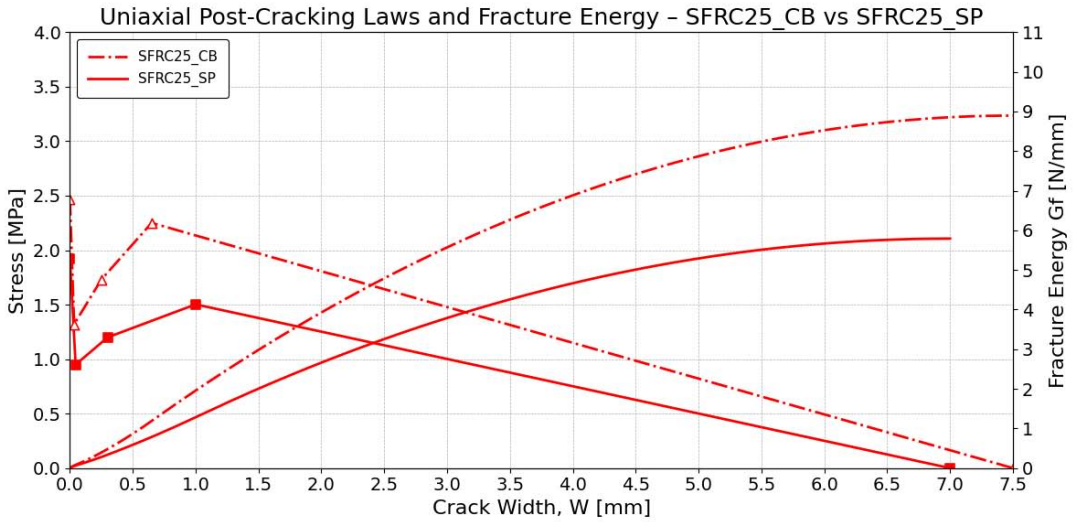

Figure 5.22: Comparison of Sprayed Panel (SFRC-25 SP) and Cast Beam (SFRC-25 CB) in terms of uniaxial post-cracking law and computed fracture energy (G_f).

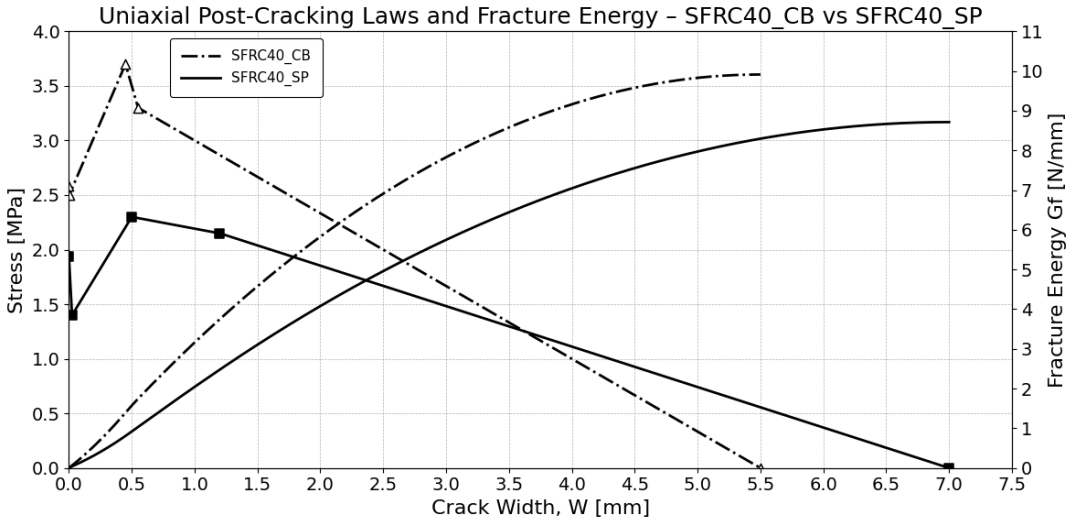

Figure 5.23: Comparison of Sprayed Panel (SFRC-40 SP) and Cast Beam (SFCR-4O CB) in terms of uniaxial post-cracking law and computed fracture energy (G_f).

The ratio of fracture energy between the series which shown in Figure 5.24 is consistent with the ratio of flexural residual strengths presented in Figure 4.53. When considering the parameters $G_{f,0.5}$, $G_{f,1.5}$, $G_{f,2.5}$ and $G_{f,3.5}$, the difference between SFRC-25 and SFRC-40 (Figure 5.21) is closely aligned with the corresponding differences in f_{R1}, f_{R2}, f_{R3} and f_{R4} obtained from the flexural response. Furthermore, the fracture energy ratio (Figure 5.24) between sprayed panel and cast beam, sprayed panel and cast panel, sprayed panel and sprayed beam, and sprayed beam and bast beam are also consistent with the flexural strength ratios described previously (Figure 4.53).

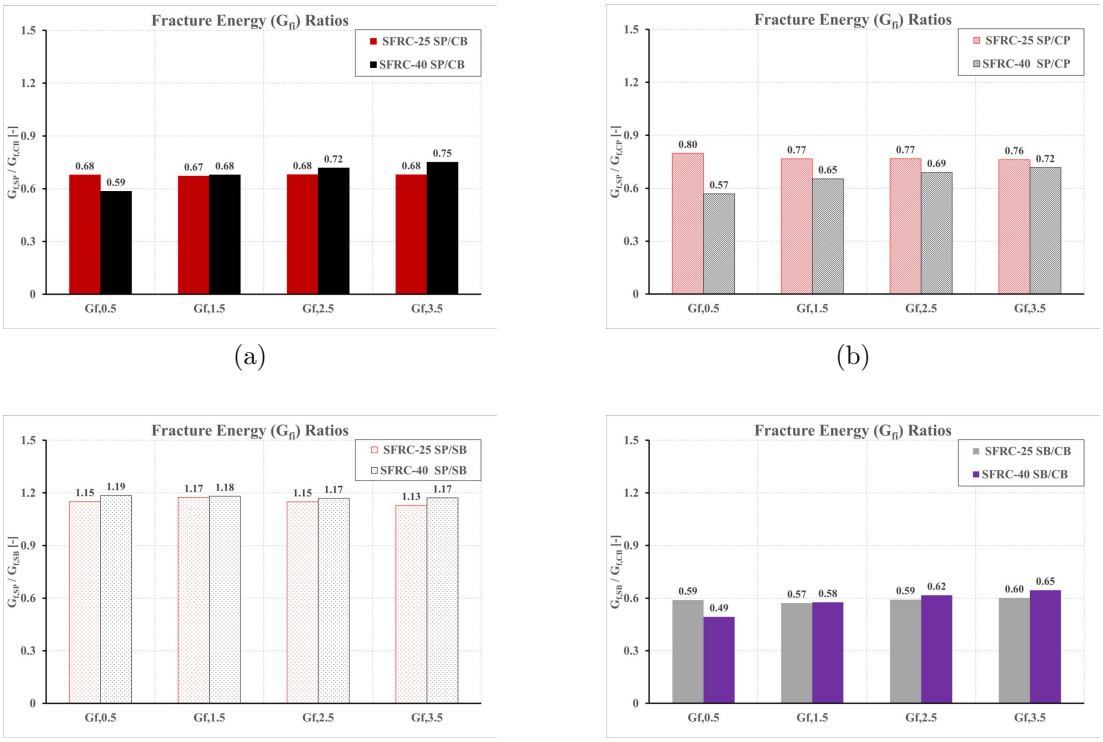

Figure 5.24: Fracture energy ratios between series: (a) SFRC-25 and SFRC-40 (SP/CB), (b) SFRC-25 and SFRC-40 (SP/CP), (c) SFRC-25 and SFRC-40 (SP/SB), and (d) SFRC-25 and SFRC-40 (SB/CB).

Chapter 6

Correlation of Main Displacement Parameters of 3PBTs

According to Eropean sprayed concrete standards, which are frequently mentioned in this thesis, EN 148488-3 [16] and EN 14487-1 [19], when calculating the residual strength of sprayed FRC materials, the crack mouth opening displacement (CMOD) of the beam EN 14651 [7] and the panel CMOD (as per EN 14488-3 [16]) are considered equivalent. However, the geometrical differences between the beam and panel, the application of the load on each, and the notches provided in both, the CMOD measurements from these two test methods cannot be considered truly and exactly equivalent. The relationship has been analysed, verified and established relationship through analytical, experimental, and numerical methods. Justify how the measurement of CMOD values differs based on these methodologies.

6.1 Analytical Correlation

The qualitative deformation configuration for the three-point bending test on the EN 14651 beam and the EN 14488-3 method B panel is shown in Figure 6.1. The geometrical relationships for a simple supported beam deformation under load, the corresponding approximate deflected configuration based on the initial assumption of small rotation equals the deflection rate over the length of the beam, and the relationships between geometric and kinematic parameters are illustrated in detail in Figure 6.2 and Figure 6.3.

From these figures, h represents the depth of the beam and δ denotes the mid-span deflection. Consequently, the width of the crack is approximated as Equation 6.1.

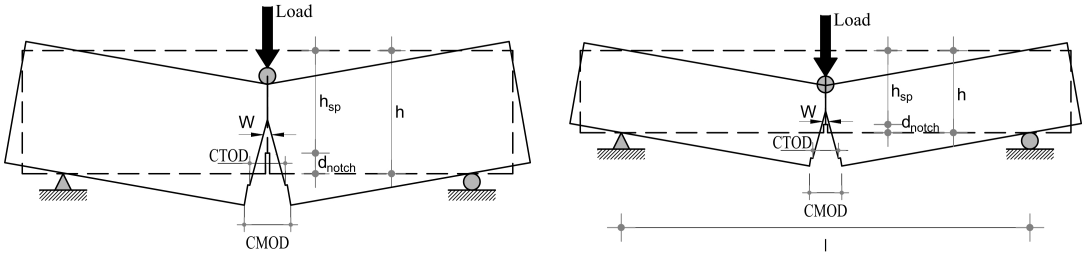

Figure 6.1: EN 14651 3PBT beam test (a) and EN 14488-3 Method B 3PBT panel test (b) - definition of CMOD and CTOD.

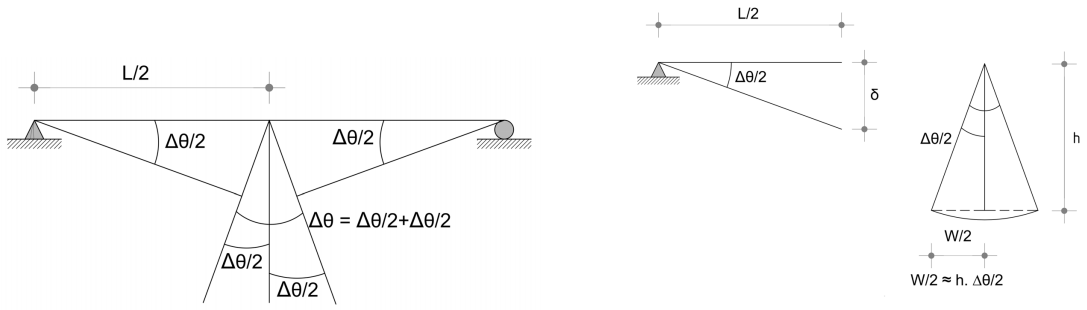

(a) (b)

Figure 6.2: For a small segment of the beam small-angle approximation to simplify the deformation of a simply supported beam.

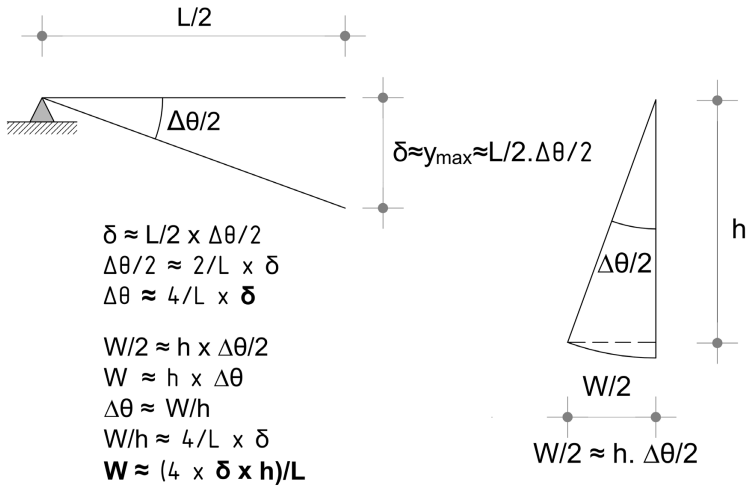

Figure 6.3: Relationship between crack width, vertical displacement, and small angle approximation for simplifying the deformation of a simple supported beam.

$$W \approx \frac{4 \times \delta \times h}{l} \tag{6.1}$$

When applying the above description to the notch beam and the notch panel below, in accordance with EN 14651 [7] and EN 14488-3 Metho B [16], respectively, the following assumptions are made:

- h_{sp} as the distance between the tip of the notch and the top of the test specimen in the mid-span section.
- The position of the neutral axis is at $0.1h_{sp}$.
- $d_{\text{neutral}} = 0.1h_{sp}$.
- d_{notch} = notch depth.

The CMOD (Crack Mouth Opening Displacement) and CTOD (Crack Tip Opening Displacement) are expressed in the Figure 6.4 and Figure 6.5 and equations Equation 6.4 and Equation 6.5.

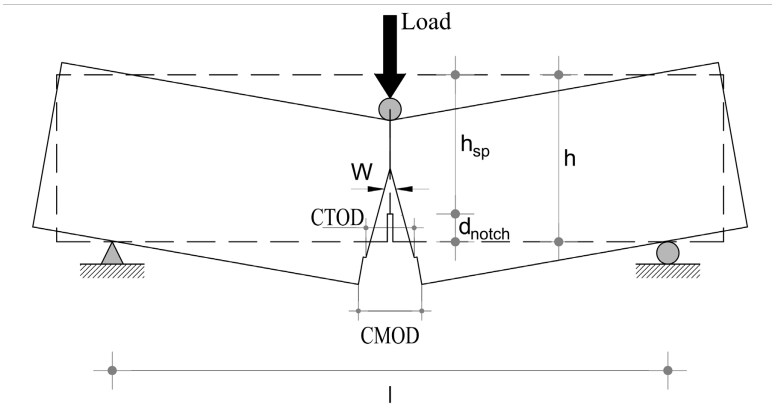

Figure 6.4: Definition of CMOD and CTOD for the three-point bending EN 14651 test methodology

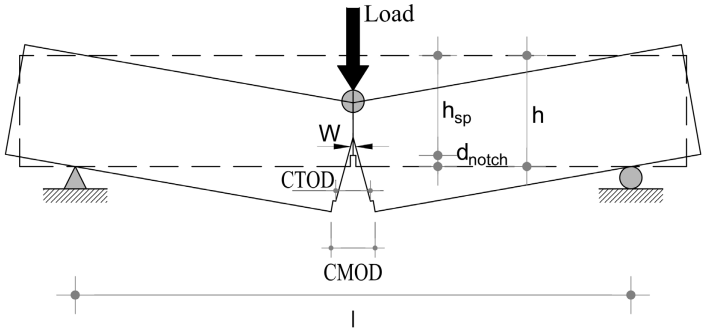

Figure 6.5: Definition of CMOD and CTOD for the three-point bending EN 14488-3 Method B test methodology.

$$\begin{aligned} \text{Distance from the NA to the tip of CMOD} &= h_{sp} - d_{\text{neutral}} + d_{\text{notch}} \\ &= h_{sp} - 0.1h_{sp} + d_{\text{notch}} \\ &= 0.9h_{sp} + d_{\text{notch}} \end{aligned} \tag{6.2}$$

$$\begin{aligned} \text{Distance from the NA to the tip of CTOD} &= h_{sp} - d_{\text{neutral}} \\ &= h_{sp} - 0.1 \times h_{sp} \\ &= 0.9h_{sp} \end{aligned} \tag{6.3}$$

$$W_{\mathrm{CMOD}} = CMOD = \frac{4 \times \delta \times (0.9h_{sp} + d_{\mathrm{notch}})}{l} \tag{6.4}$$

$$W_{\mathrm{CTOD}} = CTOD = \frac{4 \times \delta \times 0.9h_{sp}}{l} \tag{6.5}$$

6.6 and 6.8 shows the dimensions of the beam and panel, respectively, according to the relevant standards.

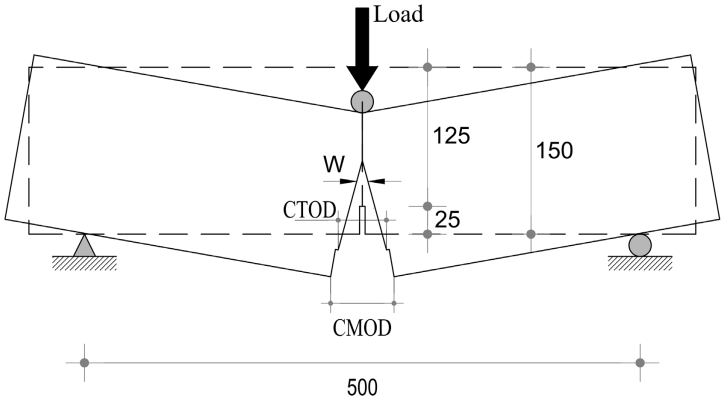

Figure 6.6: Definition of CMOD and CTOD with standard given geometrical dimensions for the EN 14651 test methodology (dimensions in mm).

$$\mathrm{CMOD}_{(\mathrm{EN\ 14651})} \approx \frac{4 \times \delta_{(\mathrm{EN\ 14651})} \times (0.9 \times 125 + 25)}{500} = 1.1 \times \delta_{(\mathrm{EN\ 14651})}$$

$$\delta_{(\mathrm{EN\ 14651})} \approx \frac{\mathrm{CMOD}_{(\mathrm{EN\ 14651})}}{1.1} \tag{6.6}$$

$$\mathrm{CTOD}_{(\mathrm{EN\ 14651})} = \frac{4 \times \delta_{(\mathrm{EN\ 14651})} \times 0.9 \times 125}{500} = 0.9 \times \delta_{(\mathrm{EN\ 14651})}$$

$$\mathrm{CTOD}_{(\mathrm{EN\ 14651})} \approx \frac{0.9 \times \mathrm{CMOD}_{(\mathrm{EN\ 14651})}}{1.1}$$

$$\mathrm{CTOD}_{(\mathrm{EN\ 14651})} \approx 0.81 \times \mathrm{CMOD}_{(\mathrm{EN\ 14651})} \tag{6.7}$$

In the Equation 6.7, the neutral axis (NA) position is assumed at 0.1 x h_{sp}. However, with the assumed NA position varies from 0.25 x h_{sp} to 0.01 x h_{sp}, the relationship also changes,

Table 6.1: Relationship between CMOD and CTOD in the EN 14651 test methodology, assuming the neutral axis position at 0.1xhsp.

CMOD EN 14651 [mm]	**CTOD EN 14651 [mm]**
0.5	0.4091
1.5	1.2273
2.5	2.0455
3.5	2.8636

causing φ to increase from 0.7895 to 0.8319, as shown in Equation 6.1 and Figure 6.7.

$$\text{CTOD}_{\text{EN 14651}} = \varphi \times \text{CMOD}_{\text{EN 14651}} \tag{6.8}$$

$$\text{where } \varphi \text{ is } 0.7895 - 0.8319$$

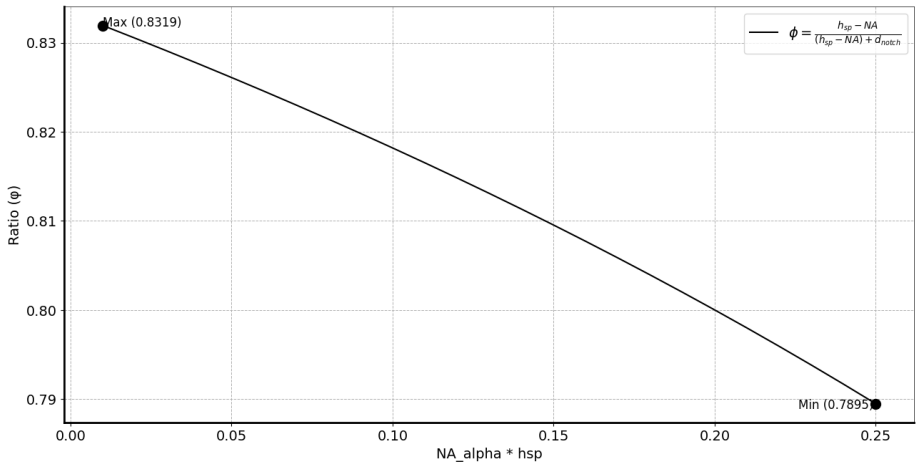

Figure 6.7: Relationship between CTOD and CMOD for EN 14651 test methodology with a varying the neutral axis position assumption from 0.25xh_{sp} to 0.01xh_{sp}.

Similarly to the correlation established between CMOD and CTOD for the EN 14651 beam, a corresponding correlation is illustrated and established for the EN 14488-3 test methodology, as presented below.

Table 6.2: Relationship between CMOD and CTOD in EN 14651 test methodology, assuming the neutral axis position varies from 0.25xh_{sp} to 0.01xh_{sp}.

CMOD EN 14651 [mm]	**CTOD EN 14651 [mm]**
0.5	0.3947 - 0.4160
1.5	1.1842 - 1.2479
2.5	1.9737 - 2.0798
3.5	2.7632 - 2.9118

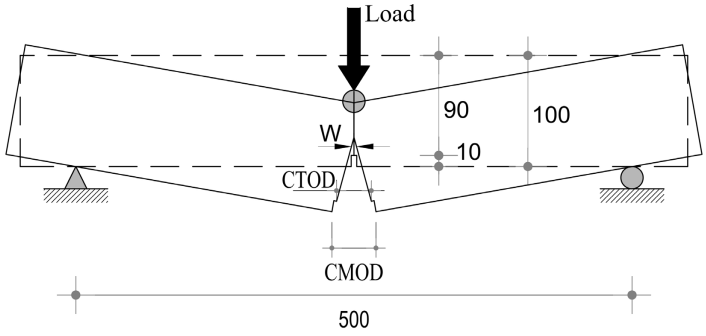

Figure 6.8: Definition of CMOD and CTOD with standard given geometrical dimensions for EN 14488-3 Method B test methodology (dimensions in mm).

$$\text{CMOD}_{\text{EN 14488-3}} \approx \frac{4 \times \delta_{\text{EN 14488-3}} \times (0.9 \times 90 + 10)}{500} \approx 0.728 \times \delta_{\text{EN 14488-3}}$$

$$\delta_{\text{EN 14488-3}} \approx \frac{1}{0.728} \text{CMOD}_{\text{EN 14488-3}} \tag{6.9}$$

$$\text{CTOD}_{\text{EN 14488-3}} \approx \frac{4 \times \delta_{\text{EN 14488-3}} \times 0.9 \times 90}{500} \approx 0.648 \times \delta_{\text{EN 14488-3}}$$

$$\text{CTOD}_{\text{EN 14488-3}} \approx 0.648 \times \frac{1}{0.728} \times \text{CMOD}_{\text{EN 14488-3}}$$

$$\text{CTOD}_{\text{EN 14488-3}} \approx 0.89 \times \text{CMOD}_{\text{EN 14488-3}} \tag{6.10}$$

In Equation 6.10 assumes that the neutral axis (NA) is positioned at 0.1xhsp. However, as

Table 6.3: Relationship between CMOD and CTOD in the EN 14488-3 Method B test methodology, assuming the neutral axis position at 0.1xh_{sp}.

CMOD EN 14488-3 1 [mm]	**CTOD EN 14488-3 [mm]**
0.5	0.4451
1.5	1.3352
2.5	2.2253
3.5	3.1154

the assumed NA position shifts from 0.25xh_{sp} to 0.01xh_{sp}, this relationship changes similarly to the EN 14651 test methodology above, causing φ to increase from 0.8710 to 0.0.8953 as detailed in Equation 6.11 and illustrated Figure 6.9. The upward shift of the neutral axis results in an increase φ.

$$\text{CTOD}_{\text{EN 14488-3}} = \varphi \times \text{CMOD}_{\text{EN 14488-3}} \tag{6.11}$$

where φ is 0.8710 to 0.8991

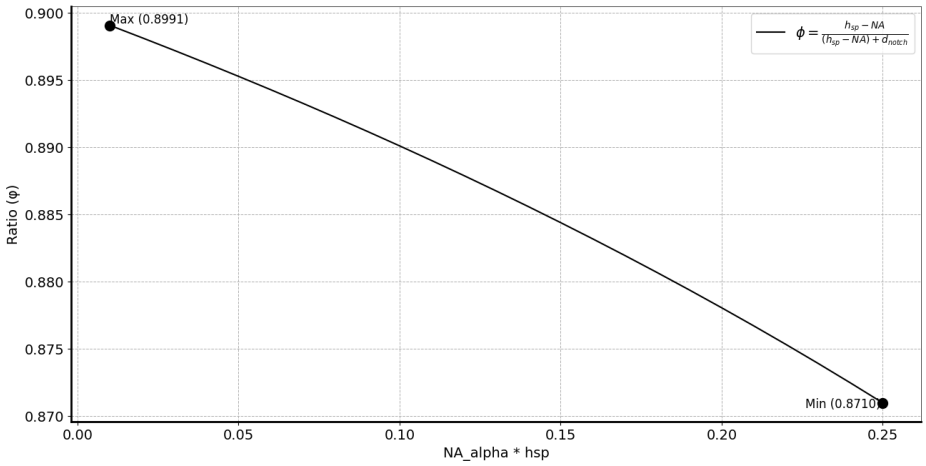

Figure 6.9: The relationship between CTOD and CMOD in the EN 14488-3 Method B test methodology with a varying the NA position assumption from 0.25 to 0.01 h_{sp}.

With the same crack width of CTOD, the test methodologies of EN 14651 and EN 14488-3 method B result in the relationship for CMOD, as shown in Equation 6.21 and Equation 6.22. The CMOD measurements, used to calculate the residual strength of the FRC according to Model 2020 [8] are 0.5mm, 1.5mm, 2.5mm and 3.5mm in EN 14651. The corresponding

Table 6.4: Relationship between CMOD and CTOD in EN 14488-3 method B test methodology, assuming the neutral axis position varies from 0.25xh_{sp} to 0.01xh_{sp}.

CMOD EN 14488-3 [mm]	**CTOD EN 14488-3 [mm]**
0.5	0.4355 – 0.4495
1.5	1.3065 – 1.3486
2.5	2.1774 – 2.2477
3.5	3.0484 – 3.1468

CMOD values for the EN 14488-3 test methodology, at equal CTOD for the beam and panel as Equation 6.7 and Equation 6.10, can be derived below and presented in Table 6.5.

$$\text{CTOD}_{\text{EN 14651}} = \text{CTOD}_{\text{EN 14488-3}}$$

$$0.81 \times \text{CMOD}_{\text{EN 14651}} = 0.89 \times \text{CMOD}_{\text{EN 14488-3}}$$

$$\text{CMOD}_{\text{EN 14651}} = 1.099 \times \text{CMOD}_{\text{EN 14488-3}} \tag{6.12}$$

$$\text{CMOD}_{\text{EN 14488-3}} = 0.910 \times \text{CMOD}_{\text{EN 14651}} \tag{6.13}$$

Equation 6.22 relationship assumes that the neutral axis (NA) is 0.1xhsp. However, it has also been computed by varying the assumption of NA position from 0.25xh_{sp} to 0.05xh_{sp}. The graph below shows the maximum and the minimum corresponding CMOD values from EN 14488-3 for CMODs (0.5, 1.5, 2.5, 3.5) according to EN 14651. As the assumption of the neutral axis position shifts to the top, the CMOD values vary.

Table 6.5: Relationship between CMOD from EN 14651 and EN 14488-3 Method B test methodologies, assuming the neutral axis at 0.1xh_{sp}.

CMOD EN 14651 [mm]	**CMOD EN 14488-3 Method B [mm]**
0.5	0.46
1.5	1.37
2.5	2.28
3.5	3.19

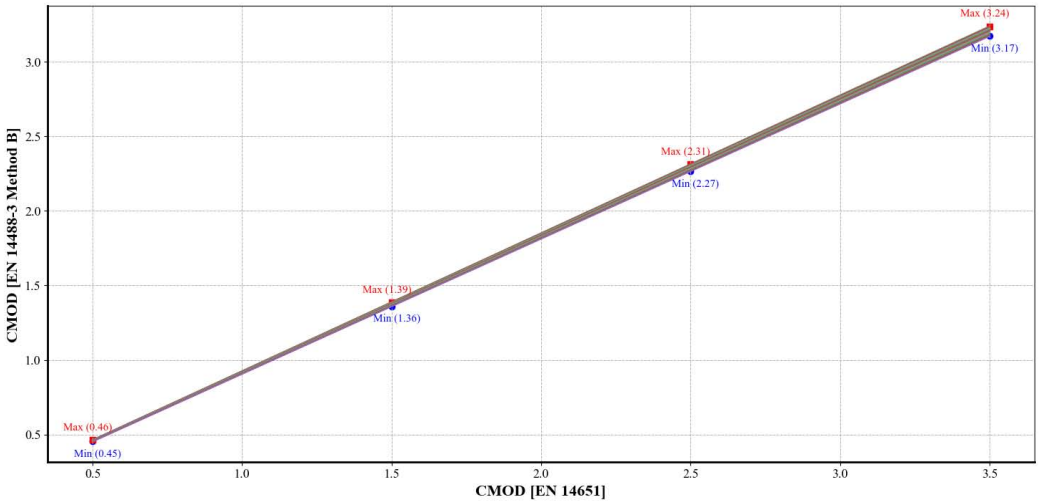

Figure 6.10: The relationship between CMOD from EN 14488-3 Method B and EN 14651 with varying the assumption of the Neutral Axis (NA) position from 0.25xh_{sp} to 0.01xh_{sp}.

Equation 6.22 assumes that the neutral axis (NA) is positioned at 0.1xhsp. However, as the location assumption of the NA changes 0.25xh_{sp} to 0.01xh_{sp}, this relationship changes, causing φ to increase from 0.906 to 0.0.923 as detailed in Equation 6.1 and illustrated in Figure 6.10. The shift of the neutral axis to the top causes φ to increase. And move the assumption of the neutral axis to the top decrease the difference between CMOD values of EN 14651 and EN 14488-3 Method B.

$$\text{CMOD}_{\text{EN 14488-3}} = \varphi \times \text{CMOD}_{\text{EN 14651}} \tag{6.14}$$

where φ is 0.906 to 0.923

Table 6.6: Relationship between CMOD of EN 14651 and EN 14488-3 Method B analytically assuming the neutral axis from 0.25xh_{sp} - 0.01xh_{sp}.

CMOD EN 14651 [mm]	**CMOD EN 14488-3 Method B [mm]**
0.5	0.45 – 0.46
1.5	1.36 – 1.38
2.5	2.27 – 2.31
3.5	3.17 – 3.23

6.2 Experimental Correlation

Similar to the analytical approach presented in the previous subsection, the experimental relationship between the two test methodologies was established by using the same CTOD values for both tests. The trendline established using the two test methodlogies between the CMOD, CTOD and DEF (Figure 6.11 and 6.12), a relationship between the CMOD of EN 14651 and that of EN 14488-3 Method B was determined experimentally by equating the corresponding trendlines. The analysis considered all experimental results included in this Ph.D. work, comprising 62 EN 14488-3 Method B notched panel tests and 125 EN 14651 notched beam tests.

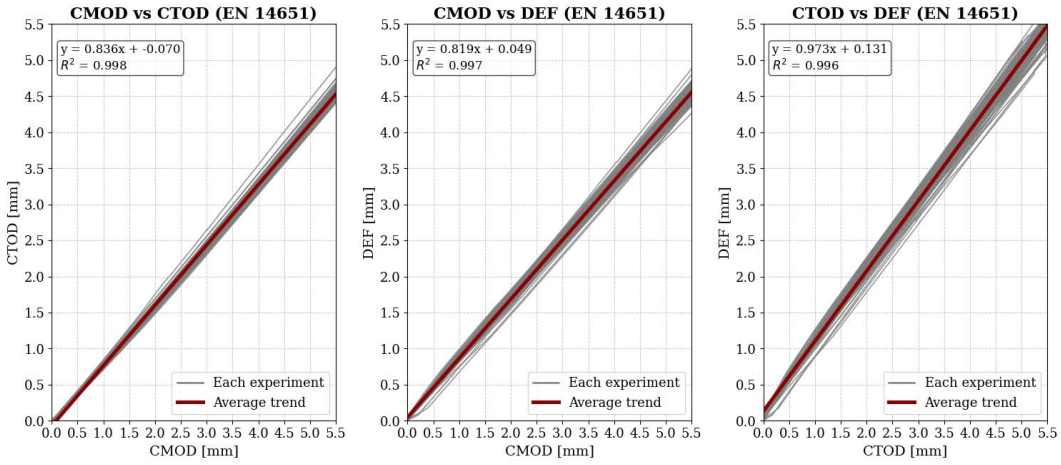

Figure 6.11: Experimental relationships between CMOD, CTOD, and DEF according to EN 14651 [7]. (a) CMOD vs CTOD (b) CMOD vs DEF (c) CTOD vs DEF.

$$\mathrm{CTOD}_{\mathrm{EN\ 14651}} = 0.83\,\mathrm{CMOD}_{\mathrm{EN\ 14651}} \pm 0.070 \tag{6.15}$$

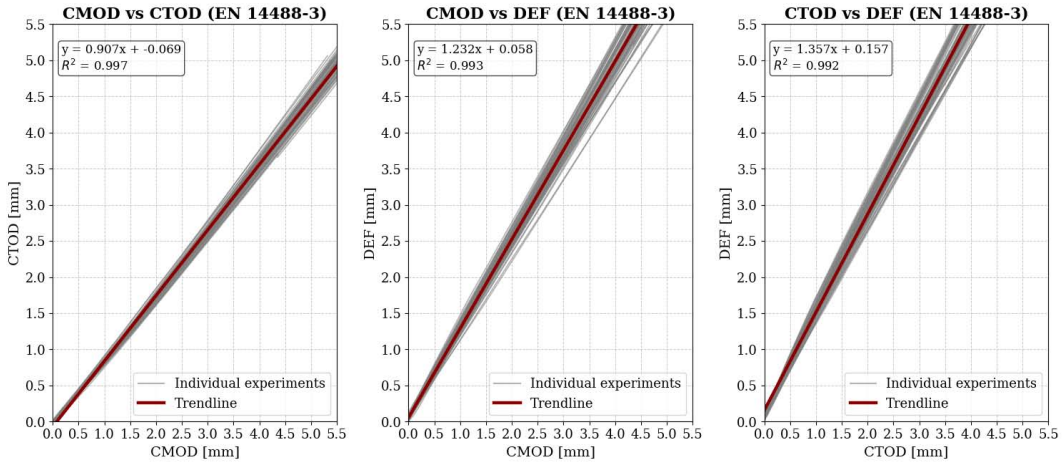

Figure 6.12: Experimental relationships between CMOD, CTOD, and DEF according to EN 14488-3 Method B [16]. (a) CMOD vs CTOD (b) CMOD vs DEF (c) CTOD vs DEF.

$$\mathrm{CTOD}_{\text{EN 14488-3}} = 0.907\,\mathrm{CMOD}_{\text{EN 14488-3}} \pm 0.069 \tag{6.16}$$

$$\mathrm{CTOD}_{\text{EN 14651}} = \mathrm{CTOD}_{\text{EN 14488-3}}$$

$$0.83\,\mathrm{CMOD}_{\text{EN 14651}} \pm 0.070 = 0.907\,\mathrm{CMOD}_{\text{EN 14488-3}} \pm 0.069$$

$$\mathrm{CMOD}_{\text{EN 14651}} = 1.093 \times \mathrm{CMOD}_{\text{EN 14488-3}} \tag{6.17}$$

$$\mathrm{CMOD}_{\text{EN 14488-3}} = 0.915 \times \mathrm{CMOD}_{\text{EN 14651}} \tag{6.18}$$

Table 6.7: Relationship between CMOD of EN 14651 and EN 14488-3 Method B based on experimental results.

CMOD EN 14651 [mm]	**CMOD EN 14488-3 Method B [mm]**
0.5	0.46
1.5	1.37
2.5	2.29
3.5	3.20

6.3 Numerical Correlation

Using the same CTOD values for both test methodologies, as in the analytically and experimentally established relationships between the CMODs of the two, the numerical correlation was developed based on the trendlines obtained from the CMOD–CTOD CMOD–DEF and CTOD-DEF relationships (Figures 6.13 and 6.14). Accordingly, a relationship between the CMOD of EN 14651 [7] and that of EN 14488-3 Method B [16] was determined numerically by equating the corresponding trendlines. The numerical correlation was derived using the inverse analysis results from the cast and sprayed beam tests for EN 14651 and the cast and sprayed panel series for EN 14488-3 Method B.

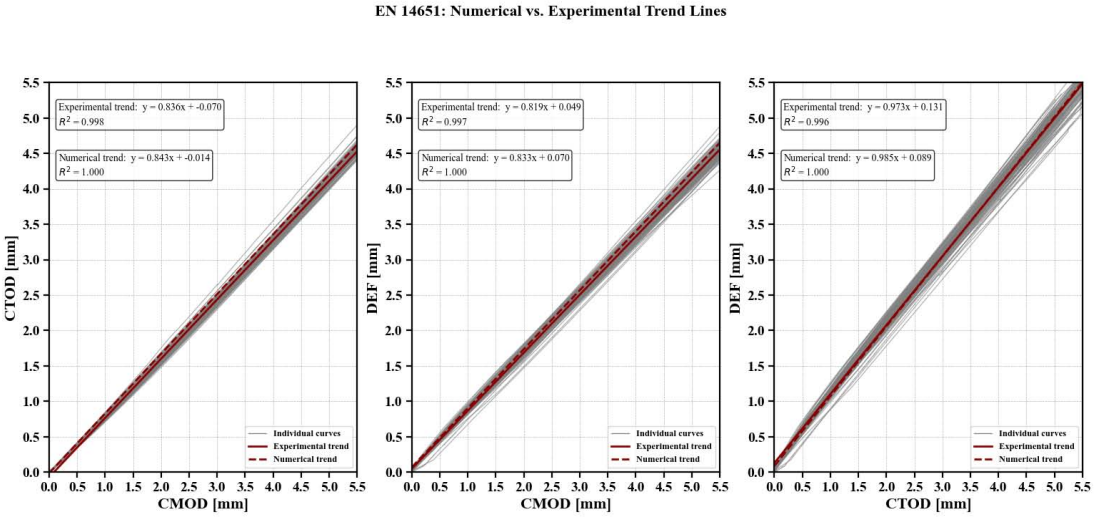

Figure 6.13: Experimental and numerical relationships between CMOD, CTOD, and DEF according to EN 14651 [7]. (a) CMOD vs CTOD (b) CMOD vs DEF (c) CTOD vs DEF.

$$\mathrm{CTOD}_{\mathrm{EN\ 14651}} = 0.843\,\mathrm{CMOD}_{\mathrm{EN\ 14651}} \pm 0.014 \tag{6.19}$$

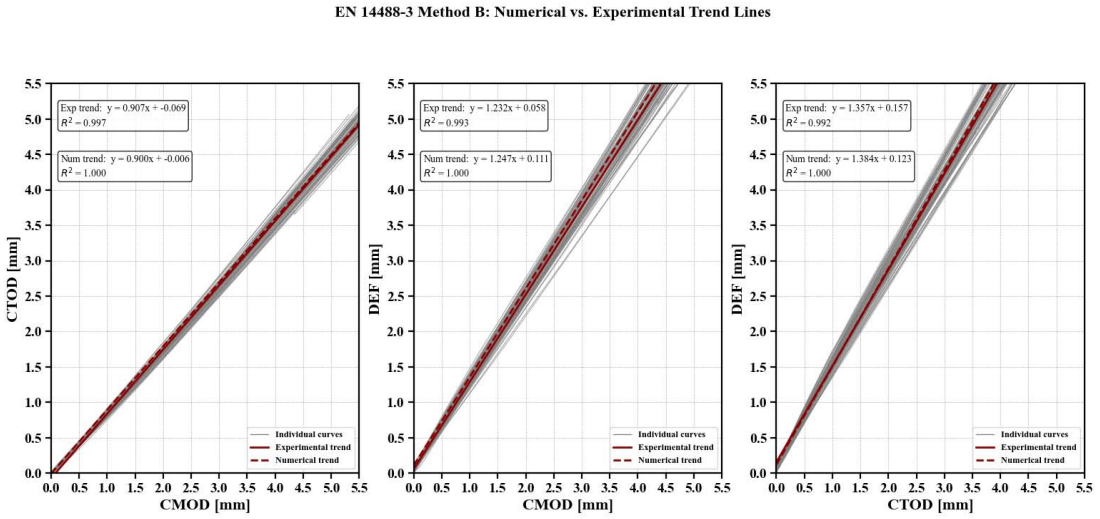

Figure 6.14: Experimental and numerical relationships between CMOD, CTOD, and DEF according to EN 14488-3 Method B [16]. (a) CMOD vs CTOD (b) CMOD vs DEF (c) CTOD vs DEF.

$$\mathrm{CTOD}_{\text{EN 14488-3}} = 0.900\,\mathrm{CMOD}_{\text{EN 14488-3}} \pm 0.006 \tag{6.20}$$

$$\mathrm{CTOD}_{\text{EN 14651}} = \mathrm{CTOD}_{\text{EN 14488-3}}$$

$$0.843\,\mathrm{CMOD}_{\text{EN 14651}} \pm 0.014 = 0.900\,\mathrm{CMOD}_{\text{EN 14488-3}} \pm 0.006$$

$$\mathrm{CMOD}_{\text{EN 14651}} = 1.067 \times \mathrm{CMOD}_{\text{EN 14488-3}} - 0.008 \tag{6.21}$$

$$\mathrm{CMOD}_{\text{EN 14488-3}} = 0.937 \times \mathrm{CMOD}_{\text{EN 14651}} - 0.008 \tag{6.22}$$

Table 6.8: Relationship between CMOD of EN 14651 and EN 14488-3 Method B based on numerical results.

CMOD EN 14651 [mm]	**CMOD EN 14488-3 Method B [mm]**
0.5	0.461
1.5	1.398
2.5	2.335
3.5	3.272

Table 6.9: Relationship between CMOD of EN 14651 and EN 14488-3 Method B—summary.

Method	**Relationship**
Analytical	$\text{CMOD}_{\text{EN 14488-3}} = 0.910 \times \text{CMOD}_{\text{EN 14651}}$
Experimental	$\text{CMOD}_{\text{EN 14488-3}} = 0.915 \times \text{CMOD}_{\text{EN 14651}}$
Numerical	$\text{CMOD}_{\text{EN 14488-3}} = 0.937 \times \text{CMOD}_{\text{EN 14651}} - 0.008$

Table 6.10: Relationship between CMOD of EN 14651 and CMOD of EN 14488-3 Method B (analytical, experimental, numerical).

CMOD EN 14651 [mm]	**CMOD EN 14488-3 Method B [mm]**		
	Analytical	**Experimental**	**Numerical**
0.5	0.46	0.46	0.461
1.5	1.37	1.37	1.398
2.5	2.28	2.29	2.335
3.5	3.19	3.20	3.272

Based on the analytical, experimental, and numerical correlations, the relationship between the CMOD values of EN 14488-3 Method B and EN 14651 was established and is summarized in the Table 6.9. Subsequently, the 6.10 presents the corresponding CMOD values of EN 14488-3 Method B [16] for the reference CMODs of EN 14651 [7] (0.5 mm, 1.5 mm, 2.5 mm, and 3.5 mm). As discussed in the introductory section of this chapter, the CMODs obtained from EN 14651 [7] and EN 14488-3 Method B [16] are not identical.

Chapter 7

Conclusions

This doctoral research focuses on an in-depth investigation of the properties and performance of fibre-reinforced sprayed concrete for use in permanent tunnel linings. The study employs experimental, numerical and analytical approaches, based on a comprehensive review of the literature used for establishing the background and objectives of the work. The research aims to determine whether sprayed fibre-reinforced concrete (FRC) represents an effective solution for final tunnel linings based on its mechanical performance, post-cracking behaviour, and compliance with existing standards. The main objectives are to clarify the performance differences of sprayed fibre reinforced concrete assessed using testing methodologies specifically developed for sprayed FRC and those mainly originally conceived for cast FRC, and to establish potential relationships among these performance outcomes. As part of the numerical approach, the study also aims to develop accurate uniaxial post-cracking constitutive laws suitable for use in the design of Permanent Sprayed Concrete Linings (PSCL).

Chapter 2 provided an overview of the current state of the art on fibre-reinforced and sprayed concrete materials, with particular emphasis on sprayed fibre-reinforced concrete for use in permanent tunnel linings. This review established the technical foundation and context for the subsequent experimental, numerical, and analytical investigations.

Chapter 3 highlighted the significance of the research and outlined the logical framework and methodology adopted to achieve the study's objectives.

The main part of the thesis, presented in Chapter 4, involved an extensive experimental investigation aimed at evaluating the mechanical properties of sprayed fibre-reinforced concrete.

The study used standard testing procedures conceived to assess post-cracking properties of the sprayed FRC. In addition, cast-in-moulds samples were produced from the same concrete

batch adopted for the spraying process. The residual strength test was conducted in accordance with EN 14488-3 Method B:2023 (three-point bending notched panel test) and the energy absorption capacity test was conducted according to EN 14488-5, Both tests are recommended by EN 14487-1:2023, the recently updated standard commonly used for sprayed concrete tunnel linings. In addition, the three-point bending notched beam test according to EN 14651 was used. The latter is recommended by Eurocode 2 Annex L and the *fib* Model Code 2020 for classification and characterisation of FRC even though the cast-in-mould beams are traditionally used for conventionally cast-FRC structures. Furthermore, the EN 14651 three-point bending notched beam test was also conducted on saw-cut sprayed beams obtained from large sprayed panels ($15 \times 80 \times 200\,\text{cm}$).

The experimental campaigns covered sprayed FRC specimens, including cast-in-mould FRC samples. The mixes incorporated a steel fibre SFRC-25 and SFRC-40, with a dosage of 25 kg/m^3 ($V_f = 0.32\%$) and 40 kg/m^3 ($V_f = 51\%$) respectively and a macro-synthetic fibre MSFRC-7 with a dosage of 7 kg/m^3 ($V_f = 0.77\%$). The concrete were produced from the same batch with a target strength class of C-35. Flexural tests were carried out at 28 and 90 days, while compressive strength and shrinkage tests were conducted at 1, 3, 7,10,14,28,56 and 90 days.

Based on this comprehensive experimental campaign, the following conclusions were drawn:

- The compressive strength of sprayed FRC (measured from samples drilled from a sprayed panel) was lower than that of cast FRC (measured on conventionally cast-in-moulds cubic specimens) at all ages. The cubic compressive strength of sprayed fibre reinforced concrete $f_{cm,\text{sprayed}}$ reached approximately 85% of the cubic cast concrete strength $f_{cm,\text{cast}}$ at 28 days. The lower compressive strength of the sprayed concrete might be attributed to several factors. Unlike cast-in-mould cubes, sprayed concrete is not subjected to vibration, which may result in less uniform compaction and a more porous internal structure. This resulted in percentage difference of 5.15% relative to the density of cast-cube samples for SFRC-25; however, this density difference was not observed in the SFRC-40 series, where a difference of 0.87% was obtained.

  In addition, since the sprayed samples were cored from sprayed panels, part of the strength reduction may be attributed to micro-defects and microcracking induced by the drilling process. A unique damage factor 1.06 has been suggested in ACI PRC-214.4-21. A damage factor is also suggested by Italian Explanatory Circular, ranging from 1.10 to 1.00 depending on the concrete strength class.

  In general, the dominant contribution is associated with the spraying process itself. The

observed reduction in bulk density indicates an increase in void content due to the spraying mechanism. Additionally, the process alters the pore structure, induces microcracking, and modifies the characteristics of the interfacial transition zone (ITZ), the interface between coarse aggregate and cement paste, thereby influencing the overall microstructural integrity of the hardened concrete. The results confirm that, in order for sprayed FRC to achieve adequate strength for final tunnel lining applications, optimisation of the spraying process and consideration of the strength difference relative to traditionally cast-in-mould elements are essential to enhance compressive performance and improve understanding of its behaviour in permanent tunnel linings.

- The energy absorption capacity or toughness of the sprayed FRC increased with increasing fibre dosage. when the fibre content was raised by 60%, 25 kg/m^3 to 40 kg/m^3, the energy absorption capacity increased by 28% and 21% for the sprayed and cast series, respectively. Compared with the variation observed for the same fibre contents in residual strengths (f_{Ri}) exhibited by notched samples (both notched panels and beams) used for the mechanical characterisation, this increase was relatively moderate. Regarding the difference between the sprayed and cast series, with the 25 kg/m^3 fibre dosage, the sprayed specimen exhibited approximately 5.90% lower energy absorption capacity, while at the 40 kg/m^3 fibre dosage, the energy absorption capacity of the cast and sprayed series is nearly identical. These differences were also relatively small compared with those observed in residual strength results for the sprayed and cast series (both panels and beams) as probably related to the high degree of redundancy provided by four-sided supports used in the energy absorption test.

- The energy absorption class (E_{25}) for the cast-panel series is E700 for FRC panels reinforced with 7 kg/m^3 of macro-synthetic fibres, and E1000 for FRC panels reinforced with steel fibres at dosages of 25 kg/m^3 and 40 kg/m^3, respectively. For the sprayed-panel series, the corresponding energy absorption classes are E700 and E1000 for steel-fibre dosages of 25 kg/m^3 and 40 kg/m^3, respectively.

- When considering mechanical post-cracking characterisation based on notched beam samples, the difference in the limit of proportionality (f_{L}) between the SFRC-25 and SFRC-40 series was approximately 15% for both cast-in-mould and beams saw-cut from sprayed panels ("sprayed beams"). This relatively small variation indicates that the (f_{L}) is primarily governed by the concrete matrix strength rather than the fibre content difference between the two series compared to the ($f_{\mathrm{R}i}$) results. For the series of cast-in-mould

beams, the residual flexural tensile strengths (f_{R1}, f_{R2}, f_{R3} and f_{R4}) increased by 76%, 49%, 36% and 30%, respectively, when comparing SFRC-40 to SFRC-25. In the case of "sprayed beams", the corresponding increases were approximately 56%, 55%, 50% and 44%, respectively. The relative difference in residual strength between the two series was observed to decrease as the crack width increased. Regarding cast-in-moulds beams and "sprayed beam" samples, consistent trends were observed with cast beams showing higher mean residual strengths with narrower statistical dispersion even though "sprayed beams" showing slightly lower variability $COV \leq 0.10$.

- Difference between the results of the f_{Ri} strengths of the cast-in-mould beam and the "sprayed beam" was significant; for both fibre contents (25 and 40 kg/m^3) the beam sawn from sprayed panels exhibited lower post-cracking strengths than cast ones: its difference was consistent for both SFRC-25 and SFRC-40. with an average proportional relationship of approximately 0.74 for f_L, 0.55 for f_{R1}, 0.58 for f_{R2}, 0.62 for f_{R3}, 0.65 for f_{R4} relative to the corresponding cast-in-mould beams.

- When considering mechanical post-cracking characterisation based on notched panel samples, the limit of proportionality (f_L) differed approximately 14% and 50% between the SFRC-25 and SFRC-40 series for sprayed and cast-in-mould panels, respectively. Regarding the effect of fibre contents, for the sprayed panels, the residual flexural tensile strengths (f_{R1}, f_{R2}, f_{R3} and f_{R4}) increased by 69%, 61%, 56% and 51%, respectively, when comparing SFRC-40 to SFRC-25. In the case of cast-in-mould panels, the corresponding increases were approximately 120%, 73%, 57% and 50%, respectively. The relative difference in residual strength between the two series was observed to decrease as the crack width increased.

- The sprayed notched panels generally exhibited lower flexural strengths and higher variability than the cast ones. Increasing the fibre content reduced the variability in sprayed fibre reinforced concrete as shown by the decrease in the coefficient of variation (COV). In comparison, the cast notched panels displayed more consistent results, with COV values of approximately 10% for both SFRC-25 and SFRC-40, and 20% for MSFRC-7. These results confirm that fibre dosage significantly influences both strength and consistency, where the spraying process introduces additional variability.

- By comparing notched panels tested according to Method B 14488-3:2023 and notched beams tested according to EN 14651, considering the overall SFRC-25 steel fibre and based on the mean flexural tensile curve, the results followed the order SFRC-25 cast-in-

mould beam > SFRC-25 cast-in-mould panel > SFRC-25 sprayed panel > SFRC-25 sprayed beam (beam sawn from sprayed panel). This indicates that the series of cast elements exhibited higher nominal flexural tensile strengths than the corresponding sprayed elements in both notched panel and notched beam tested according to EN 14488-3:2023 and EN 14651 test methodology. For SFRC-40 series, the same trend was observed, with magnitudes following the order SFRC-40 cast-in-mould panel > SFRC-40 cast-in-mould beam > SFRC-40 sprayed panel > SFRC-40 "sprayed beam". In both series, cast-in-mould notched elements showed noticeably higher post-cracking flexural strengths compared with notched sprayed elements, both tested in 3PBT configuration.

- However, by considering cast-in-mould samples: the SFRC-25 cast-beams present higher post-cracking strengths than cast-panels, whereas for SFRC-40 series, is the opposite. It is worth noticing that, for a given fiber content, the difference in terms of post-cracking performance between cast elements (panels vs. beam) is less than the that observed when comparing globally cast-in-mould elements with sprayed ones.

- In tunnelling practice, and among some researchers within the scientific community PSCL (Permanent Sprayed Concrete lining) are often designed by referring on post-cracking residual strengths retrieved from cast-in-mould beams tested according to EN 14651. However, as demonstrated in this study, the residual strength values obtained from cast-in-mould notched beam differ from those derived from notched sprayed panel results (EN 14488-3 Method B) and from beams sawn from sprayed panels ("sprayed beams") tested in accordance to EN 14651. The ratios between residual strengths obtained from notched sprayed panels and notched "sprayed beams" with respect to those obtained from typical cast-in-mould notched beam remain consistent for SFRC-25 and SFRC-40 series, with average ratios of approximately 0.82 for f_{L}, 0.67 for f_{R1}, 0.68 for f_{R2}, 0.71 for f_{R3}, 0.72 for f_{R4} relative to the corresponding cast beams. These findings indicate that while EN 14651 used for cast-in-mould beams are generally recognized as important and a useful reference for comparative assessment, the corresponding post-cracking properties overestimate the residual strengths of sprayed concrete due to the clear differences between the spraying process and traditionally casting one. Therefore, for design PSCL, test on sprayed notched panel testing (EN 14488-3 Method B, 2023) is recommended as it seems to represent the in-situ post-cracking performance.

- The flexural test on the notched sprayed panels and notched beams was also conducted at 90 days to evaluate the effect of age on the post-cracking strength, and to compare

the results with those obtained at 28 days. Across all series, the limit of proportionality (f_L) values increased considerably by approximately 33%, which can be attributed to the strong influence of compressive strength of the concrete on (f_{R1} compared to the residual strength parameters (f_{R1}, f_{R2}, f_{R3} and f_{R4}) for the residual strength, there was an overall 4-16% increase in residual strength at 90 days compared to the results at 28 days.

- The current methodology for the post-cracking mechanical characterization of sprayed FRC (method B, 3PBTs on notched panels EN 14448-3:2023) is reliable, since reliable nominal residual strengths can be obtained, well representing the actual behaviour of sprayed FRCs.

- From manual counting of number of fibres from cracked surface of notched samples, fibre-orientation numbers were estimated. The latter are not very far from the assumed values in the Model Code for the cast-in-mould beams according to EN 14651 (SFRC-25 cast-in-mould beam = 0.50, and SFRC-40 cast-in-mould beam = 0.55). For the sprayed standard panel tested according to EN 14488-3 Method B (SFRC-25 sprayed panels = 0.36, and SFRC-40 sprayed panels = 0.33). Moreover, the fibre orientation numbers estimated from beams saw-cut from sprayed panel, so-called "sprayed beam", are well aligned to those obtained from sprayed panels (SFRC-25 "sprayed beam" = 0.36, and SFRC-40 "sprayed beam" = 0.36).

- The classification of SFRC-25 cast-in-mould beam according to the Model Code 2020 and Eurocode 2 Annex L is 4d and 4e, respectively. For SFRC-40 cast-in-mould beam, the corresponding classes are 7c and 7d. The saw-cut sprayed-beam specimens tested under EN 14651 show classifications of 2.5d for SFRC-25_SB according to both the Model Code 2020 and Eurocode 2 Annex L, and 3.5d and 3.5e for SFRC-40 SB according to the Model Code 2020 and Eurocode 2 Annex L, respectively. Both SFRC-25 and SFRC-40 sprayed panels are classified as Class 3 according to EN 14487-1.

- Since the Model Code 2020 and Eurocode 2 Annex L classify FRC based on the characteristic residual strengths $f_{R,ki}$ corresponding to CMOD values of 0.5, 1.5, 2.5, and 3.5 mm obtained from cast-in-mould beam tests (EN 14651), the post-cracking residual strengths $f_{R,ki}$ retrieved from tests carried out according to EN 14488-3-Method B on notched-panels were used to determine the sprayed-panel classification. The SFRC-25 and SFRC-40 notched sprayed panels were classified as 2d and 4.5d, respectively.

- It is noted in this thesis that the classifications derived from the cast-in-mould standard

beam (EN 14651) for SFRC-25 CB and SFRC-40 CB are 4d and 7c, whereas the classifications obtained from the sprayed-panel test method (EN 14488-3 Method B) are 2d and 4.5d for SFRC-25 SP and SFRC-40 SP, respectively. These differences are probably mainly related to the different fibre orientation exhibited by sprayed SFRC as a result of the spraying process. In fact, as previously noted, the fibre orientation numbers of the cast-in-mould series are higher than those of the sprayed specimens.

- The effect of ageing on the classification results between 28 and 90 days is found to be minimal. The classification values remain essentially stable over time, with the only notable change being a slight increase in the SFRC-40 "sprayed beam" series, which shifts from Class 3.5d at 28 days to Class 4d at 90 days. This indicates that the change in residual strength between 28 and 90 days is small and does not significantly affect the classification of the material.

In Chapter 5, numerical modelling was performed for both sprayed and cast fibre-reinforced concrete (FRC) beams and panels. The following conclusions were drawn:

- The post-cracking performance trends, based on fracture energy (G_f) derived from σ–w laws (numerical results), are similar to those demonstrated by experimental flexural responses of FRCs under investigation.
- In all cases, and consistent with the flexural response, the uniaxial post-cracking behaviour of the sprayed series obtained from the numerical modelling exhibited lower values compared to the cast elements. Furthermore, the differences within each group-namely between cast beams and cast panels, and between sprayed beams and sprayed panels—were significantly smaller than the differences observed between the sprayed and cast series.
- The inverse analysis approach proposed for evaluating sprayed fibre reinforced concrete uniaxial post-cracking laws were effective and provide accurate σ–w relationships for use in structural numerical simulations of sprayed concrete tunnel linings

Chapter 6 the correlation of main displacement parameters used in notched tests was studied for getting an in-depth understanding of the comparability of residual strengths (f_{Ri}) retrieved from notched panels and beams especially with regard the range of crack widths under investigation.

- According to European sprayed concrete standards, which are frequently mentioned in this research, EN 14488-3 and EN 14487-1, when calculating the residual strength of sprayed FRC materials, the crack mouth opening displacement (CMOD) of the beam EN 14651 and the panel CMOD (as per EN 14488-3) are considered equivalent. However, as a result of the geometrical differences between the beam and panel, the application of the load on each, and the notches provided in both, the CMOD measurements from these two test methods cannot be considered truly and exactly equivalent.
- To address this, the relationship between the CMOD values obtained from the two standards has been analysed, verified, and established through analytical, experimental, and numerical methods as reported in Chapter 6. The parameters are not exactly in a 1:1 ratio, but they are acceptably close each other making reasonable within standard applications to directly compare for a given CMOD the residual strengths obtained from notched panels and notched beams. In fact, they are referring approximately to the same crack-width as measured from tip of the crack.

References

[1] International Federation for Structural Concrete. *fib Model Code 2010 for Concrete Structure: Final draft*. Ernst Sohn, Lausanne, Switzerland, 2010.

[2] Ingemar Lofgren. *Fibre-reinforced Concrete for Industrial Construction – a fraction mechanics approach to material testing and structural analysis*. PhD thesis, Chalmers University of Teechnology, Gothenburg, Sweden, 2005. PhD thesis.

[3] J.F. Guan, X.Z. Hu, C.P. Xie, Q.B. Li, and Z.M. Wu. Wedge-splitting tests for tensile strength and fracture toughness of concrete. *Theoretical and Applied Fracture Mechanics*, 93:263–275, 2018.

[4] S.H. Chao, N.B. Karki, J.S. Cho, and R.N. Waweru. Use of double punch test to evaluate the mechanical performance of fibre reinforced concrete. In Gustavo J., Parra.Montesinos, Hans W.Reinhardt, Antoine E., and Naaman, editors, *High Performance Fibre Reinforced Cement Composite 6*, volume 2 of *RILEM Bookseries*, pages 27–34. Springer, 2012.

[5] Marco di Prisco, Liberato Farrara, and L. Marco G. Double edge wedge splitting (dews): an indirect tension test to identify post-cracking behaviour of fibre reinforced cementitious composites. *Material and Strutures*, 46:1893–1918, 2013.

[6] Hussam A.Goaiz, Nabeel A.Farhan, M. Neaz Sheikh, Tao Yu, and Muhammad N.S. Hadi. Experimental evaluation of tensile strength test methods for steel fibre-reinforced concrete. *Magazine of Concrete Research*, 71(8):385–394, 2019.

[7] CEN (European Committee for Standardization). Test method for metallic fibre concrete - measuring the flexural tensile strength (limit of proportionality (lop), residual). Technical Report EN 14651:2005, European Committee for Standardization (CEN), Brussels, Belgium, 2005. Available at: `https://standards.cen.eu/`.

[8] International Federation for Structural Concrete. *fib Model Code 2020 for Concrete Structure: Final draft*. Ernst Sohn, Lausanne, Switzerland, 2023.

[9] CEN (European Committee for Standardization). Design of concrete structures, general rules and rules for buildings (annex l. Technical Report Eurocode 2 EN 1992-1-1, European Committee for Standardization (CEN), Brussels, Belgium, 2023. Available at: `https://standards.cen.eu/`.

[10] Dupont D and Vandewalle L. Distribution of steel fibres in rectangular sections. *Cement and Concrete Research*, 27:391–398, 2005.

[11] Thomas A.H. *Sprayed concrete lined tunnels*. CRC Press, Boca Raton, USA,, 2nd edition, 2019.

[12] Karl Gunnar Holter. Loads on sprayed waterproof tunnel linings in jointed hard rock: A study based on norwegian cases. *Rock Mechanics and Rock Engineering*, 47:1003–1020, 2014.

[13] Jiang Su and Alan Bloodworth. Simulating composite behaviour in scl tunnels with sprayed waterproofing membrane interface: A state-of-the-art review. *Engineering Structures*, 191:698–710, 2019.

[14] Antoine Gagnon and Marc Jolin. Three point bending test on notched beam (en 14651) and notched square panel (e3pbt). Technical report, CRIB, Laval University, Quebec, Canada, 2019. A Technical Report V 1.1 Report for Bekaert Underground Solution.

[15] Benoit De Rivaz Chris Peaston. En 14488-3 notched panel versus en 14651 notched beam testing for pre-construction trial conformance testing of sprayed concrete linings (scl). In Jinxiu Yan, Tarcisio Celestino, Markus Thewes, and Erik Eberhardt, editors, *Tunnelling for a Better Life*, Proceedings of the ITA-AITES WORLD TUNNEL CONGRESS 2024, pages 1151–1158. CRC Press/Balkema, 2024.

[16] CEN (European Committee for Standardization). Testing sprayed concrete – part 3: Flexural strengths (first peak, ultimate and residual) fibre reinforced beam specimens. Technical Report EN 14488-3, European Committee for Standardization (CEN), Brussels, Belgium, 2006. Available at: `https://standards.cen.eu/`.

[17] ASTM (American Society for Testing and Materials). Astm c1550-20 standardtest method for flexural toughness of fiber reinforced concrete (using centrally loaded round panel).". Technical Report ASTM C1550, American Society for Testing and Materials (ASTM), West Conshohocken, United State, 2020.

[18] CEN (European Committee for Standardization). Testing sprayed concrete - part 5: Determination of energy absorption capacity of fibre reinforced slab specimens. Technical

Report EN 14488-5, European Committee for Standardization (CEN), Brussels, Belgium, 2006. Available at: `https://standards.cen.eu/`.

[19] CEN (European Committee for Standardization). Sprayed concrete – part 1: Definitions, specifications and conformity. Technical Report EN 14487-1, European Committee for Standardization (CEN), Brussels, Belgium, 2022. Available at: `https://standards.cen.eu/`.

[20] International Federation for Structural Concrete. Constitutive modelling of high strength / high performance concrete: State-of-art report. Technical Report fib Bulletin No. 42, International Federation for Structural Concrete(fib), Lausanne, Switzerland, 2008.

[21] M.G. Alberti, A. Enfedaque, and J.C. Gálvez. A review on the assessment and prediction of the orientation and distribution of fibres for concrete. *Composite Part B*, 151:274–290, 2018.

[22] Alun Thomas and Ross Dimmock. The design philosophy for permanent sprayed concrete linings. In Thomas Beck and Synnøve A. Myren andSiri Engen, editors, *Eith International Symposium on Sprayed Concrete-Modern Use of Wet Mix Sprayed Concrete for Underground Support*, 2018.

[23] Bentur A and Mindess S. *Fibre Reinforced Cementitious Composites*. Taylor Francis, Abingdon, England, 2nd edition, 2007.

[24] International Federation for Structural Concrete. *Fibre Reinforced Concrete (State of Art),*. FIB, Lausanne, Switzerland, 2022.

[25] Giuseppe Tiberti, Federica Germano, Antonio Mudadu, and Giovanni Plizzari. An overview of the flexural post-cracking behavior of steel fiber reinforced concrete. *Structural concrete*, 2017.

[26] B. Barr and P.D. Newman. Toughness of polypropylene fibre-reinforced concrete. *Composites*, 16(1):48–53, 2003.

[27] Machine Hsie, Chijen Tu, and P.S.Song. Mechanical properties of polypropylene hybrid fiber-reinforced concrete. *Material Science and Engineering*, 494(1-2):153–157, 2008.

[28] O Cengiz and L Turanli. Comparative evaluation of steel mesh, steel fibre and high-performance polypropylene fibre reinforced shotcrete in panel test. *Cement and Concrete Research*, 34(8):1357–1364, 2004.

[29] Kamasani Chiranjeevi Reddy and Kolluru V.L. Subramaniam. Experimental investigation of crack propagation and post-cracking behaviour in macrosynthetic fibre reinforced concrete. *Magazine of Concrete Research*, 69(9):467–478, 2017.

[30] Kamasani Chiranjeevi Reddy and Kolluru V.L. Subramaniam. Analysis for multi-linear stress-crack opening cohesive relationship: Application to macro-synthetic fiber reinforced concrete. *Engineering Fracture Mechanics*, 169:128–145, 2017.

[31] W.S.A. Nana, H.V. Tran, T. Goubin, G. Kubisztal, A. Bennani, T.T. Bui, G. Cardia, and A. Limam. Behaviour of macro-synthetic fibers reinforced concrete: Experimental,numerical and design code investigations. 32:1271–1286, 2021.

[32] Peter J. M. Bartos. *Glassfibre Reinforced Concrete principles, production, Properties and applications*. Whittles Publishing, Dunbeath,Scotland, 2017.

[33] Jawad Ahmad, Roberto Alonso, Ali Majdi, Nabil Ben Kahla, Ahmed Farouk Deifalla, and Mohammed A. El-Shorbagy. Glass fibers reinforced concrete: Overview on mechanical, durability and microstructure analysis. *Materials*, 15(15), 2022.

[34] Ehab T. Al-Rousan, Hammad R. Khalid, and Muhammad Kalimur Rahman. Fresh, mechanical, and durability properties of basalt fibre-reinforced concrete (bfrc): A review. *Developments in the Built Environment*, 14, 2023.

[35] Zhenghua Lyu Ziming He Kate T.Q. Nguyen Wenzhen Wang, Aiqin Shen. Fresh and rheological characteristics of fiber reinforced concrete—a review. *Construction and Building Materials*, 296, 2021.

[36] Nilufer Ozyurt, Thomas O. Mason, and Surendra P. Shah. Correlation of fiber dispersion, rheology and mechanical performance of frcs. *Cement and Concrete Composites*, 29(2):70–79, 2007.

[37] Bensaid Boulekbache, Mostefa Hamrat, Mohamed Chemrouk, and Sofiane Amziane. Flowability of fibre-reinforced concrete and its effect on the mechanical properties of the material. *Construction and Buidling Materials*, 24(9):1664–1671, 2010.

[38] Liberato Ferrara and Alberto Meda. Relationships between fibre distribution, workability and the mechanical properties of sfrc applied to precast roof elements. *Material and Structures*, 39:411–420, 2006.

[39] Liberato Ferrara and Alberto Meda. The role of flaw size and fiber distribution on tensile ductility of pva-ecc. *Composite Part B Engineering*, 56:536–545, 2014.

[40] A. Hillerborg. Analysis of fracture by means of the fictitious crack model, particularly for fibre reinforced concrete. *International Journal of Cement Composites*, 2(4):536–545, 1980.

[41] H. Stang. Evaluation of properties of cementitious fiber composite materials, high performance fiber reinforced cement composites. 1:388–406, 1992.

[42] Jan G.M. van Mier. *Fracture processes of concrete*. CRC Press, Boca Raton, Florida, 1st edition, 1997.

[43] Alan Renato Estrada Cacers, Sergio H.P. Cavalaro, and Antonio Domingues de Figueiredo. Integrated approach for quality control of fibre-reinforced sprayed concrete for tunnel lining. *Tunnelling and Underground Space Technology*, 140, 2023.

[44] CEN (European Committee for Standardization). Testing hardened concrete - part 1: Shape, dimensions, and other requirements for specimens and moulds. Technical Report EN 12390-1:2021, European Committee for Standardization (CEN), Brussels, Belgium, 2021. Available at: `https://standards.cen.eu/`.

[45] CEN (European Committee for Standardization). Testing fresh concrete sampling and common apparatus. Technical Report EN 12350-1:2019, European Committee for Standardization (CEN), Brussels, Belgium, 2019. Available at: `https://standards.cen.eu/`.

[46] CEN (European Committee for Standardization). Testing hardened concrete - part 2: Making and curing specimens for strength tests. Technical Report EN 12390-2:2009, European Committee for Standardization (CEN), Brussels, Belgium, 2009. Available at: `https://standards.cen.eu/`.

[47] International Federation for Structural Concrete. *Fibre reinforced concrete State-of-the-Art report:fib Bulletin 105*. Ernst Sohn, Lausanne, Switzerland, 2022.

[48] F. Laranjeira, A. Aguado, C. Molins, S. Grünewald, J. Walraven, and S. Cavalaro. Framework to predict the orientation of fibers in frc: A novel philosophy. *Cement and Concrete Research*, 42(6):752–768, 2012.

[49] Abrishambaf A, Barros JAO, and Cunha VMCF. Relation between fibre distribution and post-cracking behaviour in steel fibre reinforced self-compacting concrete panels. *Cement and Concrete Research*, 51:57–66, 2013.

[50] Ozyurt N. *Correlating fiber dispersion, rheology and mechanical performance for fiber-reinforced cement-based materials*. PhD thesis, Istanbul Technical University Graduate Institute, Istanbul, Turkey, 2006. PhD thesis.

[51] S.H. Chao, N.B. Karki, J.S. Cho, and R.N. Waweru. Fibre spacing and specific fibre surface. In R.N.Swamy, editor, *Fibre Reinforced Cement and Concrete*, volume 9 of *RILEM Bulletin*, pages 67–79. Springer, 1975.

[52] Antonio Conforti, Estefania Cuenca, Raúl Zerbino, and Giovanni A. Plizzari. Influence of fiber orientation on the behavior of fiber reinforced concrete slabs. *Structural Concrete*, 22(3):1831–1844, 2021.

[53] R. Zerbino, J. M. Tobes, M. E. Bossio, and G. Giaccio. On the orientation of fibres in structural members fabricated with self compacting fibre reinforced concrete. *Cement and Concrete Composites*, 34(2):191–200, 2012.

[54] Sorousshian P and Lee CD. Distribution and orientation of fibres in steel fibres reinforced concrete. *ACI Material Journal*, 87(5):433–439, 1990.

[55] Kim H Lee C. Orientation factor and number of fibers at failure plane in ring-type steel fiber reinforced concrete. *Cement and Concrete research*, 40(5):810–819, 2010.

[56] Rao CK. Effectiveness of random fibres in composites. *Cement and Concrete research*, 9(6):685–693, 1979.

[57] Alberti MG, Enfedaque A, and Galvez JC. On the prediction of the orientation factor and fibre distribution of steel and macro-synthetic fibres for fibre-reinforced concrete. *Cement and Concrete Composites*, 77:29–48, 2017.

[58] Alberti MG. *Polyolefin fibre-reinforced concrete: from material behaviour to numerical and design considerations*. PhD thesis, Universidad Politecnica de Madrid, Madrid, Spain, 2015. PhD thesis.

[59] Dudley R. Morgan and E. Stefan Bernard. A brief history of shotcrete in the underground industry. *Shotcrete Magazine*, 2017.

[60] EFNARC (The European Federation of Specialist Construction Chemicals and Concrete Systems),). European specification for sprayed concrete. Technical Report EFNARC, EEFNARC, Flums, Switzerland, 1996.

[61] ASTM International. Standard practice for sampling materials for shotcrete. Technical Report ASTM C1385/C1385M-10(2017), ASTM International, West Conshohocken, PA, USA, 2017. Available at: `https://www.astm.org/`.

[62] American Concrete Institute. Guide to shotcrete reported by aci committee 506. Technical Report ACI 506R-16, American Concrete Institute (ACI), Farmington Hills, MI, USA, 2016. Available at: `https://www.concrete.org/`.

[63] Canadian Standards Association. Concrete materials and methods of concrete construction/test methods and standard practices for concrete. Technical Report CSA A23.1:19 / CSA A23.2:19, Canadian Standards Association (CSA), Toronto, ON, Canada, 2019. Available at: `https://www.csagroup.org/`.

[64] Japan Society of Civil Engineers. Jsce guidelines for concrete no.16: Standard specifications for concrete structures. Technical Report JSCE No.16, Japan Society of Civil Engineers (JSCE), Tokyo, Japan, 2007.

[65] Dudley R. Morgan. Evolution of fibre reinforced shotcrete. *Shotcrete Magazine*, 2000.

[66] Knut Garshol and O.T. Blindheim AS. Development of mechanized wet mix shotcrete application in norwegian tunnelling industry. In *Shotcrete for underground support V: proceedings of the Engineering Foundation Conference*. New York, N.Y. : American Society of Civil Engineers, 1990.

[67] S. Bernard, M.J.K. Clements, and Duffield. Development of macro-synthetic shotcrete in australia. In Thomas Beck, Synnøve A. Myren, and Siri Engen, editors, *Seventh International Symposium on Sprayed Concrete-Modern Use of Wet Mix Sprayed Concrete for Underground Support*. norsk betongforening, 2014.

[68] D. Millette and M Jolin. Shotcrete accelerators for wet-mix. *Shotcrete Magazine*, 2014.

[69] T. Ikumi, Renan P. Salvador, and A. Aguado. Mix proportioning of sprayed concrete: A systematic literature review. *Tunnelling and Underground Space Technology*, 124, 2022.

[70] David Chapman, Nicole Metje, and Alfred Stark. *Introduction to tunnel construction*. CRC Press, New York, USA, 2nd edition, 2018.

[71] V. Bindiganavile and N. Banthia. Fiber reinforced dry-mix shotcrete with metakaolin. *Cement and Concrete Composites*, 23:503–514, 2001.

[72] H Bin, Y Song, Y Shaofeng, W Jianxun, and L Jiameng. Key factors affecting pumpability, strength and rebound rate of wet sprayed concrete. *Metal Mine*, 2014.

[73] W Kusterle M Dietzel F Mittermayr I Galan, A Baldermann. Durability of shotcrete for underground support – review and update. *Construction and Building Materials*, 202:465–493, 2019.

[74] A spanish association of tunnels and underground works aetos. Design, manufacture and installation of shotcrete in underground works. Technical report, A spanish association of tunnels and underground works aetos, Spain, 2015.

[75] Luiz Roberto Prudêncio Jr. Accelerating admixtures for shotcrete. *Cement and Concrete Composites*, 20(2-3):213–219, 1998.

[76] Isaac Galobardes Reyes. *Characterization and Control of wet-mix sprayed concrete with accelerators*. PhD thesis, Universitat Politècnica de Catalunya, Barcelona, Spain, 2013. PhD thesis.

[77] Isaac Galobardes, Sergio H. Cavalaro, Antonio Aguado, and Tomàs Garcia. Estimation of the modulus of elasticity for sprayed concrete. *Construction and Building Materials*, 53:48–58, 2014.

[78] R.P. Salvador, Cavalaro S.H.P., R. Monte, and Figueiredo A.D. Relation between chemical processes and mechanical properties of sprayed cementitious matrices containing accelerators. *Cement and Concrete Composites*, 79:117–132, 2017.

[79] ITA Working Group Number 12 and ITAtech . Permanent sprayed concrete linings. Technical Report 24, International Tunnelling Association (ITA), Avignon, France, 2020.

[80] Jean-Benot Darveau and Marc Jolin. Three point bending test on square panel with notch on spraeyd specimens (3pbt on square panel)-dramix 4d 65/35 bg. Technical report, CRIB, Laval University, Quebec, Canada, 2022. Technical Report V 1.2 for Bekaert Underground Solution.

[81] Chris Peaston and Benoit De Rivaz. Notched beam and panel test alternatives for conformance testing of sprayed concrete linings consistent with limit state design. In Øyvind Bjøntegaard, Thomas Beck, and Cecilie Hagby, editors, *Ninth International Symposium on Sprayed Concrete-Modern Use of Wet Mix Sprayed Concrete for Underground Support*, Sandefjord, Norway, 2014. norsk betongforening.

[82] Bou-Young Youn-Čale, Sven Plückelmann, and Rolf Breitenbücher. Round robin test to compare flexural strength test methods for steel fiber-reinforced sprayed concretes. *Structural Concrete*, 23:255–267, 2021.

[83] N. Buratti, A. Incerti, A.R Tilocca, M. Paparella, and M. Draconte. Energy absorption tets on fibre-reinforced shotcrete round and square panels. In Daniele Peila, Giulia Viggiani, and Tarcisio Celestino, editors, *Tunnels and Underground Cities Engineering and Innovation Meet Archaeology, Architecture and Art*, page 10, Sandefjord, Norway, 2019. CRC Press.

[84] Alan Renato Estrada Cáceres, Sergio Henrique Pialarissi Cavalaro, and Antonio Domingues de Figueiredo. Evaluation of steel fiber–reinforced sprayed concrete by energy absorption tests. *Journal of Materials in Civil Engineering*, 33(9):255–267, 2021.

[85] Sergio Carmona and Climent Molins. Using energy absorption capacity to determine residual resistances of frc. In Llano-Torre A. Martí-Vargas J.R. Serna, P., editor, *Fibre Reinforced Concrete: Improvements and Innovations II*, volume 36 of *X RILEM-fib International Symposium on Fibre Reinforced Concrete (BEFIB) 2021*, pages 601–611. Springer, 2022.

[86] S. Carmona and C. Molins. Equivalence between flexural toughness and energy absorption capacity of frc. In P. Serna, A. Llano-Torre, and J. Martí-Vargas, J.R.and Navarro-Gregori, editors, *Fibre Reinforced Concrete: Improvements and Innovations*, volume 30 of *RILEM-fib International Symposium on Fibre Reinforced Concrete*, pages 253–261. Springer, 2021.

[87] P.K. Juhasz, L. Nagy, and P. Schaul. Correlation of results of the standard beam and efnarc panel test. In Bjorn and Nilsen (szerk.), editors, *Surface challenges Underground solutions*, volume 8 of *Proceedings of the World Tunnel Congress 2017*, pages 2754–2761. Tudományosr, 2017.

[88] E.S. Bernard and S.A. Hanke. Age-dependent behaviour of fibre-reinforced shotcrete. In *Fourth International Symposium on Sprayed Concrete – Modern Use of Wet Mixed Sprayed Concrete for Underground Support*, Proceedings of the Fourth International Symposium on Sprayed Concretes, 2002.

[89] R. Winterberg K.p. Juhasz, P. Schaul. The effect of testing age on the performance of fibre reinforced concrete. In Daniele Peila, Giulia Viggiani, and Tarcisio Celestino, editors, *Tunnels and Underground Cities. Engineering and Innovation Meet Archaeology, Architecture and Art*, Proceedings of the WTC 2019 ITA-AITES World Tunnel Congress (WTC 2019). CRC Press, 2019.

[90] E.S. Bernard. Long-term post-crack performance of high-strength fibre-reinforced concrete for structural applications. *Structural Concrete*, 24(1):1134–1151, 2022.

[91] Alan Bloodworth Jiang Su. Crack development and effect of aging on performance of composite shell sprayed concrete tunnel linings. In *WTC 2017: Surface challenges – Underground solutions*, Proceedings of the World Tunnel Congress 2017. Norwegian Tunnelling Society, 2017.

[92] E.S. Bernard. Age-dependent changes in post-crack performance of fibre-reinforced shotcrete linings. *Tunneling and underground space technology*, 49:241–248, 2015.

[93] Min Ook Kim and Amanda C. Bordelon. Age-dependent properties of fibre-reinforced concrete for thin concrete overlays. *Construction and Building Materials*, 137:288–299, 2017.

[94] S. Smaniotto, M. Neuner, A. Dummer, T. Cordes, and G. Hofstetter. Experimental study of a wet mix shotcrete for primary tunnel linings—part i: Evolution of strength, stiffness and ductility. *Engineering Fracture Mechanics*, 267:108409, 2022.

[95] Erik Nordstrom. Andreas Sjolander, Anders Ansell. On the design of permanent rock support using fibre-reinforced shotcrete. *Fibers (MDPI)*, 11(2), 2023.

[96] Zhiqiang Zhang, Xingyu Zhu, Yanyang Zhang, and Ruikai Gong. Experimental and numerical investigation on flexural and fracture performance of steel fiber reinforced shotcrete. *Construction and Building Materials*, 315:125645, 2022.

[97] Soner Guler, Behice Öker, and Zehra Funda Akbulut. Workability, strength and toughness properties of different types of fiber-reinforced wet-mix shotcrete. *Structures*, 31:781–791, 2021.

[98] Christopher K.Y. Leung, Raymond Lai, and Augustus Y.F. Lee. Properties of wet-mixed fibre reinforced shotcrete and fiber-reinforced concrete with similar composition. *Cement and Concrete Research*, 35(4):788–795, 2005.

[99] Ramiro Castellanos Castellón, Marcos G. Alberti, Jaime C. Gálvez, J. Vera-Agulló, and R. Pina-Zapardiel. Comparison of the mechanical properties of fiber reinforced shotcrete at laboratory and on-site conditions. *Preprints*, 2022.

[100] Mehdi Bakhshi, Christopher Barsby, and Barzin Mobasher. Comparative evaluation of early age toughness parameters in fiber reinforced concrete. *Material and Structures*, 47:853–872, 2014.

[101] CEN (European Committee for Standardization). Design of concrete structures, general rules and rules for buildings (annex l. Technical Report Eurocode 2 EN 1992-1-1, European Committee for Standardization (CEN), Brussels, Belgium, 2004. Available at: `https://standards.cen.eu/`.

[102] Isaac Galobardes, Sergio H. Cavalaro, Antonio Aguado, and Tomàs Garcia. Estimation of the modulus of elasticity for sprayed concrete. *Construction and Building Materials*, 53:48–58, 2014.

[103] Josef Kaufmann, Kurt Frech, Philipp Schuetz, and Beat Münch. Rebound and orientation of fibers in wet sprayed concrete applications. *Construction and Building Materials*, 49:15–22, 2013.

[104] M Darveau, J Jolin. Three point bending test on square panel with notch on sprayed and cast specimens (3pbt on square panel)- dramix 4d 65/35 bg. Technical report, CRIB, Laval University, Quebec, Canada, 2021. Report for Bekaert Underground Solutions,.

[105] Luis Segura-Castillo, Sergio H. P. Cavalaro, Chris Goodier, Antonio Aguado, and Simon Austin. Fibre distribution and tensile response anisotropy in sprayed fibre reinforced concrete. *Materials and Structures*, 51(29), 2018.

[106] E.S. Bernard and A.H. Thomas. Fibre reinforced sprayed concrete for ground support. *Tunneling and underground space technology*, 99:103302, 2020.

[107] T.P. Smirnoff. Tunneling in soft ground. *Developments in Geotechnical Engineering*, 59 PartA:406–459, 1989.

[108] J. Sustersic, A. Zajc, R. Ercegovic, and V. Jovicic. Early age behaviour of fibre reinforced shortcrete. In Rudolph N. Kraus, Tarun.R. Naik, Peter Claisse, and Sadeghi-Pouya, editors, *International Conferrence: Sustainable construction materials and technologies*, Special papers proceedings, pages 276–282. UW Milwaukee CBU, 2007.

[109] Erik Stefan Bernard. Early-age load resistance of fibres reinforced shotcrete linings. *Tunnelling and underground space technology*, 23(4):451–460, 2008.

[110] Raymond Ian Gilbert and Erik Stefan Bernard. Post-cracking ductility of fibre reinforced concrete linings in combined bending and compression. *Tunnelling and Underground Space Technology*, 76:1–9, 2018.

[111] Danying Gao, Zhiqiang Gu, Haitang Zhu, and Yunchao Huang. Fatigue behavior assessment for steel fiber reinforced concrete beams through experiment and fatigue prediction model. *Structures*, 27:1105–1117, 2020.

[112] Xiuling Wang, Feifei Fan, Jinxing Lai, and Yongli Xie. Steel fiber reinforced concrete: A review of its material properties and usage in tunnel lining. *Structures*, 34:1080–1098, 2021.

[113] ACI Committee 506. Fibre-reinforced shotcrete – guide. Technical Report ACI PRC-506.1-21, ACI (American Concrete Institute), Farmington Hills, USA, 2021. A Technical Report V 1.2 Report for Bekaert Underground Solution.

[114] CEN (European Committee for Standardization). Fibres for concrete – part 1: Steel fibres - definitions, specifications and conformity. Technical Report EN 144889-1, European Committee for Standardization (CEN), Brussels, Belgium, 2006. Available at: `https://standards.cen.eu/`.

[115] ASTM (American Society for Testing and Materials). Standard specification for steel fibers for fiber-reinforced concrete. Technical Report ASTM A820/A820M-22, American Society for Testing and Materials (ASTM), West Conshohocken, United State, 2022.

[116] CEN (European Committee for Standardization). Fibres for concrete – part 2: Polymer fibres - definitions, specifications and conformity. Technical Report EN 144889-2, European Committee for Standardization (CEN), Brussels, Belgium, 2006. Available at: `https://standards.cen.eu/`.

[117] ASTM (American Society for Testing and Materials). Standard specification for polyolefin chopped strands for use in concrete. Technical Report ASTM D7508/D7508M-20, American Society for Testing and Materials (ASTM), West Conshohocken, United State, 2020.

[118] Axel G. Nitschke and Ralf Winterberg. Performance of macro synthetic fibre reinforced tunnel linings. In *ITA-AITES World Tunnel Congress 2016 (WTC 2016)*. Curran Associates, 216.

[119] Organiztion member of AFTES. Design of sprayed concrete for underground support. Technical Report Recommendations GT20R1A1, AFTES (French Tunnelling and Underground Space Association), Paris, France, 2000.

[120] Donal Coughlan, Rose Diez, John Comins, and Alfred Stärk. Crossrail project: Use of sprayed concrete tunnel linings on london's elizabeth line. In *Proceedings of the Institution of Civil Engineers*, volume 170, pages 39–46, 2017.

[121] Jiang Su. Design of sprayed concrete linings in soft ground a uk perspective. In *Proceeding of World Tunnel Congress: Underground - The Way to the Future*, pages 123–136, 2013.

[122] A. Pillai, H. Jung, F. Clement, C. Wilson, and D. Traldi. Sprayed concrete composite tunnel lining – load sharing between the primary and secondary lining, and its benefit in reducing the structural thickness of the lining. In *World Tunnel Congress: Surface Challenges-Underground solutions*, Proceedings of the World Tunnel Congress 2017. Curran Associates, 2017.

[123] Ulrike Pelz and Jurij Karlovšek. Spray-applied waterproofing membranes in tunnelling: Application and research directions in australia. *Tunnelling and Underground Space Technology*, 122:104364, 2022.

[124] Thomas. Alun H and Picket Andrew P. Composite shell lining. In Wolfgang Kusterle, editor, *Spritzbeton-Tagung 2012 (Shotcrete Conference 2012)*, 2012.

[125] Thomas A.H. The design of the crossrail tunnels in uk. *Geomechanics and Tunnelling*, 14(4), 2021.

[126] Ahsan Saif Khyzer Ahmed Sheikh. Steel fibre-reinforced shotcrete as an alternative to conventional concrete tunnel lining: a case study of gulpur hydropower project. *Geomechanics and Geoengineering*, 15(4):252–262, 2019.

[127] Kurt Zeidler and Johannes Jagarf. Fibre reinforced shotcrete for tunnel final lining.

[128] Paul Rapp. Shotcrete design and construction for the stave falls project power tunnels. *Shotcrete Magazine (American Shotcrete Association)*, 2000.

[129] T.J. Ireland and S. Stephenson. Design and construction of a permanent shotcrete lining—the a3 hindhead project, uk. In Erik Stefan Bernard, editor, *Shotcrete: Elements of a system*, Proceedings of the third international conference on engineering development in shotcret, pages 143–152, Sydney, Australia, 2010. TSE Pty. Ltd.

[130] Vojkan Jovičić, Jakob Šušteršič, and Željko Vukelič. The application of fibre reinforced shotcrete as primary support for a tunnel in flysch. *Tunnelling and Underground Space Technology*, 24(6):723–730, 2009.

[131] Ulrich Gossla, Luc Buttel, Holger Wahrmund, and Bernd Mehlig. Bemessung, anwendung und qualitatssicherung von stahlfasespritzbeton im tunnelbau. (design, execution and quality management of steel fibre reinforced shotcrete in tunnels). In Michael Pauser, editor, *Conference: Concrete and reinforced concrete construction (Beton- und Stahlbetonbau)*, volume 105, pages 72–132, 2018.

[132] Leonardo M. Massone and Francisco Nazar. Analytical and experimental evaluation of the use of fibers as partial reinforcement in shotcrete for tunnels in chile. *Tunnelling and Underground Space Technology*, 77:13–25, 2018.

[133] Vitor Moreira de Alencar Monteiro and Flávio de Andrade Silva. On the design of the fiber reinforced shotcrete applied as primary rock support in the cuiabá underground mining excavations: A case study. *Case Studies in Construction Materials*, 15:e00784, 2021.

[134] Jeramy Decker, Paul Madsen, Vojtech Gall, and Timothy O'Brien. Use of synthetic, fiber-reinforced, initial shotcrete lining at devil's slide tunnel project in california. *Transportation Research Record*, 2313(1):147–154, 2012.

[135] Lihe (John) Zhang, Dudley R.Morgan, Serge Moalli, David Gagnon, and Danny Dugas. Tunnel shotcrete lining for hydroelecric projects. *Shotcrete (American Shotcerete Association*, 2019.

[136] V. Gall, K. Zeidler, N. Munfah, and D. Cerulli. Shotcrete for tunnel final linings – design and construction considerations. In Levent Ozdemir, editor, *Proceedings of the North American Tunneling Conference 2004*. Taylor Francis Group, 2004.

[137] M. Gonzalez, M. Kitson, D. Mares, B. Muir, E. Nye, and T. Schroeter. The north strathfield rail underpass – driven tunnel design and construction. In *15th Australasian Tunnelling Conference 2014*. Australasian Tunnelling Society, 2014.

[138] Carlos A. Madrid, Sergio E. Garcia, Flavio B. Rodriguez, and Claudio F. Parada. Correlation between trials of polymer fibers shotcrete (srf): Fiber content in fresh mixture, energy absorption and barcelona test. In Thomas Beck, Synnove A. Myren, and Siri Engen, editors, *8th International Symposium on Sprayed Concrete – Modern Use of Wet Mix Sprayed Concrete for Underground Support*, Trondheim, Norway, 2018. Norsk Betongforening.

[139] M. Balá, M. Uhrin, Pavel Ruzicka, and Matou Hilar. Utilisation of fibre reinforced sprayed concrete for primary lining of the povaský chlmec tunnel. *IOP Conference Series: Materials Science and Engineering*, 246, 2017.

[140] Hassan Sahranavard and Reza Aghanoori. Use of polymer fiber (hpp) reinforced shotcrete instead of final lining in khomary tunnel. *Tunnelling and Underground Space Technology*, 21(3):342, 2006. Safety in the Underground Space - Proceedings of the ITA-AITES 2006 World Tunnel Congress and 32nd ITA General Assembly.

[141] A. Kaul. Composite shell lining for tunnels and mined stations. *Water and Energy International*, 58(8):44–48, 2015.

[142] Qing Du, Shanzun Sun, Shuyi Wen, Guyi Zhan, and Yang Li. Application of composite shell lining for qingdao metro xizhen station. *IOP Conference Series: Earth and Environmental Science*, 267(4):042066, 2019.

[143] C. Aire and L. Aguilar. Fiber reinforced shotcrete control tests in the mexico city metro line 12 tunnel. *Revista ALCONPAT (Applied Research)*, 2021.

[144] C. Hauck and A.E. Mathisen. Macro-synthetic fibre reinforced shotcrete in a norwegian road tunnel. In Erik Stefan Bernard, editor, *Proceedings of second international conference on engineering development in shotcrete*, volume 105 of *Proceedings of second international conference on engineering development in shotcrete*, pages 72–132, 2004.

[145] LIU Hui and SU Bo. Property test and mixture ratio design of steel fiber shotcrete for wanjunhui tunnel. *Journal of Railway Engineering Society*, 18(3):69–78, 2001.

[146] L. Kuitenbrouwer. The use of steel fibre shotcrete on major european underground projects. In Erik Stefan Bernard, editor, *Third International Symposium on Sprayed Concrete-Modern Use of Wet Mix Sprayed Concrete for Underground Support*, Proceedings of second international conference on engineering development in shotcrete, 1999.

[147] Tom Melbye, Ross Dimmock, and Knut F. Garshol. *Sprayed concrete for rock support*. MBT International Underground Construction Group, Division of MBT (Switzerland) Ltd, Switzerland, 9 edition, 2001.

[148] T. Franzén. Shotcrete for underground support: a state-of-the-art report with focus on steel-fibre reinforcement. *Tunnelling and Underground Space Technology*, 7(4):383–391, 1992.

[149] X.R.Liu, Y.H.Zhu, and X.H.Li. Experimental research on single-layer tunnel lining of steel fibre shotcrete. *Rock and Soil Mechanics*, 30(8):2319–2323, 2009.

[150] Ulrich Gossla, Luc Buttel, Holger Wahrmund, and Bernd Mehlig. r. Design, execution and quality management of steel fbre reinforced shotcrete in tunnels. In *Conference on concrete and reinforced concrete construction (Beton- und Stahlbetonbau)*, volume 105, pages 92–101, 2010.

[151] Zhu YH. *Study on mechanical characteristics of steel fibre reinforced shotcrete and its application in single layer tunnel lining*. PhD thesis, Chongqing University, Chongqing, China, 2009. PhD thesis.

[152] Jianting Wu, Yuan Hongchao, and Xu Bo. Mechanical behavior prediction of tunnel with single-layer steel fiber shotcrete lining. *Scientific Reports*, 15:34537, 2025.

[153] Benoit De Rivaz. High-performance steel fibres offer new possibilities for permanent sprayed concrete lining. *Tunnel News*, 2023.

[154] A. Bedi, S.k. Gupta, S. Trivedi, and A. Pengelleyr. Design construction of mumbai metro line 3 sahar road crossover cavern using permanent sprayed concrete linings. In *ITA-AITES World Tunnel Congress 2022*, 2022.

[155] Verya Nasri. Initial and final shotcrete linings for edouard montpetit station of rem project. *Shotcrete Magazine*, 1st Quarter:48, 2025.

[156] ITAtech AG PFRCS. Itatech guidance for precast fibre reinforced concrete segements. Technical report, ITAtech, Avignon, France, 2016. Design Aspects.

[157] fib (International Federation for Structural Concrete). Precast tunnel segments in fibre-reinforced concrete: State of the art report. Technical report, fib (International Federation for Structural Concrete)., Lausanne, Switzerland, 2017.

[158] Working Group 2. Twenty years of frc tunnel segment practice: lessons learnt and proposed design principles - ita report number 16. Technical report, ITA and AITES, Avignon, France, 2016.

[159] CEN (European Committee for Standardization). Sprayed concrete – part 1: Definitions, specifications and conformity. Technical Report EN 14487-1, European Committee for Standardization (CEN), Brussels, Belgium, 2006. Available at: `https://standards.cen.eu/`.

[160] CEN (European Committee for Standardization). Testing sprayed concrete – part 3: Flexural strengths (first peak, ultimate and residual) fibre reinforced beam specimens. Technical Report EN 14488-3, European Committee for Standardization (CEN), Brussels, Belgium, 2006. Available at: `https://standards.cen.eu/`.

[161] EFNARC (The European Federation of Specialist Construction Chemicals and Concrete Systems),). Testing sprayed con-crete: three point bending test on square panel with notch: Flexural tensile strength of fibre concrete on sprayed test specimen. Technical Report EFNARC, EEFNARC, Flums, Switzerland, 2011.

[162] Benoit De Rivaz, A. Meda, and J. Kennedy. Fibre reinforced spray concrete performance criteria: Comparison between en14651 and efnarc three-point bending test on square panel with notch. In *Tunnels and Underground Cities. Engineering and Innovation Meet Archaeology, Architecture and Art*, Proceedings of the WTC 2019 ITA-AITES World Tunnel Congress. imprint CRC Press, 2019.

[163] CEN (European Committee for Standardization). Testing sprayed concrete-part 1: Sampling fresh and hardened concrete. Technical Report EN 14488-1, European Committee for Standardization (CEN), Brussels, Belgium, 2005. Available at: `https://standards.cen.eu/`.

[164] International Federation for Structural Concrete. *Fibre reinforced sprayed concrete in tunnels and underground spaces:fib Bulletin 116*. Ernst Sohn, Lausanne, Switzerland, 2025.

[165] CEN (European Committee for Standardization). Concrete-specification, performance, production and conformity. Technical Report EN 206:2013, European Committee for Standardization (CEN), Brussels, Belgium, 2013. Available at: `https://standards.cen.eu/`.

[166] CEN (European Committee for Standardization). Testing concrete in structures – part 1: Cored specimens taking, examining and testing in compression. Technical Report EN 12504-1:2019, European Committee for Standardization (CEN), Brussels, Belgium, 2019. Available at: `https://standards.cen.eu/`.

[167] CEN (European Committee for Standardization). Testing hardened concrete - part 3: Compressive strength of test specimens. Technical Report EN 12390-3:2019, European Committee for Standardization (CEN), Brussels, Belgium, 2019. Available at: `https://standards.cen.eu/`.

[168] CEN (European Committee for Standardization). Assessment of in-situ compressive strength in structures and precast concrete components. Technical Report EN 13791:2019, European Committee for Standardization (CEN), Brussels, Belgium, 2019. Available at: `https://standards.cen.eu/`.

[169] American Concrete Institute. Guide for obtaining cores and interpreting compressive strength results (aci prc-214.4-21). Technical report, American Concrete Institute, Farmington Hills, MI, USA, 2021.

[170] F. Michael Bartlett and James G. MacGregor. Effect of core diameter on concrete core strengths. *ACI Materials Journal*, 91(5):460–469, September–October 1994.

[171] Consiglio Superiore dei Lavori Pubblici. Istruzioni per l'applicazione dell'aggiornamento delle norme tecniche per le costruzioni [instructions for the application of the updated italian building code]. Circular No. 7 C.S.LL.PP., 21 January 2019, 2019. Official Gazette of the Italian Republic, No. 35, 11 February 2019, Rome, Italy.

[172] CEN (European Committee for Standardization). Testing hardened concrete - part 13: Determination of secant modulus of elasticity in compression. Technical Report EN 12390-13:2013, European Committee for Standardization (CEN), Brussels, Belgium, 2013. Available at: `https://standards.cen.eu/`.

[173] CEN (European Committee for Standardization). Testing hardened concrete - part 16: Determination of shrinkage and expansion. Technical Report EN 12390-16:2019, European Committee for Standardization (CEN), Brussels, Belgium, 2021. Available at: `https://standards.cen.eu/`.

[174] Chung-Chan Hung and Tuong Dat Dinh Do. Sprayed high-strength strain-hardening cementitious composite: Anisotropic mechanical properties and fiber distribution characteristics. *Construction and Building Materials*, 412:134862, 2024.

[175] A. Blanco, P. Pujadas, A. de la Fuente, S.H.P. Cavalaro, and A. Aguado. Assessment of the fibre orientation factor in sfrc slabs. *Composites Part B: Engineering*, 68:343–354, 2015.

[176] CEN (European Committee for Standardization). Basis of structural designl. Technical Report EN 1990:2023, European Committee for Standardization (CEN), Brussels, Belgium, 2023. Available at: `https://standards.cen.eu/`.

[177] DIANA FEA BV. User's manual - material library release 10.8. Technical Report DIANA 10.8, DIANA FEA BV, Delft, Netherlands, 2024.

[178] Giuseppe Tiberti. *Concrete Tunnel Segments with Combined Traditional and Fiber Reinforcement: Optimization of the Structural Behavior and Design Aspects*. PhD thesis, Department of Civil, Environmental, Architectural Engineering and Mathematics, University of Brescia, Brescia, Italy, 2014. 396 p., Aracne Editrice s.r.l., Roma, Italy.

[179] Federica Germano. *Cyclic Behavior of Steel Fiber Reinforced Concrete: From Material to Seismic Columns*. PhD thesis, Department of Civil, Environmental, Architectural Engineering and Mathematics, University of Brescia, Brescia, Italy, 2014. 339 p., Aracne Editrice s.r.l., Roma, Italy.

[180] A. Hillerborg, M. Modéer, and P.-E. Petersson. Analysis of crack formation and crack growth in concrete by means of fracture mechanics and finite elements. *Cement and Concrete Research*, 6(6):773–781, 1976.

[181] H. Dahl R. Brincker. Fictitious crack model of concrete fracture. *Magazine of Concrete Research*, 41(147):79–86, 1989.

[182] Per-Erik. Peterson. *Crack growth and development of fracture zones in plain concrete and similar materials*. PhD thesis, Devision of Building Materials. LTH, Lund University, Sweden, 1981.

[183] B. H. Oh Zdeněk P. Bažant. Crack band theory for fracture of concrete. *Materials and Structures*, 16:155–177, 1983.

[184] J.G. Rots and J. Blaauwendraad. Crack models for concrete discrete or smeared? fixed, multi-directional or rotating,. *HERON (Netherlands Technology Foundation (STW))*, 43(1), 1989.

[185] P.E. Roelfstra and F.H. Wittmann. Numerical method to link strain softening with failure of concrete. In Folker H. Wittmann, editor, *The International Conference on Fracture Mechanics: Fracture Toughness and Fracture Energy of Concrete*, Amsterdam, Netherland, 1986. Elsevier.

[186] A.G. Kooiman, C.van der Veen, and J.C. Walraven. Modelling the post-cracking behaviour of steel fibre reinforced concrete for structural design purposes. *HERON*, 45(4), 2000.

[187] H. P. Feenstra. *Computational Aspects of Biaxial Stress in Plain and Reinforced Concrete*. PhD thesis, Delft University of Technology, Delft, The Netherlands, 1993. Ph.D. Thesis.

[188] F. Lo Monte, A. Marcucci, S. Guanziroli, and L. Ferrara. Three- versus four-point bending tests for the identification of frc tensile constitutive behavior. In *Proceedings of the Italian Concrete Days: Innovation and Sustainability in Concrete Structures*, pages 725–730, 2024. Italian Concrete Days Conference.